Light utilization in microalgae : the marine diatom Phaeodactylum tricornutum and the green algae Chlamydomonas reinhardtii

Serena Flori

Communauté
UNIVERSITÉ Grenoble Alpes

THÈSE

Pour obtenir le grade de

DOCTEUR DE LA COMMUNAUTE UNIVERSITE GRENOBLE ALPES

Spécialité : **Biologie Végétale**

Arrêté ministériel : 7 août 2006

Présentée par

Serena FLORI

Thèse dirigée par **Giovanni FINAZZI** et
codirigée par **Dimitris PETROUTSOS**

préparée au sein du **Laboratoire de Physiologie Cellulaire et Végétale**
dans **l'École Doctorale Chimie et Science du Vivant**

Light utilization in microalgae:

the marine diatom *Phaeodactylum tricornutum* and the green algae *Chlamydomonas reinhardtii*.

Thèse soutenue publiquement le **15 Septembre 2016**
devant le jury composé de :

Mme Christelle, BRETON
Professeur à l'Université Grenoble Alpes (Président)
Mme Claire, REMACLE
Professeur à l'Université de Liège, Belgique (Rapporteur)
M Maurizio, RIBERA D'ALCALA'
Directeur de Recherche SZN, Italy (Rapporteur)
Mme Xenie, JOHNSON
Ingénieur CEA Cadarache (Examinateur)
M Jun, MINAGAWA
Professeur National Institute for Basic Biology, Japan (Examinateur)
M Dimitris, PETROUTSOS
CR1 CNRS Grenoble (Co-encadrant de thèse)
M Giovanni, FINAZZI
Directeur de Recherche CNRS Grenoble (Directeur de thèse)

Pour ma famille…



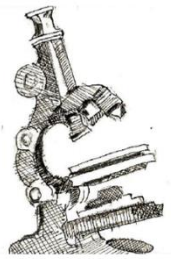
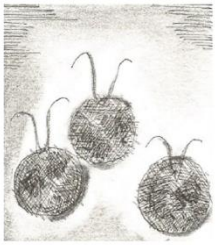
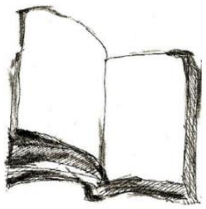

Summary

Light utilization in microalgae: the marine diatom *Phaeodactylum tricornutum* and the green algae *Chlamydomonas reinhardtii*.

Microalgae have developed distinct approaches to modulate light absorption and utilization by their photosystems in response to environmental *stimuli*. In this Ph.D Thesis, I characterised different strategies employed by freshwater (*Chlamydomonas reinhardtii*) and marine algae (*Phaeodactylum tricornutum*) to optimise their acclimation to the environment.

In the first part of this work, I used spectroscopic, biochemical, electron microscopy analysis and 3-dimentional reconstitution to produce a model of the entire cell of the marine diatom *Phaeodactylum tricornutum.* This model has been used to address the following questions: *i.* how the cellular organelles interact to optimise CO_2 assimilation via ATP/NADPH exchanges? *ii.* how is a secondary chloroplast structured to facilitate exchanges with the cytosol via its four membranes envelope barrier? and *iii.* how have diatoms shaped their photosynthetic membranes to optimise light absorption and downstream electron flow?

In the second part, I have focused on the regulation of light harvesting and dissipation in *C. reinhardtii* by studying the role of perception of light colour and metabolism on excess light dissipation via the Non-Photochemical Quenching of energy (NPQ). Using biochemical and spectroscopic approaches, a molecular link between photoreception, photosynthesis and photoprotection was found in *C. reinhardtii* via the role of the photoreceptor phototropin on excess absorbed energy dissipation (NPQ). I also demonstrated that besides light, downstream metabolism can also affect this acclimation process.

Overall this Ph.D work reveals the existence and integration of different signal pathways in the regulation of photoprotective responses by microalgae living in the ocean and in the land.

Résumé

L'utilisation de la lumière chez les microalgues : la diatomée marine *Phaeodactylum tricornutum* et l'algue verte *Chlamydomonas reinhardtii*.

Les microalgues ont développé des approches distinctes pour moduler l'absorption de la lumière et son utilisation par leurs photosystèmes en réponse à des stimuli environnementaux. Dans ce rapport de Thèse je présente les différentes stratégies employées par une algue d'eau douce (*Chlamydomonas reinhardtii*) et une algue marine (*Phaeodactylum tricornutum*) pour optimiser leur acclimatation à l'environnement.

Dans la première partie de ce rapport, je propose un modèle de cellules entières de la diatomée marine *Phaeodactylum tricornutum* obtenue par analyses spectroscopiques et biochimiques ainsi que par l'obtention d'images par microscopie électronique et reconstitution 3-D. Ce modèle a été utilisé pour répondre aux questions suivantes *i.* comment les chloroplastes et les mitochondries sont organisés pour optimiser l'assimilation du CO2 par échange ATP / NADPH *ii.* comment est structuré un chloroplaste secondaire pour faciliter les échanges avec le cytosol à travers les quatre membranes qui le délimitent et *iii.* comment sont structurées les membranes photosynthétiques afin d'optimiser l'absorption de lumière et le flux d'électrons.

La deuxième partie de ce rapport porte sur la régulation de la lumière et de sa dissipation chez *C. reinhardtii* grâce à l'étude d'une part du rôle de la perception de la couleur de la lumière et d'autre part du métabolisme sur la dissipation de l'excès de lumière par quenching non photochimique (NPQ). En utilisant des approches biochimiques et spectroscopiques, on a mis en évidence un lien moléculaire entre la photoréception, la photosynthèse et la photoprotection chez *C. reinhardtii* via le rôle du photorécepteur phototropine, démontrant ainsi que le métabolisme, en plus de la lumière, peut aussi affecter ce processus d'acclimatation.

En conclusion, ce travail de thèse révèle l'existence et l'intégration des différentes voies de signalisation dans la régulation des réponses photoprotectrices mises en place chez les microalgues marines et d'eau douce.

Chapter 1

1.1 Introduction

I realized my Ph.D thanks to a Marie Curie ITN grant in the frame of the AccliPhot network. The main aim of the AccliPhot consortium was to investigate and understand short-term acclimation mechanisms in photosynthetic organisms integrating theoretical and experimental research from academia and industry. My Ph.D program took place in the Cell and Plant Physiology Laboratory (LPCV, BIG) at CEA Grenoble. The experimental work, divided into two main tasks, aimed at understanding how the different processes linked to photosynthesis (light absorption, dissipation electron flow and carbon assimilation for metabolism) are regulated to allow microalgae to successfully acclimate to their environment.

1.2 From light perception to light utilization

Microalgae are an ensemble of marine and freshwater organisms adapted to live in differentiated aquatic environment and are at the basis of the trophic network. Although they represent only a small percentage of the biomass on Earth, these organisms (also called “primary producers”) contribute significantly to the global primary productivity (Field et al., 1998). Their activity influences the major biogeochemical cycles, playing a crucial role in CO_2 sequestration from the atmosphere (through the so-called biological pump). Via photosynthesis, they can alter CO_2 concentrations enriching the surrounding environment with oxygen, thereby influencing global climate. Under favourable conditions, light can trigger exponential growth mechanisms called "algal blooms" in which the density of these species can reach several millions cells per milliliter. In aquatic environment, microalgae undergoes strong variations of incident irradiance due to its transport along the water column and to the effect of water mixing (induced by wind or currents). Light variability can influence photosynthetic organisms, which must regulate their photosynthetic apparatus in order to adapt to the limiting, saturating or over-saturating light input. Acclimation to low irradiance requires an increased efficiency in light-harvesting achieved by *de novo* synthesis of photosynthetic pigments (Sukenik et al., 1987). On the other hand, oversaturating irradiance leads to damaged photosynthetic apparatus (Bowler et al., 1992; Osmond et al., 1997; Anderson et al., 1998) resulting in the redirection of the energy into dissipative processes with an overall reduction in the photosynthetic yield.

When light excites a chlorophyll (Chl) molecule, it enters in a fist singlet-state excitation (^{1}Chl*). This “energy rich” state *i.* can be used to drive photosynthesis (qP, Figure 1.1), *ii*. can relax into the ground state via chlorophyll fluorescence (Figure 1.1) or *iii.* can be dissipated in the form of heat

(through non radiative thermal emission, in a process that is the basis of Non-Photochemical Quenching, NPQ, Figure 1.1). In both plants and microalgae, the rapid regulation of these mechanisms is an essential component for the successful acclimation to their environmental *niche*.

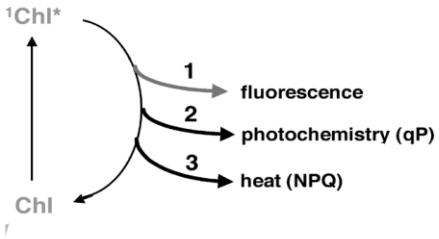

Figure 1.1 – **Fate of the excited chlorophyll**. Representation of the possible relaxation pathways of the singlet excited state of chlorophyll (1Chl*). (1) fluorescence (2) photochemistry (qP) or (3) dissipation as heat (or NPQ; from Muller et al., 2001).

1.3 The photosynthetic process

The first route, and the most advantageous one, is the use of this energy to drive photochemistry, i.e. shuttling electrons through the photosynthetic electron transport chain. In photyosynthetic eukaryotes, this process occurs in a specific organelle, the chloroplast, which contains a membrane system (the thylakoids), which are the sites of photosynthetic electron transport and an aqueous matrix (the stroma), where CO_2 is assimilated into carbohydrates.

While some phototrophic prokaryotes (Béjà et al., 2000; Kolber et al., 2000) perform an ancestral, anoxygenic type of photosynthesis (Whitmarsh, 1999), most photosynthetic organisms use water as an electron donor to reduce CO_2 and produce carbohydrates generating oxygen as secondary product. Consistent with this event, photosynthesis permits the proliferation of life on Earth and the overall process can be represented as follows (Figure 1.2).

$$nH_2O + nCO_2 + Light \rightarrow (CH_2O)n + $$

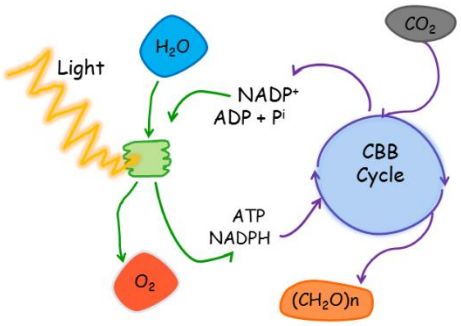

Figure 1.2 – **Representation of the oxygenic photosynthesis**

The major players in the photosynthetic process are two multiproteic complexes called photosystems I (PSI) and II (PSII). Their structure is design into two distinct units, one devoted to the light-harvesting processes (the antenna complexes) and one (the core-complexes) the site of photochemical reactions. PSI and PSII are structurally different, however they share common features like some chlorophyll binding proteins, responsible for light absorption and special chlorophylls pair located in the core complexes, which drive electron transport.

Photosynthetic organisms belonging to *viridiplantae* (plants and green algae) possess the antenna complexes composed by proteins members of the light-harvesting complexes (LHC) superfamily. These proteins binds a high concentration of light-harvesting pigments (chlorophylls *a* and *b* and carotenoids) at various stoichiometries as a consequence of adaptation to different environmental conditions (Green & Durnford, 1996; Nelson & Ben-Shem, 2005). These antenna complexes are encoded by the nuclear genome and they are associated with photosystems I (LHCI or LHCA) and with photosystems II (LHCII or LHCB). In the model plant *Arabidopsis thaliana* four isoforms are associated with PSI (LHCA1-4) and six with PSII (LHCB1-6; Jansson, 1999). Microalgae, on the other hand, possess a more complex organization of LHC. In the model organism *Chlamydomonas reinhardtii*, the LHCI antenna is larger than plants with nine LHCAs subunits (Büchel, 2015) and nine genes encode for the LHCII. In diatoms, the peripheral antennae are mainly composed of fucoxanthin chlorophyll proteins (FCP), which bind chlorophyll *c* instead of *b* and fucoxanthin instead of lutein. Due to the homology of FCP genes with LHC genes of higher plants (Apt et al.,1994; Eppard & Rhiel, 1998), the FCP are commonly placed into the CBP family (Chlorophyll Binding Proteins, Dittami et al., 2010). However, the specific characterization of these LHC complexes to photosystem I or II in diatoms is still matter of debate (for a recent review see Büchel, 2015).

The photosystems core-complexes include reaction centres and internal (core) antennae. These proteins are well conserved during evolution and present only small differences between organisms. The PSII core-complex for example, contain two similar proteins (D1 and D2) which directly bind pigments (special pair of chlorophyll *a*, P680), electron transport cofactors (2 pheophytins, 2 plastoquinones and a non-heme iron) and two proteins of the internal antenna (CP43 and CP47). In *viridiplantae*, the PSI core complex contains 14 subunits. The “central” part is composed by the subunits PsaA, B and C (three large proteins associated with the cofactors A0, A1, FX, FA and FB) and special pair of chlorophylls (P700) responsible for the photochemical conversion (Nelson & Yocum, 2006).

The light phase of photosynthesis starts with the absorption of photons by the antenna complexes of the photosystems (LHCI and LHCII). Once a photon is captured by this "net-trap" the energy is transferred in a down-hill reaction to specific Chl *a* molecules in the PSs core complexes (P700 and P680, respectively for PSI and PSII) thanks to the specific arrangement of pigments within the antennas. When these pigments become excited, they perform charge separation to feed a chain of redox reactions. This ultimately generates reducing power in the form of nicotinamide adenine dinucleotide phosphate (NADPH) molecules. At the same time, charge separation (in PSI and PSII) and the protonation/deprotonation reactions that occur on the two side of the thylakoid membranes during electron transfer, lead to the generation of an electro-chemical potential gradient (ΔpH) between the stroma and the lumen (internal aqueous space) side of the thylakoid membranes. This gradient is used to synthesize adenosine triphosphate (ATP), according to the Mitchell's theory. A schematic representation of the pathway for photosynthetic electron flow is presented in Figure 1.3.

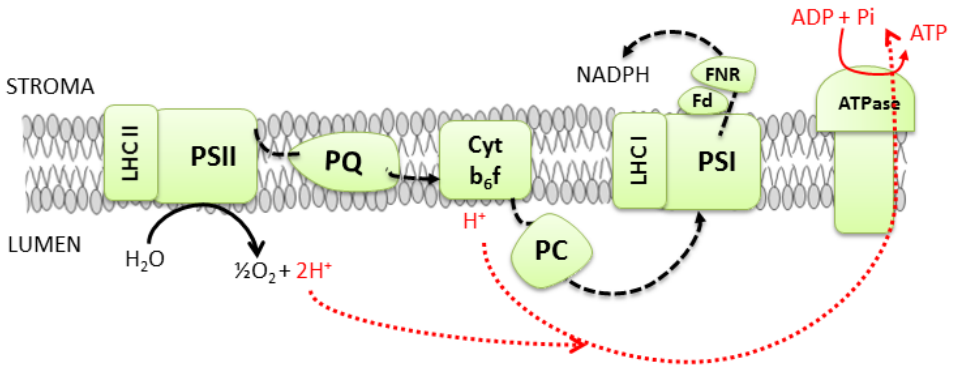

Figure 1.3 – **Schematic representation of the pathway for the photosynthetic linear electron flow**. Black rows represent the electrons pathway through the major components of the photosynthetic electron flow chain: photosystem II (PSII), the plastoquinone (PQ) the cytochrome b_6f complex (Cyt $_{b6f}$) the plastocyanin (PC), the light harvesting complex of the photosystems I (LHCI), the photosystems I (PSI), the ferredoxin (Fd), the enzyme Fd-NADP+-oxidoreductase (FNR) and the ATP synthase. Red rows represent the protons pathway.

At the level of PSII, excited P680 transfers an electron to a pheophytin, the primary electron acceptor molecule. Afterwards, the electron is delivered to secondary quinone acceptors (QA and QB), and is carried through a chain of transporters molecules (according to their redox potential). In parallel, excitation of the primary electron donor of PSI (P700) transfers an electron to the primary PSI acceptors A0, and then again to a chain of electron transporters (A1, ferredoxin (Fd) and the enzyme Fd-NADP+-oxidoreductase, FNR), ultimately leading to the reduction of NADP+ to NADPH on the stroma side. Electrons flow between PSII to PSI occurs via two soluble electron carriers PQ and PC, which reduce and oxidize the Cyt b_6f complex, respectively, during the so called "Z-scheme" (Hill & Bendall, 1960).

The ATP and NADPH provided by the light phase are used during the light-independent phase (erroneously described dark phase). This stage (where the light is not directly needed) comprise a series of reactions indicated with the name Calvin-Benson-Bassham Cycle (CBB, Benson & Calvin, 1950; Benson, 2002; Bassham, 2003) in which atmospheric CO_2 is reduced to carbohydrates to sustain cellular metabolism. The synthesis of the 3-carbon molecule (glyceraldehyde 3-phosphate, GAP) is catalyzed by the enzyme Ribulose-1,5-Bisphosphate Carboxylase/Oxygenase (RuBisCo) located in the stroma of the chloroplast. Thanks to the uptake of CO_2 the Ribulose-5-phosphate (Ru5P) is regenerated at the end of the process to preserve the cyclic characteristic of the CBB cycle. This process requires ATP and NADPH in a stoichiometry of 1.5. However, the linear electron flow described above produces ATP at lower amounts (likely 1.3, e.g. Allen 2002; Petersen et al., 2012). Therefore, photosynthetic organisms must adjust and optimize the ATP/NADPH ratio in order to produce biomass. In *viridiplantae*, it is believed that the higher demand for ATP than for NADPH, leads to the rerouting of photosynthetic electrons around PSI in a cyclic electron flow. This process involves the transfer of electrons from the ferredoxin back to the Cyt b_6f complex, producing a proton gradient (and thus ATP) during the reduction of PC. PSII is not involved in this process and as consequence, this alternative pathway does not lead to the production of NADPH or O_2. On the other hand, in diatoms, our recent results (see section 2.5) show that optimization of the photosynthetic ATP/NADPH ratio is achieved through an extensive interaction between the photosynthetic and the respiratory process, which occurs in the mitochondria.

1.4 *"Too much of a good thing…"*

Citing Barber & Anderson, 1992 "*light can be bad for photosynthesis".* Indeed, as mentioned above, the excited Chl *a* has several ways to relax to its ground state, one of them is fluorescence. Fluorescence consists in the emission of an energy photon at longer wavelength (and lower energy) than the absorbed photon. Changes in the quantum yield of fluorescence allow calculating the capacity of PSII reaction centres to drive photosynthesis (Genty et al., 1989) and nowadays these parameters are a common proxy used to evaluate photochemical efficiency. The three fates of light described by Muller and coworkers are in competition and the relative yield of fluorescence is dependent on the efficiency of the other two pathways (qP and NPQ; Niyogi, 1999; Muller et al., 2001). Using *in vivo* fluorometers (called pulse amplitude modulation, PAM) changes in fluorescence emission in dark adapted and illuminated cells can be measured providing information on changes in the efficiency of photochemistry (qP) and heat dissipation (Non photochemical quenching; NPQ). The PAM principles are based on the selective amplification of the fluorescence signal emitted by the Chl *a* after excitation using different light sources and modulated light frequency pulses (Baker, 2008). Measuring the progressive reduction of chlorophyll fluorescence in response to illumination we can have information about the activation of NPQ mechanisms. The analysis starts with dark-adapted cells and a short (200 ms long) saturating pulse. During this condition, cells, as consequence of the transient reduction of Q_A, re-emit the maxium amount of absorbed energy in the form of fluorescence (Fm; maximal fluorescence of dark-adapted cells). Then saturating pulses are applied in parallel with illumination. After each pulse, the maximal fluorescence of light-adapted cells (Fm') is recorded. The activation of thermal dissipation mechanisms (NPQ) can be quantified by the decrease of Fm'. The amplitude of NPQ, according to Bilger and Björkman (1990), is related to the differences between these two conditions (dark- versus light-adapted cells) and calculated as: (Fm/ Fm') – 1).

1.5 Photoprotection

The highly variable nature of the environment surrounding photosynthetic organisms exposes them to possibly dangerous situations. In particular, light, which is the driving force for life strongly affects the performance and growth of photosynthetic organisms. While low light can limit growth by limiting the photosynthetic performances, excess light can led to the production of reactive oxygen species (see e.g. Niyogi & Truong, 2013; Finazzi & Minagawa, 2014). Plants and algae can optimize energy capture and conversion efficiency under different light conditions by adapting their photosynthetic apparatus thanks to a variety of short and long-term responses.

Short-term responses act in the timescale of seconds to minutes and allow reversible responses of the photosynthetic machinery. Under high light exposure, excessive photon flux leads to the over-excitation of the light-harvesting complexes. This increases the possible accumulation of chlorophyll triplets (Chl*), which in turn trigger the production of reactive oxygen species (ROS; Krieger-Liszkay et al., 2008), i.e. dangerous compounds for the cell. To reduce this risk, photosynthetic organisms can increase the thermal dissipation of the excess light. This is typically achieved via NPQ, which represents a major strategy for rapid regulation of photosynthesis.

On the other hand, long-term responses are also observed and involve ultrastructural changes in the cell and in most cases *de-novo* synthesis or breakdown of proteins, pigments and redox cofactors. For instance, during limiting light conditions, photosynthetic cells tend to increase their light-harvesting capacity to maximize light capture. This requires an increased biosynthesis of photosynthetic pigments (Sukenik et al., 1987), as well as the increased expression of the genes encoding for the light harvesting proteins (LHC in plants). Conversely, plants tend to decrease the size of the LHC proteins in high light (Anderson et al., 1995) to avoid absorption of excess light. This leads to a feedback regulation, where the level of irradiance regulate the antenna size of photosystems on the long-term scale of several hours/days (Smith et al., 1990; Melis, 1991; Ballottari et al., 2007). In the following, I will shortly describe the molecular mechanisms of both the short and long-term responses.

1.6 Short-term responses

1.6.1 Non-photochemical quenching

The NPQ is the major fast responses to light *stimuli*. In plants, it has been reported that three NPQ components can be distinguished based on their different relaxation kinetics (Horton et al., 1996; Dall'Osto et al., 2005; Joliot & Finazzi, 2010). The fastest component is the energy-dependent component, qE. In plants qE relax in around one minute. The next one is state transitions qT, which relaxes within minutes. Finally, the photoinhibitory quenching qI, shows the slowest relaxation kinetics. The exact contribution of each component can vary depending on photosynthetic organisms and environmental conditions. As a general rule, qE is the major component from moderate to high light conditions, development of qT is supposed to play a role in balancing light quality excitation between the two photosystems. Therefore, this process is prominent under low light, where photosynthesis is limited by absorption. Finally, qI becomes predominant when light is oversaturated and exceeds the photosynthetic capacity.

1.6.1.1 Energy-dependent quenching qE

The major process contributing to the non-photochemical quenching of the chlorophyll fluorescence is qE. This process mostly occurs at the level of the LHC of photosystem II (LHCII, Horton et al., 1996). qE is triggered by *i.* the acidification of the lumenal space, because the saturated electron flow leads to the building of a large pH gradient across the thylakoid membranes *ii*. changes in pigment composition in the LHCII (through the xanthophyll cycle, XC) and *iii.* activation of specific qE protein effectors (Niyogi & Truong, 2013). The exact role of each component is still matter of debate and can vary within autotrophs.

i. During photosynthesis, the activation of the electron transport chain generates a transmembrane ΔpH across the thylakoid membranes. The lumen becomes acidic, while the the stroma of the chloroplast becomes slightly basic. In high light, when the absorption of light exceeds the actual capacity for carbon fixation, the acidification of the thylakoid lumen immediately switches a signal for the feedback regulation of light harvesting.

ii. When the lumen pH drops below 6, it activates specialized enzymes which can convert specific pigments (oxygenated carotenoids called xanthophylls) into a closely related de-epoxidated one. This conversion occurs on a timescale of minutes and is supposed to facilitate a conformational change in the LHCII, switching the PSII into a quenched state.

iii. The decrease in lumenal pH also results in the protonation of specific PSII-proteins that vary within organisms and evolution.

1.6.1.1.1 Xanthophyll cycle and its variants

As mentioned above, the pigments contained in the light harvesting complexes are extremely variable between organisms. Carotenoids are key players in acclimation/regulation processes because they can directly contribute to both light harvesting (between 350 and 750 nm of the visible spectrum) and photoprotection, through the xanthophyll cycle. In plants, light-harvesting proteins binds lutein, neoxanthin, violaxanthin (Vx) and β-carotene. During NPQ, the violaxanthin de-epoxidase enzyme (VDE) converts violaxanthin to zeaxanthin (Zx) through antheraxanthin; whereas under low light intensities the conversion of Zx again into Vx is catalyzed by a zeaxanthin epoxidase (ZEP; Hager, 1967). Diatoms LHC antennae (FCP) bind different pigments like fucoxanthin, chlorophyll *a/c* (Beer et al., 2006) and xantophylls (Büchel & Wilhelm, 1993; Hiller et al., 1993). These microalgae possess not only the Vx/Zx cycle but also the diadinoxanthin cycle (Lohr, 2011) which comprises a one-step de-epoxidation that converts diadinoxanthin (Dd) into diatoxanthin (Dt) through the activity of the enzyme diadinoxanthin de-epoxidase (DDE, active at low pH). It was demonstrated by Goss and coworkers in 2006 that the accumulation of the photoprotective pigment diatoxanthin is linearly correlated with the extent of qE in diatoms. The reverse reaction is catalysed by the diatoxanthin epoxidase enzyme (DTE) and consists in the back conversion of Dt into Dd activated under low light conditions.

1.6.1.1.2 Light-harvesting complex protein superfamily and its variants

Another essential component of qE is the presence of specific proteins effectors present in all eukaryotic photoautrophs. These nuclear encoded proteins possess a core structure composed by transmembrane alpha-helices, which are located in the thylakoid membranes. While “genuine” light harvesting complexes proteins contain conserved residues that bind chlorophylls and carotenoids, some of the qE effector proteins do not bind pigments. This is typically the case of the PSBS (photosystem II subunit S) protein (Bonente et al., 2008), which contains four-helices (at variance with the three found in the LHCII). Genetic analysis, in the model plant *Arabidopsis thaliana* has demonstrated that this protein is an essential component of the qE response (Li et al., 2000; Figure 1.4 A). PSBS acts as sensor of lumenal pH. It is generally accepted that the protonation of acidic residues in the lumenal site of the PSBS promotes the rearrangement of the LHCII-PSII supercomplex (Betterle et al., 2009; Goral et al., 2012) leading to the activation of qE. Because of its role in photoprotection (Li et al., 2000) PSBS is needed for plant survival under fluctuating light conditions in the field (Külheim et al., 2002). On the other hand, a different qE type machinery is found in algae. In the chlorophyte *Chlamydomonas reinhardtii* the *PSBS* gene is present (Anwaruzzaman et al., 2004) but the protein is not expressed in qE promoting conditions (Bonente et al., 2008). Conversely, two light-harvesting complex stress-response proteins are present in the genome of this alga (LHCSR1 and LHCSR3; Peers et al., 2009; Tokutsu & Minagawa, 2013), which actively participate in the NPQ response. The two LHCSR isoforms possess similar promoter regions followed by an almost identical polypeptide sequence (Maruyama et al., 2014). At difference with PSBS, LHCSR shares the typical three helix protein motif and the pigment binding capacity of a true LHCII protein (Bonente et al., 2011; Figure 1.4 B). LHCSR3 binds pigments like: chlorophyll *a* /*b*, lutein, violaxanthin and zeaxanthin (Bonente et al., 2011) and presumably acts also as a quenching site (Tokutso & Minagawa, 2013). Moreover, LHCSR3 also acts as a sensor of luminal acidification, with several residues (aspartate and glutamate) being essential for NPQ induction (Ballottari et al., 2016). However, LHCSR proteins are not constitutively present in the chloroplast of *C. reinhardtii*, and require high light (Allorent et al., 2013) an active photosynthetic electron flow (Petroutsos et al., 2011; Maruyama et al.,2014) Ca^{2+} signalling and the calcium Ca^{2+} binding protein CAS (Petroutsos et al., 2011) to accumulate in the thylakoids. While the LHCSR proteins are not found in the plant genomes, they are present in all the algal genomes investigated so far, as well as in mosses (Alboresi et al., 2010). In diatoms, these proteins (named LHCX) play a similar role in the activation of qE (Bailleul et al., 2010; Zhu & Green, 2010; Lepetit et al., 2013). In this group of microalgae the

induction of some LHCX isoforms is strongly correlated with light changes (Bailleul et al., 2010; Lepetit et al., 2013; Nymark et al., 2013). However, amongst the four isoforms identified in the genome of the pennate diatom *P. tricornutum* (Bowler et al., 2008) only three are inducible (Taddei et al., 2016) while one, LHCX1, is constitutively expressed and contributes to a constant qE capacity (Bailleul et al., 2010).

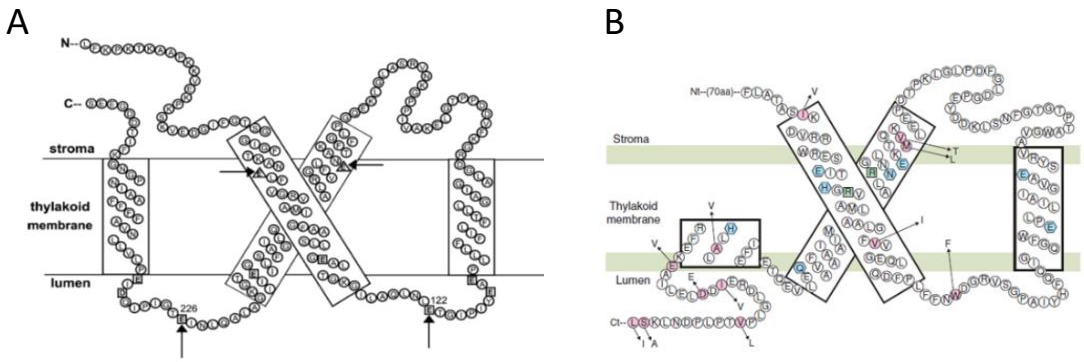

Figure 1.4 – **Schematic representation of the structure of Lhc proteins.** (A) PSBS protein in *Arabidopsis thaliana* (modified from Li et al., 2002). (B) LHCSR3 protein in *C. reinhardtii* (from Maruyama et al., 2014).

1.6.1.2 State transitions, qT

Another component of the non-photochemical quenching is state transitions, a mechanism that redistributes the excitation energy between photosystems (Allen, 1992). In plants and green algae, the physical segregation of PSII and PSI imposes the existence of different antennae systems, which excite the two photosystems independently. State transitions optimize the relative absorption capacity of PSs via a redox regulated migration of antenna complexes between the two PSs. In particular, under light conditions that promote a preferential excitation of PSII (compared to PSI) the reduced state of the PQ pool will activate a protein kinase (Stt7/STN7) via its binding to the Cyt b_6f complex. The kinase phosphorylates some light-harvesting complex of PSII (LHCII), which migrate laterally towards PSI increasing its absorption capacity during the so called state 1 to state 2 transition. The reverse reaction is driven by a protein phosphatase (PPH1/TAP38) that dephosphorylates the LHCII associated with PSI and allows its re-association with PSII (state 2 to state 1 transition). This mechanism, is absent in diatoms (Owens, 1986), of moderate amplitude in plants (Niyogi, 1999) and it represents a much larger component in the green algae *C. reinhardtii*, where it can reallocate up to 80% of its mobile antenna between photosystems (Delosme et al., 1996; Figure 1.5). While in plants, state transitions only plays the role of optimizing light absorption

in low light, in *Chamydomonas* this process also contributed to photoprotection in high light (Allorent et al., 2013) and it is still debated whether it involves a different mechanism than the simple physical displacement of LHCII between the two photosystems (Nawrocki et al., 2016; Ünlü et al., 2014; Nagy et al., 2014).

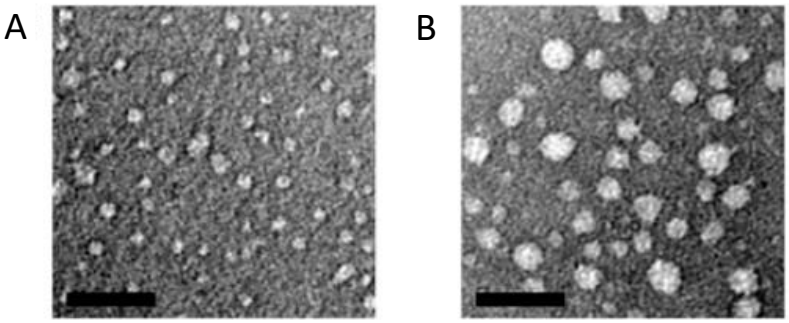

Figure 1.5 – **LHCII fractions in *C. reinhardtii*.** EM picture of the purified thylakoid membranes obtained after sucrose gradient fractionation during state 1 (A). State 2 condition (B), in this picture large aggregates are visible (Iwai et al., 2010).

In other organisms, such as red algae and cyanobacteria, different NPQ mechanisms are observed, which reflect the specific features of the light harvesting complexes of these organisms (the phycobilisomes, PBS). In these peculiar situation another mechanisms of PSII fluorescence quenching called energy spillover seems to play a major photoprotective role (Kowalczyk et al., 2013).

1.6.1.3 Energy spillover as photoprotective mechanism

In red algae and cyanobacteria, the "classic" NPQ effectors (i.e. the xanthophyll cycle and PSBS proteins) are missing. Therefore, these organisms possess peculiar responses to cope with a changing light environment. Cyanobacteria contain specific stromal-exposed antennae called phycobilisomes, which bind an orange carotenoid protein (OCP; Kirilovsky & Kerfeld, 2012) shown to be an essential component of NPQ in this group. In red algae (which also possess the PBSs, but lack the PSBS or OCP proteins) most of the energy absorbed by the PBS is transferred from photosystem II to photosystem I through the energy spillover (direct energy transfer). Kowalczyk and coworkers demonstrated that the excitonic flux at PSII level controls the amount of energy transfer toward PSI via a still unknown mechanism. Overall, despite the fact that all these photosynthetic organisms are able to dissipate excess light at the level of PSII, the molecular mechanisms differ significantly between cyanobacteria, red alga, green algae and plants.

In diatoms, the two photosystems share similar antennas (FCPs), although recent data suggest that the two photosystems could contain specialized antennae pools (Veith et al., 2009). The similarity between FCPs translates into a more homogeneous absorption spectrum of the two photosystems than in plants. Thus, diatoms do not perform light driven state transitions (Owens, 1986), and have succeeded in optimizing light utilization achieving an efficient excitation energy balance at both limiting and saturating light conditions. Consistent with the peculiar structure of their thylakoids, which is intermediate between the unstructured situation seen in cyanobacteria (and red algae) and the highly structured one observed in plants (and green algae) the possible photoprotection of PSII via energy spillover was tested in this project of thesis (see section 2.5).

1.6.1.4 Photoinhibition, qI

The slowest contribution of the non-photochemical quenching is attributed to photoinhibition of the photosystems due to prolonged overexcitation of the photosynthetic machinery. This process describes the degradation and disassembly of the core subunit of the photosystem II (PsbA or D1 protein; Aro et al., 1993; Barber & Andersson, 1992) leading to a general decrease of its photosynthetic quantum yield (Krause, 1988). Overall, the extent of photoinhibition depends on the balance between PSII photodamage and repair (Murata et al., 2007). Despite the fact that the degradation of the D1 proteins is a fast process (Neidhardt et al., 1998; Sundby et al., 1993), high amounts of reactive oxygen species (ROS) can enhance the degradation of this protein (Murata et al., 2007) leading to a decrease in photosynthetic quantum yield in excess light.

1.7 Long-term responses

Prolonged stress exposure plants and algae leads to multiple responses that modify and fine tune the photosynthetic apparatus. Long-term photoprotective responses involve the expression and/or repression of nuclear and chloroplast specific genes, with the ultimate goal of preventing photoinihibition in chronic high light or enhancing absorption in a shade environment.

To mention only a few examples, multiple signal cascades control the accumulation of light-harvesting antennae complexes, chloroplast movement, changes in the PSII/PSI ratios and in proportion of stacked and unstacked thylakoids membranes. These responses are mainly mediated by the *de-novo* synthesis and/or degradation of the protein complexes involved in the light harvesting and electron flow processes (Falkowski & LaRoche 1991; Raven & Geider, 2003).

1.8 AIM of the thesis

In nature, photosynthetic organisms need to optimize energy capture and conversion efficiency adjusting their photosynthetic apparatus in response to environmental *stimuli*. In particular microalgae have developed distinct approaches to modulate light absorption and utilization capacity of their photosystems. During my Ph.D thesis I aimed to investigate the mechanisms of light utilization in two algal model organisms: the marine diatom *Phaeodactylum tricornutum* and the freshwater green alga *Chlamydomonas reinhardtii*. In the first project, I focused on the structure/ function relationship using the pennate species *Phaeodactylum tricornutum* as a model. Due to the simplified structure of its chloroplast, with no apparent structural segregation between PSII and PSI (see Chapter 2) we tested the possibility of the existence of the energy spillover. Using several complementary approaches (spectroscopy, biochemistry, immunolabelling and three-dimentional (3D) reconstitution) we generate a comprehensive 3D map of the photosynthetic membranes and complexes. This multidisciplinary study reveals *i.* how diatoms regulate exchanges of ATP/NADPH between chloroplast and mitochondria (see section 2.3). *ii.* how the external membranes system (the envelope) organized and operate for the transfer of compounds produced in other intracellular compartments (see section 2.4). *iii.* how these organisms have adapted their internal membrane system (the thylakoids) in order to optimize photosynthesis (see section 2.5).

In the second project, novel insights into the regulation of photoprotection mediated by both perception of light colour and metabolism in the green alga *Chlamydomonas reinhardtii* were obtained (see Chapter 4). We first showed the existence of a molecular link between photoreception, photosynthesis and photoprotection. Our data show that *Chlamydomonas* is able to detect changes in light wavelength thanks to photoreceptors, and this also affects photorotection *via* the regulation of the induction of the protein LHCSR3 (see section 4.3). Moreover, we demonstrate that besides light, downstream metabolism can affect the NPQ capacity of *C. reinhardtii*, via negative feedback of the LHCSR3 accumulation in the thylakoids (see section 4.4).

Overall, these projects underline how the different processes linked to photosynthesis (light absorption, dissipation electron flow and carbon assimilation for metabolism) are tightly interconnected to achieve a successful acclimation to the environment of microalgae.

Chapter 2

2.1 Introduction

This chapter is organized in four sections. In the first section (section 2.2), I will give an introduction and on the chloroplast origin and on the structural arrangements of the photosynthetic membranes (the thylakoids) in the chloroplast. In the second section (section 2.3) the article "Energetic Coupling Between Plastids and Mitochondria Drives CO_2 Assimilation in Diatoms" will be presented. Afterwards, in the third section (section 2.4) I will introduce the article "Ultrastructure of the Periplastidial Compartment of the Diatom *Phaeodactylum tricornutum"*. Finally (in section 2.5) the manuscript in preparation "Chloroplast thylakoid architecture optimizes photosynthesis in diatoms" will be presented.

2.2 The chloroplast

The chloroplast is a specific organelle of plants and algae. It contains the molecular machinery that performs photosynthesis. Chloroplasts represent a particular form of plastids, which are dynamic organelles that can differentiate in response to environmental *stimuli* and developmental stage. The typical plastids found in plants are (Figure 2.1) *i.* the undifferentiated form called proplastid *ii.* the etioplast, i.e. the progenitor of the chloroplast *iii.* the chloroplast, the photosynthetic organelle *iv.* the chromoplast, mostly containing carotenoids *v.* the gerontoplast, the senescent form of the chloroplast *vi*. the amyloplast, the starch storage reservoir and *vii.* the elaioplast, the lipids storage plastid.

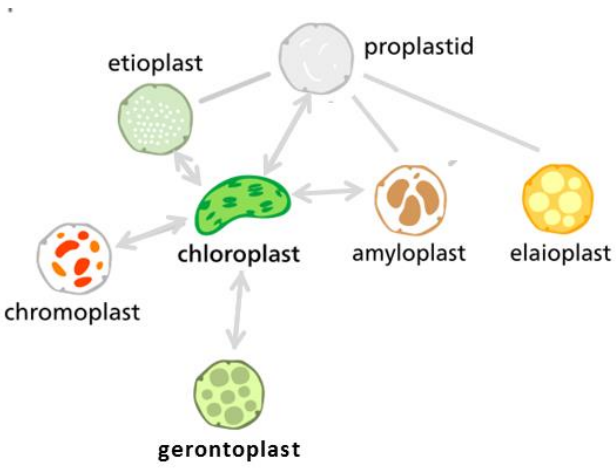

Figure 2.1– **Representation of the principal plastids found in plants.** The proplastid, etioplasts, chloroplasts, chromoplasts, gerontoplasts, amyloplasts and elaioplasts are represented. Grey lines show possible route of plastids differentiation (modified from https://commons.wikimedia.org/w/index.php?curid=28879042).

The chloroplast originated between 1.6 and 0.6 billion years ago (Yoon et al., 2004; Cavalier-Smith, 2006; Figure 2.2 A) when a cyanobacterial type of organism (α-proteobacterium-like ancestor) was engulfed by a eukaryote host. This endosymbiosis led to primary plastids characterized by two limiting membranes derived from the inner and outer membranes of the gram-negative cyanobacterium (Jarvis & Soll, 2001). These membranes control the exchanges between the plastid and the rest of the cell. This symbiotic event permitted the evolution of autotrophic organisms and the proliferation of oxygenic life on Earth. Primary plastids are found in three major lineages: Glaucophytes, red algae (Rhodophytes) and green algae (like Chlorophytes and Charophytes; Keeling, 2004). The latest is believed to be the progenitor of modern plants. During evolution both the red (Figure 2.2 B) and green lineage have been engulfed independently by another eukaryotic cell leading to the origin of secondary plastids between 1.2 and 0.55 billion years ago (Yoon et al., 2004; Cavalier-Smith, 2006; Figure 2.2 B). Over time, the engulfed host cell was reduced to a multiple membrane-bound plastid. In fact, these membranes represent *i.* the remaining of the phagocytosis of the primary alga plus *ii.* the two previous membranes of the gram-negative cyanobacterium. Seven major lineages possess secondary plastids: Euglenids, Chlorarachniophytes, Cryptomonads, Haptophytes, Heterokonts (diatoms), Dinoflagellates and Apicomplexa (Keeling, 2004).

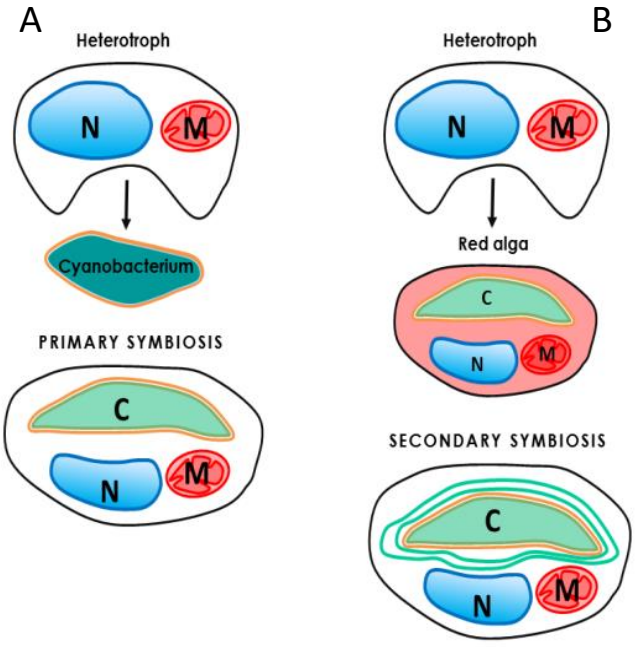

Figure 2.2 – **Schematic representation of primary and secondary symbiosis.** (A) Primary endosymbiosis. (B) Secondary endosymbiosis.

In general, the chloroplast structure is about 3–5 µm in diameter and contains three distinct sub-compartments:

i. The chloroplast envelope (Figure 2.3 A) is the site of the synthesis and translocation of many components (ions and metabolites) between the cytosol and the chloroplast. In primary plastids, the envelope is formed by two layers which surround the organelle. These membranes (the inner and outer membranes) are reminiscent of the symbiont's host.

ii. The stroma (Figure 2.3 B) is the soluble phase contained in the chloroplasts where most of the enzymes required for carbon fixation, amino acids or vitamins synthesis are located. It also contains the chloroplast DNA and the ribosomes for protein synthesis.

iii. The thylakoids (from the greek word thylakoides = sac; Menke, 1962) is a network of internal membranes, which hosts the proteins performing the light-phase of photosynthesis. Thylakoids form one continuous compartment within the chloroplast (Mustárdy & Garab, 2003; Staehelin, 2003). These membranes, typically enriched in galactolipids, present a lateral heterogeneity, already noticed in 1960 by Menke. He introduced two distinct terms to describe the sub-compartments of the chloroplast in plants: the “sac-like” appressed thylakoids and the large thylakoids. The first one, now called grana (singular granum) are made of stacks of thylakoid membranes with a diameter of 300-600 nm and a thickness of ~4 nm (Kirchhoff et al., 2011; Figure 2.3 C). The second term is referred to the connecting membranes now called stroma lamellae (Figure 2.3 D). Every single thylakoid vesicle contains an aqueous space that is named the lumen. The diameter of this space can vary depending on the conditions (Kirchhoff et al., 2011).

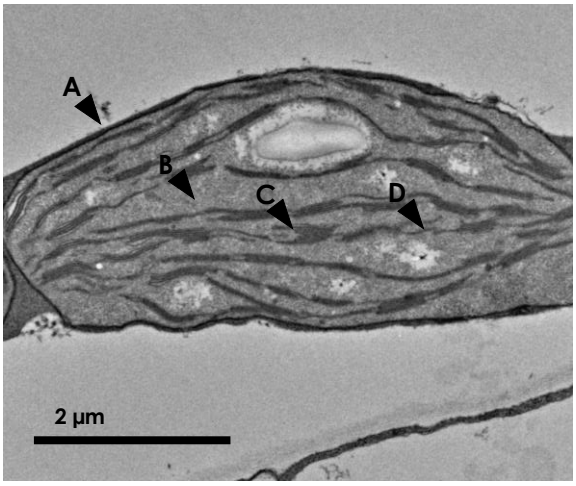

Figure 2.3 – **Chloroplast details of *Arabidopsis thaliana.*** (A) the envelope, (B) the stroma, (C) a grana and (D) stroma lamellae. The thylakoid lumen is not visible at this magnification.

The exact three-dimensional architecture of the grana in plant is still a matter of debate and several models have been proposed to interpret the structural arrangements of thylakoid in plant chloroplasts (reviewed in Daum et al., 2011). The first one, the fork model (Arvidsson & Sundby, 1999; Figure 2.4 A) considers that grana as repetitive units of three disks formed by symmetrical invaginations of a thylakoid pair. The second (Shimoni et al*.,* 2005; Figure 2.4 B) considers grana as formed by paired membranes emerging from bifurcations of stroma lamellae connected by membranes upwards and downwards. Finally the helix model, probably the most correct one, proposes that stroma lamellae rotate around the grana stacks as a right-handed helix, connecting every granum with multiple stroma lamellae (Paolillo et al., 1967; Paolillo, 1970; Mustardy & Garab 2003; Mustardy et al., 2008; Daum et al., 2011; Austin & Staehelin, 2011; Ruban & Johnson, 2015; Figure 2.4 C).

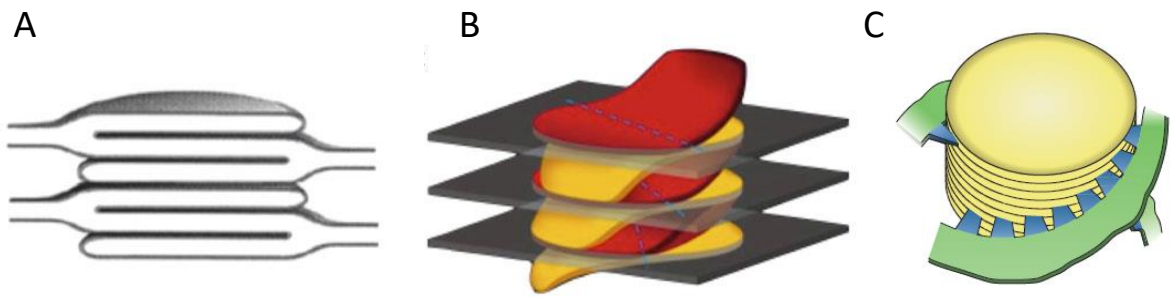

Figure 2.4 – **Current models of the structural arrangements of thylakoids in plant chloroplast**. (A) the fork model of Arvidsson &Sundby, 1999. (B) the bifurcated model of Shimoni et al., 2005 (picture from Daum et al. 2011). (C) the right-handed helix model predicted by Paolillo 1970 (picture from Ruban & Johnson, 2015).

These membranes are densely populated by proteins, which occupy up to 70% of the total membrane area (Kirchhoff et al., 2002). These proteins are the key players of photosynthesis (see section 1.3): the photosystem II (PSII), the cytochrome b_6f complex (Cyt b_6f), the photosystem I (PSI) and the ATP-synthase. In plants, extensive biochemical, fractionation and immunolocalisation studies have shown that PSI and the ATP synthase complexes accumulate preferentially in the stroma exposed membrane (the stroma lamellae and the grana margins) due to the steric hindrance of their stromal protrusions (Dekker & Boekema, 2005; Amunts et al., 2008; Junge et al., 2009). Conversely, PSII which has flat stromal surfaces, is mostly localized in the grana, while the cytochrome b_6f complex, which functionally connects PSI and PSII, has a more homogeneous localization in these compartments (reviewed in Albertsson, 2001; Kouřil et al., 2012; Figure 2.5). This heterogeneous distribution of photosynthetic complexes has deep consequence on light harvesting and electron flow. Most likely, the main reason for segregating the photosystems in two different domains of the membranes is to prevent a physical contact beween them, which will lead to excitation energy spillover (section 1.6.1.3) from PSII (which has the photochemical trap of the higher energy) to PSI (which has a lower energy trap).

A second reason for the formation of stacked grana in plants is the necessity to increase the light harvesting capacity of the chloroplast (Barber, 1980) creating extreme folding surfaces to concentrate the maximum amount of antenna complexes in the smallest volume. Consistent with this idea, changes in light intensity can largely affect the spatial organization of thylakoid membranes. This flexible interconnected networks can rapidly vary its architectural organization adjusting the number of layers within the grana stacks under low light conditions (Anderson, 1986), or increment the unstacking of grana discs under high light conditions (Fristedt et al., 2009; Khatoon et al., 2009; Herbstova et al., 2012). These structural rearrangements, in plants, tend also to facilitate light harvesting but also photoprotective mechanisms like turnover of photodamaged D1 (Herbstova et al., 2012; Kirchhoff, 2013) or state transitions (see section 1.6.1.2).

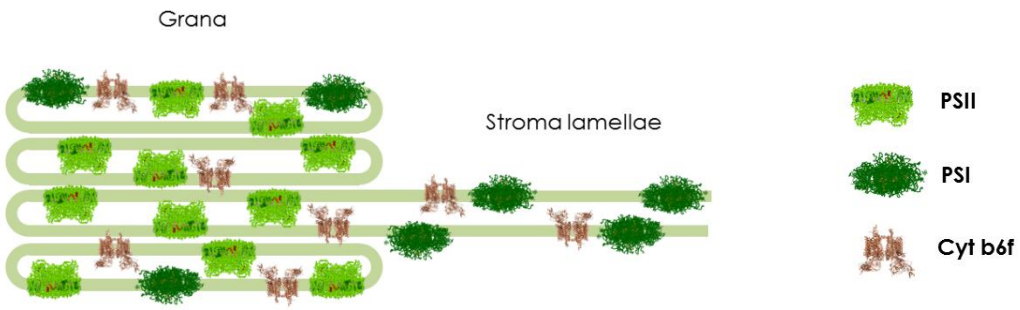

Figure 2.5 – **Representation of the thylakoid membranes in plants**. (A) the grana stack mostly enriched in PSII (B) the stroma lamellae enriched in PSI. The Cyt b_6f is equally distributed between the two regions.

One of the main goal of this Ph.D thesis was to understand the structure of a secondary chloroplast and to investigate the functional consequences of this structure on the photosynthetic light absorption, electron flow and ATP and NADPH synthesis and consumption. Our structural, biophysical and biochemical results unveil for the first time these complex structures in diatoms using the model organism *Phaeodactylum tricornutum*.

2.2.1 Case of study *Phaeodactylum tricornutum* (Bohlin, 1897)

Phaeodactylum tricornutum is a pennate diatom (Heterokonts) wich displays different morphotypes, *i.e.* fusiform, triradiate and oval (Figure 2.6). Cells of this pleiomorphic species are ~10 µm in diameter and a large part of their volume is occupied by a single chloroplast (3-9 µm).

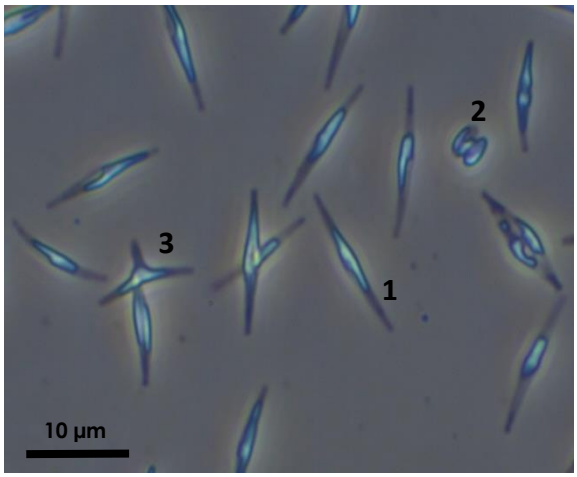

Figure 2.6 – **Morphotypes of *P. tricornutum.*** (1) Fusiform, (2) oval and (3) triradiate.

Within this plastid the three classical main subcompartments (Figure 2.7 A) can be easily identified: *i*. the envelope *ii.* the stroma and *iii.* the thylakoids. However, diatom chloroplast exhibit peculiar differences.

i. The envelope system is formed by two internal membranes the inner and the outer envelope membranes (iEM and oEM, Botte & Marechal, 2014; Petroutsos et al., 2014; Figure 2.7 B; 1-2) of the secondary symbiont's chloroplast, sourrounded by the periplastidial membrane (PPM, Figure 2.7 B; 3) and the chloroplast endoplasmic reticulum membrane (cERM, Figure 2.7 B; 4). Between the PPM and oEM lies a minimized symbiont cytoplasm, the periplastidial compartment (PPC, Grosche et al., 2014; see section 2.3).

ii. The chloroplast stroma containing most of the enzymes needed for carbon fixation (as the RuBisCO). In algae, this essential enzyme is concentrated in a specialized region called the pyrenoid (Holdsworth, 1971; Lacoste-Royal & Gibbs, 1987; Borkhsenious et al., 1998; Figure 2.7 D). Moreover, the stroma also contains the chloroplast DNA and the ribosomes for protein synthesis.

iii. Unlike higher plants, diatoms thylakoids do not possess a clear distinction between grana and stroma lamellae. Their membranes are generally organized in stacks of three lipid bilayers oriented parallel to the envelope membranes (Figure 2.7 A,B,C). A single stack of thylakoids forms the girdle lamella that encircles the whole structure (Figure 2.7 C). Only near the pyrenoid region we found that the tips of thylakoids from multiple stacks merged, oriented perpendicularly towards the envelope (Figure 2.7 A, B, C).

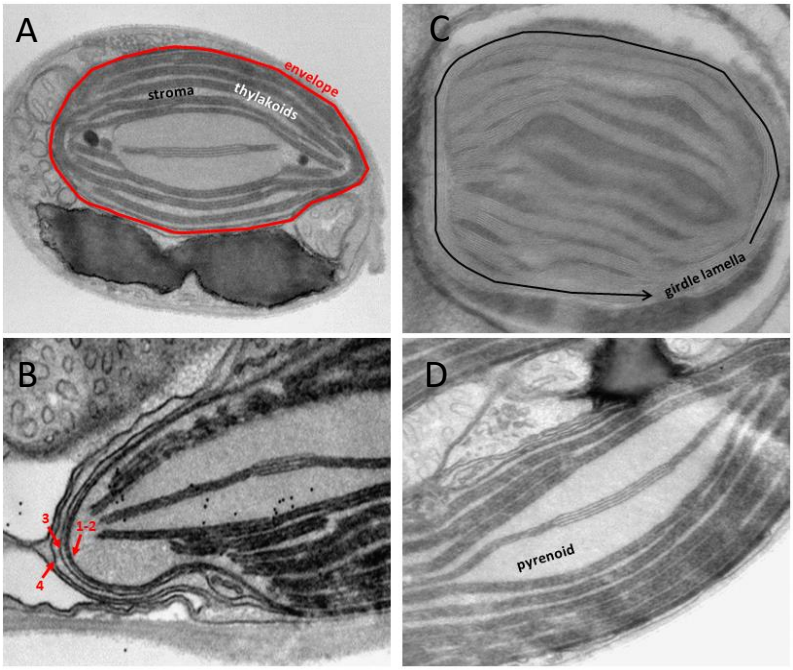

Figure 2.7 – **Chloroplast details of *P. tricornutum.*** (A) Whole cell view, the envelope is highlighted in red, the thylakoids in white and the stroma space in black. (B) Details of the envelope. in this picture the four membranes are visible. (C) Detail of the girdle lamella which surround the chloroplast (D) Pyrenoid region with the typical enlarged 2 lipid bilayers in the center.

As explained above, the main reasons to investigate the the structural organization of secondary plastids were to understand:

i. how diatoms regulate exchanges of ATP/NADPH between chloroplast and mitochondria (see section 2.3).
ii. how external membranes system (the envelope) are organized and operate for the transfer of compounds produced in other intracellular compartments (see section 2.4).
iii. how these organisms have adapted their internal membrane system (the thylakoids) in order to optimize photosynthesis (see section 2.5).

Thanks to a multidisciplinary approach, we provide relevant information to answer these questions.

2.3 Energetic interactions between chloroplasts and mitochondria

2.3.1 Preface

The article Bailleul et al., 2015 presented in this section represents my first contribution to the characterization of the model diatom *Phaeodactylum tricornutum*. This work is part of a collaboration between different laboratories in Europe, which was coordinated by my host laboratory.

In photosynthesis, the efficient conversion of CO_2 into organic matter requires the optimization of the ATP/NADPH ratio (Allen, 2002). In most photosynthetic organisms (i.e. *viridiplantae*), this optimization relies principally on processes localized within the plastid (for more information see Shikanai, 2007; Allen, 1975; Asada, 2000; Cardol et al., 2008; Ort & Baker, 2002). However, in diatoms, all the mechanisms described so far, seems to be not relevant to balance this ratio. Thus, the main question addressed in this project was how diatoms regulate photosynthetic process being one of the most successful group of microalgae in the ocean.

In the article below, we were able to show that diatoms regulate ATP/NADPH ratio through energetic interactions between plastids and mitochondria. The hypothesis proposed in this study explain the optimization of carbon fixation through the re-routing of reducing power (NADPH) generated in the plastid towards mitochondria (the site of respiration) and the import of mitochondrial ATP into the chloroplast. These extensive exchanges are mediated by the physical contacts between the two organelles, which I was able to document by studying the structure of chloroplast and mitochondria in intact *P. tricornutum* cells. The interesting results here obtained convinced me to pursue the structural characterization of the chloroplast membranes, which will be presented in the two following sections. In conclusion, the cross-talk chloroplast-mitochondria in diatoms facilitate the optimization of carbon fixation demonstrating the high photosynthetic efficiency achieved by these organisms worldwide.

2.3.2 Energetic coupling between plastids and mitochondria drives CO_2 assimilation in diatoms

Benjamin Bailleul[1,2,3,4,], Nicolas Berne[1], Omer Murik[4], Dimitris Petroutsos[5], Judit Prihoda[4], Atsuko Tanaka[4], Valeria Villanova[6], Richard Bligny[5], Serena Flori[5], Denis Falconet[5], Anja Krieger-Lizkay[7], Stefano Santabarbara[8], Fabrice Rappaport[3], Pierre Joliot[3], Leila Tirichine[4], Paul Falkowski[2], Pierre Cardol[1], Chris Bowler[4,], Giovanni Finazzi[5,]

[1] Genetics and Physiology of Microalgae, Department of Life Sciences and PhytoSYSTEMS, University of Liège, B-4000 Liège, Belgium

[2] Environmental Biophysics and Molecular Ecology Program, Department of Marine and Coastal Sciences and Department of Earth and Planetary Sciences, Rutgers University, New Brunswick, NJ 08901, USA

[3] Institut de Biologie Physico-Chimique (IBPC), UMR 7141, Centre National de la Recherche Scientifique (CNRS), Université Pierre et Marie Curie, 13 Rue Pierre et Marie Curie, 75005 Paris, France

[4] Ecology and Evolutionary Biology Section, Institut de Biologie de l'Ecole Normale Supérieure (IBENS), Centre National de la Recherche Scientifique (CNRS), UMR 8197, INSERM U1024, 46 Rue d'Ulm, 75005 Paris, France

[5] Laboratoire de Physiologie Cellulaire et Végétale, UMR 5168, Centre National de la Recherche Scientifique (CNRS), Commissariat à l'Energie Atomique et aux Energies Alternatives (CEA), Université Grenoble Alpes, Institut de Recherche en Sciences et Technologies pour le Vivant, CEA Grenoble, 38054 Grenoble cedex 9, France

[6] Fermentalg SA, F-33500 Libourne, France

[7] Institute for Integrative Biology of the Cell (I2BC), Commissariat à l'Energie Atomique et aux Energies Alternatives (CEA), Centre National de la Recherche Scientifique (CNRS), Université Paris-Sud, Institut de Biologie et de Technologie de Saclay, F-91191 Gif-sur-Yvette cedex, France

[8] Istituto di Biofisica, Consiglio Nazionale delle Ricerche, Via Celoria 26, 20133 Milan, Italy

Abstract

Over the past ~ 35 million years, diatoms have been one of the most successful classes of photosynthetic marine eukaryotes, and are believed to have contributed to climate cooling by absorbing carbon dioxide from the atmosphere and sequestering it via the biological carbon pump (Falkowski, 2004). Today the proportion of planetary primary production performed by diatoms is equivalent to that of terrestrial rainforests (Field et al., 1998). In photosynthesis, the efficient conversion of CO_2 into organic matter requires a tight control of the ATP/NADPH ratio which, in other photosynthetic organisms, relies principally on a range of plastid-localized ATP generating processes (Shikanai, 2007; Asada, 2000; Cardol, et al., 2008; Ort & Baker, 2002). Here we show that diatoms regulate ATP/NADPH through extensive energetic exchanges between plastids and mitochondria. This interaction comprises the rerouting of reducing power generated in the plastid towards mitochondria and the import of mitochondrial ATP into the plastid, and is mandatory for optimized carbon fixation and growth. We propose that the process may underlie the ecological success of diatoms in the ocean.

In oxygenic photosynthesis, light drives a linear electron flow from water to NADPH by the two photosystems (PSI and PSII), and the generation of an electrochemical proton gradient (or proton motive force, PMF) across the thylakoid membranes which fuels ATP synthesis by an ATP synthase. Although the ratio of ATP/NADPH generated by linear electron flow is not entirely resolved (Petersen et al., 2012; Allen, 2002), it is considered to be insufficient to fuel CO_2 import into the plastid and assimilation by the Calvin cycle (Allen, 2002; Lucker et al., 2013). Additional ATP must therefore be produced by alternative electron pathways, i.e., electron flow processes that generate a PMF without net NADPH synthesis. In *Viridiplantae* (including green algae and higher plants), these alternative electron pathways are mostly chloroplast localized and comprise cyclic electron flow (CEF) around PSI (Shikanai, 2007) and/or the water-to-water cycles (Allen, 1975), i.e., flows of electrons resulting from the oxidation of water at PSII and rerouted to an oxidase activity. The latter oxidases include the Mehler reaction at the PSI acceptor side (Asada,2000; Radmer & Kok, 1976; Badger, 1985), the activity of the plastoquinone terminal oxidase downstream of PSII (Cardol et al., 2008), and the oxygenase activity of RuBisCO (photorespiration; Ort & Baker, 2002). Although genes encoding the majority of components for these processes appear to be present in diatoms (Prihoda et al., 2012; Bowler et al., 2008; Grouneva, et al., 2011), it is currently unknown what mechanisms

are utilized to balance the ATP/NADPH ratio. We therefore investigated the question using the model species *Phaeodactylum tricornutum*.

2.3.2.1 Results

The PMF generated across thylakoid membranes comprises an electric field (ΔΨ) and a proton gradient (ΔpH). The ΔΨ can be probed *in vivo* by measuring the Electro-Chromic Shift (ECS) of photosynthetic pigments, i.e., a modification of their absorption spectrum caused by changes in the transmembrane electrical field in the plastid (Witt, 1979). An ECS signal is present in *P. tricornutum* (Figure 2.8 A), and an analysis of the ECS signal relaxation after light exposure (Supplementary Figure 2.13) reveals that it comprises two components displaying different spectra (Figure 2.8 A). One follows a linear dependence on the amplitude of the ΔΨ whereas the other follows a quadratic relationship (Figure 2.8 B). The existence of a "quadratic ECS" is predicted by theory (Witt, 1979) but has only been observed so far in mutants of green algae with altered pigment composition (Joliot & Joliot, 1989). The peculiar existence of two different ECS probes in wild-type *P. tricornutum* cells allows an absolute quantification of the electrical field, providing a valuable tool to analyze the PMF in a living cell (see methods).

We plotted the amplitude of the quadratic vs linear ECS signals during the relaxation of a light-induced PMF and obtained, as expected, a parabola (Figure 2.8 C, D and Supplementary Figure 2.13). However, the ECS signals did not reach the minimum of the parabola in the dark, but rather remained positive. This indicates that a PMF is maintained across the thylakoid membrane of diatoms even without illumination ($\Delta\Psi_d$, Figure 2.8 C). The $\Delta\Psi_d$ can be dissipated with an uncoupler (FCCP), but also by anaerobiosis or inhibition of mitochondrial respiration by Antimycin A (AA) to block Complex III in the so-called cyanide-sensitive respiratory pathway, combined with salicylhydroxamic acid (SHAM) to inhibit the alternative oxidase (AOX) in the cyanide-insensitive respiratory pathway (Figure 2.8 D). These results suggest that the PMF present in the diatom plastid in the dark is generated by the chloroplast ATPase by hydrolysis of ATP derived from mitochondria (Figure 2.8 E; Diner & Joliot, 1976). Furthermore, the extent of the $\Delta\Psi_d$ observed in *P. tricornutum* is larger than that previously reported in green algae (Finazzi & Rappaport, 1998), suggesting that the ATP exchange could be more efficient in diatoms.

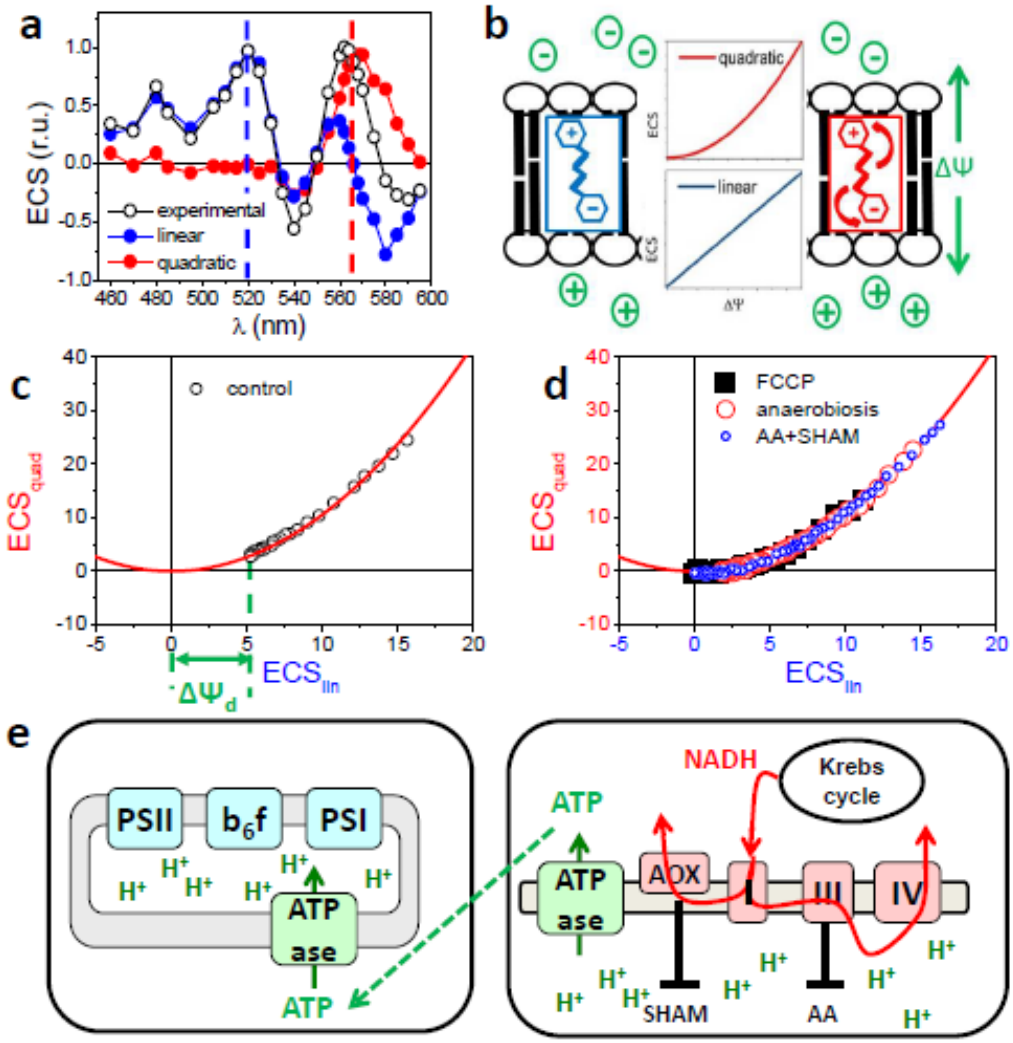

Figure 2.8 – **ECS allows measuring the proton motive force in *P. tricornutum*.** (A) Deconvolution of the experimental Electro-Chromic Signal (ECS) spectrum (black) into linear (blue) and quadratic (red) spectral components, as described in Methods. (B) Schematic representation of polar and polarizable pigments, and theoretical dependencies of their associated ECS responses upon the electric field. Green "+" and "-": ΔΨ. Blue and red "+" and "-": pigment dipoles. Red arrows: pigment polarization induced by ΔΨ. (C,D) Relationship between quadratic and linear ECS in control (C) and in uncoupler (8 nM FCCP, black squares), anaerobic (red circles), and respiratory inhibitors (AA, 5 µM, and SHAM, 1 mM, blue circles) treated cells (D). Green arrow: value of the dark electric field (ΔΨd). (E) Schematic representation of the plastid-mitochondria energetic interactions in the dark. Red arrows: respiratory electron flows. Green dashed line: putative ATP/ADP exchange pathway between the organelles. PS = photosystem, b6f = cytochrome b6f, ATPase = ATPase/synthase, I/ III/ IV = respiratory complexes I, III and IV, and AOX = Alternative Oxidase.

To evaluate what mechanism regulates ATP/NADPH in the light in *P. tricornutum*, we first used the linear ECS to probe the CEF capacity. CEF turned out to represent only a very low fraction of the maximum electron flow capacity (Figure 2.9 A and Supplementary Figure 2.14 A, C) and was insensitive to changes in the photosynthetic flux (Figure 2.9 A). Thus, it appears very unlikely that CEF could regulate ATP/NADPH levels. Next we explored the water-to-water cycle using membrane-inlet mass spectrometry (MIMS) on cells incubated with O_2 (Diner & Joliot, 1976). O_2 consumption increased with light, being ~2.5-fold higher at saturating light intensities than in the dark (Supplementary Figure 2.14 B, D). We also found that the light-stimulated O_2 consumption was blocked by DCMU, which inhibits O_2 production by PSII (Supplementary Figure 2.14 B, D), indicating that this process is fed by electrons generated by PSII. O_2 consumption increased linearly with O_2 production, in agreement with earlier findings in another diatom species (Waring et al., 2010), indicating that a constant proportion (~10%) of the electron flow from PSII is rerouted to an O_2 consuming pathway, regardless of light intensity (Figure 2.9 B).

To test whether the O_2 consuming pathway occurs in the plastid or relies on mitochondrial activity, we used increasing concentrations of mitochondrial inhibitors to titrate respiration and tested possible consequences on photosynthesis. We reasoned that if mitochondrial respiration consumes reducing equivalents generated in the plastid to generate additional ATP, any mitochondrial dysfunction should negatively impact photosynthesis. We found that this was indeed the case, as photosynthetic electron transfer rates (ETR_{PSII}) linearly followed changes in respiration (Figure 2.9 C and Supplementary Figure 2.15). We conclude that a partial rerouting of the photosynthetic flow towards mitochondrial respiration rather than CEF optimizes photosynthesis in diatoms, providing commensurate ATP per NADPH at all irradiances (Figure 2.9 D).

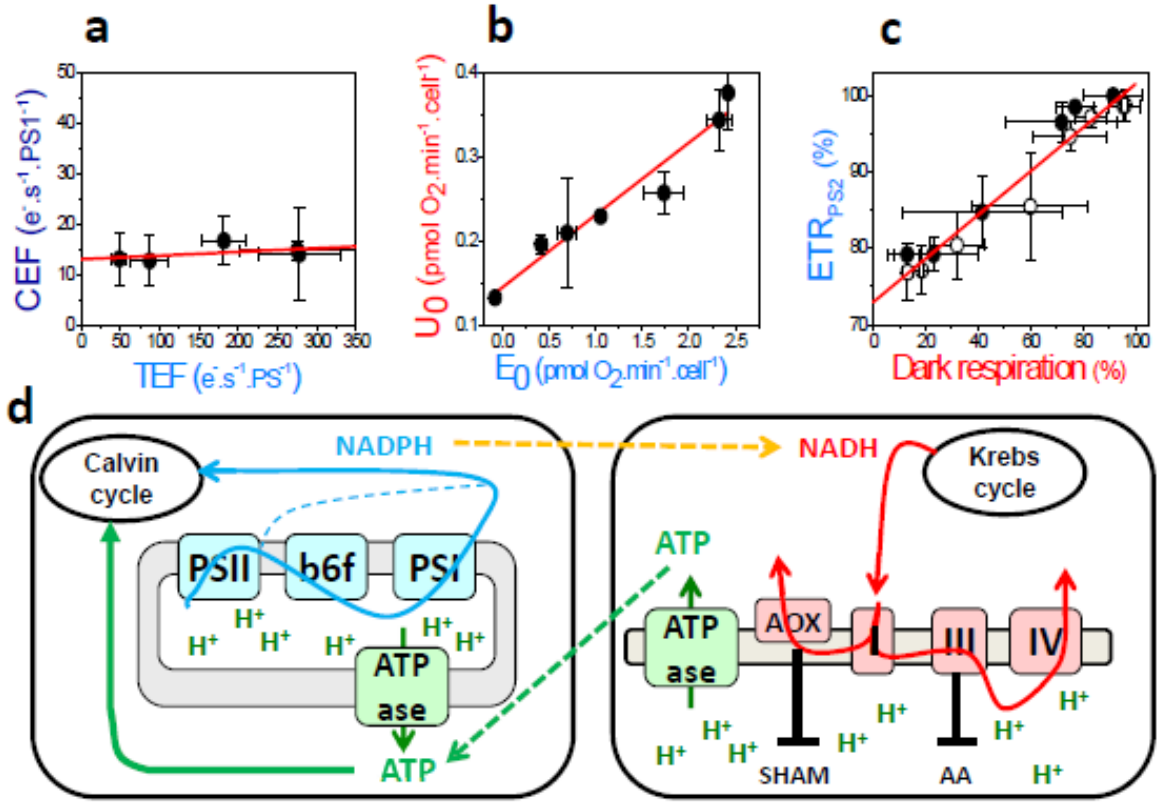

Figure 2.9 –**Mitochondria-plastid energetic interactions in *P. tricornutum*.** (A) Relationship between CEF capacity and total electron flow (TEF). (B) Relationship between oxygen uptake (U0) and gross photosynthesis (E0) as measured by MIMS. (C) Dependency of photosynthetic activity (ETRPSII) on respiration rates. Closed circles: SHAM + AA; open circles: SHAM + Myxothiazol treatments (see Methods). (D) Schematic representation of possible plastid-mitochondria metabolic interactions in the light. Same as in Figure 2.8 E + Blue lines: photosynthetic linear (light blue arrow), and cyclic (dark blue dashed line) flows. Yellow dashed arrow: exchange of reducing equivalents between the organelles.

The increasing sensitivity of photosynthesis to alternative oxidase (AOX) inhibitor with light (Figure 2.10 A) suggests that the cyanide-insensitive respiration becomes prominent in high light. This prompted us to generate AOX knockdown cell lines of *P. tricornutum*. Two independent clones were selected based on reduced AOX protein accumulation (Figure 2.10 B) and decreased activity (measured as the SHAM-sensitive, AA insensitive component of respiration; Supplementary Figure 2.16 A). The AOX contribution, representing ~50% of dark respiration in wild-type cells (Supplementary Figure 2.15 E), was decreased 2-fold in the two knockdown lines. Confocal microscopy confirmed the mitochondrial localization of the targeted gene product (Supplementary Figure 2.17 A). The reduced AOX activity in the knockdown lines paralleled a diminished PMF in the

dark ($\Delta\Psi_d$), despite the fact that overall dark respiration was slightly higher (Supplementary Figure 2.16 B). This effect was strongly enhanced by addition of AA (Supplementary Figure 2.16 B). The decreased AOX activity also correlated with a decreased photosynthetic capacity, especially under high light intensities (similar to SHAM-treated wild-type cells; Figure 2.10 A), and a diminished growth rate (Figure 2.10 C), which was exacerbated further by inhibiting Complex III using AA (Supplementary Figure 2.16 C). The growth and photosynthetic phenotypes were not due to changes in the accumulation of the photosynthetic complexes, for which we detected comparable levels of representative proteins in all cell lines (Figure 2.10 B). The only exception was a small decrease in the Cytochrome *b_6f* content in the knockdown cell lines, which nonetheless did not decrease its catalytic efficiency (Supplementary Figure 2.18).

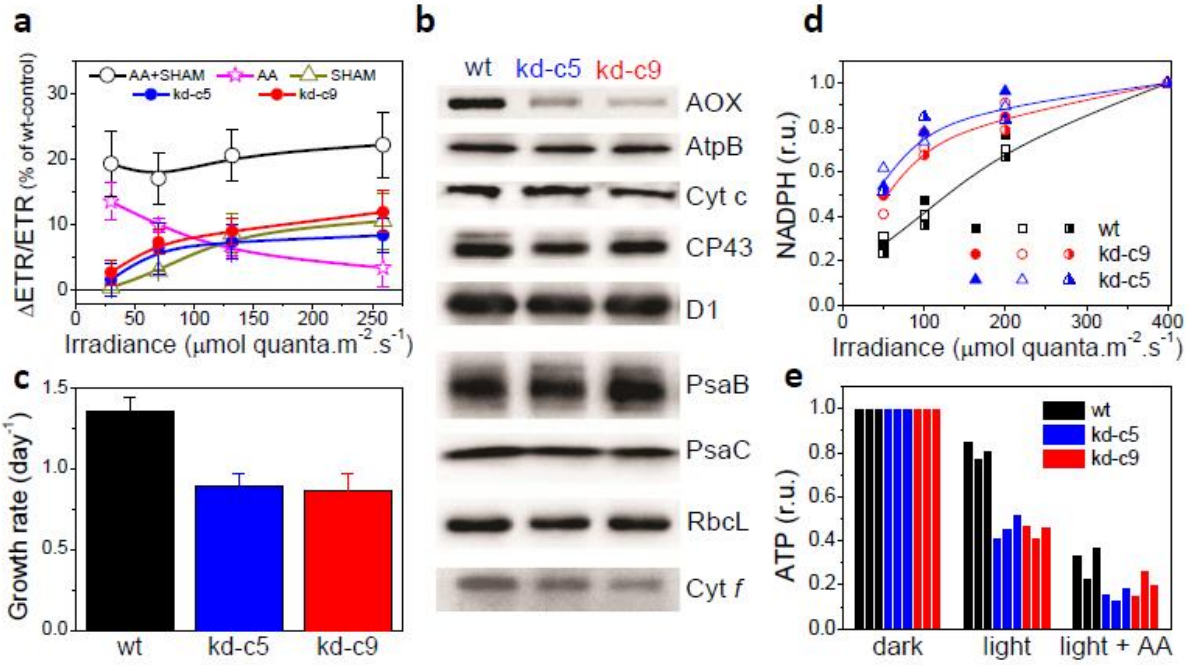

Figure 2.10 – **Phenotypic traits of AOX mutants in *P. tricornutum*.** (A) Relative sensitivity of photosynthesis (ETRPSII) to the presence of inhibitors of respiration: AA (blue), SHAM (red) and AA+SHAM (black) (n = 2 ± S.E), or to the knock-down of AOX (n = 5 ± S.D.). Green and magenta are used for kd-c5 and kd-c9, respectively, in all panels. (B) Western blot analysis of photosynthetic and respiratory complexes. (C) Growth rates of the wild type (dark blue) and AOX mutants (n = 7 ± S.D.). (D) In vivo assessment of NADPH redox changes as a function of irradiance, in wild-type and AOX mutants (n = 3 ± S.D.). (E) In vivo 31P-NMR evaluation of the NTP content in wild-type and AOX mutants, in the dark or in low light (with or without AA).

Our working model presented in Figure 2.9 D predicts that disruption of the plastid-mitochondria interaction in the knockdown cell lines should lead to the accumulation of NADPH and a decreased cellular content of ATP in the light. *In vivo* assessments of the pools of NADPH and ATP in wild-type and knockdown cell lines indeed confirmed an increase in the NADPH/$NADP^+$ ratio with light intensity (Figure 2.10 D and Supplementary Figure 2.19 A) accompanied by a net decrease of cellular ATP levels (Figure 2.10 E and Supplementary Figure 2.19 B), both of which were more drastic in AOX knockdown cells compared to wild-type cells. These observations confirm that mitochondrial respiration is directly involved in the adjustment of the ATP to NADPH ratio in the plastid.

We then examined the generality of our findings in other diatom species. The similar ECS features (linear and quadratic components) in *Thalassiosira pseudonana* and *Thalassiosira weissflogii*, *Fragilaria pinnata* and *Ditylum brightwelii* (Figure 2.11 A) were used to confirm the presence of a PMF in the plastids in the dark at the expense of hydrolysis of ATP supplied by the mitochondria in all cases (Figure 2.11 B). Moreover, a negligible contribution of CEF (Supplementary Figure 2.20) and a significant involvement of mitochondrial respiration to photosynthesis (Supplementary Figure 2.21) were found in all these species. The involvement of mitochondrial respiration in the optimization of photosynthesis therefore appears be a general and conserved feature in diatoms.

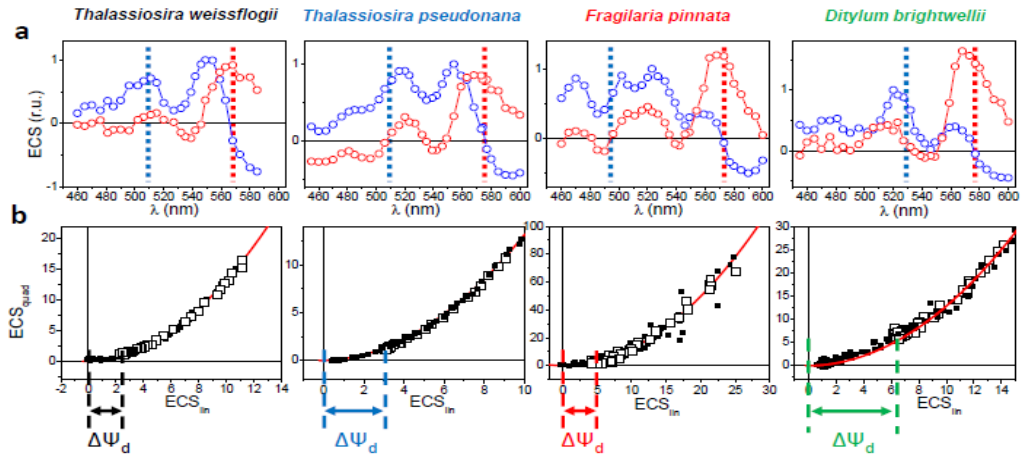

Figure 2.11 – **ATP transfer from mitochondria to plastid in representative diatoms.** (A) Spectra of the linear (blue) and quadratic (red) ECS probes in *T. weissflogii* (black), *T. pseudonana* (blue), *F. pinnata* (red), and *D. brightweli* (green). Blue and red vertical dashed lines represent the wavelengths used for linear and quadratic ECS, respectively. (B) Relationship between the quadratic and the linear ECS in control conditions (open green squares) and in the presence (closed green circles) of respiratory inhibitors AA and SHAM (representative of at least 3 independent experiments for each diatom). ΔΨd is represented as a horizontal arrow.

2.3.2.2 Conclusions

We conclude that ATP limits photosynthetic carbon assimilation in diatoms, as suggested in other photosynthetic organisms (Allen, 2002), but that at variance with the *Viridiplantae*, optimization of diatom photosynthesis does not rely on plastid-localized processes. Instead, constitutive energetic interactions between diatom mitochondria and plastids ensure the sharing of reducing equivalents and ATP to fuel CO_2 assimilation in the light (Figure 2.9 D). While the process we have uncovered has some similarities to the export of reducing equivalents from the plastids towards mitochondria in plants and green algae, the fundamental difference is that in these latter organisms the process serves as a valve to dissipate excess electrons (Kinoshita et al., 2011), and can only participate in the regulation of ATP/NADPH ratio when the chloroplast capacity to make extra ATP is genetically disrupted (Dang et al., 2014; Lemaire et al., 1988; Cardol et al., 2009). We propose that the presence of triose phosphate transporters such as the malate shuttle (Kinoshita et al., 2011), which are encoded in diatom genomes (Prihoda et al., 2012), as well as the very tight physical interactions observed in diatoms between plastids and mitochondria (Supplementary Figure 2.17 B), may make these energetic interactions possible between the two organelles. Because diatom plastids are surrounded by four membranes, rather than two as in *Viridiplantae* (Bowler et al., 2008) it will be of interest to elucidate the configuration of such transporters. More generally, the coupling of respiratory and photosynthetic activities in diatoms should be explored in the context of resource utilization in the ocean and as a means to boost the production of useful metabolites for biotechnology.

Supplementary Figures

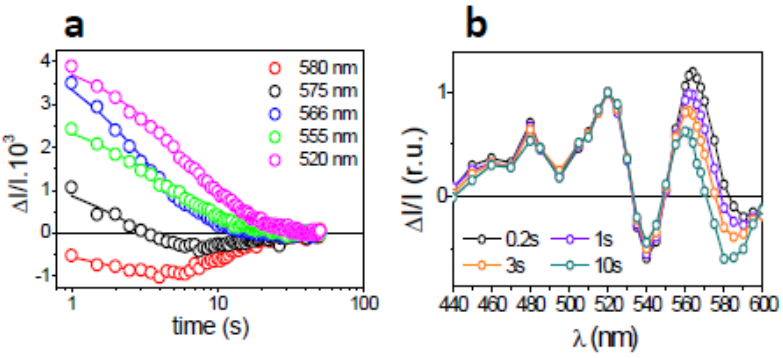

Supplementary Figure 2.12 – **Deconvolution of the quadratic and linear ECS in *P. tricornutum*.** (A) Absorption difference (ΔI/I) kinetics followed at different wavelengths in *P. tricornutum*, after a series of six saturating laser flashes, in anaerobic conditions. Solid lines correspond to the global fit of the experimental data with a sum of two exponential decays, with time constants t and 2t respectively, as expected for linear and quadratic dependencies (see Methods). (B) ΔI/I spectra are shown at different times during ECS relaxation. All spectra were normalized to 1 at 520 nm for better comparison. The observation that the blue and green parts of the spectrum are homothetic during relaxation, while changes are seen in the red most part of it, reflects the presence of the two ECS components, having different relaxation kinetics.

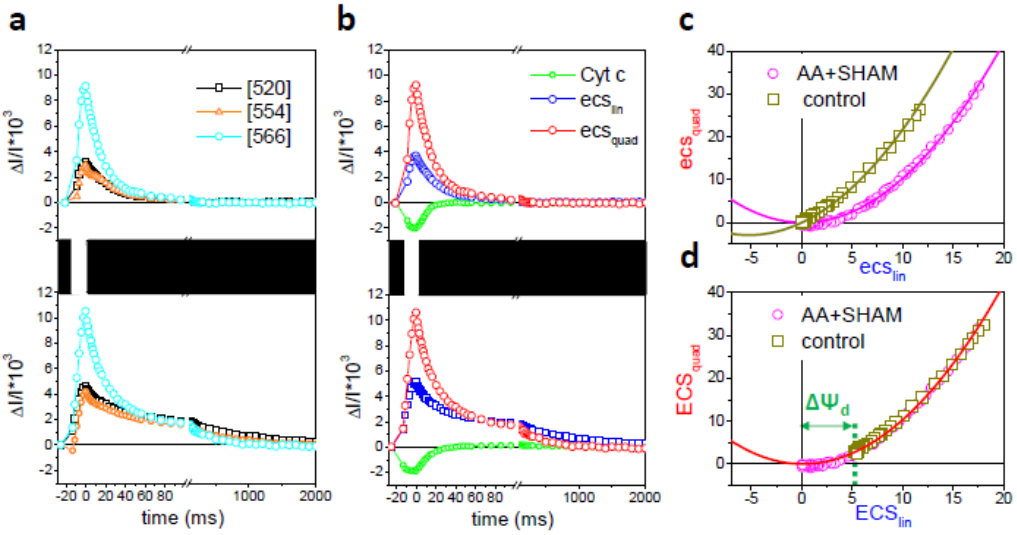

Supplementary Figure 2.13 – **Separation of c-type cytochromes signals, and linear and quadratic ECS signals in *P. tricornutum.*** (A) Kinetics of ΔI/I changes at 520, 554 and 566 nm during a ~10ms pulse of saturating red light (4500 µmol. quanta.m-2.s-1) and the subsequent dark relaxation (top: control conditions, bottom: AA+SHAM). (B) Kinetics of of ecslin, ecsquad changes and c-type cytochrome redox state, from kinetics in panel a, after deconvolution as explained in Methods. (C, D) Relationship between the quadratic and the linear ECS, before (ecslin, ecsquad, panel c) and after (ECSlin, ECSquad, panel D) correction for the dark electric field (see Methods). Dark yellow and magenta circles correspond to control and AA+SHAM conditions, respectively. The green arrow indicates the value of the ΔΨd in control conditions.

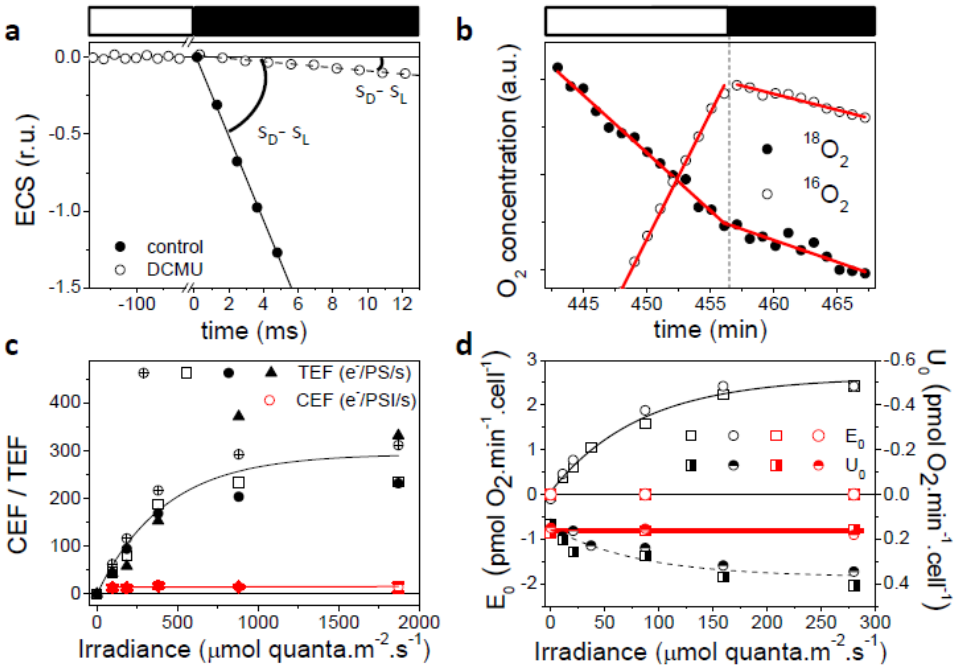

Supplementary Figure 2.14 – **Cyclic electron flow and water-to-water cycles in *P. tricornutum*.** (A) Representative traces of changes in linear ECS (normalized as explained in Methods) to evaluate linear and cyclic electron flow. Cells were illuminated with 1870 µmol quanta.m-2.s-1 of red light, in absence (closed circles) and presence (open circles) of DCMU and then transferred to the dark. Traces represent changes in the linear ECS. (B) Representative traces of the 16O2 and 18O2 concentrations at the offset of a 280 µmol quanta/m2/s blue light. In panels A and B, light and dark periods are represented by white and black boxes, respectively. (C) The photochemical rate corresponding to TEF and CEF can be estimated by measuring the initial slope of the ECS decay, as explained above25 (see Methods) at difference irradiances (n = 2-4 ± S.D.). (D) Light- dependencies of oxygen uptake (U0, open circles) and gross photosynthesis (E0, closed circles) in control conditions (dark) and in the presence of DCMU (red) (n = 2 ± S.E.).

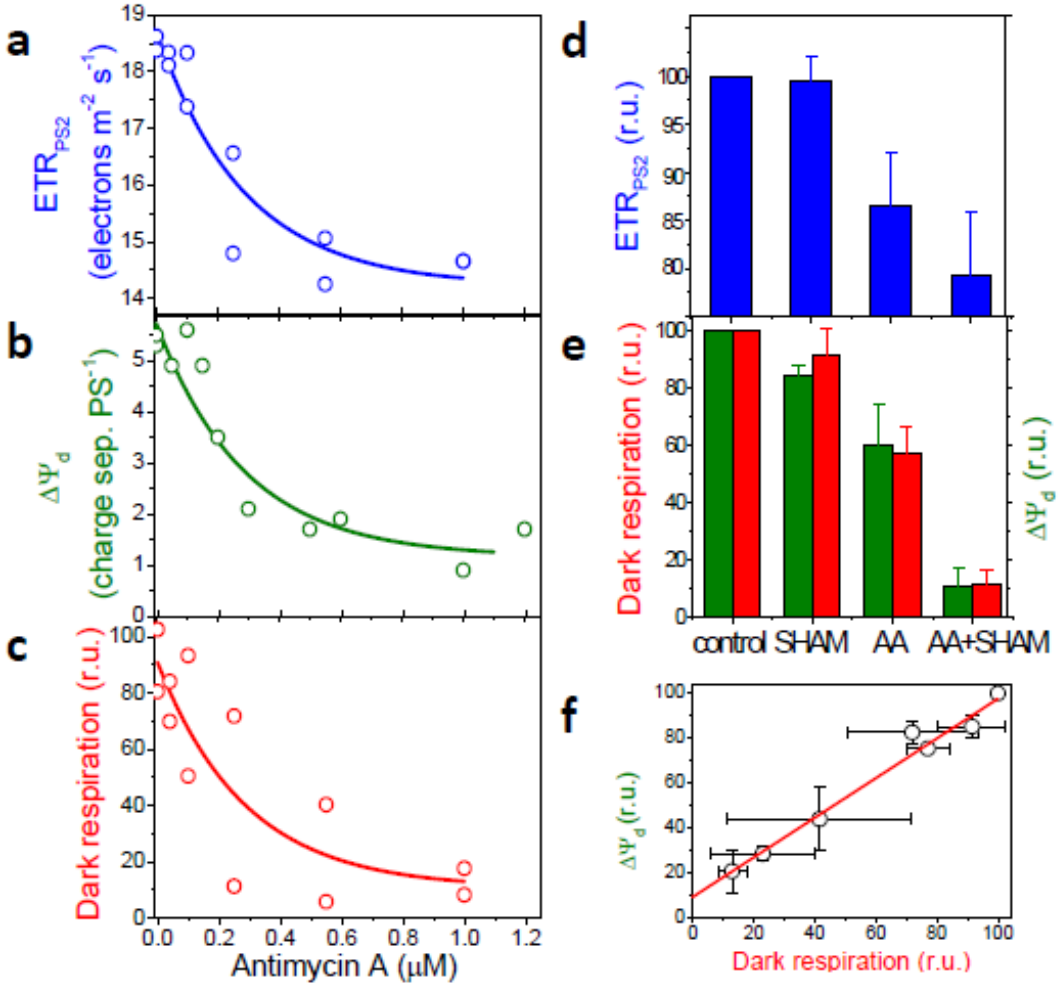

Supplementary Figure 2.15 – **ΔΨd and photosynthesis under respiratory inhibition.** (A,B,C) Dependency of the ETRPSII (A), ΔΨd (B) and dark respiration (C), expressed as a % of the values measured in untreated *P. tricornutum* wt cells, and following inhibition of the cyanide sensitive respiratory pathway with different concentrations of Antimycin A, in the presence of saturating SHAM (1 mM). Experimental data were fitted with a monoexponential decay function. (D,E) Effect of AA, SHAM and AA+SHAM on ETRPSII (D), ΔΨd and dark respiration (E), expressed as % of control, in wild-type cells of *P. tricornutum*. [SHAM]: 1mM. [AA]: 5µM. (n = 2-4 ± S.D.). (F) Relationship between ΔΨd and mitochondrial respiration in samples poisoned with increasing concentrations of AA in the presence of SHAM (from panels B and C).

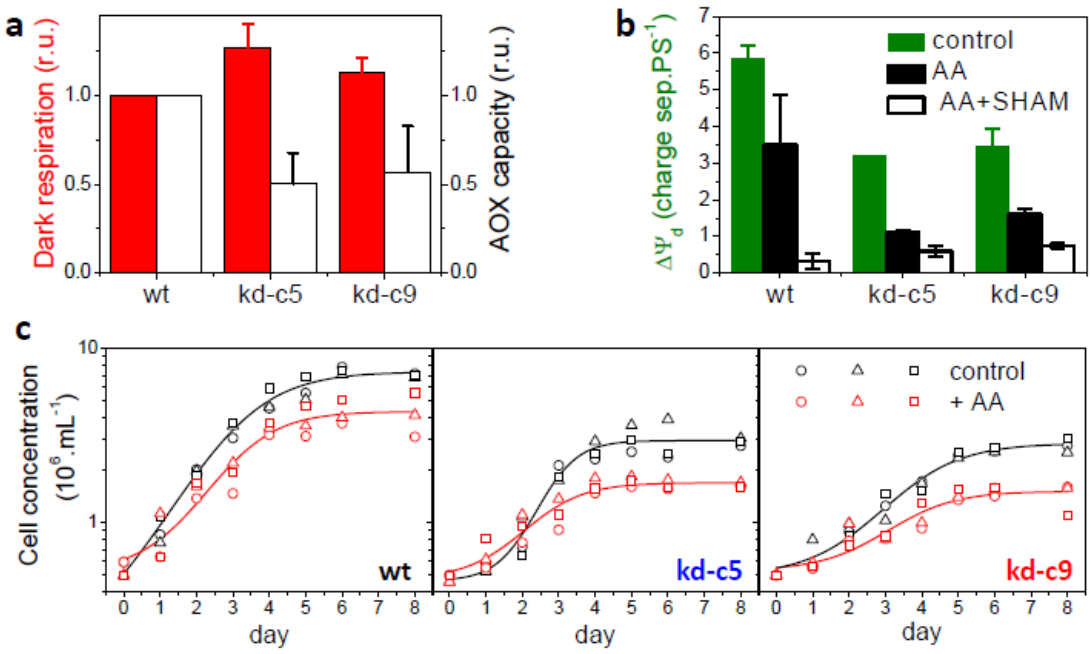

Supplementary Figure 2.16 – **Dark respiration, PMF and growth in AOX mutants in *P. tricornutum*.** (A) Respiratory activity of wild type and AOX knockdown lines. Total respiration rate (red bars) and the contribution of the AOX capacity (white bars, see Methods) were normalized to wild-type values. (n = 5 ± S.D.). (B) ECS-based measurements of ΔΨdark in wild type and AOX knockdown lines, in control conditions (dark), in the presence of AA (grey), and in the presence of AA+SHAM (white). (n = 2-3 ± S.D.). (C) Growth curves of wild type and AOX knockdown cell lines in the presence/absence of AA (2µM). AA was added every day and cells were grown in continuous light to prevent them from dying in the dark because of lack of respiration. (n = 3 ± S.D.).

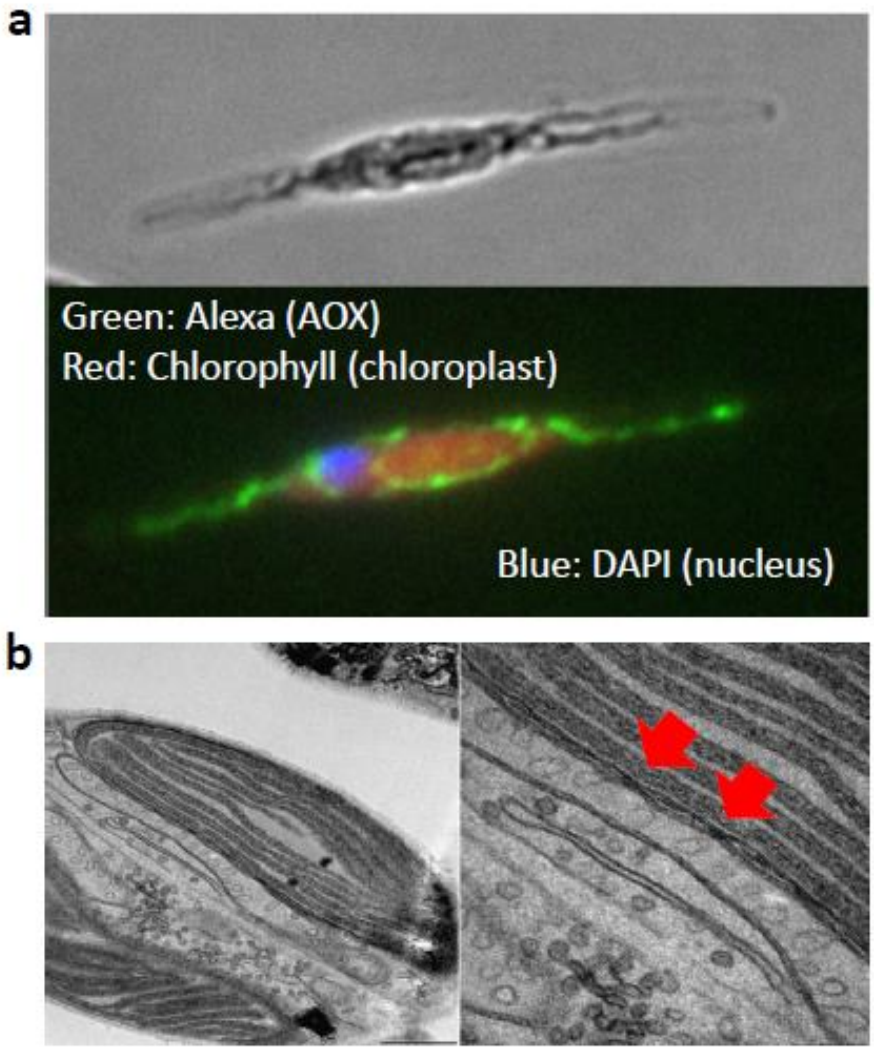

Supplementary Figure 2.17 – **Subcellular localization of AOX in *P. tricornutum* and plastid-mitochondria interaction in *P. tricornutum* wild-type cells**. (A) Subcellular localization of AOX. Cells were treated with an anti-AOX antibody and then with a secondary Alexa Fluor 488 antibody (see Methods). Positions of plastid and nuclei are indicated by chlorophyll a autofluorescence (red) and DAPI staining (blue), respectively. The pattern of AOx localization is similar to what was observed with a mito-tracker. (B) EM pictures of the plastid-mitochondria juxtaposition in *P. tricornutum*. Arrows indicate possible physical contacts between the plastid and mitochondrial membranes.

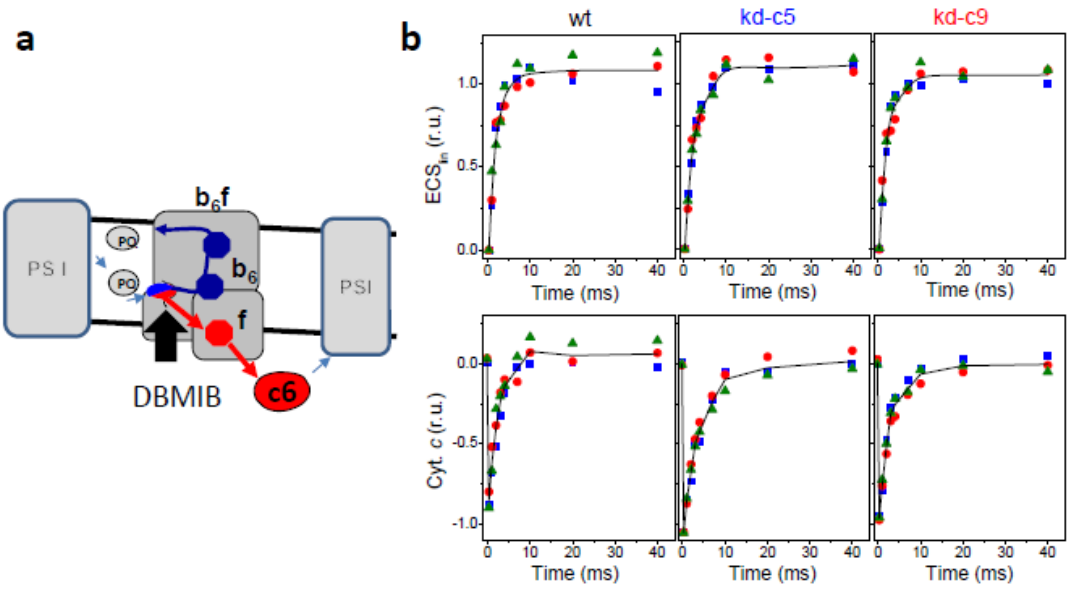

Supplementary Figure 2.18 – **Cytochrome b6f turnover in Pt1 and AOX mutants.** (A) Schematic representation of the electron flow reaction steps in the cytochrome b6f complex, which can be evaluated by spectroscopic measurements. (B) Slow phase of ECSL indicating cytochrome b6 (blue) and time resolved redox changes of cytochrome c/f (red) in wild type Pt1 and AOX knockdown mutants. *P. tricornutum* cells were exposed to saturating single turnover laser flashes given 10 s apart. Data were normalized to the amplitude of the fast phase of the ECSlin signal. Cyt. c and ECSlin were deconvoluted as explained in Methods. (n = 4 ± S.D.). Cell concentration was 2. 10 7 cells mL-1. Note that both the slow phase of the ECSlin and reduction of cytochrome c/f were completely abolished by the plastoquinone competitive inhibitor DBMIB 10 µM (black arrow).

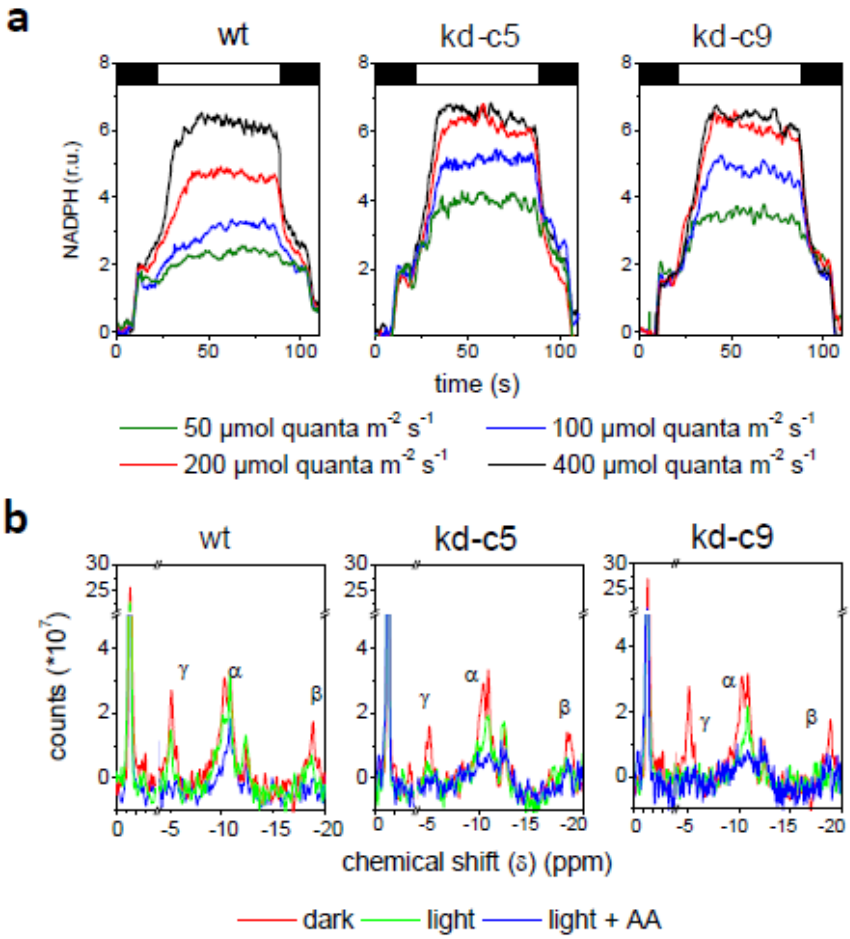

Supplementary Figure 2.19 – **In vivo changes in the NADPH redox state and ATP in wild type and AOX knockdown mutants.** (A) Changes in NADPH at different light intensities. Light and dark periods are represented by white and black boxes, respectively. Light intensities were 50, 100, 200 and 400 µmol. quanta m-2 s-1 (green, blue, red, and black traces, respectively). Chl concentration was ~5 µg mL-1. (B) Representative spectra from cells of wild type (left panel) and AOX knockdown C5 (middle panel) and C9 (right panel) in the dark (red), light (green) and light + AA (blue) conditions are shown, with normalization to the internal standard (methylenediphosphonate; pH 8.9). The positions of the α, β and γ phosphates of NTPs are shown. Inserts show the quantification of the NTP content in wild-type and AOX knockdown mutant cells, as reported in Supplementary Figure 2.14 E (± S.D.).

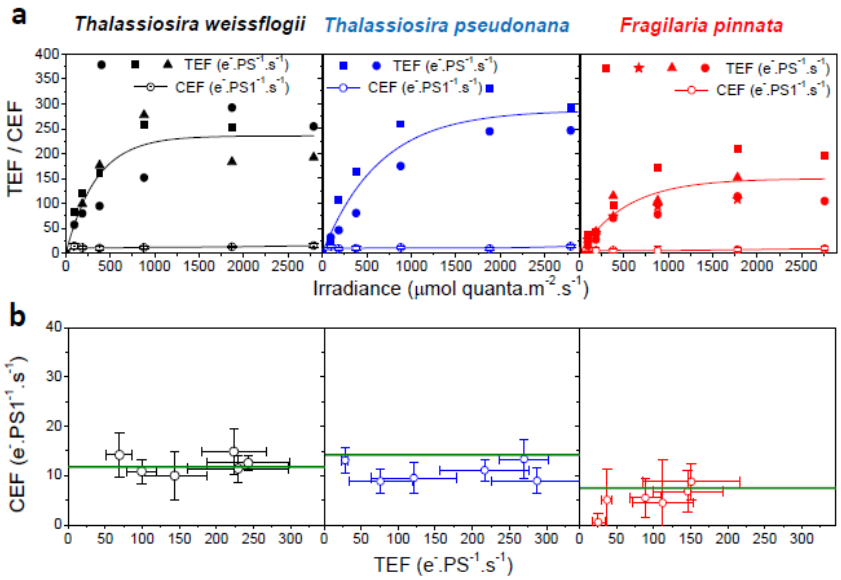

Supplementary Figure 2.20 – **Cyclic electron flow in representative diatoms.** (A) Linear (closed circles) and cyclic (in the presence of DCMU) electron flows were measured at different light intensities, as in Supplementary Figure 2.13, in *Thalassiosira weissflogii* (black), *Thalassiosira pseudonana* (blue) and *Fragilaria pinata* (red). (B) CEF was plotted against LEF. The red line corresponds to CEF = 5% of the maximal total electron flow. (n = 3-5 ± S.D.).

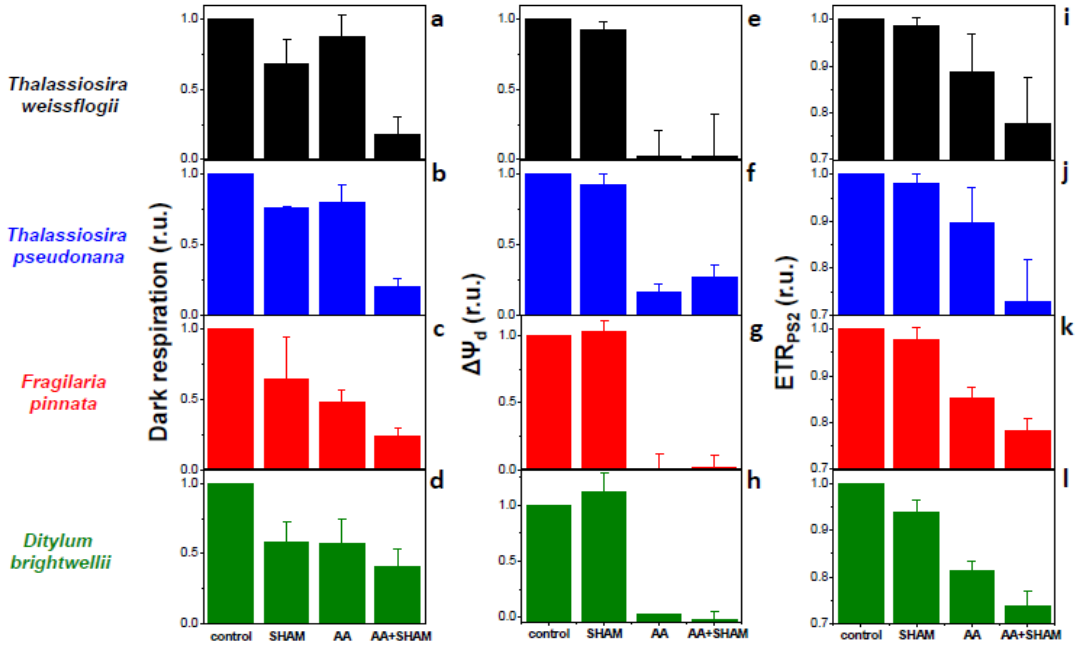

Supplementary Figure 2.21 –**ΔΨd and photosynthesis under conditions of respiratory inhibition in representative diatoms.** Dark respiration (A,B,C,D), ΔΨd (E,F,G,H) and ETRPSII (I,J,K,L), in conditions of different levels of inhibition of the respiratory pathway with saturating Antimycin A, and/or saturating SHAM. Panels a, e and i: T. weissflogii (black). Panels B, F and J: *T. pseudonana* (blue). Panels C, G and K: *F. pinnata* (red). Panels D, H and l: *D. brightwelii* (green). (n= 2-6 ± S.D.).

2.3.2.3 Materials and methods

Growth conditions: Wild type and AOX transformant lines of *Phaeodactylum tricornutum* Pt1.86 (CCMP 2561) were grown in artificial sea water (ASW; Vartanian et al., 2009). *Thalassiosira pseudonana* (CCMP 1335), *Thalassiosira weissflogii* (CCMP 1336), *Fragilaria pinnata* (CCAP 1029/2) and *Ditylum brightwelii* (CCMP 359) were grown in F/2 medium, supplemented with silica (Guillard, 1975). All strains were grown at 19 ± 1 °C, in semi-continuous batch culture with moderate shaking. The photoperiod was 12 h light/12 h dark, and light irradiance was 70 µmol quanta m^{-2} s^{-1}. Cell concentration was determined daily with a Z2 Coulter Counter analyzer (Beckman Coulter), to ensure all the experiments were performed with cells in exponential phase. For biophysical measurements, cells were concentrated by centrifugation and resuspended in their growth medium (supplemented with 10% w/v Ficoll to prevent cell sedimentation), and kept in the dark at least 30 minutes before measurements.

Inhibitors: 3-(3,4-dichlorophenyl)-1,1-dimethyl-urea (DCMU), Carbonyl cyanide-4-(trifluoromethoxy)phenylhydrazone (FCCP), Antimycin A (AA), Myxothiazol and salicylhydroxamic acid (SHAM) (Sigma-Aldrich, Munich, Germany) were dissolved in ethanol, whereas Hydroxylamine (HA), glucose, glucose oxidase and catalase (Sigma-Aldrich, Munich, Germany) were dissolved in deionized water. FCCP was used at a very low concentration (8 nM, Figure 2.9 B) to allow the disruption of the dark PMF without preventing the light-induced generation of PMF needed to quantify the $\Delta\Psi_d$. AA and Myxothiazol were used at 5µM, unless otherwise stated (Figure 2.9 B and Supplementary Figure 2.15). DCMU was used at a concentration of 15µM. In every measurement involving HA or SHAM, the lowest inhibitor concentration to induce a full inhibition of PSII activity or maximum inhibition of respiration, respectively, was used. The range of concentrations used was 30-100µM and 500-1000µM for HA and SHAM, respectively. Anaerobic conditions were obtained through incubation with catalase (1000 U/mL), glucose (10 mM) and glucose oxidase (2 mg/mL). Note that AA has been described as an inhibitor of cyclic electron flow, affecting the NDH-related pathway (Joët et al., 2001). However, this potential effect was ruled out in diatoms, where no change in cyclic electron flow was noticed upon addition of AA, consistently with the fact that genes encoding for the NDH complex are invariably lacking in diatom chloroplast genomes. AA and Myxothiazol were preferred to potassium cyanide to block the cyanide sensitive pathway of respiration, because potassium cyanide also affects RuBiCO activity (Wishnick & Lane, 1969), ascorbate peroxidase (Nakano & Asada, 1987) and Cu/Zn superoxide dismutase (Asada et al., 1974).

Deconvolution of linear and quadratic ECS components: To deconvolute the linear and quadratic contributions to the ECS signals, cells were left for an hour in the cuvette to reach complete anaerobiosis. In these conditions, the ATP synthase activity is slowed down, and long-living ECS signals are no longer contaminated with other light-induced absorption changes (principally c-type cytochromes redox change signals). Light stimulation of cells was achieved with a series of 6 laser single turnover (duration ~7 ns) saturating flashes, provided by a laser dye (LDS 144 698) pumped by a double frequency Nd-YAG laser (Quantel, Brilliant, France). We considered that the relaxation of the electric field generated by the light stimulus is described by the exponential function: $\Delta\Psi = \Delta\Psi_0 .\exp(-t/t)$, where t is time, $\Delta\Psi_0$ is the initial electric field generated by the light, and t is the electric field decay lifetime. The linear and quadratic components of the ECS are theoretically proportional to $\Delta\Psi$ and $\Delta\Psi^2$ respectively. Therefore, the $\Delta I/I$ spectro- temporal matrixes (from 460 to 600 nm) can be described by a sum of two exponentials: $y(\lambda, t) = A(\lambda).\exp(-t/t) + B(\lambda).\exp(-2.t/t) + C(\lambda)$. The kinetics of ECS relaxation were fitted by a global routine, which considers the lifetime t as a global (wavelength independent) variable, and the amplitudes of linear and quadratic components (A and B, respectively) as local (wavelength dependent) variables. A non-decaying component (C) was also included in the fit to account for a small fraction of residual signal at long delay times. The plot of the A and B amplitudes as a function of the wavelength provides the Decay Associated Spectra of the linear and quadratic contributions to the ECS signal, respectively, which are reported in Figure 2.17 A. The fit was performed using a home-made software, which uses the MINUIT package, developed and distributed by CERN, Geneva, Switzerland, implemented in FORTAN77. It minimizes the reduced sum of squared residues between the model function and the experimental data, employing a two-steps protocol involving an initial search that utilises the Simplex method (Nelder-Mead algorithm) and a refined search using the Levenberg-Marquardt algorithm as described in Santabarbara et al., 2009. The quality of the fit description was judged on the basis of reduced sum of squared residues statistics, visual inspection of the fit residuals, residuals autocorrelation and stability of the solutions upon random perturbation of the best-fit.

Measurements of c-type cytochromes and linear and quadratic ECS: Absorption difference signals were measured at different wavelengths with a Joliot-type spectrophotometer (JTS-10, Biologic, France), equipped with a white probing LED and the appropriate interference filters (3 to 8 nm bandwidth). For $\Delta\Psi_d$ measurements, the PMF was increased using a ~10ms pulse of saturating (4500 µmol quanta.m^{-2}.s^{-1}) red light (see Supplementary Figure 2.14 for representative ECS kinetics). For

P. tricornutum, ECS signals were evaluated using 3 wavelengths, to eliminate contribution from c-type cytochrom*es* (see Supplementary Figure 2.14). The latter was calculated as Cyt. *c* = [554]-0.4.[520]-0.4.[566], where [554], [520] and [566] are the absorption difference signal at 554 nm, 520 nm and 566 nm, respectively. The very similar relaxation of c-type cytochromes in aerobic and anaerobic conditions, despite very different ECS relaxations (Supplementary Figure 2.14 B), demonstrates the validity of the Cyt. *c* deconvolution procedure. Then ecs_{lin} and ecs_{quad} (ECS signals before correction for the $\Delta\Psi_d$) were estimated form the following relationships: ecs_{lin}=[520]-0.25.Cyt. *c* and ecs_{quad}=[566]+0.15.Cyt. *c*. For the other diatoms, appropriate wavelengths were chosen for calculating ecs_{lin} and ecs_{quad} (red and blue lines in Figure 2.11) to minimize the cytochrome contributions. ECS data were then normalized to the ecs_{lin} increase upon a saturating laser flash (i.e., 1 charge separation per photosystem, see Melis, 1982). The relationships between ecs_{quad} and ecs_{lin} were fitted with the parabolic equation ecs_{quad}+ a. $\Delta\Psi_d{}^2$ = a.(ecs_{lin}+ $\Delta\Psi_d$)^2, where $\Delta\Psi_d$ is the electric component of the PMF in the dark (expressed in charge separation per PS) and a is constant for all the experiments related to a diatom species (see Supplementary Figure 2.14 C). The ecs_{lin} and ecs_{quad} values represent ECS changes relative to dark values. Therefore, we corrected them for the dark electric field. This leads to ECS_{lin} = ecs_{lin} + $\Delta\Psi_d$, and ECS_{quad} = ecs_{quad} + a.$\Delta\Psi_d{}^2$, i.e. absolute values of the ECS signals. This simply corresponds to a shift of the x and y axis to allow the minimum of the parabola to coincide with the origin of the axes (see Supplementary Figure 2.15 D), and leads to ECS_{quad} = a.$ECS_{lin}{}^2$. This leads to evaluation of $\Delta\Psi_d$ as the minimal ECS_{lin} value of the experimental data (for example, the $\Delta\Psi_d$ in *P. tricornutum* as ~ 5 charge separations by PS, i.e., 100 mV[12] , Figure 2.8 C and Supplementary Figure 2.14 D). The presence of linear and quadratic ECS components allows measuring the absolute value of the $\Delta\Psi$ in the dark ($\Delta\Psi_d$). Indeed the amplitude of the linear ECS response (ecs_{lin}) observed upon a light stimulus increasing the $\Delta\Psi$ is constant, i.e. independent on the value of the field pre-existing the illumination ($\Delta\Psi_d$). Conversely, the amplitude of the quadratic ECS response (ecs_{quad}) is a function of the value of the $\Delta\Psi_d$. Therefore, plotting the amplitude of the ecs_{quad} vs ecs_{lin} allows quantifying the absolute value of the electric field in the dark ($\Delta\Psi_d$).

Cyt b_6f turnover was measured though the slow phase (phase B; Joliot & Delosme, 1974) of the linear ECS, which reflects b_6f-catalysed charge transfer across the membranes, and through the reduction rate of the c-type cytochromes (*c6/f),* using the 3 wavelengths deconvolution procedure described above. Measurements were performed after a saturating laser flash.

Measurements of photosynthetic flows: For calculation of the total electron flow (TEF, the sum of linear and cyclic electron flows) and cyclic electron flow (CEF) capacities, we measured the photochemical rates in the absence and presence, respectively, of DCMU. In brief, under steady state illumination conditions, the ECS signal results from concomitant transmembrane potential generation by PSII, the cytochrome b_6f complex and PSI and from transmembrane potential dissipation by the plastid ATP synthase When light is switched off, PS activities stop immediately, while ATP synthase and cytochrome b_6f complex activities remain (transiently) unchanged. Therefore, the difference between the slopes of the linear ECS signal (ECS_{lin}) measured in the light and after the light is switched off (s_D-s_L) is proportional to the rate of PSI and PSII photochemistry (i.e. to the rate of "total" electron flow, Supplementary Figure 2.13 A). Because the linear ECS has been normalized to the amplitude of the linear ECS signal induced by a saturating laser flash (Nakano & Asada, 1987; see above), the difference of slopes evaluates the number of charge separations per photosystem and per second. The rate of CEF can be evaluated using the same approach under conditions where PSII activity is inhibited by DCMU, and dividing this slope by the linear ECS signal induced by a saturating laser flash in the presence of PSII inhibitors (1 charge separation per PSI; Bailleul et al., 2010). This was done using saturating concentrations of DCMU, which block PSII oxidation by PSI and of hydroxylamine, to avoid charge recombination within PSII.

Fluorescence-based measurements: Fluorescence-based photosynthetic parameters were measured with a fluorescence imaging setup described in Johnson et al., 2009. Photosynthetic electron transfer rate ETR_{PSII} and NPQ were calculated, respectively, as (Fm'-F)/Fm'.I and (Fm-Fm')/Fm', where F and Fm' are the steady state and maximum fluorescence intensities in light acclimated cells (respectively), Fm is the maximal fluorescence intensity in dark-adapted cells, and I is the light irradiance in µmol quanta.m^{-2}.s^{-1} (Genty et al., 1989; Bilger & Björkman, 1990). The light saturation curves of ETR_{PSII} were fitted with the exponential rise function $P = P_{max}(1- \exp(E/E_k))$, where P_{max} is the maximal photosynthetic electron transport rate and E_k is the optimal light. ΔETR/ETR (Figure 2.10 A) was calculated as (ETR_{ref}-ETR).100/ ETR_{ref}, the reference being the wt in control conditions.

Membrane inlet mass spectrometer (MIMS) measurements: Samples were introduced in a 3 mL thermostated cuvette, which was connected to a Quadrupole Mass Spectrometer (QMS 200, Pfeiffer Vacuum Prisma, Asslar, Germany) by a stainless steel vacuum tube (0.125 inch) passing

through a water trap filled with ethanol and dry ice. The sample was separated from the tube via a gas permeable inlet system (PTFE membrane). $^{18}O_2$ was added as a bubble to the algal suspension, and the bubble was removed prior to the experiment. The measurements of the partial pressure of $^{16}O_2$ ($P^{16}O_2$, m/z = 32), $^{18}O_2$ ($P^{18}O_2$, m/z =36) and Argon (m/z =40) were performed after the cuvette was sealed. A blue LED source was connected to the cuvette, and the light irradiance was manually adjustable in the 0 to ~800 µmol quanta.m^{-2}.s^{-1} range. The temperature was kept at 19 ± 1 °C in the cuvette during the experiment.

To calculate gross O_2 production (E_0) and uptake (U_0), respectively, production and consumption by the cells, we adapted the equations from Peltier & Thibault, 1985:

$U_0 = (\Delta[^{18}O]/\Delta t + k[^{18}O]).([^{18}O]+[^{16}O]/[^{18}O])$

$E_0 = (\Delta[^{16}O]/\Delta t + k[^{16}O]) + U_0.([^{18}O]+[^{16}O]/[^{16}O])$

Where k is the rate constant of O_2 decrease measured in the absence of algae. We normalized O_2 to Argon- a biologically inert gas with very similar solubility properties, which decreases the sensitivity of O_2 measurements to fluctuations by ~80% (Kana, 1994). The gas concentrations were calibrated by measuring air-equilibrated O_2 concentration (stirring deionized water in the open cuvette for at least 5 hours) and background O_2 (bubbling with N_2).

Respiration rates were measured as O_2 exchange rates using a Clark-type oxygen electrode at 19°C (Hansatech Instrument, King's Lynn, UK). AOX capacity was measured as SHAM-sensitive respiration in conditions where the cyanide-sensitive pathway was beforehand inhibited (AA, 5µM).

ATP/NADPH *in vivo* measurements: $NADP^+$/NADPH redox changes were followed in living cells using a dual PAM (Walz, Germany). NADPH fluorescence was measured at 460 nm, upon excitation in the near UV. Chlorophyll *a* concentration was ~ 5 µg. mL^{-1}. ATP content was measured using an *in vivo* (Santabarbara et al., 2009) P- AMX 400 NMR spectrometer equipped with a 25-mm multinuclear probe tuned at 161.9 MHz, and a home-made lighting system, as described in Rivasseau et al., 2009. The relative ATP content was estimated *in vivo* from the surface of α-, β- and γ-phosphorus resonance peaks corresponding to the three phosphates of NTPs, which dominate the NMR spectra with inorganic phosphate and polyphosphates (Bligny & Douce, 2001).

Western blots and immunolocalization: Protein samples (5-10 µg) were loaded on 13% SDS-PAGE gels and blotted to nitrocellulose. Primary AOX antibody was customly designed (Sdix, USA,

1:4000 dilution). All other antisera used were obtained from Agrisera (Vännäs, Sweden). The blots were developed with ECL detection reagent and images of the blots were obtained using a CCD imager (Chemidock MP Imaging, Bio-Rad). Immunolocalization of AOX was generally done as described in (Bailleul et al., 2010). Briefly, cells were fixed with 2% formaldehyde in culture media for 20 minutes, washed 3 times with marine phosphate buffer (mPBS, see Van de Meene & Pickett-Heaps, 2004) and premeabelized by 1% Triton X-100 in mPBS for 10 minutes. The cells were washed again, blocked for 30 minutes in 1% BSA in mPBS and incubated over night at room temperature with anti-AOX antibody from rabbit (custom design, Sdix, USA, 1:200 dilution in mPBS). The cells then were rinsed with mPBS and incubated with donkey Alexa 488-conjugated anti-rabbit IgG antibody (Life Technologies, USA, at 1:100 dilution in mPBS) for 2 h at room temperature. Cells were then stained with 0.5µg/ml DAPI (4',6'-diamidino-2-phenylindole, Life technologies) for 10 min and mounted with Vectashield (Vector Laboratories, Inc., USA) after a rinse. Finally the cells were observed using a Leica SP5 confocal microscope (Leica Microsystems, Germany).

Electron microscopy: For transmission electron microscopy (TEM), *P. tricornutum* cells were fixed in 0.1 M cacodylate buffer (Sigma-Aldrich) pH 7.4 Containing 2.5% glutaraldehyde (TAAB), 2% formaldehyde (Polysciences, Inc.) for one hour at room temperature and then prepared according to a modified protocol from Deerinck et al. (http://ncmir.ucsd.edu/ sbfsem-protocol). After the dehydration steps, the cells were infiltrated with ethanol/Epon resin mixture (2/3-1/3 for one hour and 1/3-2/3 for one hour) and finally embedded in Epon in a 60°C oven for 48 hours or longer. Ultrathin sections (60 nm) were prepared with a diamond knife on an UC6 Leica ultramicrotome and collected on 200 µm mesh nickel grids before examining on a JEOL 1200 EX electron microscope.

Contributions

B.B., L.T., C.B., G.F. designed the study. B.B., N.B., O.M., D.P., J.P., A.T., V.V., R.B., S.F., D.F., A.K-L, S.S., F.R., P.J., L.T., P.C., G.F. performed experiments. B.B., N.B., O.M., D.P., R.B., A.K-L, F.R., P.J., L.T., P.F., P.C., C.B., G.F. analyzed the data. B.B., C.B., G.F. wrote the manuscript, and all authors revised and approved it.

2.3.3 Perspectives

The presented work discloses the energetic interactions between chloroplast and mitochondria that are required for optimization of photosynthesis in diatoms. Since its publication I have performed new structural studies, taking advantage of the FIB-SEM technology, thereby addressing new questions. According to literature, the number and size of mitochondria, in this group of algae, remain a mystery. Round and collaborators in 1990 proposed that its morphology follow a long structure localized in the cytoplasm. The lacking of comparative studies on mitochondria structure in diatoms switched on our curiosity and comprehensive studies have been performed. Our recent 3D reconstitution of an intact cell of *P. tricornutum* indicate that every cell contain a single chloroplast, but also a single mitochondrion, which is highly ramified and sits on the chloroplast. This mitochondria is partially sandwiched between the chloroplast and the nucleus and reinforces our conclusion about the physical exchanges between the two organelles but also raises the important question on the mechanism of these exchanges. The optimization of protocols for scanning electron microscopy should address this question. One approach to move a step forward will be the improvement of the 3D reconstitution of *Phaeodactylum tricornutum* cells enhancing the resolution of the chloroplast and mitochondria-fused membranes. Furthermore, an interesting point will be to visualize these “fusion junction” and elucidate the configuration of the transporters that underline the energetic exchanges reported in the paper presented here. A promising strategy is the use of cryo-EM tomography linked with the correlative light EM (CLEM), to localize the carriers within the fusion membranes. Combining molecular and structural techniques, in a comprehensive approach, will be possible to identify these transporters and finally unravel the structural arrangement of the machineries that optimize photosynthesis in diatoms.

2.4 *Phaeodactylum* periplastidial compartment

2.4.1 Preface

The article presented in this section focuses on the periplastidial compartment of the model organism *Phaeodactylum tricornutum*.

Diatoms plastids derives from the engulfment of a red alga by another eukaryotic cell, followed by reduction of symbiont cell structures. In the pennate diatom *Phaeodactylum tricornutum,* like in all the other photosynthetic organisms studied so far, most plastid proteins are encoded in the nucleus and imported through these membranes. However, consistent with the fact that four membranes (instead of two in plants and green algae) constitute the chloroplast envelope of diatoms, the translocation of many components between the cytosol and the chloroplast should require a different transport machinery. So far it is not clear if transport through the periplastidial compartment (PPC) could occur *via* membrane translocators or *via* unknown vesicular trafficking systems. Consistent with the latter, a vesicular network (VN) was observed in the PPC of *Ochromonas danica* (Gibbs, 1979), a Chrysomonad close to, but distinct from diatoms. Ultrastructural studies also support the existence of a VN in the PPC in diatoms (Bedoshvili et al., 2009) but their location within the cell has not been assessed so far. Taking advantage of ultrathin sections of disrupted *P. tricornutum* cells obtained using the focus ion beam-scanning electron microscopy (FIB-SEM; see section 3.4.2) we revealed the presence of a vescicular network in the PPC of *Phaeodactylum tricornutum*. This network represents a potential candidate for the trafficking process mentioned above. Moreover, we saw direct membrane contacts between the periplastidial membrane (PPM) and the nuclear inner envelope membrane at the level of the chloroplast-nucleus isthmus. Overall, this study not only provides insights into the subcellular organization of membrane compartments in diatoms, but also allows corroborates previous hypotheses for the protein import, i.e. a process that is fundamental to understand the function, biogenesis and dynamics of secondary plastids, at the structural level.

2.4.2 Ultrastructure of the Periplastidial Compartment of the Diatom *Phaeodactylum tricornutum*

Serena Flori[a], Pierre-Henri Jouneau[b], Giovanni Finazzi[a], Eric Maréchal[a,] and Denis Falconet[a]

[a]Laboratoire de Physiologie Cellulaire et Végétale; Unité Mixte de Recherche 5168 CNRS – CEA – INRA – Université Grenoble Alpes; Institut de Recherche en Sciences et Technologies pour le Vivant; CEA-Grenoble; 17 rue des Martyrs; 38054 Grenoble Cédex 9, France

[b]Laboratoire d'Etudes des Matériaux par Microscopie Avancée; Institut Nanosciences et Cryogénie; Service de Physique des matériaux et Microstructures; CEA-Grenoble; 17 rue des Martyrs; 38054 Grenoble Cédex 9, France

Abstract

Diatoms contain a secondary plastid that derives from a red algal symbiont. This organelle is limited by four membranes. The two outermost membranes are the chloroplast endoplasmic reticulum membrane (cERM), which is continuous with the host outer nuclear envelope, and the periplastidial membrane (PPM). The two innermost membranes correspond to the outer and inner envelope membranes (oEM and iEM) of the symbiont's chloroplast. Between the PPM and oEM lies a minimized symbiont cytoplasm, the periplastidial compartment (PPC). In *Phaeodactylum tricornutum*, PPC-resident proteins are localized in "blob-like-structures", which remain associated with plastids after cell disruption. We analyzed disrupted *Phaeodactylum* cells by focused ion beam scanning electron microscopy, revealing the presence of a vesicular network (VN) in the PPC, at a location consistent with blob-like structures. Presence of a VN in the PPC was confirmed in intact cells. Additionally, direct membrane contacts were observed between the PPM and nuclear inner envelope membrane at the level of the chloroplast-nucleus isthmus. This study provides insights into the PPC ultrastructure and opens perspectives on the function of this residual cytoplasm of red algal origin.

Diatoms constitute a major group of phytoplankton in oceans and freshwater ecosystems, and are so ecologically successful that they are responsible for up to one fourth of global primary productivity (Field et al., 1998). Based on comprehensive surveys of oceanic biodiversity, diatoms are spread globally and are the most diverse photosynthetic eukaryotic lineage (de Vargas et al., 2015; Massana et al., 2015). A striking feature of diatoms is their sophisticated ultrastructure, inside highly packed cells, including a chloroplast bounded by four membranes, known as a 'secondary' or 'complex plastid'. Our understanding of the structure of this organelle and its relationship with the rest of the cell is fragmentary. Plastid-mitochondrion metabolic interactions were recently shown to optimize bioenergetic coupling, being one of the reasons for diatoms' performance in ecosystems (Bailleul et al., 2015; see section 2.3). The stroma of diatoms' chloroplast is also the site of production of fatty acids, which are precursors for the biosynthesis of all membrane and storage glycerolipids, but it is still unknown how these fatty acids and glycerolipids can traffic across and inside subcellular membranes to reach their final destination (Abida et al., 2015). Important shuttling of proteins, lipids and other metabolites is therefore expected to occur through the four membranes limiting the plastid. Diatom glycerolipids are considered a promising feedstock for biofuels and other lipid-derived chemicals (Levitan et al., 2014). It is therefore essential, but challenging, to advance knowledge on the subcellular organization and connectivity of membranes within diatom cells.

The secondary plastid derives from the engulfment of a red alga by another eukaryotic cell, followed by the reduction of the symbiont subcellular structures (Cavalier-Smith, 2003; McFadden, 2014; McFadden & van Dooren, 2004; Nisbet et al., 2004). Such secondary plastids are found in groups that are distant from diatoms (Heterokonta), like Cryptophyta, Haptophyta, Chromerida or Apicomplexa (Cavalier-Smith, 2003; Dorrell & Smith, 2011; Gibbs, 1962a, b, c, 1979, 1981; Maréchal & Cesbron-Delauw, 2001; Petroutsos et al., 2014). Secondary plastids are therefore chimeric organelles, combining host and symbiont-derived structures. The outermost membrane, termed the 'chloroplast endoplasmic reticulum membrane' (cERM, Figure 2.22; Gibbs, 1979) is supposed to derive from the host phagocytic membrane (Cavalier-Smith, 2003; McFadden & van Dooren 2004; Nisbet et al., 2004) and is therefore expected to be phospholipid rich (Abida et al., 2015; Petroutsos et al., 2014).

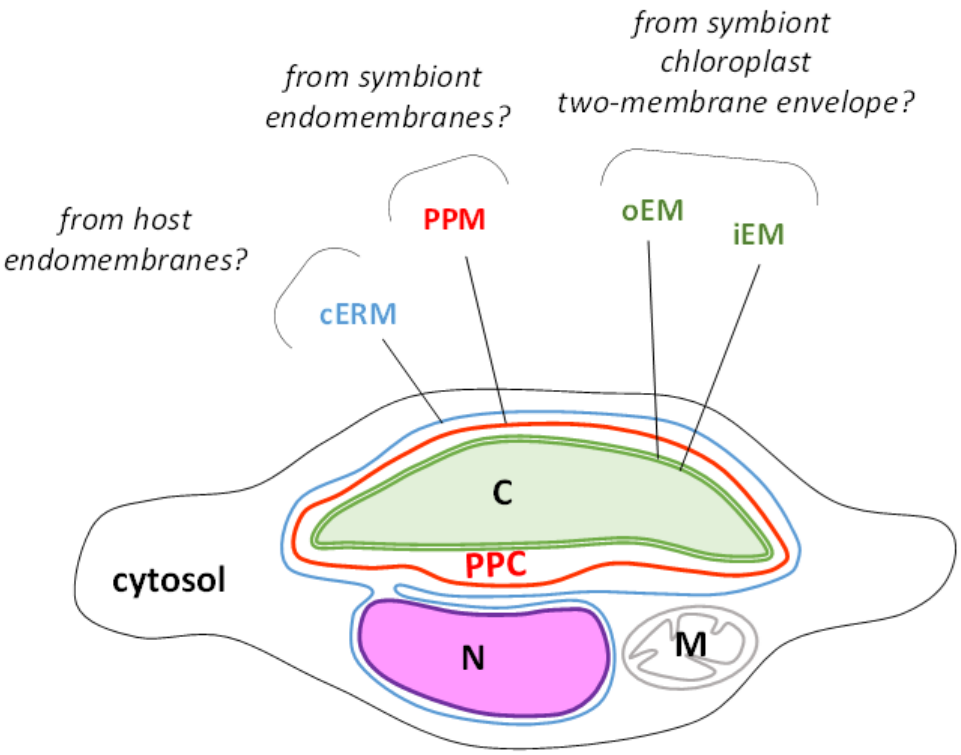

Figure 2.22 – **Chimeric organization of the secondary plastid in diatoms.** The scheme shows a fusiform cell of *Phaeodactylum*. The plastid is limited by 4 membranes. The chloroplast endoplasmic reticulum membrane (cERM), shown in blue, is continuous with the outer nuclear envelope membrane. The periplastidial membrane (PPM) is shown red. The outer and inner envelope membrane (oEM and iEM), shown in light green, are tightly apposed. The presence of a specific periplastidial compartment (PPC) is based on the detection of blob-like structures observed by confocal microscopy, in which protein precursors fused to GFP and crossing only the cERM and the PPM reside. The presence of VN in this PPC is addressed here. C, chloroplast; N, nucleus; M, mitochondrion.

In diatoms, the cERM is directly connected to the host outer nuclear envelope membrane (oNE) and the ER (Bouck, 1969; Kroth et al., 2008). In other groups, like Apicomplexa, the cERM and the endomembrane system are not continuous and transfers of material occurs *via* vesicular trafficking (Heiny et al., 2014; van Dooren et al., 2001; van Dooren et al., 2000). Underneath, the 'periplastidial membrane' (PPM, Figure 2.22) is considered to derive from the symbiont plasma membrane (Grosche et al., 2014), although an alternative origin from the host ER has been recently proposed (Gould et al., 2015). The nature of the two innermost membranes of the chloroplast is not debated, being reminiscent of the galactolipid-rich chloroplast envelope of the symbiont, called the 'outer' and 'inner envelope membranes' (oEM and iEM, Figure 2.22; Botté & Maréchal, 2014; Petroutsos

et al., 2014). Between the PPM and oEM lies a minimized symbiont cytoplasm, the 'periplastidial compartment' (PPC, Figure 2.22; Grosche et al., 2014). The cytoplasmic remains of the red algal symbiont show different degrees of reduction. Cryptophytes like *Guillardia theta* contain a minimized version of the nucleus in the PPC, called the nucleomorph (Curtis et al., 2012), whereas other groups including diatoms have completely lost the symbiont nucleus.

Phaeodactylum tricornutum is by far the most studied pennate diatom, following the complete sequencing and annotation of its genome (Bowler et al., 2008), the development of molecular tools for gene expression and functional characterizations (Apt et al., 1996; De Riso et al., 2009; Falciatore et al., 1999; Siaut et al., 2007) and the production of reference data for membrane lipidomic studies (Abida et al., 2015). *P. tricornutum* is pleiomorphic, with three major morphotypes, *i.e.* fusiform (shown in Figure 2.22), triradiate and oval. A series of axenic strains have been collected in various marine environments worldwide, including Pt1, which has been analyzed here (De Martino et al., 2007). Subcellular localization of proteins in the secondary plastid of *P. tricornutum* relies on confocal imaging of cells expressing the green fluorescent protein (GFP) fused to various addressing sequences (Gould et al., 2006; Grosche et al., 2014; Gruber et al., 2007; Hempel et al., 2009; Kilian & Kroth, 2005; Moog et al., 2011; Peschke et al., 2013; Sommer et al., 2007).

Most plastid proteins in *P. tricornutum* are nuclear encoded: their sequences contain a bipartite topogenic signal (Bts), comprising an N-terminal signal peptide (Sp), a chloroplast-like transit peptide (Ctp) and an amino acid motif at the cleavage site of the Sp, termed the ASAFAP motif (Gould et al., 2006; Gruber et al., 2007; Kilian & Kroth, 2005; Moog et al., 2011). Three major translocating systems are involved to import plastid proteins harboring a Bts (Supplementary Figure 2.29). Firstly, a sec61 complex operates by co-translational mediation of pre-proteins across the cER (Bolte et al., 2009). Secondly, the symbiont endoplasmic reticulum-associated degradation (ERAD) machinery has evolved to give rise to a translocon called the 'symbiont-specific ERAD-like machinery', or SELMA (Felsner et al., 2011; Hempel et al., 2007; Hempel et al., 2009; Lau et al., 2015; Sommer et al., 2007; Stork et al., 2012; Stork et al., 2013). Thirdly, transport across the oEM and iEM involves components related to the classic chloroplast translocon, *i.e.* TOC and a TIC respectively (Bullmann et al., 2010; Heinz & Lithgow, 2014; Schleiff & Becker, 2011; Schleiff et al., 2011; Sommer et al., 2011; Stork et al., 2013; Wunder et al., 2007).

Following docking of ribosomes at the surface of the secondary plastid, the Sp determines the targeting *via* the cERM and PPM (Supplementary Figure 2.29). The presence of a phenylalanine (F) or an aromatic residue at position +1 of the Ctp determines the transport across the oEM and the

iEM. In the absence of such aromatic amino acid, proteins remain resident in the PPC (Gould et al., 2006; Gruber et al., 2007; Kilian & Kroth 2005; Moog et al., 2011). A recent study has shown that pre-proteins could be N-glycosylated prior their transport through the PPM (Supplementary Figure 2.29), probably by the action of an oligosaccharide transferase (OST; Peschke et al., 2013). An important question is then posed by this discovery, regarding the possibility to import some of the plastid proteins, most notably folded glycoproteins, *via* membrane translocators or *via* unknown vesicular trafficking systems.

The evidence for a protein to reside (or be blocked) inside the PPC lies on the detection of GFP fusions inside single spot-like structures at the periphery of the plastid, called "blob-like-structures' (Gould et al., 2006; Gruber et al., 2007; Kilian & Kroth, 2005; Moog et al., 2011). The presence of membrane vesicles in blob-like structures was considered as possible based on the arrest of protein import by treatment with Brefeldin A (Kilian & Kroth, 2005), however in following studies, this hypothesis was never confirmed. Consistently with the absence of vesicles, no PPC-specific component involved in vesicular lipid trafficking, such as Rabs, SNAREs, COPI, COPII, chlathrin, calveolin, ESCRT, GEFs or GAPs could be predicted (Moog et al., 2011).

In a comprehensive electron microscopy study of the chrysomonad *Ochromonas danica*, a vesicular network (VN) was observed in the PPC (Gibbs, 1979). This VN has been initially called a periplastidial reticulum (Gibbs ,1979). This network did not extend around the whole chloroplast of *O. danica*, but was found restricted to particular locations, close to the nucleus (Gibbs, 1979). Apparent increase of this VN after treatment with cycloheximide and disappearance after treatment with chloramphenicol suggested a relation with protein import (Gibbs, 1979). This study is often considered a reference to suggest that the PPC of diatoms may contain a VN, but the detection of membrane translocators and the lack of putative PPC proteins acting in lipid trafficking have been repeatedly used as an argument to consider the presence of vesicles as unlikely, or generated by unknown components (Gould et al., 2006; Moog et al., 2011; Peschke et al., 2013; Sommer et al., 2007). Ultrastructural study of chloroplasts in diatoms other than *Phaeodactylum* has supported the existence of a VN in the PPC (Bedoshvili et al., 2009), but location within the cell and conservation in the diatom phylum have not been assessed. The ultrastructure of the PPC needs therefore to be characterized in *P. tricornutum*. We analyzed by electron microscopy series of ultrathin sections of *P. tricornutum* cells, revealing the presence of a VN in the PPC, at a location corresponding to blob-like structures.

2.4.2.1 Results and Discussion

Since blob-like structures remain associated to chloroplasts after cell disruption (Kilian & Kroth, 2005), we took advantage of this property and analyzed by electron microscopy series of ultrathin sections of disrupted *P. tricornutum* cells (Figure 2.23 A and B). Series of thin sections allow the detection of membrane connectivity in the three dimensions. Here, the thickness of section slices was 4 nm, and 200 to 600 sections were collected per sample, allowing the ultrastructure scanning of single organelles (chloroplast, mitochondrion or nucleus) from tangential sections (edges) to cross sections (Figure 2.23 C).

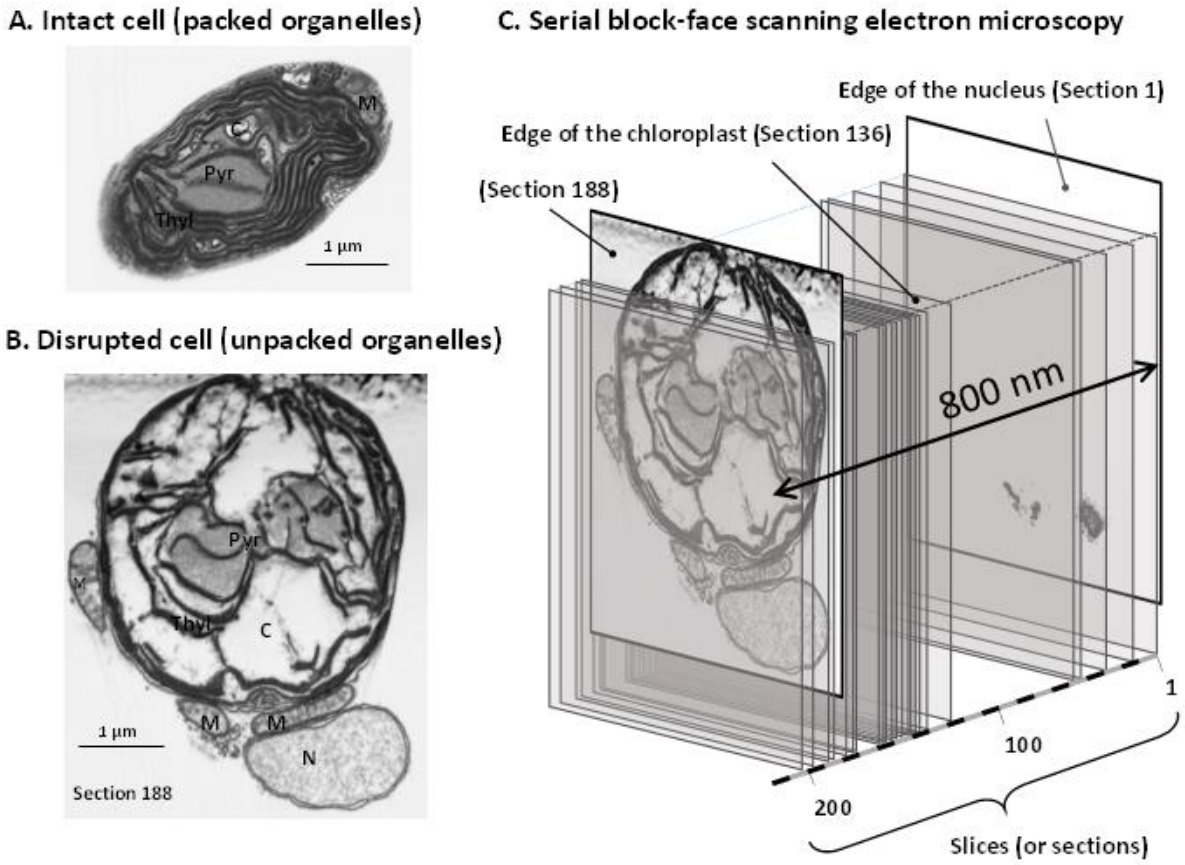

Figure 2.23 – (A) Electron micrograph of an intact *Phaeodactylum* cell. (B) Disrupted cell. (C) Lateral view of the serial scanning method. Slices or section are 4 nm-thin, and allow the detection of membrane continuity between successive cross sections. For 200 sections, the depth of the scanning is 1 µm. In the disrupted cell shown in Figures 2.10, 2.11 and 2.12, the tangential view of the nucleus is in section 1, and that of the chloroplast is in section 136. C, chloroplast; M, mitochondrion; N, nucleus; Pyr, pyrenoid; Thyl, thylakoids.

Focusing on a disrupted unpacked cell, the scanning of the region between a nucleus and a secondary plastid is shown in Figures 2.24, 2.25 and 2.26. In these series, the identity of the membranes is assessed by the connectivity in the two dimensions of the sections and the conservation from one section to the following, i.e. the third dimension. To help trace membrane identity and connectivity between sections, schematic representations are also shown: sections 1', 48', 140', 145', 152', 178', 184' and 208'.

Firstly, Figure 2.24 shows the most tangential region of the nucleus. Section 1 corresponds to the edge of this organelle, i.e. a tangential view of the oNE. Section 16 shows the tangential view of the iNE. The following sections, e.g. 30, 44 or 48, are transverse views of the nucleus, containing the chromatin, and allowing the visualization of nuclear pores (Figure 2.24, section 48, NP). The uncondensed chromatin indicates that the cell is in interphase. In section 120, the cross section of the nuclear envelope is slightly irregular and shows a constricted area (Figure 2.24, section 120, dashed circle). In this constricted region of the nucleus the oNE is connected to the cERM (Figure 2.24, sections 136, bold dark arrows). In section 140, this oNE-cERM isthmus gets larger (Figure 2.24, sections 140, bold dark arrows) and irregular tangential sections of the PPM are visualized facing directly the iNE. Here, and in following sections, the oEM and the iEM appear as closely apposed membranes.

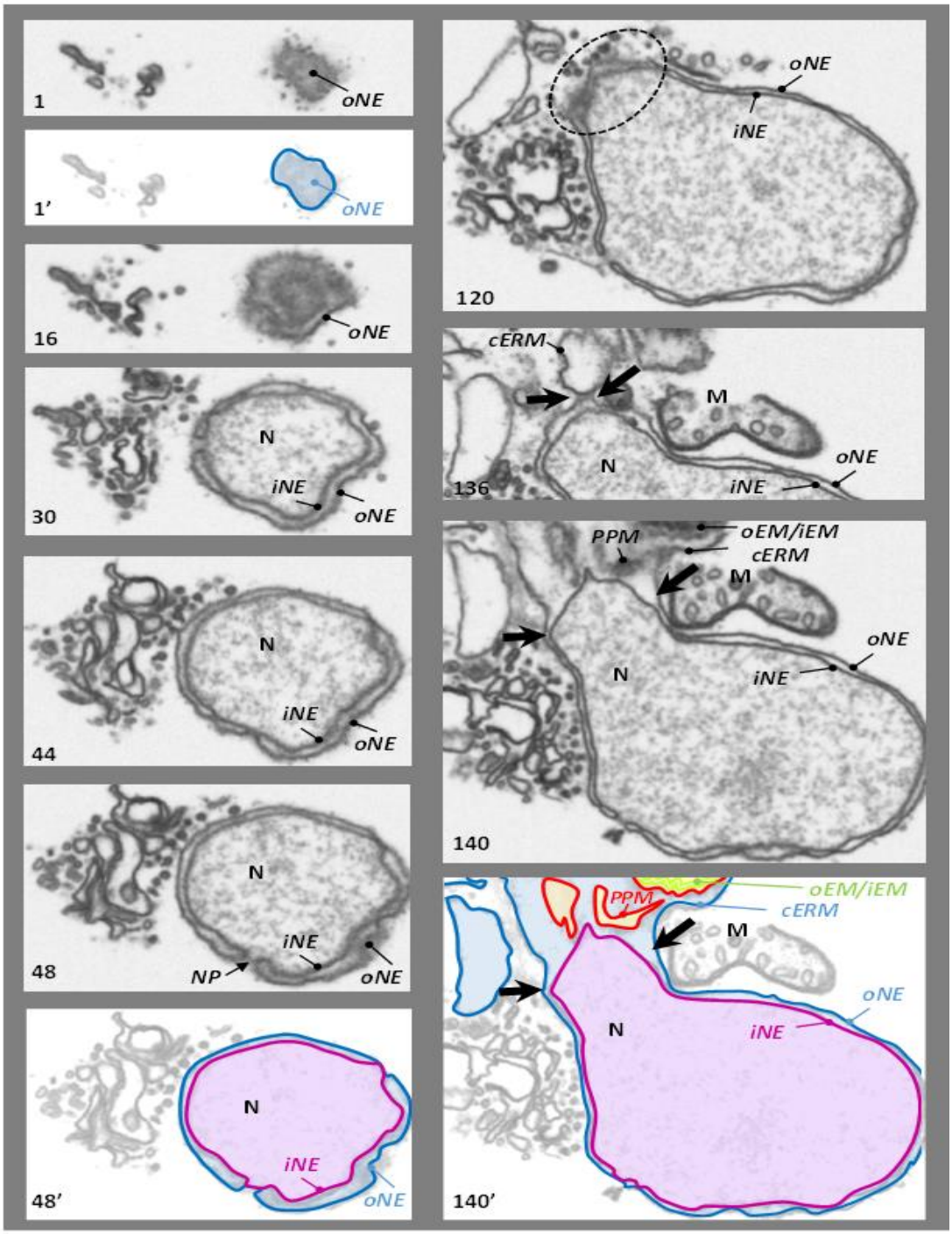

Figure 2.24 **– Serial electron micrograph scanning of a *Phaeodactylum* disrupted cell at the level of the cERM–oNE isthmus.** The outer nuclear envelope is shown in blue from a tangential section (1) to the level of sub-spherical nucleus (48 and 48'), where it is lined with the inner nuclear envelope (iNE) shown in purple. The nucleus then forms a constricted area shown in dashed lines (120). In the vicinity of the chloroplast, the oNE becomes continuous with the chloroplast endoplasmic reticulum membrane (cERM). The edges of the isthmus are shown with arrows. M, mitochondrion; N, nucleus; NP, nuclear pore.

Secondly, Figure 2.25 shows a focus in the region where the iNE faces directly the PPM. In sections 142, 144 and 145 the PPM is less irregular and shows an increased apposition with the iNE. A vesicular network (VN) appears between the PPM and the oEM/iEM. The PPM/iNE membrane contact site expands from sections 148 to 152, becoming as large as the oNE-cERM isthmus.

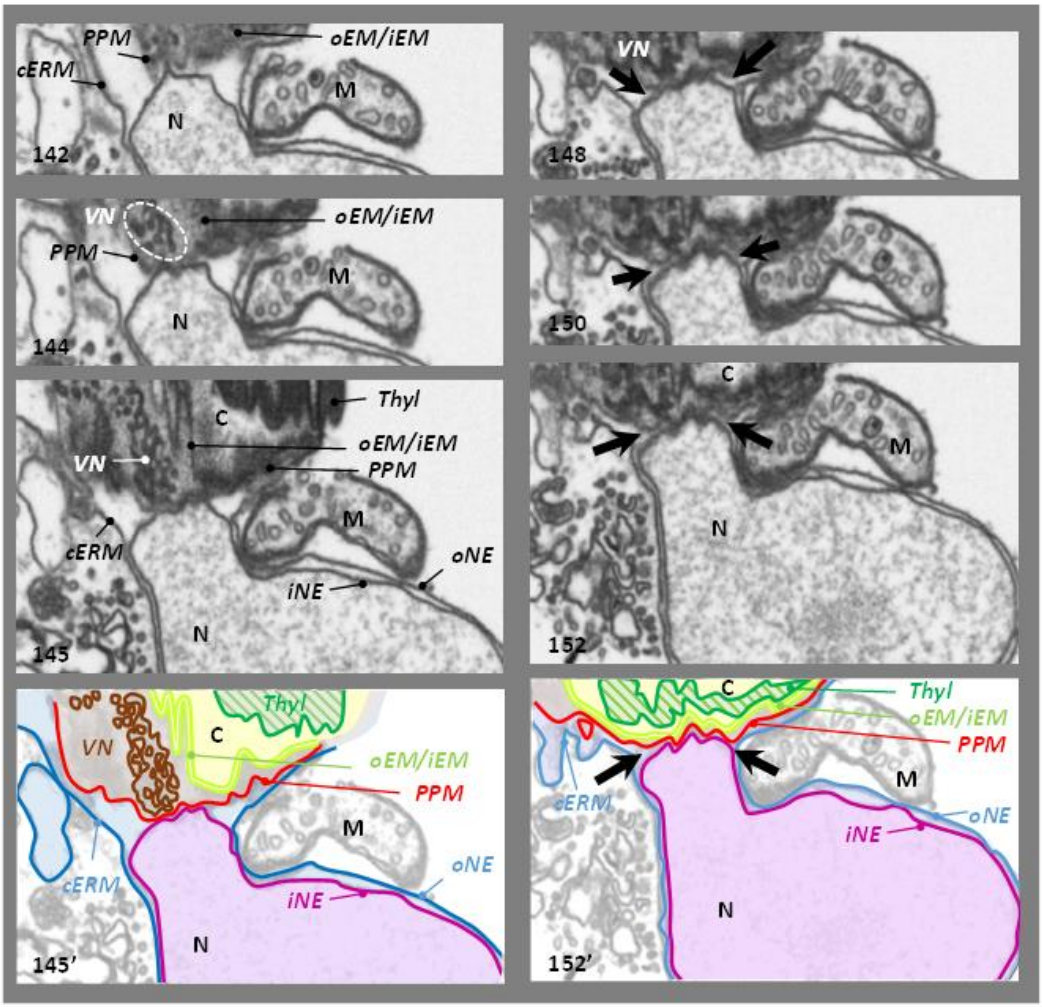

Figure 2.25 – **Serial electron micrograph scanning of a *Phaeodactylum* disrupted cell at the level of the iNE-PPM membrane contact.** The outer nuclear envelope (oNE) is shown in blue in continuity with the cERM. The inner envelope membrane (iNE) is shown in purple and gets in very tight contact with the irregular periplastidial membrane (PPM; from 142 and further). A vesicular network (VN) fills the space between the PPM and the two innermost membranes of the chloroplast, the outer and inner envelope membranes (oEM and iEM, respectively), shown in light green. C, chloroplast; M, mitochondrion; N, nucleus; Thyl, thylakoids.

Thirdly, Figure 2.26 allows visualizing the expansion of the VN in regions where the oEM and cERM are not connected. From sections 158 to 160 and 162, the oNE-cERM isthmus and the PPM/iNE membrane contact site are clearly visible, whereas section 174 shows disconnected cross sections of the chloroplast and the nucleus (Figure 2.26, sections 174, star). The VN is still visible, indicating that the VN is close, but not strictly dependent on the nucleus-chloroplast isthmus. In sections 176 and 178, direct connections between the VN and the PPM are visible (Figure 2.26, section 178/178', bold arrow), whereas no link between the VN and the oEM could be detected. The VN is visible in sections 188, 192 and is tangentially observed in section 200. Section 208 shows a second connection between the nucleus and the chloroplast (Figure 2.26, section 208/208', bold arrows), but this time without any VN.

Thus this series illustrates that at the level of a large cERM-oNE isthmus a PPM/iNE membrane contact site is established and a VN appears between the PPM and the oEM, connected to the PPM but not to the oEM. The VN in the PPC is therefore at a location corresponding to that of blob-like structures observed by confocal microscopy in *Phaeodactylum* cells broken by osmotic shock, and initially reported to possibly contain membrane vesicles (Kilian & Kroth, 2005).

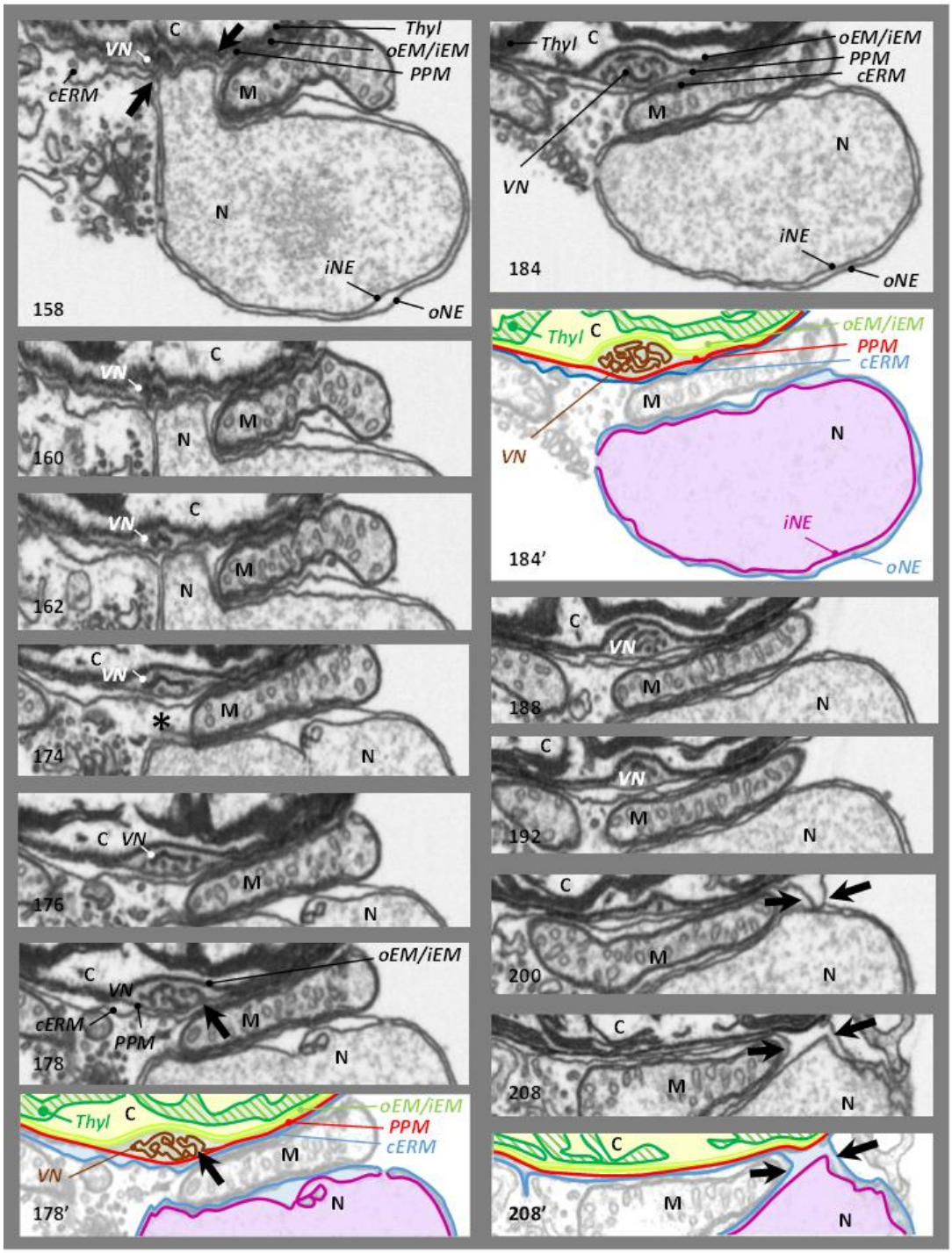

Figure 2.26 – **Serial electron micrograph scanning of a *Phaeodactylum* disrupted cell at the level of the periplastidial compartment.** The outer nuclear envelope (oNE) is shown in blue in continuity with the cERM. The inner envelope membrane (iNE) is shown in purple in tight contact with the periplastidial membrane (PPM) at the level of the nucleus-chloroplast contact zone. The vesicular network (VN) fills the space between the PPM and outer envelope membranes (oEM), shown in light green. The VN is also present in regions where the chloroplast and the nucleus are not connected (star in 174, and further). The VN shows continuity with the PPM (178) but not with the oEM. Additional direct connections between the oNE and cERM are visible in regions where no VN can be observed (208). C, chloroplast; M, mitochondrion; N, nucleus; Thyl, thylakoids.

Based on this analysis of disrupted and unpacked cells, we sought to establish whether the VN could be detected in intact cells. Figure 2.27 shows three examples. In cell 1, the VN lies within a groove between the PPM and the oEM, and appears therefore at two opposite locations of the chloroplast periphery in the vicinity of the nucleus (Figure 2.27 A, sections 203, 320 and 332, black arrows), in particular at the level of the nucleus-choroplast isthmus (sections 332, star). In cell 2, the VN appears more distant from the nucleus (Figure 2.27 B, sections 235, 330 and 378, black arrow). In cell 3, the VN appear close to the nucleus, but not in the area where the chloroplast-isthmus occurs. Overall, the VN is therefore most often present close to the chloroplast-nucleus isthmus, where it might play a functional and structural role, although other locations are possible. Using the complete set of sections of cell 1 (Figure 2.27 A) we used the volume viewer of Fiji image analysis tools (Schindelin et al., 2012) to reconstitute cross sections perpendicular to the main axis of the cell (Figure 2.27 D).

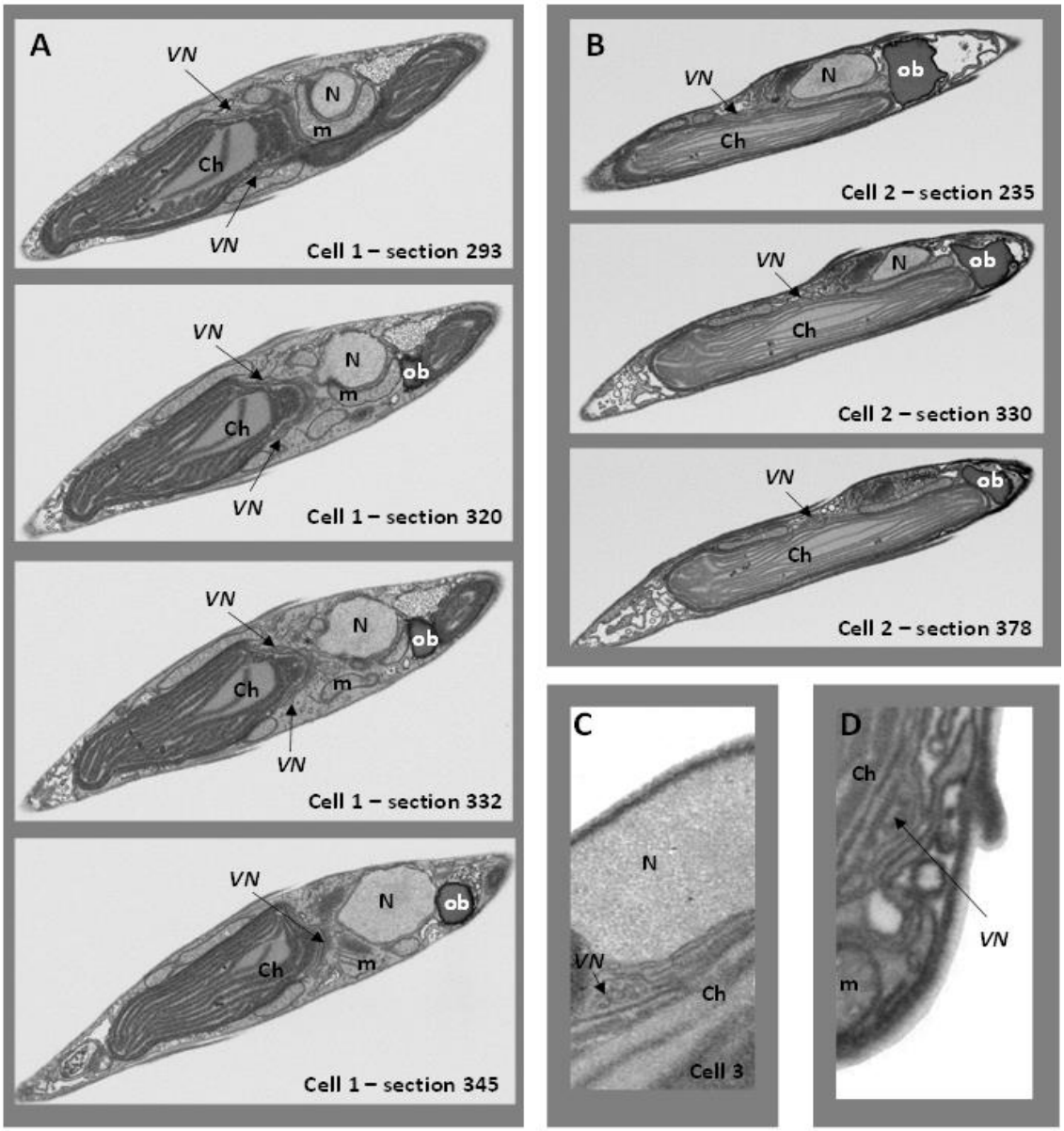

Figure 2.27 – **Serial electron micrograph scanning of *Phaeodactylum* intact cells at the level of the periplastidial compartment.** Three cells are shown (cell 1, 2 and 3) in A, B and C. (A) magnified cross-section of cell 1 is shown in (D) corresponding to the video provided in supplementary data. The vesicular network (VN) within the periplastidial compartment is shown with arrows. Ch, chloroplast; m, mitochondrion; N, nucleus; ob, oil body.

The three-dimensional organization of the VN can thus be viewed in Supplementary Materials Video A (http://dx.doi.org/10.1016/j.protis.2016.04.001). The ultrastructure of the VN in *Phaeodactylum* is therefore similar to that of the VN observed in the *Ochromonas*, although in this chrysomonad, the VN was only located close to the nucleus and appeared to have some direct connection with the oEM in addition to the PPM (Gibbs, 1979).

We also examined previously published *Phaedoctylum* electron micrographs. In most cases, it is barely possible to identify the limiting membranes of the chloroplast. In the in-depth study of dividing cells published recently (Tanaka et al., 2015), one can see in some of sections, membrane vesicular or reticulated structures in the periphery of the chloroplast, the precise nature of which could not be assessed at that time, and which might be a VN within the PPC. In other diatoms like *Thalassiosira proshkinae*, *Attheya ussurensis*, *Chaetoceros muelleri*, *Aullacoseira baicalensis*, *Synedra acus*, a similar VN structure could be observed at the periphery of chloroplasts (Bedoshvili et al. 2009). A PPM/iNE direct contact could also be observed in *Thalassiosira proshkinae* and *Chaetoceros muelleri* (Bedoshvili & Likhoshvai, 2012). Thus, the organization of the PPC characterized here in *Phaeodactylum* is likely conserved in both pennate and centric diatoms.

Probably the most important result of this study is that the PPC of diatoms is not empty. A residual cytoplasm exists, containing vesicles. None of the proteins that were reported to reside, or possibly reside, in the PPC could be predicted to act in vesicle formation, like SNAREs, Rabs, COPI, COPII, chlathrin, calveolin, ESCRT, GEFs or GAPS (Moog et al., 2011). The VN must therefore be generated by an unknown process. The identification of the proteins generating the VN in the PPC represents therefore an important challenge for future works.

The glycerolipid composition of each of the four membranes that surround the plastid is unknown, but the present study will be also crucial in future investigation related to membrane lipid biogenesis. It is difficult to speculate on the location of the classical lipids found in the envelope of primary chloroplasts in secondary plastids *i.e.* galactoglycerolipids (monogalactosyldiacylglycerol, MGDG and digalactosyldiacylglycerol, DGDG), sulfoquinovosyldiacylglycerol (SQDG) and phosphatidyldiacylgycerol (PG; Abida et al., 2015; Boudiere et al., 2014; Petroutsos et al., 2014) or if phospholipids of the ER or nuclear envelope are also present and in the same proportions in the cERM. Lipid composition of the PPM could be related to that of the cERM, by importing phosphoglycerolipids, or to that of the oEM, by importing chloroplast lipids. In photosynthetic organisms, it is usually considered that in standard conditions phospholipids are mostly present in the endomembrane system, whereas non-phosphorus glycolipids are in the plastid. The analysis of

isolated secondary plastids has been possible in Apicomplexa, which is non-photosynthetic and disconnected from the nucleus (Botte et al., 2013) and in that peculiar case, presence of galactoglycerolipids could not be shown (Botté et al., 2008; Botte & Marechal, 2014; Botte et al., 2013), whereas plastid membranes were clearly enriched in phosphoglycerolipids and even sterols (Botte et al., 2013). Galactolipids could be detected in the photosynthetically active secondary plastid of a Chromerida by immunofluorescence confocal imaging (Botte et al., 2011). The comprehensive analysis of the lipidome of *Phaeodactylum* has shown the presence of MGDG, DGDG, SQDG and even a form of SQDG acylated on its polar head (Abida et al., 2015). Based on our observations, we speculate that galactoglycerolipids are present in the iEM and oEM and that phosphoglycerolipids and betaine lipids are likely present in the cERM and the PPM. Membrane lipid transfers might occur at the level of membrane contact sites, such as that observed here between the PPM and the INE, or via dedicated platforms, such as the VN, or by other non-vesicular systems between adjacent membranes.

The continuity between the PPM and the VN suggests that the biogenesis of the VN depends on the PPC and not on the oEM. A summary of a possible scenario for the origin of the PPM and VN is thus given in Figure 2.28.

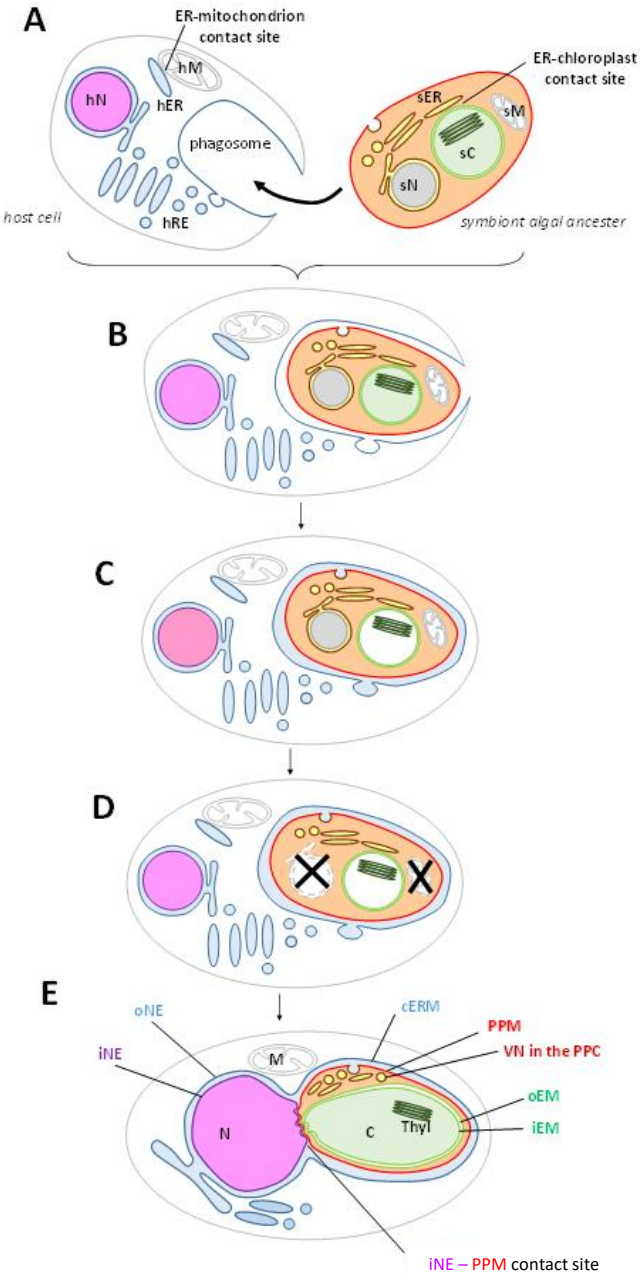

Figure 2.28 – **Stepwise reduction of the symbiont cytosol following secondary endosymbiosis in the diatom lineage.** (A) The host cell and red algal symbiont. (B) Engulfment of the red alga. (C) Residence and transmission of the red alga within the phagotrophic membrane. (D) disappearance of symbiont organelles, including the nucleus, and cytosolic structures. (E) Present status. C, chloroplast; cERM, chloroplast endoplasmic reticulum membrane; iEM, inner envelope membrane; iNE, inner nuclear envelope; M, mitochondrion; N, nucleus; oEM, outer envelope membrane; oNE, outer nuclear envelope; PPC, periplastidial compartment; PPM, periplastidial membrane; Thyl, thylakoid, VN, vesicular network.

Important questions raised by the present study lie in the molecular organization and the function of the membrane compartments we have unraveled. Are there structural proteins involved in the opening of a circular isthmus connecting the oNE and the cERM? What are the components maintaining the iNE and the PPM closely apposed inside the opened oNE-cERM isthmus? Is the iNE/PPM membrane contact site involved in the exchange of metabolites, ions, proteins or nucleic acids? The plastid of diatoms seem to encode its required set of tRNAs and rRNAs (Oudot-Le Secq et al., 2007), but other transfers of RNAs might occur. Retrograde signaling from the chloroplast to the nucleus (Lepetit et al., 2013) might also occur at the level of this chloroplast-nucleus isthmus. What are the proteins involved in the elaboration of the VN? How are the PPM and VN physically connected? What is the function of the VN? The VN could be an important platform for the import of some protein precursors, most importantly those that are folded and glycosylated after crossing the cERM and PPM (Peschke et al., 2013). Protein transport from the VN to the oEM would therefore need a non-vesicular process. This study provides therefore novel insights into the PPC ultrastructure, opening fascinating perspectives to comprehend the origin of the secondary plastid in diatoms, its protein and membrane lipid biogenesis and its sophisticated relationship with other cell compartments.

Supplementary Figure

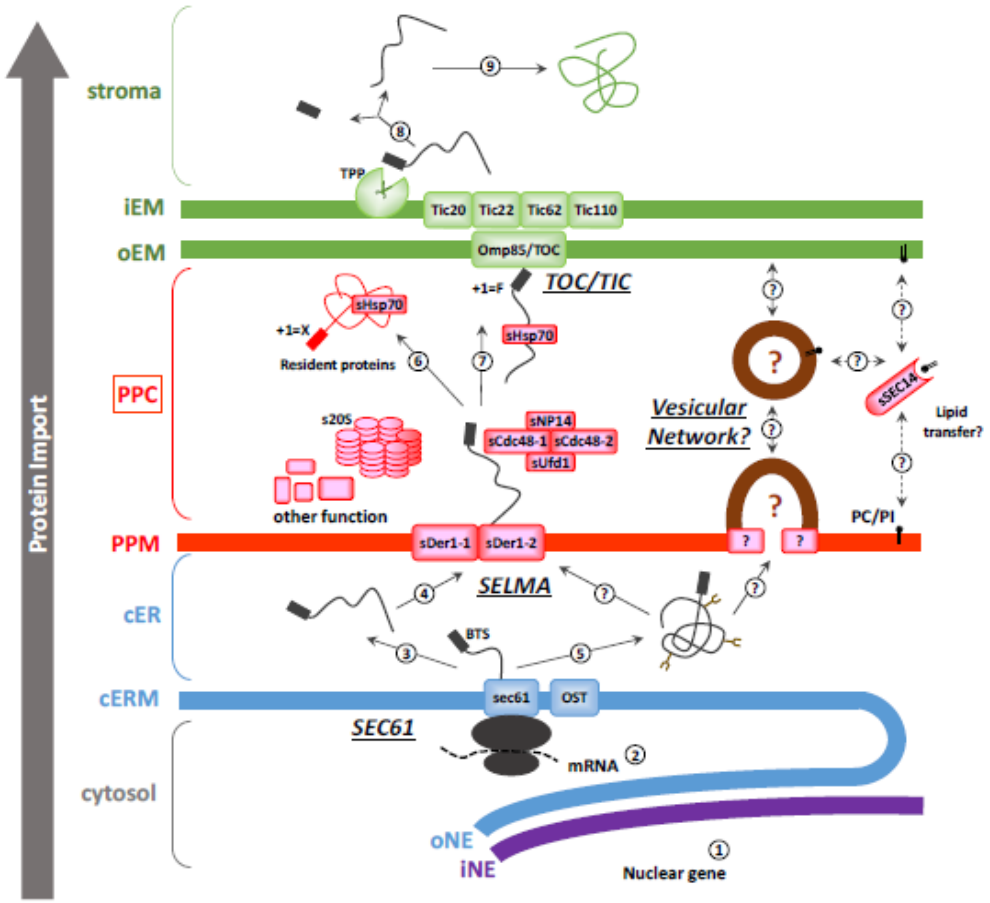

Supplementary Figure 2.29 – **Protein import across the four chloroplast limiting membrane and via the periplastidial compartment.** Following mRNA transcription (1) and translation (2), plastid protein precursors harbor a bipartite topogenic signal (Bts). A sec61 complex operates very early by co-translational mediation of pre-proteins across the cERM (3) and release an unfolded protein precursor in the lumen of the chloroplast ER (cER). This unfolded protein can be directed to the next membrane (4). Pre-proteins can also be N-glycosylated prior their transport through the PPM (5), probably by the action of an oligosaccharide transferase (OST). A translocon called the 'symbiont-specific ERAD-like machinery' (SELMA) is located in the PPM. In the SELMA, Derlin proteins, sDer1-1 and sDer1-2, interact together and with the Bts. Components of a symbiont ERAD machinery, i.e. sCdc48 ubiquitin-dependent AAA-ATPases, and their cofactors sUfd1 and sNP14, reside in the PPC. In the absence of an aromatic amino acid at position +1 of the Ctp (+1=X), proteins remain resident in the PPC. Presence of a phenylalanine or an aromatic residue (+1=F) determines the transport across the oEM and the iEM. Transport across the oEM and iEM involves components related to the chloroplast translocon, i.e. TOC and a TIC respectively. The TOC core component derives from a prokaryotic Omp85 sequence. Important TIC subunits well characterized in plant and alga chloroplasts are conserved in the iEM, i.e. Tic20, Tic22, Tic62 and Tic110. Cleavage of the Bts (8) by a transit peptide peptidase (TPP) releases mature proteins in the stroma (9). In this scheme the transfer of folded proteins is not deciphered. Possible routes via a vesicle network (VN) in the PPC are shown.

2.4.2.2 Materials and methods

***Phaeodactylum tricornutum* cultivation:** The Pt1 *Phaeodactylum tricornutum* strain (CCAP 1055/3) was obtained from the Culture Collection of Algae and Protozoa, Scottish Marine institute, UK. Culture was grown in exponential phase in ESAW (Enriched Seawater, Artificial Water) medium, using 50 mL single-use flasks with 100 rpm shaking (Certomat BS-1 incubator; Sartorius stedim biotech), a low light intensity of 20 µmol photon $m^{-2}.s^{-1}$ and a 12/12 hour light/dark photoperiod at 19°C.

Sample preparation for electron microscopy: Cells of *P. tricornutum* were harvested at logarithmic phase before the offset of the light period at 5000 x g, 10 min, 4 °C. Cells were then fixed in 0.1 M cacodylate buffer (Sigma-Aldrich), pH 7.4, containing 2.5% glutaraldehyde (TAAB), 2% formaldehyde (Polysciences) for 1 h at room temperature and prepared according to a modified protocol from T. J. Deerinck (http://ncmir.ucsd.edu/sbem-protocol).

Focused ion beam – scanning electron microscopy (FIB-SEM): Focused ion beam (FIB) tomography has been realized in a Zeiss NVision 40 dual-beam microscope. In this technique, the Durcupan embedded cells of *P. tricornutum* were cut in cross-section, slice by slice, with a Ga+ ion beam (of 700 nA at 30 kV), and each slice was imaged in scanning electron microscopy (SEM) at 5 kV using the in-column EsB back-scatter detector. For each slice, a thickness of 4 nm has been removed, and the SEM images are recorded with a pixel size of 4 nm. The image stack is then registered by cross-correlation using the StackReg plugin in the Fiji software. This procedure gives us directly an image the 3D structure of the sample with an isometric voxel size of 4x4x4 nm^3.

Video A **- The three-dimensional organization of the vesicular network (arrow) in cross sections of *Phaeodactylum tricornutum***. (http://dx.doi.org/10.1016/j.protis.2016.04.001).

2.4.3 Perspectives

The presence of a specific periplastidial compartment (PPC) was deduced based on confocal microscopy. In particular, GFP-fused protein precursors able to cross only the cERM and the PPM membranes were found in blob-like structures, which were identified as the PPC space. Taking advantage of an innovative technique used in EM, this study provides new insights into the subcellular organization of membrane compartments in diatoms unveiling the presence of a vesicular network, opening new perspectives on the mechanisms for protein import in secondary plastids. Although our knowledge on these organisms has been improved in recent years, our understanding on the dynamics of secondary plastids is still limited. Nevertheless, additional biochemical and structural techniques should be applied to provide more details on chloroplast structure, proteins and metabolites transport across the four envelope membranes. Overall this article represents a proof of concept of the use of new technologies to address previously unanswered questions. Another interesting challenge in this field would be to identify the proteins generating the vescicular network in the periplastidial compartment. To achieve this goal, correlative light electron microscopy (CLEM) can be a good strategy by combining the recognition of specific targets labelled with the green fluorescent protein (GFP) with the high resolution of images obtained by electron microscopy and possibly with the 3-Dimenstional reconstruction. Although the optimization of this technique is both time and technically demanding, it will open new opportunity to analyze transport pathways in organisms originated by different endosymbiosis events.

2.5 Ultrastructure of diatoms photosynthetic membranes

2.5.1 Preface

This article (Flori et al., 2016 manuscript in preparation) represents a significant part of my Ph.D work and focuses on the ultrastructure of the chloroplasts in the model organism *Phaeodactylum tricornutum*. In particular, this study addresses the question of how thylakoid membranes are 3-dimentionally structured in their native environment.

Unlike plants, photosynthesis in diatoms occurs within chloroplasts originated by a secondary endosymbiosis event, where no differentiation in the photosynthetic membranes between appressed regions (Grana= rich in photosystem II) and non-appressed regions (Stroma lamellae= rich in photosystem I) was reported. The more homogeneous thylakoid structure in diatoms, should promote mixing of the photosynthetic complexes, physical interaction between them and consequent energy spillover from PSII to PSI, ultimately impacting light capture and photosynthetic electron transport. In both higher plants and microalgae, light harvesting and electron flow rely on chloroplast's architecture. The completely different structural features of diatoms photosynthetic membranes could have deeply modified the light responses and electron flow properties in these organisms. So far, none of the existing model for plants chloroplast topology can interpret the available pictures of thylakoids in diatoms. In this comprehensive study, the 3D structure of *Phaeodactylum tricornutum* plastid reveals how secondary endosymbiosis algae have optimally shaped light harvesting and photosynthetic electron flow. Using *in vivo* absorption spectroscopy, limited energy spillover was found, suggesting that photosystems are largely segregated in the thylakoids. Biochemical and immunolocalization analyses support this conclusion revealing a refined compartmentation of photosystems between the external and the innermost thylakoid membranes. The model here proposed explains how absorbed light can be partitioned between the photosystems without generating restricted diffusion domains limiting electron transfer, as required for optimum photosynthesis. Thus, this study provides insights into structural and functional features of diatoms challenging the common view that photosynthetic membranes are loosely organized in chloroplasts derived form a secondary endosymbiosis.

2.5.2 Chloroplast thylakoid architecture optimizes photosynthesis in diatoms

Serena Flori[1], Pierre-Henri Jouneau[2], Benjamin Bailleul[3], Benoit Gallet[4], Leandro Estrozi[4], Christine Moriscot[4], Olivier Bastien[1], Simona Eicke[5], Alexander Schober[6], Carolina Rio Bartulos[6], Eric Maréchal[1], Peter G. Kroth[6], Dimitris Petroutsos[1], Samuel Zeeman[5], Cécile Breyton[4], Guy Schoehn[4], Denis Falconet[1], Giovanni Finazzi[1].

[1] Université Grenoble Alpes (UGA), Laboratoire de Physiologie Cellulaire et Végétale, UMR 5168, Centre National de la Recherche Scientifique (CNRS), Commissariat à l'Energie Atomique et aux Energies Alternatives (CEA), Institut National Recherche Agronomique (INRA), Institut de Biosciences et Biotechnologie de Grenoble (BIG), Grenoble, 38100 France

[2] UGA, Laboratoire d'Etudes des Matériaux par Microscopie Avancée; Institut Nanosciences et Cryogénie; Service de Physique des matériaux et Microstructures. Grenoble, France.

[3]UMR 7141 CNRS, Université Pierre et Marie Curie, Institut de Biologie Physico-Chimique (IBPC), Paris, France

[4] UGA, UMR 5075 CNRS, CEA, UGA, Institut de Biologie Structurale, Grenoble, France.

[5]Plant Biochemistry, Department of Biology, ETH Zurich, CH-8092, Zürich, Switzerland

[6]Department of Biology, University of Konstanz, 78457 Konstanz, Germany

Abstract

Photosynthesis allowed open ocean colonisation by phytoplankton and plant establishment on the land. Unlike plants, we are still unlocking the mechanisms evolved by phytoplankton to optimize their photosynthesis. Here, we reveal the unexpected complexity of plastid structure in diatoms, prominent marine eukaryotes. Biochemical and immunolocalization analyses reveal segregation of photosystems (PSs) in the loosely stacked thylakoid membranes typical of secondary plastids. Isolation of PSs within subdomains minimize physical contacts between them, thus optimizing their light utilization. However, 3D tomography shows that these domains are connected by intermingling thylakoids, to ensure fast equilibration of electron carriers and improve photosynthetic electron flow. Overall, we propose a revised topology of diatom plastid that accounts for optimum performances of secondary endosymbiotic algae in modern oceans.

Photosynthesis is the unique process converting sunlight energy into organic matter, feeding the entire planetary food chain. Photosynthesis is nearly equally accomplished on the land, which is dominated by plants, and in the ocean, which is mostly colonised by microbial phototrophs. Plant chloroplasts are derived from a cyanobacterium-like organism *via* primary endosymbiosis, while the majority of phytoplankton chloroplasts derive from a red eukaryotic microalgae *via* secondary endosymbiosis. The different phylogenetic origins have led to distinct structural chloroplast designs. Primary plastids contain a two membranes envelope, while four membranes are generally found in secondary plastids (Cavalier-Smith, 2003). Primary plastids also contain differentiated thylakoid domains where the two PSs, which are responsible for light photochemical utilization, are localized. PSII is in the appressed grana stacks, while PSI is found in the non-appressed stroma lamellae. The physical segregation of PSI and PSII avoids energy withdrawal from PSII *via* the thermodynamically unavoidable transfer to PSI (energy spillover; Dekker & Boekema, 2005). In turn, the physical confinement of the two PSs imposes the need for long-range diffusionof intermediary electron carriers (plastoquinones, plastocyanins or soluble cytochromes) within the crowded thylakoid membranes and restricted luminal space. The constraints on diffusion capacity is kinetically limiting maximum photosynthetic electron flow (Kirchhoff et al., 2004, 2011). No thylakoid subdomains are visible in secondary plastids, where available electron micrographs show loose stacks of three thylakoids with few anastomoses in some species (Bedoshvili et al., 2009). The mechanisms for optimizing light absorption and downstream electron flow in these marine algae has not been rigorously studied, despite them contributing ~20% of the planetary photosynthesis (Field et al., 1998). Here we combine functional analyses with 3D ultrastructural imaging to unveil a sophisticated thylakoid membrane network, which orchestrates photosynthesis *via* subtle subthylakoid segregation of the PSs.

2.5.2.1 Results and discussion

In diatoms, the reported loose thylakoid structure should result in random distribution of PSII and PSI, thereby favoring energy spillover via physical contacts. We tested this hypothesis by measuring changes in the absorption capacity of PSI upon inhibition of PSII photochemistry in the pennate diatom *Phaeodactylum tricornutum*. We reasoned that if PSI and PSII are in contact (Figure 2.30 A), inhibition of PSII photochemistry should increase utilization of PSII absorbed light by PSI, thus

enhancing its activity. Consistent with this idea, a faster PSI activity was observed in red algae upon inhibition of PSII (Ley & Butler, 1977; Kowalczyk et al., 2013), and interpreted as a signature of spillover in these organisms, which are considered as the ancestors of secondary plastids. Conversely, no change in activity is expected if PSI and PSII are physically separated and do not share their excitation energy, as in plants (Figure 2.30 B).

We found that in *P. tricornutum* the inhibition of PSII with 3-(3,4-dichlorophenyl)-1,1-dimethylurea (DCMU) and hydroxylamine (HA, Figure 2.30 C) did not accelerate significantly the rates of PSI (Figure 2.30 E), as revealed by the very mild increase in the oxidation rate of P700 (the primary electron donor to PSI, Figure 2.30 D) and, ultimately, of the total PSI donors pool. (Figure 2.30 E).

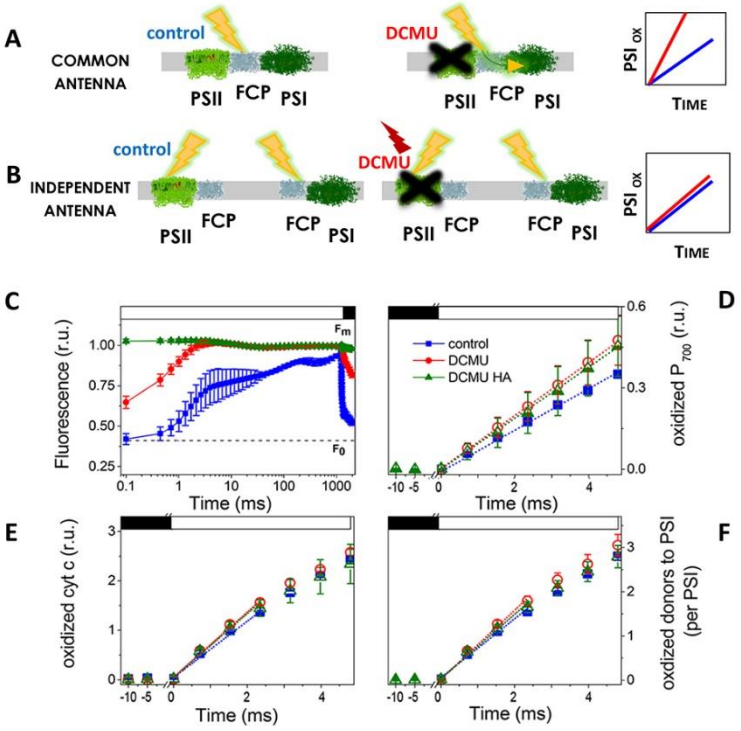

Figure 2.30 - **Experimental design to assess energy spillover in diatoms.** (A) Consequences of energy spillover from PSII to PSI on PSI activity: common antenna case. (B) Consequences of energy spillover from PSII to PSI on PSI activity: independent antenna case. (C) Fluorescence emission kinetics confirm full inhibition of PSII by DCMU and HA. (D) Kinetics of P_{700} oxidation in the light. (E) Kinetics of cyt c oxidation in the light. (F) Kinetics of oxidation of the entire pool of PSI electron donors in the light. A cyt c/PSI ratio of 3 was assumed (Supplementary Figure 2.34). Light intensity was 1100 µmol photons m^{-2} s^{-1}. Solid blue squares: control; empty red circles: DCMU 40µM, blue tringles: DCMU 40µM + HA 0.2 mM. Mean ± SEM (n = 6, for 3 biological samples). FCP: Fucoxanthin Chlorophyll light harvesting antenna Protein. F_0: mimimum fluorescence emission (active PSII). Fm: maximum fluorescence emission (inactive PSII).

Similar results were found in cells exposed to limiting or saturating light intensities (Supplementary Figure 2.35). The observed increase (less than 15 %) is much smaller than the two-fold effect reported in red algae (Kowalczyk et al., 2013), suggesting that, although detectable (Yokono et al., 2015), spillover is limited in *P. tricornutum*. Two possibilities can account for this finding: *i.* the existence of interaction barriers (due to lipid/biochemical surroundings) preventing energy exchange between the PSs or *ii.* the physical segregation of PSI and PSII in different thylakoid domains. To distinguish between them, we immunolocalized the two PSs in intact cells prepared with the Tokuyasu protocol (Tokuyasu, 1973), an optimal method to preserve membrane structures (Supplementary Figure 2.36). We found that PSI was preferentially localized in the "peripheral" stromal-facing thylakoid membranes (Figure 2.31 A and Figure 2.31 C, green sectors). Conversely, PSII was mostly found in the "core" thylakoid membranes (Figure 2.31 B and Figure 2.31 C, violet). These findings were substantiated by a statistical analysis (principal component analysis) of 149 images (Figure 2.31 D, E and F, Table S1, Table S2).

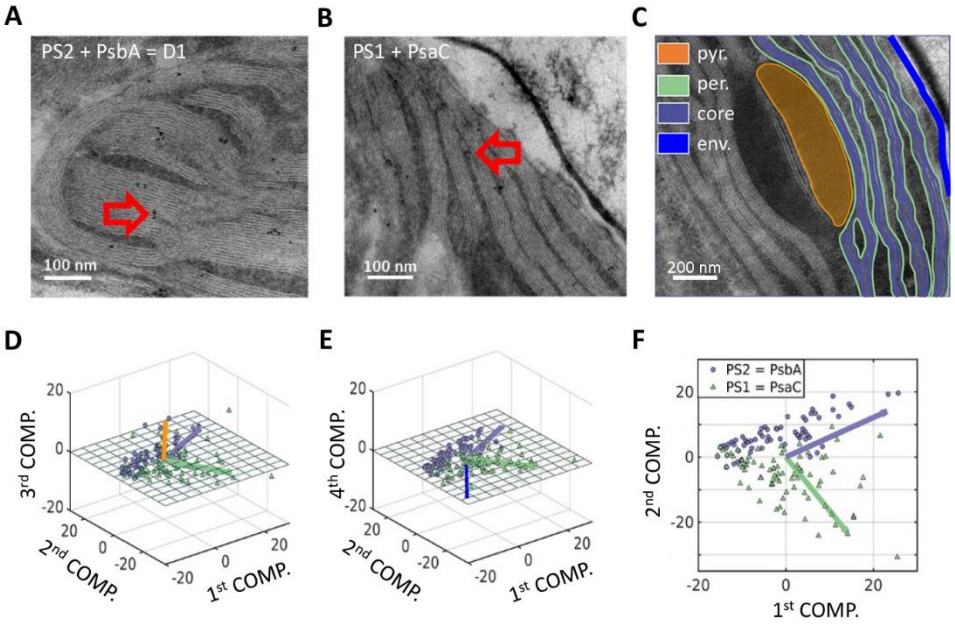

Figure 2.31 - **Immunolocalization of PSI and PSII in the thylakoid membranes of *P. tricornutum*.** (A) Localization of PSII using an antibody against the PsbA (D1) subunit. (B) Localization of PSI using an antibody against the PsaC subunit. (C) EM picture of *P. tricornutum* thylakoid membranes; showing four areas: the internal part (CORE, violet) the external, peripheral one (PERIPH., green), the pyrenoid (Orange) and the envelope (blue). (D), (E), (F) Principal Component Analysis of PSI and PSII immunolocalization. Analysis was performed on 149 images (violet dots: localization of PSII; green triangles: localization of PSI). The first two components represent more than 93% of the variance (Table S1). See methods for further explanation. Green arrow: peripheral variable. Violet arrow: core variable. Orange arrow: Pyrenoid variable. Blue arrow: envelope variable.

We complemented the immunolocalization analyses with biochemical fractionation. In grana-containing thylakoids (see *e.g*. Berthold et al., 1981), PSI is located in the stromal-exposed thylakoid lamellae and more accessible to mild detergents than PSII, which is contained in the appressed membranes of the grana. Chloroplasts isolated from *P. tricornutum* cells were solubilized using increasing concentration of the mild detergent digitonin. Supernatant and pellet were recovered after centrifugation, and analyzed for PSII and PSI by immunoblotting. We found (Supplementary Figure 2.37) that the detergent concentration required to solubilize PSI was lower (0.2%) than that needed to extract PSII (0.5%), supporting their differing locations in stroma-accessible and less accessible membranes of the diatom chloroplasts, respectively.

Since it optimally preserves membrane structures, the Tokuyasu method allowed us to observe unexpected, and previously undescribed features of the *P. tricornutum* thylakoids. We detected regions where membranes are apparently interconnected (Supplementary Figure 2.38, A and B) and regions where additional layers abruptly "disappear" in cross sections (Supplementary Figure 2.38 C, red arrows) as if tilting out of the micrograph plane. These pictures suggested the existence of a more complex 3D thylakoid network than the simple layout of 3 loosely juxtaposed thylakoids proposed so far. We thus collected 1200 ultrathin sections with focused ion-beam scanning electron microscopy (FIB-SEM) to reconstruct the 3D structure of the entire *P. tricornutum* cell (Figure 2.32 A, Video B). We first observed the organelles and their interactions (Supplementary Figure 2.39): the mitochondrion (red) appears as a continuous network of membranes sitting on the chloroplast (green, Supplementary Figure 2.39 A). The mitochondrion is partially sandwiched between the plastid and the nucleus (blue, Supplementary Figure 2.39, A and B), the two latter directly in contact at a single point (Supplementary Figure 2.39 C, Video C). We confirmed the presence of parallel layers of thylakoids in the plastid, but also revealed the presence of connecting thylakoids (green) linking the different thylakoid layers (Figure 2.32 B violet). These "bridging" thylakoids were distinct from the chloroplast lipoprotein particles, the plastoglobules (Supplementary Figure 2.40).

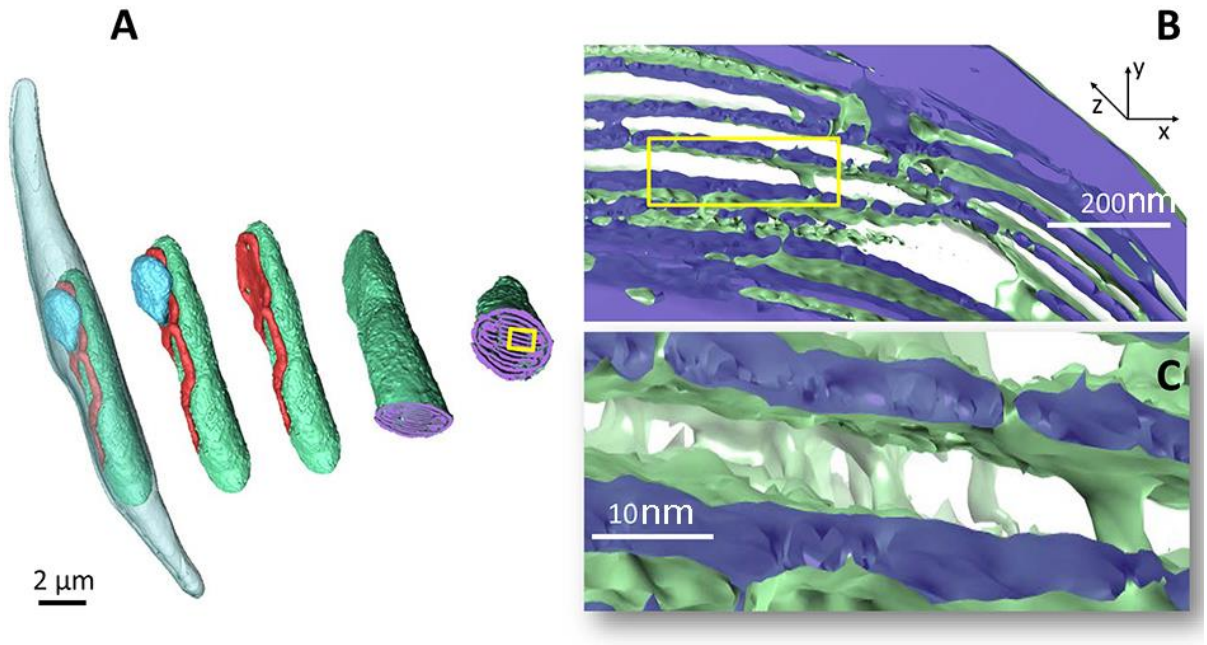

Figure 2.32 **- Three-dimensional organisation of thylakoid membranes in *P. tricornutum* cells.** (A) 3D reconstruction of an intact *P. tricornutum* cell, based on FIB-SEM images. (B) Reconstruction of thylakoid membranes in the region indicated by the yellow box in (A). (C) Magnification of the region indicated by the yellow box in B. The greater depth in the "z" direction highlights the presence of several connecting thylakoids. Data are representative of three different tomograms.

Unlike plants (Kirchhoff et al., 2004, 2011), the continuum of both the lipid and luminal compartments would prevent isolation of the two PSs in slow diffusion domains. To assess their presence in *P. tricornutum*, we used a previously employed functional approach (Kirchhoff et al., 2004). We first evaluated the theoretical equilibrium constants between PSI and its electron donor (K_{th} = 16) from the redox potentials of cyt c_6 (349 mV, Akazaki et al., 2009) and of P_{700} (420 mV, Witt et al., 2003; Nakamura et al., 2005). We then compared K_{th} with the experimental equilibrium constant (K_{exp}). The latter was calculated (using eq. 2, see methods) from an 'equilibration plot' (Figure 2.33 A), *i.e.* the relationship between oxidized P_{700} and oxidized c-type cytochromes (cyt c^+) during dark re-reduction after illumination (Supplementary Figure 2.41, B and C). In the absence of diffusion domains, $K_{exp} = K_{th}$. In this case P_{700}^+ is almost entirely reduced prior to c-type cytochromes, owing to the high K_{th} value (Supplementary Figure 2.34). Conversely, deviation from thermodynamic equilibrium ($K_{exp} < K_{th}$) is expected if electron flow is limited by diffusion domains. In this case, the fate of PSI and cyt c is determined by their relative stoichiometry in every domain. In compartments with a low PSI/cyt c ratio (*e.g.* domain 2 in Figure 2.33 B), a complete reduction of P_{700}^+ and a partial reduction of cytochromes is predicted. At the same time, P_{700}^+ reduction is incomplete in domains with a high P_{700}/cyt ratio (*e.g.* domain 1 in Figure 2.33 B), leading to P_{700}^+ accumulation. Because the equilibration plot averages the redox state of P700 and cyt c in all domains, the concomitant presence of P_{700}^+ (in domains 1) and of reduced cyt c (in domains 2) will lead to a K_{exp} value lower than K_{th}. We generated several equilibration plots by poisoning electron flow with increasing concentrations of DCMU (Figure 2.33 A and Supplementary Figure 2.41 D), and found that diffusion is restricted (*i.e*. $K_{exp} < K_{th}$), when PSII generates more than 150 electrons per seconds (Figure 2.33 A, blue and green data points). However, thermodynamic equilibration is achieved when this rate is lowered below 100 electrons s^{-1} (Figure 2.33 A, red points). We conclude that compartmentation of PSI and PSII in different thylakoid domains also generates diffusion domains in diatoms (Figure 2.33 B). However, their equilibration time (100 s^{-1} or 10 ms) is much faster than in plants (7 s^{-1} ca or 150 ms, Kirchhoff et al., 2004), likely reflecting the lower degree of structural heterogeneity of diatoms thylakoids.

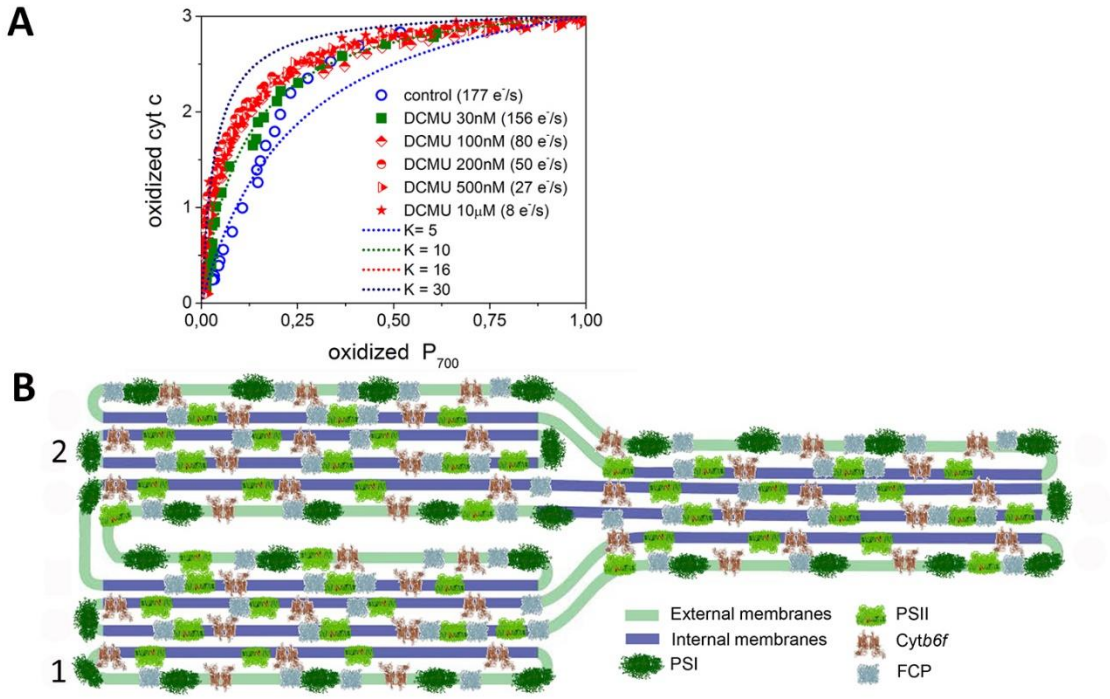

Figure 2.33 - **Structural arrangement of the photosynthetic membranes in *P. tricornutum.*** (A) Equilibrium plots for the components of the high potential chain. Redox signals of cyt c and P_{700} in the light were plotted against each other. The dotted lines represent simulations corresponding to different values of the equilibrium constant. The rate of electron flow is calculated from data in Supplementary Figure 2.40. (B) Cartoon representing a possible arrangement of the photosynthetic complexes in a likely 3 thylakoid layers arrangement of the photosynthetic membranes in *P. tricornutum*. The different PSI and PSII localization within the peripheral (green) and the core membranes (violet) is shown. PSI: photosystem 1; PSII: photosystem 2, FCP: fucoxanthin chlorophyll antenna protein, $Cytb_6f$: cytochrome b_6f complex.

2.5.2.2 Conclusions

Overall, our 3D reconstruction of *P. tricornutum* with FIB-SEM reveals an intricate network of the photosynthetic membranes (Figure 2.32, Supplementary Figure 2.40), reversing previous ideas (Spetea et al., 2012) that photosynthetic membranes of secondary endosymbiosis chloroplasts are loosely structured. Biochemical and immunolocalization analyses further reveal a subtle compartmentation of the PSs between the peripheral and core thylakoid membranes (Figure 2.33 B). Their location is compatible with the proposed lipid composition of the two fractions, because the core membranes are apparently enriched in lipids that favor PSII stability and function (Lepetit et al., 2012). The observed thylakoid structure accounts for optimum partitioning of absorbed light between the photosystems (very limited spillover), thus providing a rationale for the previously-observed high capacity of PSII to dissipate excess light thermally (Lavaud et al., 2002). Indeed, no such response is expected if surplus energy in PSII were to be dissipated *via* spillover to PSI, as in red algae (Kowalczyk et al., 2013). Moreover, the thylakoid structures avoid restriction of electron flow. On one side, the inter-thylakoid membrane bridges (Figure 2.32, Supplementary Figure 2.40) provide a continuum of the membranous and luminal compartments, avoiding diffusional limitations. On the other side, possibly because of the loose thylakoid stacking, the size of the thylakoid lumen (7.1 ± 15 nm, average of 100 estimates from 6 different preparations) is much larger than in plants (4.5 nm, Kirchhoff et al., 2011), where it is equal to that of plastocyanin, and thus limits its diffusion between PSI and the cyt b_6f (Kirchhoff et al., 2004). Conversely the lumen size in diatoms is twice larger than the size of the soluble electron carrier, cyt c_6 (~ 33 x 23 Å, Akazaki et al., 2009). This should facilitate diffusion of this redox carrier, and contribute to the very fast redox equilibration in diatoms. Consistently, lumen widening (up to values similar to those measured in diatoms), has been shown in high light exposed plants to facilitate electron flow and reduce photodamage (Kirchhoff et al., 2011). Overall, optimal absorption with no kinetic limitation of photosynthesis likely represents the strategy evolved in diatoms to implement their photosynthetic performances in the ocean.

Our data also show the intimate physical contacts between all the organelles. This not only reveals the cellular framework for the extensive energetic exchanges between chloroplast and mitochondria recently reported (Bailleul et al., 2015), but also pinpoints a site at which redox signalling between the plastid and the nucleus could occur (e.g. Lepetit et al., 2013). In line with this hypothesis, recent results in plants suggest that chloroplast evaginations (*i.e.* stromules) transiently

connect to the nucleus for metabolic exchanges and retrograde signalling between these compartments (Dietz et al., 2016).

2.5.2.3 Materials and Methods

***Phaeodactylum tricornutum* cultivation.** The *Phaeodactylum tricornutum* Pt1 strain (CCAP 1055/3) was obtained from the Culture Collection of Algae and Protozoa, Scottish Marine institute, UK. Cells were grown in the ESAW (Enriched Seawater, Artificial Water) medium (Berges et al., 2001), in 50 mL flasks in a growth cabinet (Certomat BS-1, Sartorius Stedim, Germany), at 19°C, a light intensity of 20 µmol photon $m^{-2}.s^{-1}$, a 12/12 hours light/dark photoperiod and 100 rpm shaking . Cells were collected in exponential phase, concentrated to a density of 2 * 10^7 cells mL^{-1} and used for experimental characterization.

Spectroscopic measurements. Spectroscopic analysis was performed at room temperature, using a JTS-10 spectrophotometer (Biologic France). To assess energy spillover from PSII to PSI, redox changes of P_{700} and of its electron donor pool were followed. In diatoms, a c-type cytochrome is the PSI electron donor, replacing plastocyanin as the electron donor to PSI. We will refer to the latter as cytochrome c_6 (as in Inda et al., 1999), instead of alternative nomenclatures proposed earlier (e.g. cytochrome c*x*, Weigel et al., 2003; cytochrome c_6A, Howe et al., 2006). We will also define the pool of photosynthetic type proteins (cyt c_6 + cyt *f* of the cytochrome b_6f complex) as "cyt c". Indeed, due to the absorption features, it is not possible to distinguish spectroscopically cyt c_6 form cytochrome *f*. Because of the high equilibrium constant between P_{700} and the cytochrome pool, kinetic analysis was extended also to the latter, to quantify the whole amount of electrons that was delivered to PSI in the presence and absence of PSII activity. P_{700} redox changes were measured at 705 nm. To verify that the possible contribution of fluorescence emission was not interfering with the measurements, experiments were repeated at 820 nm (where fluoresce emission is not detected). Similar results were obtained at both wavelengths, indicating that interference from fluorescence emission was negligible. Cyt c was calculated as [554]-0.4.[520]-0.4.[566], where [554], [520] and [566] are the absorption difference signals at 554 nm, 520 nm and 566 nm, respectively (Bailleul et al., 2015). Indeed, due to the absorption features, it is not possible to distinguish spectroscopically cyt c_6 form cytochrome *f*.

Kinetics of oxidation of P_{700}, cyt c and of the total donors to PSI oxidation result from concomitant electron injection by PSII and withdrawal by PSI. Therefore, to calculate the true PSI oxidation rates,

we calculated first their respective reduction rates, which were evaluated as the slope of signal relaxation upon switching the light off (Supplementary Figure 2.34 B, S_D slope). By adding this slope to the apparent oxidation rates, which we evaluated from the slope in the light (Dl), we obtained the absolute oxidation kinetics (see Supplementary Figure 2.34 for an example in the case of the total PSI electron donors pool). This procedure is needed because, by inhibiting PSII activity, DCMU modifies the reduction rates of cyt c and P_{700}, This leads to an apparent increase of the PSI and cyt c oxidation rates, which mimics the occurrence of energy spillover.

Inhibition of PSII by DCMU and HA was probed measuring the changes in chlorophyll emission from F_0 (minimum fluorescence level in which Q_A, the primary quinone acceptor of PSII is oxidized) to the Fm level, in which Q_A is fully reduced because PSII activity is blocked. As shown in Figure 2.30 C and Supplementary Figure 2.35 A, addition of DCMU alone cannot fully reduce Q_A in the short time (4 ms) employed to measure oxidation of P_{700} and of cyt c, expecially at low light. Because induction of spillover required the full reduction of Q_A, this inhibitor alone could not be sufficient to probe energy spillover in all the experimental conditions employed in this work (e. g. low light in Supplementary Figure 2.35). On the other hand, complete reduction of Q_A is achieved in the presence of HA, because this inhibitor prevents reoxidation of reduced Q_A in PSII (Cheniae & Martin, 1971). By ensuring QA reduction (Fm level) at the beginning of illumination (Figure 2.30 C, Supplementary Figure 2.35 B and C, dark), HA ensures optimum condition to evaluate spillover even in low light (Supplementary Figure 2.35 A).

To evaluate the equilibrium constants between cytochrome c and P_{700} the following equation was used to relate redox changes of P_{700} and of cyt c to the equilibrium constant *K*:

$$K = \frac{[cytc^{ox}].[P_{700}]}{[cytc].[P_{700}^{ox}]} \qquad [1]$$

where [*cytc*], [$cytc^{ox}$], [P_{700}] and [P_{700}^{ox}] represent the concentration, at equilibrium, of the oxidized and reduced form of the cyt *c* and P_{700} pools.

From equation [1] the relationship between the relative amount of oxidized P_{700} and of cyt *c* can be derived as:

$$y = \frac{K.x}{1 + x.(K - 1)}, \qquad [2]$$

with $y = \frac{cytc^{ox}}{cytc + cytc^{ox}}$ [3]

and $x = \frac{P_{700}^{ox}}{P_{700}^{ox} + P_{700}}$ [4]

Chloroplast purification. To purify intact chloroplasts from *P. tricornutum,* cells were harvested by centrifugation at 5000 *g*, 10 min, 4 °C allowing to get a pellet, which was then resuspended gently with 10 mL of isolation buffer (0.5 M Sorbitol; 50 mM Hepes-KOH; 6 mM EDTA; 5 mM $MgCl_2$; 10 mM KCl; 1 mM $MnCl_2$; 1% Poly Vinyl Pyrrolidone 40 [K30]; 0.5% BSA; 0.1% cysteine, pH 7.2-7.5) and passed slowly through a French Press at 9,000 bars. Ten milliliters of the isolation buffer were added to the mixture of broken cells on ice in the dark before centrifugation at 300 *g* for 8 min to remove intact cells. The supernatant was collected and centrifuged at 2,000 g for 10 min at 4 °C. The pellet was gently dissolved with a soft paint-brush in 2 ml of washing buffer (0.5 M Sorbitol; 30 mM Hepes-KOH; 6 mM EDTA; 5 mM $MgCl_2$; 10 mM KCl; 1 mM $MnCl_2$; 1% PVP 40 [K30]; 0.1% BSA, pH 7.2-7.5) and loaded on a discontinuous Percoll gradient (10%, 20%, 30%) in the same buffer. The mixture of broken cells and plastids was centrifuged in an ultracentrifuge (with SW41Ti rotor) at 10 000 *g* for 35 min. The chloroplast fraction accumulated in the 20 % layer of the Percoll gradient. The band was collected and diluted in the washing buffer (without BSA) and centrifuged again at 14,000 *g* for 10 min at 4°C. Chloroplasts intactness was tested with a Clark electrode (Hansatek, UK) using sodium ferricyanide as an electron acceptors. Oxygen evolution in saturating light was measured before and after an osmotic shock (induced by incubation for 5 min in the washing buffer without sorbitol). The ratio between the two rates was used to evaluate intactness, which turned out to be > 80% in our case.

Membrane solubilization and immunoblot analysis. To solubilize the two different chloroplast compartments (INTERNAL and EXTERNAL), digitonin ($C_{56}H_{92}O_{29,}$ Sigma Aldrich) was prepared at different concentrations (0.2-0.5-1.5%). Chloroplasts were incubated for up to 30 min at 4°C with the detergent and centrifuged at 11,000 g for 5 min (Beckmann rotor TLA-100). Both the supernatant and the pellet were collected and their protein content evaluated by immunoblot analysis. Samples (0.75 µg of protein) were loaded on 7% or 13% SDS-PAGE gels and blotted onto nitrocellulose membranes. Antisera against PSI (PsaC, PSI-C core subunit of photosystem I, Agrisera,

Sv) and PSII (PsbA, D1 protein of PSII, Agrisera, Sv) were detected by ECL using a CCD (charge-coupled device) imager (Chemidock MP Imaging, Bio-Rad, USA).

Sample preparation for immunolocalization using the Tokuyasu protocol. Cells of *P. tricornutum* were fixed in a double-strength fixative (4% (w/v) formaldehyde, 0.4% (v/v) glutaraldehyde) in PHEM buffer (PIPES 60 mM, HEPES 25 mM, EGTA 10 mM, $MgCl_2$ 2 mM; pH 7) in an equal volume to the culture medium (ESAW), and then diluted into a standard strength fixative (2% (w/v) formaldehyde (EMS, USA) and 0.2% (v/v) glutaraldehyde (EMS, USA)). After 15 min, fresh standard strength fixative was replaced and fixation proceeded for 30 min at room temperature, under agitation. Cells were washed 3 times with 50 mM glycine in PHEM buffer and after centrifugation were embedded in 12% gelatin in PHEM. The gelatin-embedded blocks were cryo-protected in 2.3 M sucrose in rotating vials at 4°C (overnight). Samples vitrification was obtained in liquid nitrogen following the plunge and freezing technique (*9)*. Thin sections (80 nm) were prepared at -110°C with a diamond knife (Diatome) and the blocks were prepared with an ultracryomicrotome (UC7, Leica Microsystems, Germany). Ribbons were picked-up with a drop of 1% (w/v) methylcellulose/1.15 M sucrose in PHEM buffer. Sections were thawed and transferred to Formvar carbon-coated nickel grids.

Immunolabelling was performed using an automated system (Leica microsystems EM IGL). The sucrose/methyl cellulose mixture was removed washing the grids with PBS 3 times for 2 min. Then the free aldehyde groups were inactivated on phosphate buffer saline solution (PBS) + 0.05 M glycine, pH 7.4, 15 min. The hydrophobic areas were blocked with the Aurion blocking solution for 30 min before washing three times in PBS + 0.1% BSA-c pH 7.4 for 2 min. The grids were incubated for 60 to 90 min in the diluted primary antibody (1-5 µg/ml in PBS + 0.1% BSA-c pH 7.4). Negative controls were incubated only with BSA-c buffer. After six washing steps (PBS + 0.1% BSA-c pH 7.4 for 5 min) the grids were incubated for 90 to 120 min in the diluted secondary antibody coupled to ultrasmall 6 nm gold particles in PBS (1:20 in PBS + 0.1% BSA-c pH 7.4). The grids were then extensively washed (6 times for 5 min in PBS + 0.1% BSA-c pH 7.4 and 6 times for 2 min in PBS, pH 7.4). Samples were post-fixed with 2% glutaraldehyde in PBS, pH 7.4, for 5 min and finally washed (3 times in PBS, pH 7.4, for 2 min and 6 times with deionized water for 2 min). Sections were enhanced with silver (Aurion R-Gent SE-EM) for 25 min and again washed on deionized water (6 times for 2 min). Finally, samples were contrasted with heavy metal treatment (4% neutral uranyl acetate for 5 min followed by 0.4% uranyl acetate in 2% methylcellulose for 5 min at 0°C), then

washed on liquid droplets (PBS, pH 7.4) and dried. For observation, grids were incubated 5 min on 2% uranyl oxalate (pH 7) and transferred to a mixture of 1.6% methyl cellulose and 0.4% uranyl acetate on ice, the excess of the viscous solution was drained away and the grids were let to dry. Grids were examined in an electron Tecnai 12 microscope (FEI, USA).

FIB-SEM analysis. *P. tricornutum* cells were fixed in 0.1 M cacodylate buffer (Sigma-Aldrich), pH 7.4, containing 2.5% glutaraldehyde (TAAB), 2% formaldehyde (Polysciences) for 1 h at room temperature and prepared according to a modified protocol from (https://ncmir.ucsd.edu/sbem-protocol). Focused ion beam (FIB) tomography was performed with a Zeiss NVision 40 dual-beam microscope. In this technique, the Durcupan (Sigma-Aldrich) resin embedded cells of *P. tricornutum* were cut in cross-section, slice by slice, with a Ga+ ion beam (of 700 nA at 30 kV), and each slice was imaged in scanning electron microscopy (SEM) at 5 kV using the in-column EsB back-scatter detector. For each slice, a thickness of 4 nm was removed, and the SEM images were recorded with a pixel size of 4 nm. The image stack is then registered by cross-correlation using the StackReg plugin in the Fiji software. For 3D reconstitution a stack of 600 images were analyzed with FIJI Image J software and projected in 3-dimension (x,y,z axis) using the AVIZO (FEI, USA) and CHIMERA softwares (https://www.cgl.ucsf.edu/chimera/, UCSF, USA).

Principal components analysis (PCA). The principal components analysis (PCA) is an exploratory technique that is used both to describe the structure of high dimensional data by reducing its dimensionality (Lebart et al., 2000) and to detect any groupings in the data set (Takeuchi et al., 2003). It is a linear transformation that converts n original variables (here, the localization) into n new variables (the principal components), which (i) are ordered by the amount of variance explained (ii) are uncorrelated and (iii) explain all variation in the data. We performed PCA considering four possible subcellular compartments for our antibodies: the internal and external thylakoid membranes, as well as the pyrenoid and the envelope, to account for possible aspecific labelling. This led to a 4-dimension localization space (INTERNAL, EXTERNAL, PYRENOID and ENVELOPE) of the 149 images where values are the number of immunolabeling in the given localization. First, the localization space of each of the 149 images is normalized, by subtracting the mean and dividing by the standard deviation of values for each localization.

To represent the distribution of these normalized dimensional data for the 149 images, the direction (a 4-dimensional vector) giving the largest possible variance of the distribution (that is, accounts for

as much of the variability in the data as possible) is selected as the direction for the first principal component. Then, the direction (another 4-dimensional vector) orthogonal to the previous one(s) giving the largest possible variance of the distribution is selected as the direction for the second principal component. The repetition of this procedure automatically selects vectors representing the scatter of the distribution from major ones to minor ones**.** Based on singular values decomposition, PCA is a principal axis rotation of the original variables that preserves the variation in the data. Therefore, the total variance of the original variables is equal to the total variance of the principal components. The principal component coefficients correspond to the percentage of explained variance. All statistical analysis has been done with the R software (R Development Core Team, 2008).

Logistic regression. The logistic regression is the appropriate regression analysis to conduct when the dependent variable is dichotomous and is assumed to be a stochastic event. Logistic regression is used to describe data and to explain the relationship between one dependent binary variable and one or more independent variables. The two major assumptions are: (i) that the outcome must be discrete, otherwise explained as, the dependent variable should be dichotomous in nature (ii) there should be no high intercorrelations (as demonstrated by Tabachnick & Fidell, 2012), the assumption is met for values less than 0.9) among the predictors.

The two type of antibody are variables that can have only two possible discrete values: PsaC=PSI or PsbA=PSII. We use a model dose-response relationship where the predictors are the multiple continuous variables: number of immunolabeling in the different localizations (INTERNAL, EXTERNAL, PYRENOID and ENVELOP). Since probabilities have a limited range and regression models could predict off-scale values below zero or above 1, it makes better sense to model the probabilities of getting a given antibody on a transformed scale; this is what is done in logistic regression analysis (Hosmer et al., 2013). A linear model for transformed probabilities can be set up as $\log it(p) = \alpha_0 + \alpha_1 x_1 + ... + \alpha_k x_k$ in which $\log it(p) = \log(\frac{p}{1-p})$ is the log odds. Each x_i is the number of gold beads in the localization *i* and statistics about the coefficients $alpha_i$ will provide insight about the impact of the localization *I* on the probability to get a given antibody. The analysis of deviance table and the Akaike information criterion allows the identification of the relevant predictors (Dalgaard, 2002).

The table of correlations shows that there are no strong intercorrelations between the variables (supplementary materials). Starting from a complete model (supplementary materials) and based on the variables coefficients p-values (Pr(>|z|)), we see that we can recursively delete the two variables ENV and PYR without significantly reduce the Akaike information criterion (AIC; Akaike, 1974) which is a common measure of the relative quality of a statistical model for a given set of data. The final model demonstrates that the relevant variables to predict the antibody are the number of immunolabeling in INTERNAL (p-value=5.54e-06) and EXTERNAL (p-value<0.0032) area. Bootstrap procedure allows the evaluation of the average percentage of wrong prediction: 9.4% of the image will have a wrong immunolabeling (Table S2).

Appendix: output results of the Logistic regression from the R software.

Original model: Antibody = CORE = PERIPHERAL + ENVELOP + PYRENOID

```
  > summary(glm(ANTIBODY~INT+EXT+ENVELOP+PYRENOID,binomial))
Call:
glm(formula = ANTIBODY ~ CORE + PHERIPHERAL + ENVELOP + PYRENOID, family = binomial)
Deviance Residuals:
   Min      1Q  Median      3Q     Max
-3.0638  -0.4587   0.2385   0.6176   3.1801
Coefficients:
            Estimate Std. Error z value Pr(>|z|)
(Intercept)  1.99757    0.96646   2.067   0.0387 *
CORE        -0.07048    0.01541  -4.574 4.79e-06 ***
PERIPHERAL   0.04284    0.01628   2.632   0.0085 **
ENVELOP     -0.01526    0.03754  -0.407   0.6843
PYRENOID    -0.01797    0.02578  -0.697   0.4858
---
Signif. codes:  0 ‘***’ 0.001 ‘**’ 0.01 ‘*’ 0.05 ‘.’ 0.1 ‘ ’ 1
(Dispersion parameter for binomial family taken to be 1)
   Null deviance: 205.42  on 148  degrees of freedom
Residual deviance: 114.74  on 144  degrees of freedom
AIC: 124.74
Number of Fisher Scoring iterations: 5
  > glm1 <- glm(ANTIBODY~CORE+PERIPHERAL+ENVELOP+PYRENOID,binomial)
>
> glm2 <- glm(ANTIBODY~CORE+PERIPHERAL+PYRENOID,binomial)
>
> anova(glm1,glm2,test="Chisq")
Analysis of Deviance Table
Model 1: ANTIBODY ~ CORE + PERIPHERAL + ENVELOP + PYRENOID
Model 2: ANTIBODY ~ CORE + PERIPHERAL + PYRENOID
  Resid. Df Resid. Dev Df Deviance Pr(>Chi)
1       144     114.74
2       145     114.90 -1  -0.1633   0.6861
```

Second model: Antibody = CORE = PERIPHERAL + PYRENOID

```
> summary(glm2)
Call:
glm(formula = ANTIBODY ~ CORE + PERIPHERAL + PYRENOID, family = binomial)
Deviance Residuals:
   Min      1Q  Median      3Q     Max
-3.0994  -0.4713   0.2454   0.5992   3.1901
Coefficients:
            Estimate Std. Error z value Pr(>|z|)
(Intercept)  1.91291    0.93737   2.041  0.04128 *
CORE        -0.06995    0.01530  -4.573  4.8e-06 ***
PERIPHERAL   0.04323    0.01618   2.672  0.00754 **
PYRENOID    -0.01621    0.02531  -0.640  0.52194
---
```

```
Signif. codes:  0 ‘***’ 0.001 ‘**’ 0.01 ‘*’ 0.05 ‘.’ 0.1 ‘ ’ 1
(Dispersion parameter for binomial family taken to be 1)
    Null deviance: 205.42  on 148  degrees of freedom
Residual deviance: 114.90  on 145  degrees of freedom
AIC: 122.9
Number of Fisher Scoring iterations: 5
> drop1(glm2,test="Chisq")
Single term deletions
Model:
ANTIBODY ~ CORE + PERIPHERAL + PYRENOID
           Df Deviance    AIC     LRT  Pr(>Chi)
<none>          114.90 122.90
CORE       1   143.08 149.08 28.1799 1.105e-07 ***
PERIPHERAL      1   122.73 128.73  7.8320  0.005133 **
PYRENOID  1   115.32 121.32  0.4215  0.516171
---
Signif. codes:  0 ‘***’ 0.001 ‘**’ 0.01 ‘*’ 0.05 ‘.’ 0.1 ‘ ’ 1
>
Final model: Antibody = CORE + PERIPHERAL
> glm3 <- glm(ANTIBODY~INT+EXT,binomial)
>
> anova(glm2,glm3,test="Chisq")
Analysis of Deviance Table
Model 1: ANTIBODY ~ CORE + PERIPHERAL + PYRENOID
Model 2: ANTIBODY ~ CORE + PERIPHERAL
  Resid. Df Resid. Dev Df Deviance Pr(>Chi)
1       145     114.90
2       146     115.32 -1 -0.42154   0.5162
>
> summary(glm3)
Call:
glm(formula = ANTIBODY ~ CORE + PERIPHERAL, family = binomial)
Deviance Residuals:
    Min       1Q   Median       3Q      Max
-3.0857  -0.4916   0.2485   0.5906   3.2036
Coefficients:
             Estimate Std. Error z value Pr(>|z|)
(Intercept)  1.67779    0.86027   1.950  0.05114 .
CORE        -0.06803    0.01497  -4.543 5.54e-06 ***
PERIPHERAL         0.04612    0.01562   2.953  0.00315 **
---
Signif. codes:  0 ‘***’ 0.001 ‘**’ 0.01 ‘*’ 0.05 ‘.’ 0.1 ‘ ’ 1
(Dispersion parameter for binomial family taken to be 1)
    Null deviance: 205.42  on 148  degrees of freedom
Residual deviance: 115.32  on 146  degrees of freedom
AIC: 121.32
Number of Fisher Scoring iterations: 5
> drop1(glm3,test="Chisq")
Single term deletions
Model:
ANTIBODY ~ CORE + PERIPHERAL
       Df Deviance    AIC     LRT  Pr(>Chi)
<none>      115.32 121.32
CORE     1   143.52 147.52 28.2010 1.093e-07 ***
PERIPHERAL     1   125.06 129.06  9.7361  0.001807 **
---
Signif. codes:  0 ‘***’ 0.001 ‘**’ 0.01 ‘*’ 0.05 ‘.’ 0.1 ‘ ’ 1
>
>
```

Supplementary Figures

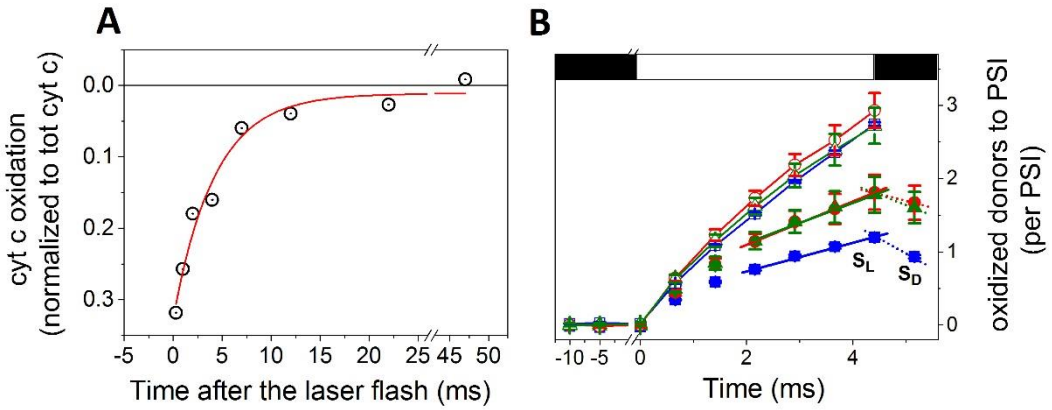

Supplementary Figure 2.34 - **PSI/cytochrome c stoichiometry and oxidation kinetics in *P. tricornutum*. Cyt c/PSI stoichiometry.** Cells were exposed to a saturating single turnover laser flash to generate 1 turnover per PSI and the amount of oxidized c-type cytochrome was calculated 300µs after the flash (i.e. when P700 is fully rereduced by the cytochromes) This amount was normalized to the total amount of cyt c oxidized in continuous light in the presence of DCMU (20µM). Because the flash oxidizes 33% of the cyt c type cytochromes, we conclude there are ~3 c-type cytochromes per PSI. (B) procedure employed to evaluate the rates of PSI oxidation in the light in the case of the total donors to PSI pool. Open bar: light on. Closed bar: light off. The slope measured after the light is switched off (S_D) allows calculating the dark rereduction rates of the PSI donor pool in the control (closed blue squares), DCMU treated samples (closed red circles) and DCMU + HA treated samples (closed green triangles). The sum of this rate plus the apparent oxidation rate in the light (S_L) .provides the real rate of oxidation of the total donors to PSI oxidation kinetics, (open symbols). See methods for further description.

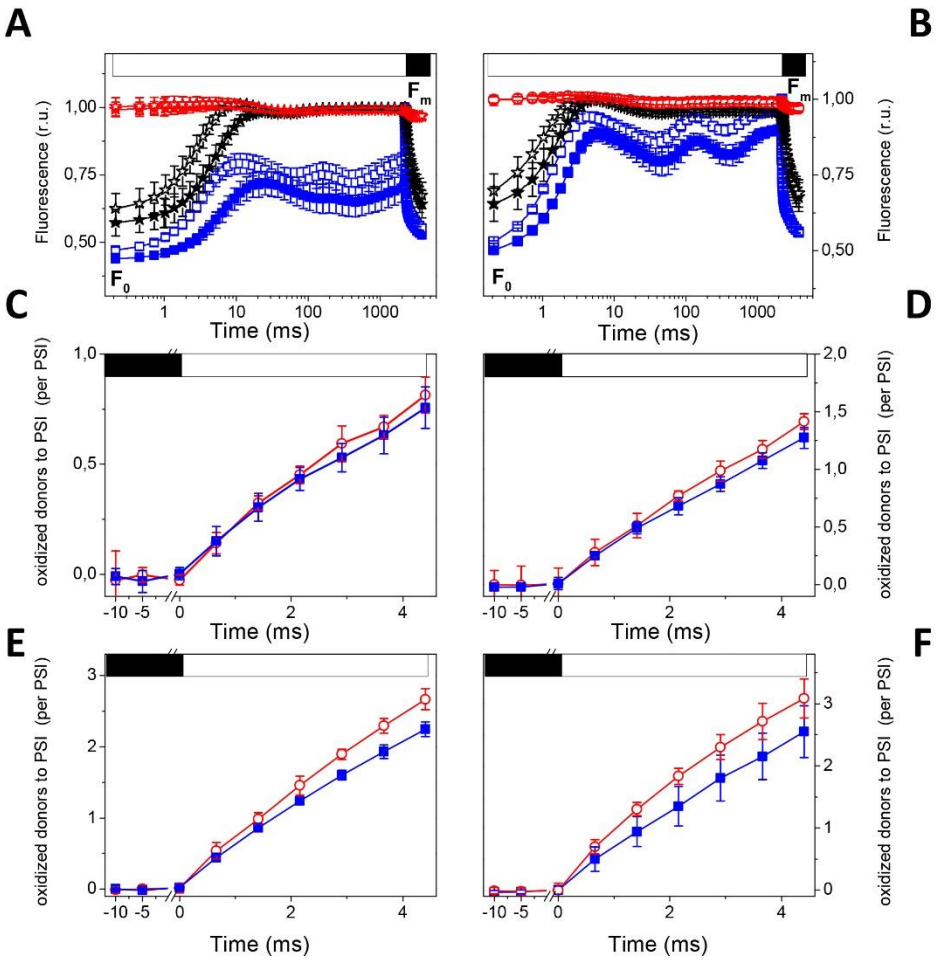

Supplementary Figure 2.35 - **Light energy spillover in *P. tricornutum* cells exposed to different light intensities.** (A) Fluorescence emission kinetics in the presence of DCMU 40 µM and HA 0.2 mM. Squares: control, triangles: DCMU; circles: DCMU and HA; open symbols 150 µm photons m^{-2} s^{-1}; closed symbols: 300 µm photons m^{-2} s^{-1}. (B) Fluorescence emission kinetics in the presence of DCMU 40 µM and HA 0.2 mM. Squares: control, triangles: DCMU; circles: DCMU and HA; open symbols: 590 µm photons m^{-2} s^{-1}; closed symbols: 1100 µm photons m^{-2} s^{-1} (C) Kinetics of oxidation of the entire pool of PSI electron donors at a light intensity of 150 µm photons m^{-2} s^{-1}. (D) Kinetics of oxidation of the entire pool of PSI electron donors at a light intensity of 300 µm photons m^{-2} s^{-1}in the light. (E) Kinetics of oxidation of the entire pool of PSI electron donors at a light intensity of 590 µm photons m^{-2} s^{-1}. (F) Kinetics of oxidation of the entire pool of PSI electron donors at a light intensity of 1100 µm photons m^{-2} s^{-1}Solid blue squares: control; empty red circles: DCMU 40µM, blue tringles: DCMU 40µM + HA 0.2 mM. Mean ± SEM (n = 2). FCP: Fucoxanthin Chlorophyll light harvesting antenna Protein. F_0: mimimum fluorescence emission (active PSII). Fm: maximum fluorescence emission (inactive PSII)**.** Closed bar: actinic light off. Open bar: actinic light on.

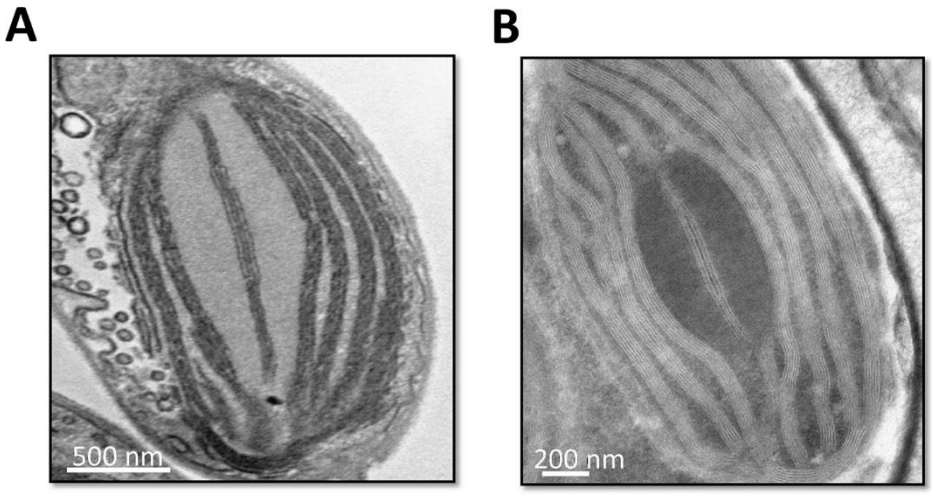

Supplementary Figure 2.36 - **Tokuyasu preparation enhances the resolution of EM pictures of *P. tricornutum* thylakoid membranes.** EM images of *P.tricornutum* from a sample fixed in resin (A) and using the Tokuyasu technique (B).

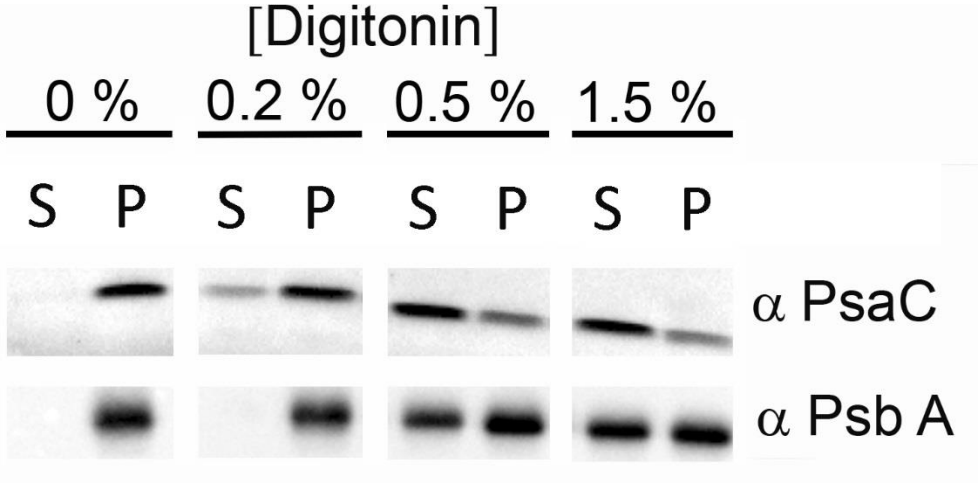

Supplementary Figure 2.37 **- Biochemical evidences for a different localization of PSI and PSII in thylakoid domains in *P. tricornutum*.** Solubilization of *P. tricornutum* thylakoid membranes with increasing concentration of digitonin (0.2, 0.5, 1.5%). Pellet (P) and supernatants (S) were analyzed by western blotting with the same anti PSI and anti PSII antibodies

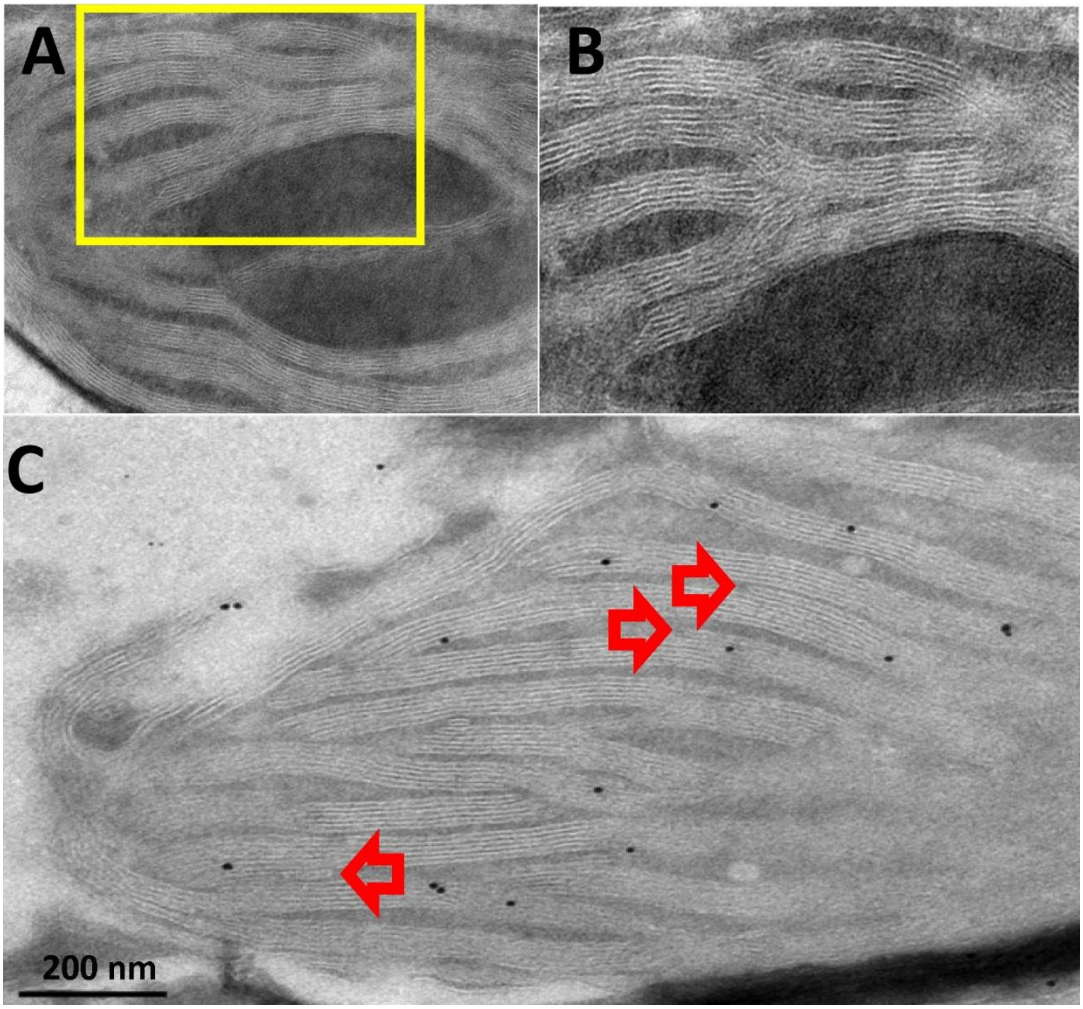

Supplementary Figure 2.38 - **Peculiar structural features of thylakoid membranes in *P. tricornutum* cells fixed using the Tokuyasu technique.** (A) EM images of *P.tricornutum* using the Tokuyasu technique reveal the existence of crosspoints between the thylakoid layers. (B) Magnification of the thylakoid layers intersections in the region indicated by the yellow box in A. (C) "Truncated" thylakoid membranes are observed in *P. tricornutum* cells prepared with the Tokuyasu technique. Red arrows point thylakoid layers that comprise an additional fourth membrane, which abruptly disappears, suggesting the existence of 3D interconnection between different layers of thylakoids

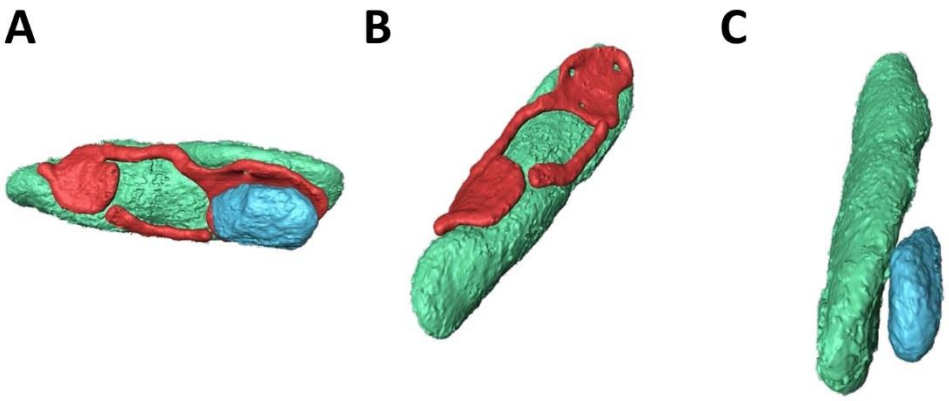

Supplementary Figure 2.39 - **Physical contacts between the organelles in *P. tricornutum* cells.** The chloroplast (green), mitochondrion (red), and nucleus (blue) structures, obtained from 3D reconstruction of intact diatom cells, are shown under different rotation angles (A to C), to highlight the physical contact between the organelles

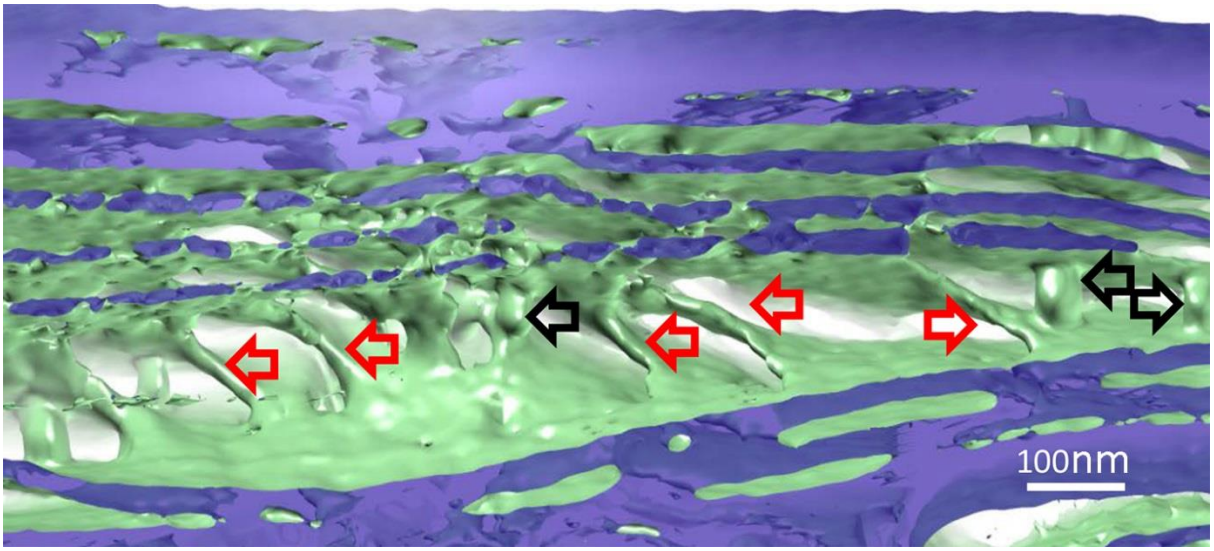

Supplementary Figure 2.40 - **3D structure of the thylakoid membranes in *P. tricornutum* cells.** Same colour code as in Figure 2.31. Note that the linking membranes (red arrows) can be clearly differentiated form the plastoglobules (black arrows), which appear as globular structures.

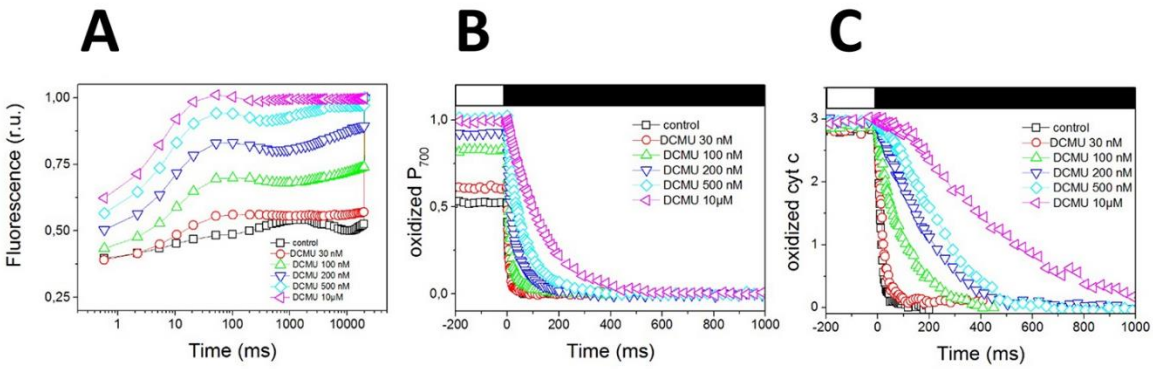

Supplementary Figure 2.41 - **Spectroscopic features of the cytochrome c_6 and P_{700} components of the electron flow chain in *P. tricornutum* cells.** (A) Fluorescence induction kinetics in the absence and in the presence of increasing DCMU concentrations. The progressive inhibition of PSII is highlighted by the increased rate of fluorescence rise. (B) Redox kinetics of P_{700} upon illumination. (C) Redox kinetics of cyt c_6 upon illumination. The rate of electron transfer were changed by addition of increasing concentrations of DCMU as in (A). Closed bar: actinic light off. Open bar: actinic light on.

	Comp. 1	Comp. 2	Comp. 3	Comp. 4
Standard deviation	10.9997641	9.8433476	3.64706862	1.67398543
Proportion of Variance	0.5170947	0.4140845	0.05684487	0.01197586
Cumulative Proportion	0.5170947	0.9311793	0.98802414	1.00000000

Table S1 **- Principal Component Analysis Results.** The first two components represent more than 93% of the variance

	INT	EXT	ENVELOP	PYRENOID
INT	1.00000000	0.099003554	0.200634040	-0.01200587
EXT	0.09900355	1.000000000	0.005308018	0.15697362
ENVELOP	0.20063404	0.005308018	1.000000000	-0.03471890
PYRENOID	-0.01200587	0.156973620	-0.034718900	1.00000000

Table S2 **- Correlation table of the number of immunolabeling in the four possible localizations**

Video B - **Focus Ion Beam Scanning Electron Microscopy (FIB-SEM) based 3D reconstitution of a whole cell of *P. tricornutum*.**

Video C - **3D structure of the chloroplast (green) mitochondrion (red) and nucleus (blue) in *P. tricornutum* cells.**

2.5.3 Perspectives

The model proposed here provides a rationale for several observations concerning photosynthesis in *Phaeodactylum tricornutum*, opening new stimulating questions on the ecological success of diatoms worldwide.

The first question I would like to answer is whether this structural arrangement is conserved in different diatoms: are the thylakoid membranes always structured as in *P. tricorntum*? Is the mitochondrion always sitting on the chloroplast, with physical contacts?

Diatoms grow in very different environments, characterized by changing light and nutrient conditions. Therefore, it is conceivable that the situation observed in *P. tricornutum* grown in laboratory conditions might not represent a real paradigm for diatoms. Consistent with this possibility, I have sometimes observed that the Fv/Fm parameter can drop below 0.5 in *P. tricornutum* cultures. The quantum yield of PSII could simply reveal that some photodamage has occurred to this complex (e.g. by nutrient starvation) but could also reveal the occurrence of a larger spillover to PSI. A systematic analysis of cultures grown under different conditions could help solving this problem.

Another important question is the role of membrane compartmentation of the PSs in the physiology of the algae. Previous work has underlined that the observed variability in the NPQ response of diatoms (Lavaud & Lepetit, 2013) is inversely proportional to their capacity to recover from photoinhibition via the synthesis of the D1/D2 subunits of PSII (Lavaud et al., 2016). In plants, the PSII repair cycle requires the re-location of this complex in the stroma exposed unstacked lamellae to enhance its accessibility of proteases (Nath et al., 2013). Assuming a similar mechanisms in diatoms, one would expect the migration of PSII from the inner thylakoid membranes to the outer ones to be a committed step of the repair process. It is tempting to speculate that possible differences in the PSII and PSI localization within the membranes could hinder or facilitate PSII repair after photoinhibition, thereby directly modulating photoprotection and consequently photoacclimation responses via NPQ. A comparative analysis of diatom species with a different NPQ capacity and or PSII repair could help solving this problem.

Then, particular attention should be given to the pyrenoid region. As recently shown in *Chlamydomonas reinhardtii* (Engel et al., 20015) the photosynthetic membranes form a peculiar array within this structure, possibly to facilitate the CO_2 assimilation. Our 3D structure of the chloroplast form *P. tricornutum* also reveal interesting features of the pyrenoid, which however cannot be entirely solved because of the low resolution of this structure. The possibility to increase

3D resolution by lower the voxel size to 2 nm should help answering the question of the arrangement of photosynthetic membranes around the pryrenoid in chloroplasts issued form a secondary endosymbiosis.

Finally, our analysis also pinpoints the existence of a physical connection between the chloroplast and the nucleus. This interaction reminds the transient connections observed in higher plants, which are mediated by stromules. It is possible therefore to speculate that this junction could play a similar role (i.e. the exchange of signals and proteins). In the previous work (see section 2.4) we highlight the presence of a chloroplast-nucleus isthmus in which the inner nuclear envelope (iNE) is in contact with the periplastidial membrane (PPM). In this area, the vesicular network (probably the machinery involved in the trafficking of proteins and other metabolites) appear to be close to the nucleus, but not in the area where the chloroplast-isthmus occurs. Further investigation is needed to understand the functional and structural role of this “bridge”. An example is to test high-light stress conditions which can enhance the plastid-to-nucleus retrograde signalling (as in Lepetit et al., 2013).

Chapter 3

3.1 Protocols

In this chapter, the optimization and development of protocols used for the experiences described in the above manuscripts are presented. Using the model organism *Phaeodactylum tricornutum* we investigate chloroplast's architecture taking advantage of different microscopic techniques. These experiences have required the optimization of the following protocols and analysis:

- Electron microscopy samples preparation
- Immunolabeling protocol
- Immunolabeling protocol through Tokuyasu technique
- Tomographic studies
- The Gatan 3View2XP analysis
- Focused Ion Beam – Scanning Electron Microscopy (FIB-SEM) analysis
- Data processing and 3-Dimentional reconstruction
- 3-Dimentional analysis of the thylakoid membranes
- The Atomic Force Microscopy analysis (AFM)
- Thylakoid membranes preparation for AFM analysis
- Protocol for the purification of intact chloroplasts of *P. tricornutum*
- Improved protocol of isolated thylakoid membranes preparation
- Experimental procedure INSERM Marseille for AFM analysis
- Experimental procedure SSL Grenoble for AFM analysis

3.2 Electron microscopy samples preparation

Cells of *P. tricornutum* in exponential phase were harvested before the offset of the light period at 5000 xg, 10 minutes, 4 °C and then fixed in 0.1 M cacodylate buffer (Ted Pella Inc., Redding, CA), pH 7.4, containing 2.5% glutaraldehyde (Electron Microscopy Sciences, Hartfield, PA), 2% formaldehyde (EMS) for 1 hour at room temperature and prepared according to a modified protocol from "NCMIR METHODS FOR 3D EM: A NEW PROTOCOL FOR PREPARATION OF BIOLOGICAL SPECIMENS FOR SERIAL BLOCK FACE SCANNING ELECTRON MICROSCOPY" T. J. Deerinck and M. H. Ellisman, in the Center for Research in Biological Systems and the National Center for Microscopy and Imaging Research, University of California, San Diego, La Jolla, CA, USA (https://ncmir.ucsd.edu/sbem-protocol). The cells were washed 3 times for 3 minutes at 1000 xg in cold 0.1 M cacodylate buffer containing 2mM $CaCl_2$ and then incubated in a solution of 3% potassium ferrocyanide in 0.1 M

cacodylate buffer and 4mM $CaCl_2$ with an equal volume of 4% aqueous osmium tetroxide (EMS) for 1 hour, on ice. Then the cells where washed 3 times for 3 minutes at 1000 xg with ddH_2O and incubated for 20 minutes, at room temperature in a fresh filtered thiocarbohydrazide (TCH) solution (0.1 g thiocarbohydrazide in 10 ml ddH_2O gently swirling at 60° C in the oven for 1 hour). The cells were then rinsed 3 x 3 minutes 1000 xg in ddH_2O at room temperature and placed in 2% osmium tetroxide in ddH_2O for 30 minutes, at room temperature. After 3 washing steps of 3 minutes at room temperature in ddH_2O the cells were transferred in 1% aqueous uranyl acetate overnight at 4°C. The next day cells of *P. tricornutum* were then washed 3 x 3 minutes 1000 xg in ddH_2O at room temperature. In the meantime a solution containing 0.066 g of lead nitrate in 10 ml of aspartic acid solution (dissolving 0.998 g of L-aspartic acid (Sigma-Aldrich) in 250 ml of ddH_2O) was prepared adjusting the pH to 5.5 with 1N KOH. The lead aspartate solution was then placed in the oven at 60°C for 30 minutes. The cells were then transferred in the lead aspartate solution and returned in the oven for 30 minutes. The heavy metal contrast performed on *P. tricornutum's* cells was controlled at the optical microscope (Figure 3.1 A). After a washing step with ddH_2O cells were dehydrated 20-30 minutes at 20%, 50%, 70%, 90%, 100%, 100% ethanol (anhydrous) and then placed in anhydrous ice-cold acetone and left at room temperature for 30 minutes. Inclusion of resin was performed after a centrifugation to remove the supernatant. The Durcupan ACM resin (EMS) was prepared mixing 11.4 g part A with 10 g part B for 2 hours then adding 0.3 g of part C for 1hour and finally with 0.05-0.1 g of part D for 1 hour. After the dehydration steps, the cells were infiltrated with acetone/Durcupan resin mixture (2/3–1/3 two times for 1 h and 1/3–2/3 for 1 h) and embedded in 100% Durcupan 2 times for 2 hours and finally into fresh 100% Durcupan in the oven at 60°C for 48 hours (Figure 3.1 B). Ultrathin sections (60 nm) were prepared with a diamond knife on an UC6 Leica ultramicrotome and collected on 200 mM mesh nickel grids before examining on a JEOL 1200 EX electron microscope in collaboration with Denis Falconet (LPCV).

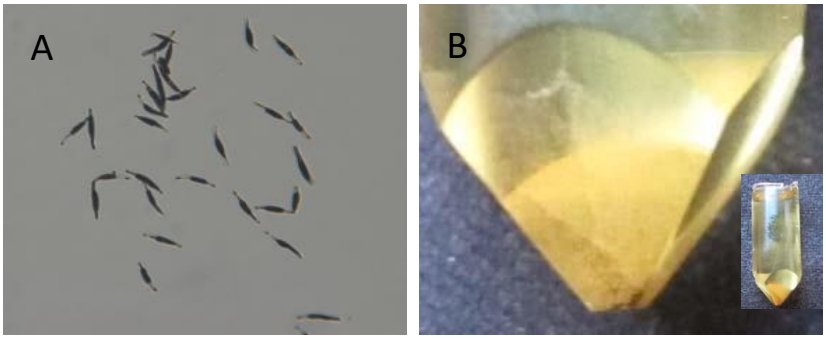

Figure 3.1 – **Samples preparation for EM.** (A) Heavy metal contrast on *P. tricornutum's* cells. (B) Final specimen embedded in resin.

3.2.1 Results and discussion

The optimization of the procedure of sample preparation has required extensive effort due the scattered character and the not exhaustive amount of information available in literature. Different staining conditions (uranyl acetate, osmium tetroxide, potassium ferrocyanide) resins (epon, durcupan, LR-white) were tested starting from protocols for mammalian cells or plants. Overall, the final protocol, which combines sample fixation, heavy metal staining, dehydration steps and embedding in resin, has led to good contrast and high lateral resolution as visible in Figure 3.2.

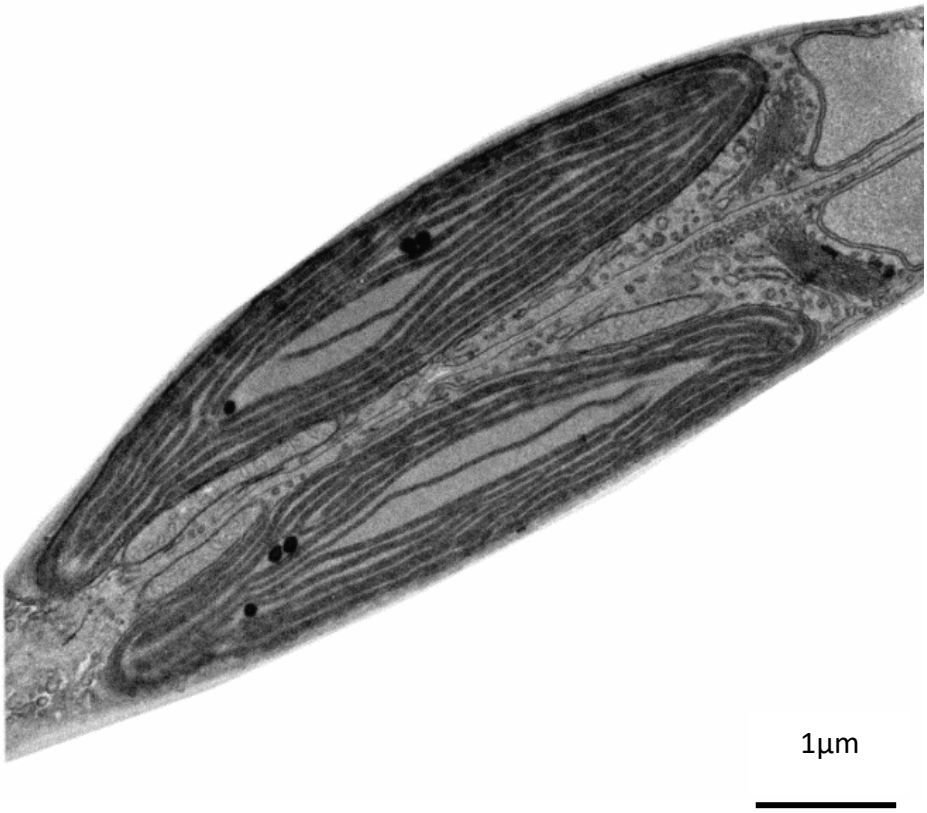

Figure 3.2 – ***P. tricornutum*** **during cell division**

3.3 Immunolabeling protocol

In order to understand the localization of the photosynthetic complexes in the thylakoid membranes of the model organism *Phaeodactylum tricornutum* different experiments were performed to optimize the dilution factor of the antibodies and the thickness of the gold marbles.

Starting from a protocol described in Vardi et al., 2008 we used sections of the specimen placed in grids with different dilutions of primary antibodies: anti PsaC | PSI-C core subunit of photosystem I (1:30/1:100) and anti PsbC | CP43 protein of PSII (1:10/1:50) in Phosphate Buffered Saline (PBS)– 5% and Bovine Serum Albumin (BSA). Then grids were incubated for 90 min with the secondary antibody anti rabbit IgG (1:20) AURION Immunogold Reagents, with 25 nm nanogold particles. Where the antibody binds, electrons from the microscope are scattered by the gold, leaving a black spot visible in the picture (Figure 3.3 A).

3.3.1 Immunolabeling protocol through Tokuyasu technique

Using the facilities of the integrated structural biology platform (IBS) in Grenoble we used an epoxy-free procedure to enhance antibody accessibility and prevent distortion effect, called Tokuyasu (Tokuyasu, 1973). This technique allows the study of the thylakoid membranes directly in their biological environment after a rapid and *in situ* vitrification (Figure 3.3 B). Cells of *P. tricornutum* were fixed in a double-strenght fixative (4% (w/v) formaldehyde, 0,4% (v/v) glutaraldehyde) in PHEM buffer (PIPES 60 mM, HEPES 25 mM, EGTA 10 mM, MgCl2 2mM; pH 7) in an equal volume to the culture medium (ESAW), and then diluted into a standard strength fixative (2% (w/v) formaldehyde (EMS) and 0,2% (v/v) glutaraldehyde, (EMS)). After 15 minutes, fresh standard strength fixative was replaced and fixation proceeded for 30 minutes at room temperature, under agitation. Cells were washed 3 times with 50 mM glycine in PHEM buffer and after centrifugation were embedded in 12% gelatin in PHEM. The gelatin-embedded blocks were cryo-protected in 2,3M sucrose in rotating vials at 4°C (overnight). Samples vitrification was obtained in liquid nitrogen following the plunge and freezing technique. Thin sections (80 nm) were prepared at -110°C with a diamond knife (Diatome) and the the blocks were prepared with an ultracryomicrotome (UC7,Leica, Microsystems). Ribbons were picked-up with a drop of 1% (w/v) methylcellulose/1,15 M sucrose in PHEM buffer. Sections were thawed and transferred to Formvar carbon-coated nickel grids.

The immunolabelling was performed using an automated system (Leica EM IGL). The sucrose/methyl cellulose mixture was removed washing the grids with PBS 3 times for 2 minutes. Then the free aldehyde groups were inactivated on PBS + 0.05 M glycine, pH 7.4, 15 minutes. The

hydrophobic areas were blocked with the Aurion Blocking Solution for 30 minutes. Then three washing steps on PBS + 0.1% BSA-c pH 7.4 for 2 minutes were performed. The primary antibody was diluted 1-5 µg/ml in PBS + 0.1% BSA-c pH 7.4 and the grids were incubated for 60 to 90 minutes. Negative controls were incubated only with BSA-c buffer. Then six washing steps on PBS + 0.1% BSA-c pH 7.4 for 5 minutes were performed. The secondary antibody with ultrasmall 6 nm gold particle was diluted in PBS (1:20) + 0.1% BSA-c pH 7.4 and grids were incubated for 90 to 120 minutes. Then six washing steps on PBS + 0.1% BSA-c pH 7.4 for 5 minutes and additional six washing steps on PBS pH 7.4 for 2 minutes were realized. After a post fixation with 2% glutaraldehyde in PBS pH 7.4 for 5 minutes, three washing steps on PBS pH 7.4 for 2 minutes and six wash with deionized water for 2 minutes were performed. Sections were enhanced with silver (Aurion R-Gent SE-EM) for 25 minutes and again washed on deionized water six times for 2 minutes. Subsequently, a first heavy metal contrast was performed on 4% neutral uranyl acetate for 5 minutes followed by another heavy metal contrast with 0.4% uranyl acetate in 2% methylcellulose (on ice) for 5 minutes. Grids were let dry, using a loop and filter paper, after switching to a fresh droplet of PBS pH 7.4. Before observation, grids were left 5 minutes on 2% uranyl oxalate (pH 7) and transferred to a mixture of 1,6% methyl cellulose and 0,4% uranyl acetate on ice, the excess of the viscous solution was drained away and the grids were let to dry. Grids were examined in an electron Tecnai 12 microscope (FEI).

3.3.2 Results and discussion

The traditional EM technique used for immunolocalization show a limited bind affinity with the incubated antibody (Figure 3.3 A) while the images obtained using the “clean” procedure Tokuyasu (Figure 3.3 B), displayed a reduced distortion effect, and an enhanced antibody accessibility. As shown in the pictures below (Figure 3.3 C) the incubated antibody is more often detected inside the thylakoid membranes leaving numerous black spots in the EM picture. The analysis was performed using the epoxy-free technique and the automated system for immunolabeling on more than 300 images and 10.000 gold particles were counted on the thylakoids of *Phaeodactylum tricornutum*.

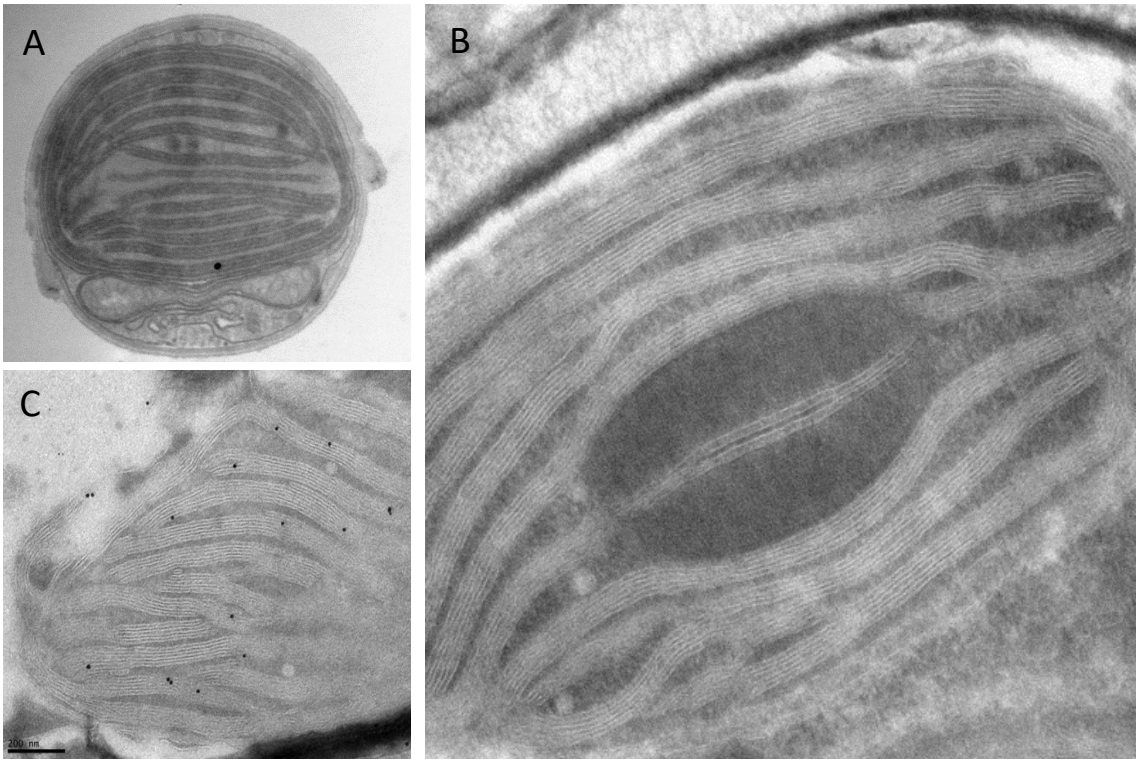

Figure 3.3 – **Immunolocalization protocols.** (A) Classic technique of immunolocalization using intact cells of *P. tricornutum.* (B) Tokuyasu technique (C) Tokuyasu technique of immunolocalization using intact cells of *P. tricornutum.*

3.4 Tomographic studies

This method was adopted to fill the "2D-3D gap" limited by the thickness of the samples. Image stacks were acquired automatically at high lateral resolution using two different techniques.

A first analysis was performed at the Technische Hochschule Zürich (ETH) using the Gatan 3View2XP within the I.T.N. Marie Curie in collaboration with Samuel Zeeman and Simona Eicke.

A second analysis was performed in the *Laboratoire d'Etudes des Matériaux par Microscopie Avancée* LEMMA of CEA Grenoble using a Focused ion beam scanning electron microscopy (FIB-SEM) in collaboration with Pierre-Henri Jouneau.

Durcupan embedded cells of *Phaeodactylum tricornutum* were analysed using the following techniques.

3.4.1 The Gatan 3View2XP analysis

The Gatan 3View2XP Microscope is an electron microscopy (Figure 3.4 A) equipped with an automatic diamond knife which develops serial block-face sections using a beam of electrons to scan across a surface (Figure 3.4 B) and reconstruct the different section to generate a high-resolution tomogram. All the images resulted (Figure 3.4 C) were optimized with specific software (FIJI ImageJ) and the three-dimensional reconstruction were performed with AMIRA® software (Figure 3.4 D).

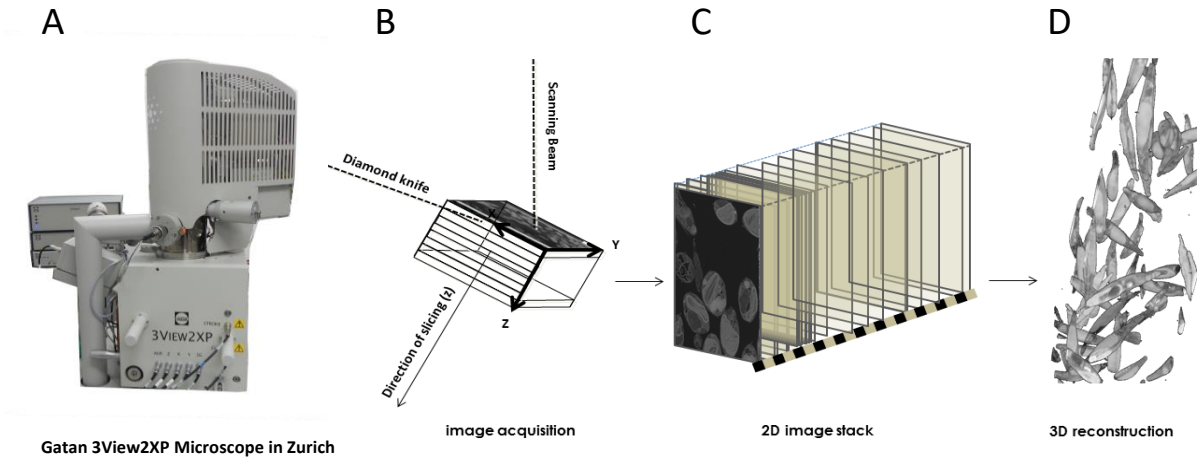

Figure 3.4 – **The Gatan 3View2XP procedure.** (A) Gatan 3View2XP Microscope in Zurich. (B) Image acquisition. (C) Automatic 2D images stack acquisition. (D) 3D reconstruction.

3.4.1.1 Results and discussion

This study reports the recording of several tomograms of intact cells of *Phaeodactylum tricornutum*. The analysis of approximately 2000 slice images reveal a complex interconnected networks of thylakoids membranes. Unfortunately, despite repetitive analysis the four acquired tomograms were not satisfying for the following segmentation and 3-D reconstruction analysis. Nevertheless a pioneering collaboration was establish in the laboratory of advance microscopy for the study of new materials in nanotechnology at CEA Grenoble using the Focused Ion Beam – Scanning Electron Microscopy (FIB-SEM) to characterize the connections between thylakoids and reveal the real chloroplast architecture in diatoms.

3.4.2 Focused Ion Beam – Scanning Electron Microscopy (FIB-SEM) analysis

Focused ion beam tomography has been realized using a Zeiss NVision 40 dual-beam microscope (Figure 3.5 A) which possess a Ga^+ ion beam (of 700 nA at 30 kV). The main devices composing this system are an ion column, an electron optic column and a field emission gun. After protecting an area of the specimen with a layer of platinum or carbon, a section is abrade by the FIB to expose a face of the sample free of artefact associated to mechanical sectioning. Then a cascade of Ga^+ ions is focused through to a needle tip that starts to erode a limited area of the sample and the newly layer exposed is imaged by a SEM (Figure 3.5 B). Each slice was imaged in a scanning electron microscopy (SEM) at 5 kV using the in-column EsB back-scatter detector. For each slice, a thickness of 4 nm has been removed and the SEM images were recorded with a pixel size of 4 nm. The images stack (Figure 3.5 C) is then registered by cross-correlation using the StackReg plugin in the Fiji software. This procedure gives us directly an image in 3D with an isometric voxel size of 4x4x4 nm. For the projection in 3-Dimension (x,y,z axis) different software were used (Figure 3.5 D).

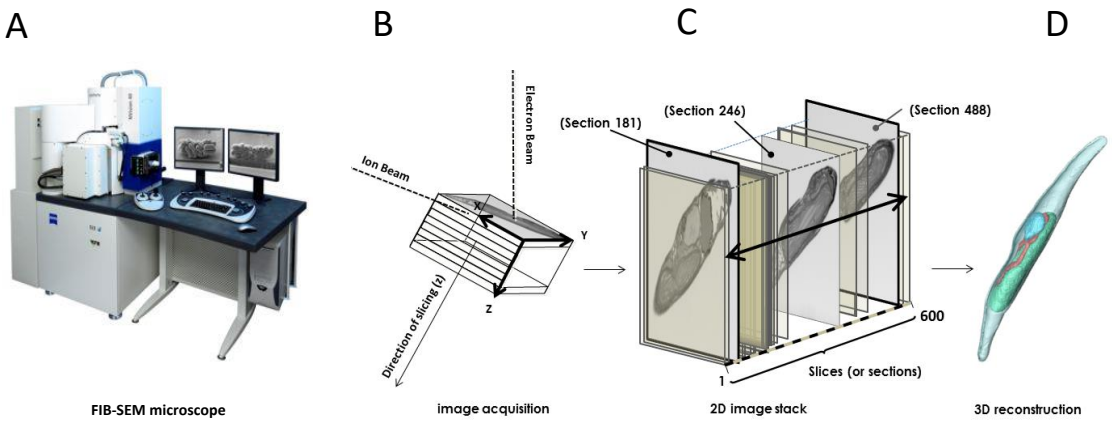

Figure 3.5 – **The FIB-SEM procedure.** (A) The Zeiss NVision 40 dual-beam microscope http://www.southampton-nanofab.com/fabrication/fib.php. (B) Image acquisition. (C) Automatic 2D images stack acquisition. (D) 3D reconstruction.

3.4.2.1 Results and discussion

During this investigation, three tomograms of intact cells of *Phaeodactylum tricornutum* were recorded. The first analysis was performed on a broken cell; this event led us to discover some particular features concerning the periplastidial reticulum in *P. tricornutum* (section 2.3). The second analysis of approximately 600 images revealed a complex and highly structured network of membranes (section 2.3 and 2.4). The third tomogram was performed to reduce the thickness of the slices at 2 nm, the resulted images were recorded with pixel size of 2 nm. The implemented voxel size didn't improve the resolution of the thylakoid membranes in the pictures that appeared blurred probably due to the affinity of these membranes to bind the heavy-metal ions of the osmium. Nevertheless combining other techniques for sample preparation (like the freeze fracture technique) it is possible to reduce the risk of distort information due to invasive steps (chemical fixations, dehydration, etc) providing more details for the 3-D analysis of the chloroplast structure.

3.5 Data processing and 3-Dimentional reconstruction

For the alignment and treatment of the second stack of *P. tricornutum* images FIJI image J software was used. Subsequently the segmentation was achieved semi-automatically using the open source software Ilastik and the 600 images were corrected manually. The 3-Dimentional reconstruction and the final movie were performed with Avizo® software.

3.5.1 Results and discussion

The 3-Dimentional reconstruction of the chloroplast (in green), the mitochondria (in red) and the nucleus (blue; Figure 3.6) led us to understand for the first time the connection between these essential component of the cell in *Phaeodactylum tricornutum*.

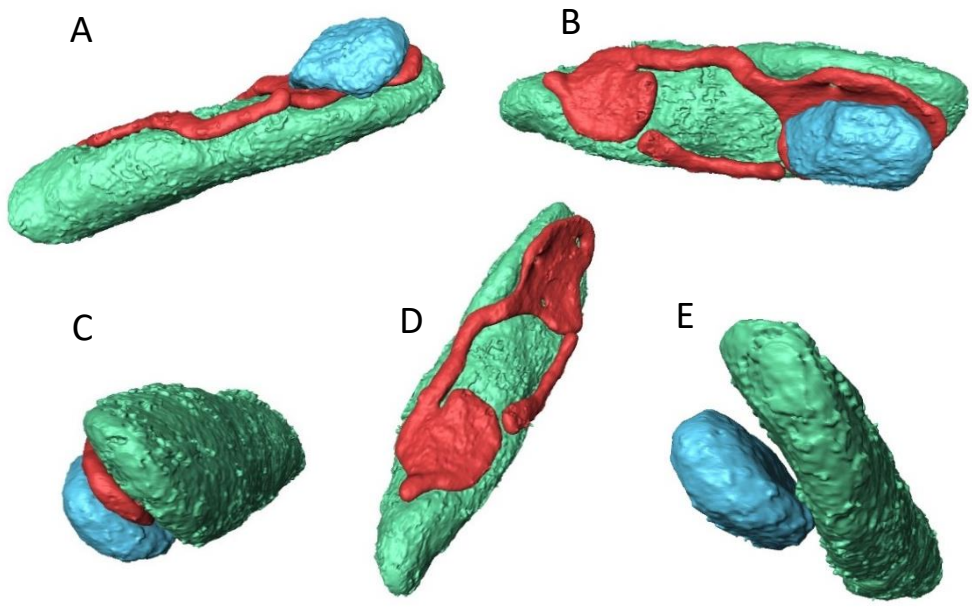

Figure 3.6 – **3D segmentation of *P. tricornutum*.** (A) Image reconstruction of the chloroplast (in green), the mitochondria (in red) and the nucleus (in blue) xy-view. (B) xz-view of the reconstruction. (C) yz-view of the reconstruction. (D) Frontal view of the connection between the chloroplast (in green) and the mitochondria (in red). (E) Lateral view of the connection between the chloroplast (in green) and the nucleus (in blue).

3.6 Three-Dimentional analysis of the thylakoid membranes

The second stack of acquired images of *P. tricornutum* was also used to unveil the 3-Dimentional architecture of the photosynthetic membranes. The analysis (represented in Figure 3.7) was performed following these steps: the alignment and treatment of the 600 images was performed with the software FIJI image J and then converted in .ccp4 files (.ccp4 is the abbreviation for collaborative computational project number 4 and is the file format of electron density data used in structural biology) for the subsequent volumetric analysis with CHIMERA software.

3.6.1 Results and discussion

The 3-D analyses performed with CHIMERA software disclose for the first time the complex dynamic structure of the thylakoid membranes in *P. tricornutum.* The study leads to a completely different opinion of the undifferentiated plastid issued by a secondary endosymbiosis. The connecting membranes founded between the thylakoid layers (Figure 3.8 A) form a basket structure near the pyrenoid region (Figure 3.8 B). So far, much of our understanding of *P. tricornutum* comes from conventional transmission electron microscopy (TEM) studies. Analyzing microalgae ultrastructure with these innovative techniques led us to scratch just the surface like Paolillo did in 1970 with serial section of EM pictures revealing the presence of right-handed lamellae in the thylakoids of plants. If we consider that nowadays the exact three-dimensional architecture of the grana in plant (for review Daum et al., 2011) is still matter of debate, we are just at the beginning.

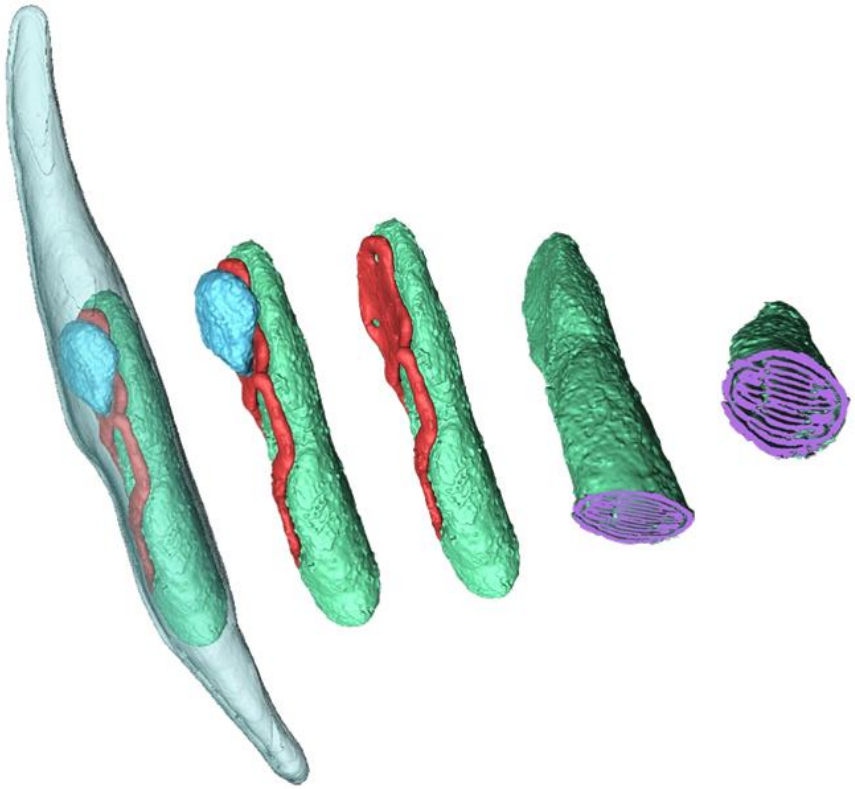

Figure 3.7 – **Sequential images analysis.** From the whole segmentation on the left (with the chloroplast, the mitochondria and the nucleus) to the study of the photosynthetic membranes of *P. tricornutum* (in violet) on the right.

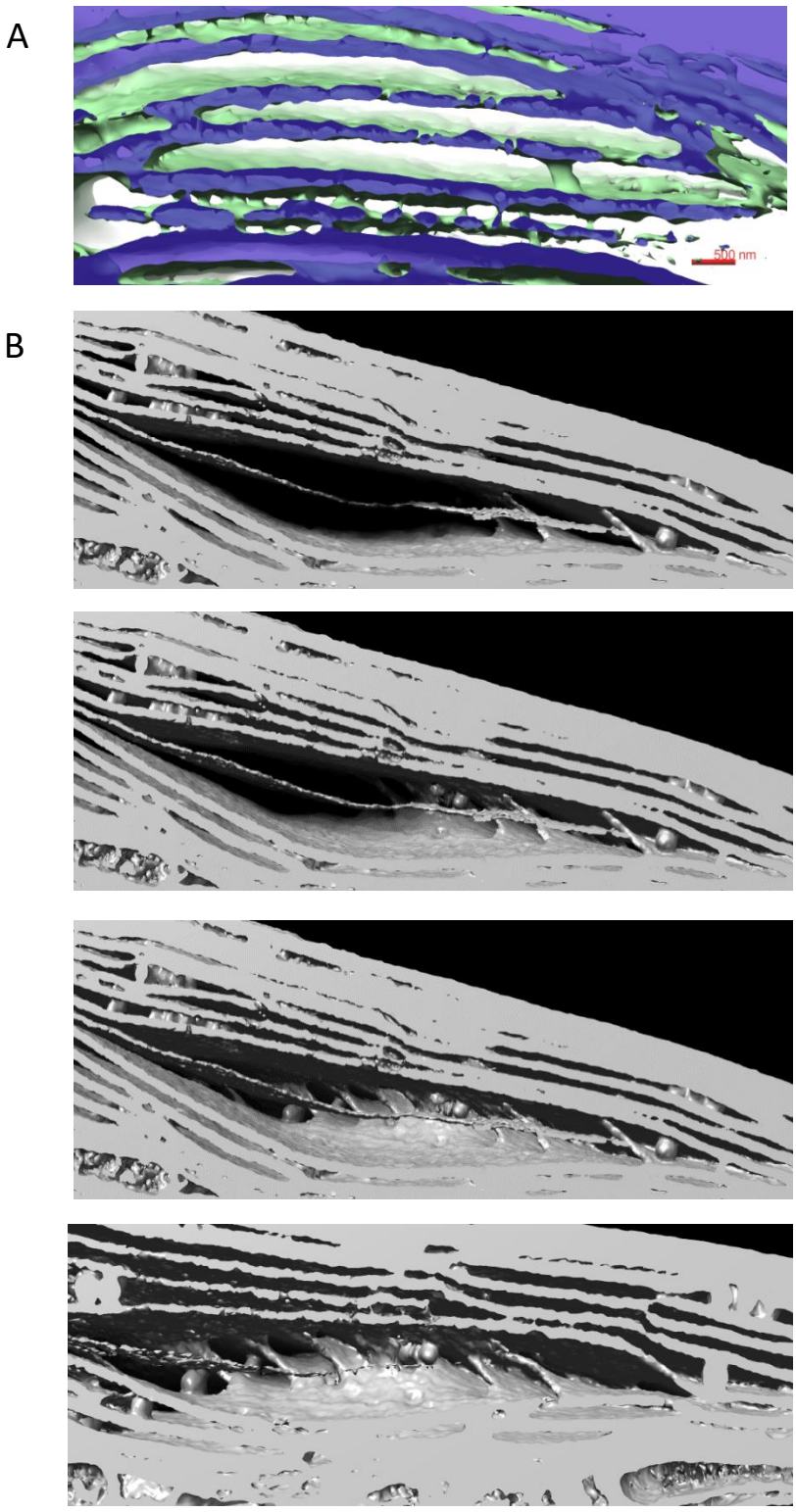

Figure 3.8 – **Images analysis with CHIMERA software.** (A) Detail of the thylakoid membranes. The violet areas correspond to the internal membranes while the green areas correspond to the external membranes. (B) Sequential images analysis of the "basket" structure near the pyrenoid region of *P. tricornutum. S*imilar to the stroma lamellae of plants, these structures connect different layers of the thylakoids and differ from the plastoglobules present in these pictures.

3.7 The Atomic Force Microscopy (AFM)

This method was chosen to better understand the topology of the thylakoid membranes and to improve the resolution at nanoscale level of the organization of photosynthetic complexes, in non fixed membranes.

The heart of the AFM (Figure 3.9 A) is a sharp tip attached to a flexible Si_3N_4 cantilever that scans the sample. During the scan, the probes touch the sample, controlled by the piezoelectric material that apply a force on the cantilever base and makes it vibrate. The movements of the probe over the surface, thanks to the laser focused on the cantilever give back a signal that is reflected to a detector (Figure 3.9 B). As result the vertical bending (deflection) of the cantilever gives us a measurement of the movement of the probe and, consequently, information about the surface of the sample. Different techniques allow studying the topography of membranes proteins directly in their biological environment (contact mode, tapping mode and noncontact mode). For the analysis we used the contact mode (CM-AFM) where the force between the tip of the cantilever and the probe is constant, commonly used for analysis of flat membranes (for more information see Liu & Sheuring, 2013) and Tapping Mode where the tip touch the sample only intermittently reducing dragging forces during the scanning (Tamayo & Garcia, 1996). The samples were deposited on a mica holder, due to the fact that the tip and the samples are immersed in a buffer solution the mica surface is attached to a teflon plate and subsequent to a metal plate (Figure 3.9 C).

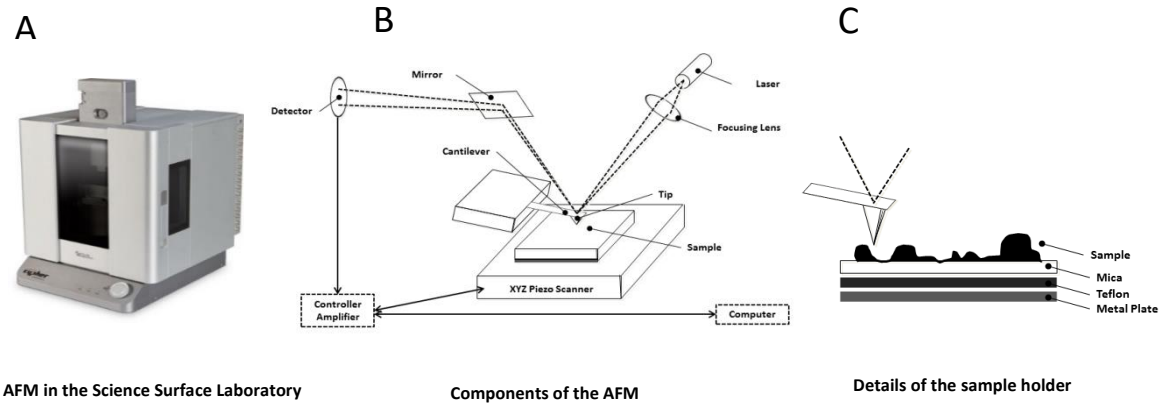

Figure 3.9 – **The AFM procedure.** (A) The Cyper AFM Microscope in the Science Surface Laboratory. (B) Major component of the AFM technique (laser, focus lens, sample, x y z piezo scanner, tip, cantilever, mirror, detector, controller amplifier and computer). (C) Details of the samples holder (from the bottom to the top: metal plate, teflon plate, mica holder and the sample).

A first investigation was performed at the *Institut National de Santé et de la Recherche Médicale* INSERM Marseille in collaboration with Simon Scheuring and Nikolay Buzhynskyy.
A second investigation was performed in the SSL (Science Surface Laboratory) of the European Synchrotron Radiation Facility (ESRF) of Grenoble in collaboration with Luca Costa.
Isolated thylakoid membranes of *Phaeodactylum tricornutum* were analysed using the following techniques.

3.7.1 Thylakoid membranes preparation for AFM

Different procedures were taken into consideration to prepare isolated thylakoid membranes for atomic force microscopy analysis. A first set of experiments was set up with a technique created in 1998 by Wittpoth and collaborators. This protocol was designed for two marine centric diatoms *Odontella sinensis* and *Coscinodiscus granii* with a silicified cell wall and as expected, some difficulties had emerged. In fact, this protocol was not adequate to open cells of *P. tricornutum*. To solve this problem, different setups, pressures and centrifugation steps were tested to improve the quality of the obtained memebranes. Unfortunately no substantial improvements were achieved and a second set of experiments was established according to Martinson *et al*., 1998 (Figure 3.10 A). The procedure was the followed. Cells were harvested and concentrated at 2000 xg for 10 minutes (Multifuge X1R Thermo Scientific) and then resuspended in buffer 1 (2 M sorbitol, 20 mM MES-NaOH (pH 6), 5 mM ε-aminocaproic acid (ACA), 1 mM benzamidine (BAM), 1 mM $MgCl_2$). Afterwards, the following sequence of sonication (15 sec burst, 30 sec cool, 15 sec burst at 105 W) and centrifugation (750 xg for 5 minutes) were realized 6 times. The supernatants were collected and centrifuged for 15 minutes at 12400 rpm in a Sorvall RC5 centrifuge with a SS-34 rotor in 50 mL polycarbonate tubes. The crude membrane pellets were resuspended in buffer 2 (2 M sorbitol, 20 mM MESNaOH (pH 6), 5 mM ACA, 1 mM BAM) homogenised and centrifuged again. Pellets were resuspended homogenised and gently transferred into four 13 ml ultracentrifuge tubes SW32Ti Beckman and overlaid with the gradient buffers 3 (5 mM MES-NaOH (pH 6), 5 mM ACA, 1 mM BAM, with sorbitol at 3.2M and 2.5 M). Thylakoids were purified by flotation in Beckman SW32Ti swinging bucket rotor after one hour at 32000 rpm, recovered, diluted in the washing buffer 6 (containing: 5 mM MES-NaOH (pH 6), 5 mM ACA, 1 mM BAM) and centrifuged for 15 minutes at 12400 rpm in a Sorvall RC5 centrifuge with a SS-34 rotor in 50 mL polycarbonate tubes. Pellets were frozen at -80°C and used for the first analysis with the AFM.

3.7.2 Protocol for the purification of intact chloroplasts of *P. tricornutum*

In order to improve the preparation of isolated thylakoid membranes first of all we developed a protocol for the purification of intact chloroplasts of *P. tricornutum* which was combined with the protocol for the fractionation of *Arabidopsis thaliana* chloroplasts (Salvi et al., 2004) following the procedure highlighted in Figure 3.10 B. Cells were harvested ($2*10^6$ cells/mL) before the offset of the light period at 5000 xg, 10 min, 4 °C, and then concentrated at 2500 xg, 10 min, 4 °C. The pellet was resuspended gently with 10 mL of Isolation buffer (0.5 M Sorbitol; 50mM Hepes -KOH ph8; 6mM EDTA; 5mM $MgCl_2$; 10mM KCl; 1mM $MnCl_2$; 1% PVP 40 (K30); ph 7,2-7,5. And fresh 0,5% BSA; 0,1% Cystein) and passed slowly through a French Press 700 scale parts (9000 bar). The mixture of broken cells was fill up with additional 10 mL of Isolation buffer on dark and ice and centrifuged at 300 xg for 8 minutes. Only the supernatant was collected and centrifuged at 2000 xg, 10 min, 4 °C. Using a soft paint-brush the pellet was gently dissolved into 2 ml of washing buffer (0,5 M Sorbitol; 30mM Hepes-KOH ph8; 6mM EDTA; 5mM $MgCl_2$; 10mM KCl; 1mM $MnCl_2$; 1% PVP 40 (K30); ph 7,2-7,5. And fresh 0,1% BSA) and loaded (max 2mL) to one Percoll gradient (0,5 M Sorbitol; 30mM Hepes-KOH ph8; 6mM EDTA; 5mM $MgCl_2$; 10mM KCl; 1mM MnCl2; 0,1% PVP 40 (K30); ph 7,2-7,5. Percoll at desired concentration 10%, 20%, 30%). The mixture of broken cells and plastids was centrifuged in a Ultra-centrifuge (with SW41Ti rotor) at 9000 rpm 35 min. The two bands resulted were collected and dissolved in the washing buffer (without BSA, 5-6 mL each) centrifuging at 9000 rpm, 10 min, 4°C. The resulted pellet was then resuspend in a hypotonic buffer (10mM MOPS-NaOH pH 7.8; 4mM $MgCl_2$; 1mM PMSF; 1mM benzamidine; 0.5mM ε-aminocaproic acid) and loaded in a sucrose gradient (10mM MOPS-NaOH pH 7.8; 4mM $MgCl_2$ with sucrose at 0.93 M, 0.6 M and 0.3 M) and centrifuge it at 20000 rpm for 1.10 hours. The bottom fraction resulting from the sucrose gradient was washed (max 4-5 mL of washing buffer) at 25000 rpm for 1.10 hours and collected for the subsequent analysis at INSERM of Marseille.

3.7.3 Improved protocol of isolated thylakoid membranes preparation

In collaboration with Nikolay Buzhynskyy we improved the protocol previous developed adding another step of French press (Figure 3.10 C). The resulting sucrose gradient performed contained 3 fractions: the upper fraction corresponding to light membrane fragments, the middle fraction which is supposed to contain stack of thylakoids and the bottom fraction of intact chloroplasts. The aliquot of the middle fraction was additionally homogenized to create isolated membrane stacks. This sample were directly transferred and analyzed at the INSERM of Marseille.

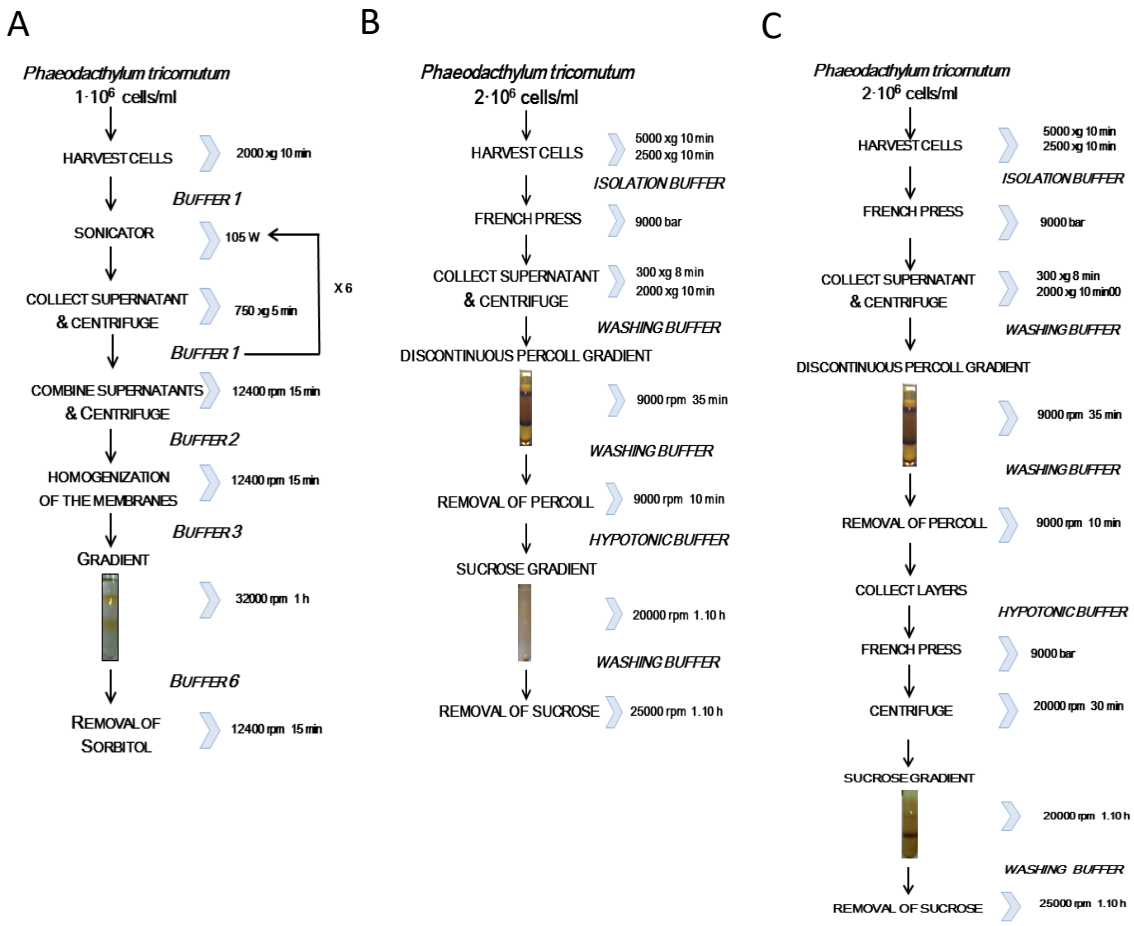

Figure 3.10 – **Experimental protocols for sample preparation for AFM analysis.** (A) Thylakoid membranes preparation following the protocol of Martinson et al., 1998. (B) Developed protocol for the purification of intact chloroplasts of *P. tricornutum*. (C) Improved protocol of isolated thylakoid membranes preparation.

3.7.4 Experimental procedure INSERM Marseille

The AFM analysis was performed according to Scheuring & Sturgis, 2009. Membranes were initially diluted 50 times with the adsorption buffer (10 mM Tris buffer 150 mM KCl and 25 mM $MgCl_2$). Afterwards, 40 µl of the solution were deposited on mica surface (freshly cleaved) and incubated for 30 minutes. Non-bound membranes were washed away with recording buffer (10 mM Tris-HCl buffer 150 mM KCl pH 7.5). The acquisition of the data were performed with a commercial Nanoscope-E contact-mode AFM (from Digital Instruments, Santa Barbara, CA, USA) equipped with a low-noise laser, and a 160 lm scanner (J-scanner) using oxide-sharpened Si_3N_4 cantilevers with a length of 100 lm (k = 0.09 N/m; Olympus Ltd., Tokyo, Japan).

3.7.4.1 Results and discussion

During this investigation several analyses were performed. The first one has provided details of thylakoid membranes revealing the presence of some flat zones (attributable to lipid membranes) surrounded by protruding and corrugated areas where small fragments are attached forming dense aggregates (Figure 3.11 A). The second analysis with the improved protocol (protocol for the purification of intact chloroplasts of *P. tricornutum*) reveals membranes on mica surface carrying a number of protruding elements (potentially assigned to the protein complexes of interest, Figure 3.11 B). During the third analysis, the sample (prepared with the improved protocol of isolated thylakoid membranes) shows membranes patch carried protruding corrugations probably constitute of protein domains (10-20 nm in size, Figure 3.11 C). However, despite several tests, the continuous scanning of the tip led to the gradual destruction of the membranes probably related to the quality of the samples. Indeed to avoid potential damage of the thylakoid membranes during the transport, we establish another collaboration in Grenoble at the Science Surface Laboratory.

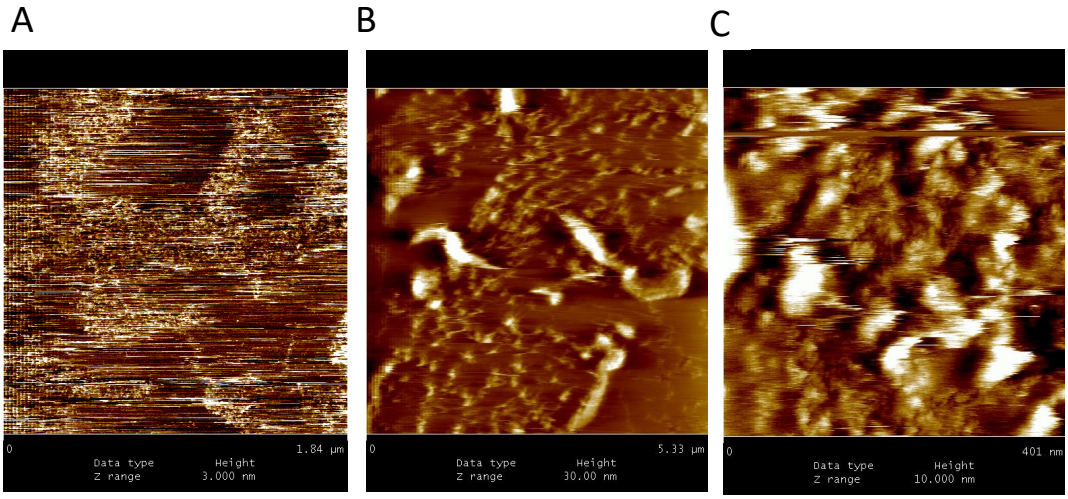

Figure 3.11 – **Results procedure INSERM Marseille.** (A) First analysis of the sample prepared with the protocol of Martinson et al., 1998. (B) Second analysis of the sample prepared with the developed protocol for the purification of intact chloroplasts of *P. tricornutum*. (C) Sample analysis prepared with the improved protocol of isolated thylakoid membranes.

3.7.5 Experimental procedure SSL Grenoble

During the second investigation fresh samples obtained with the developed protocol were diluted 50 times in the adsorption buffer (10 mM Tris buffer 150 mM KCl and 25 mM $MgCl_2$). Then, ~30µl of the solution were deposited on mica surface (freshly cleaved) and incubated for 30-45 minutes. Non-bound membranes were washed away with recording buffer (10 mM Tris-HCl buffer 150 mM KCl pH 7.5). Buffers at pH 7.4 and pH 8 were also tested. The analyses were performed in Contact Mode and in Tapping Mode (see Hansma et al., 1994). The acquisition of the data was performed with a Cypher AFM (Asylum Research, Santa Barbara, CA, USA) in Amplitude-Modulation mode AFM (one of the most common technique) using BL-AC40 (BL-AC40 Olympus Ltd. Tokyo, Japan), Si_3N_4 cantilevers with nominal stiffness of 0.150 N/m.

3.7.5.1 Results and discussion

During this analysis we achieved to have fresh preparation of thylakoids membranes and it was possible to identify three different regions: lipid bilayer, debris of membranes and packed membranes (Figure 3.12 A 1,2,3, respectively). After many tests, several interesting structures were observed at nm scale, probably protein domains organized in filaments with a regular orderliness

(Figure 3.12 B). Nevertheless, as verified in different occasions, the continuous scanning of the tip damaged the delicate membranes.

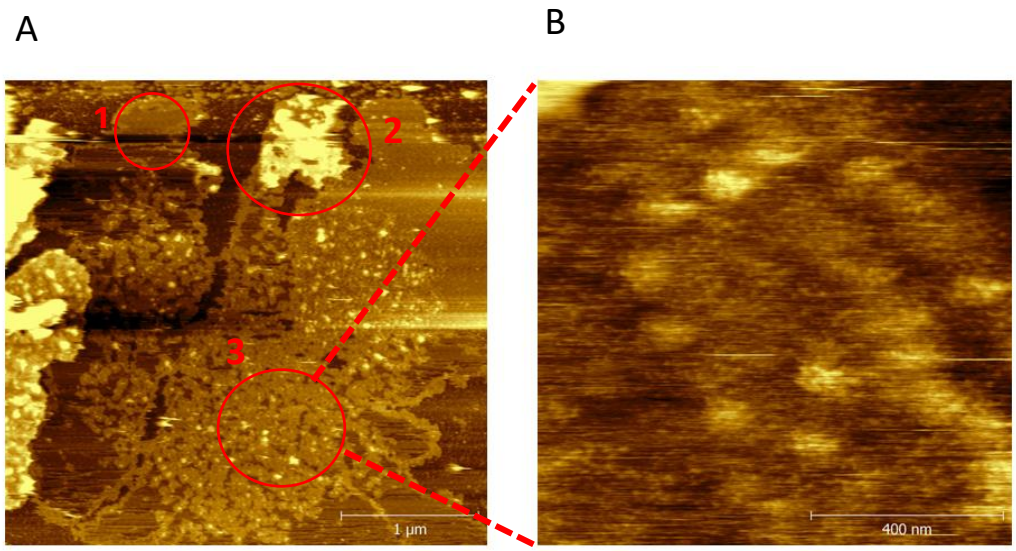

Figure 3.12 – **Results procedure SSL Grenoble.** (A) First analysis showing three different regions in the thylakoid membranes: (1) lipid bilayer (2) debris of membranes (3) packed membranes. (B) Details of the photosynthetic membranes of *P. tricornutum* showing ordered protein domains.

Overall, we concluded that the study with the Atomic Force Microscopy was not adequate for our purposes. The development of the procedure for sample preparation has required extensive effort due to the different organization of the thylakoid membranes in diatoms which has deeply modified the starting procedure (for review see Scheuring & Sturgis, 2009) adding repetitive purification steps. We consider that these additional steps might modify the natural assembly of the proteins in their natural environment. However, the advantage of this technique to study protein complexity and assembly in native membranes opens many possibilities for the future. The AFM should be employed as a supplementary tool to study the natural supramolecular organization of membranes. A future perspective can consider the application of the protocols here developed to plan new experiments and implement the knowledge on this technique.

Chapter 4

4.1 Introduction

This chapter is organized in three sections. In the first one (section 4.2) I will introduce the model organism *Chlamydomonas reinhardtii* and present some specific features of this alga. In particular, I will focus on the protein LHCSR3 (Light Harvesting Complex-Stress Related 3) which is the effector of the qE component of NPQ. I wil also describe acetate assimilation in *C. reinhardtii* and finish with a description of the nature and function of photoreceptors. In the second section (section 4.3) the article "A Blue Light Photoreceptor Mediates the Feedback Regulation of Photosynthesis" will be presented. In the third section (section 4.4), I will present data about the metabolic regulation of NPQ and LHCSR3 in *Chlamydomonas reinhardtii*.

4.2 *Chlamydomonas reinhardtii*

The model organism studied in this part of my Ph.D manuscript is the unicellular green alga *Chlamydomonas reinhardtii* (Greek *chlamys*: cloak and *monas*: solitary) belonging to the *phylum* Chlorophyta. It is a 10 µm fresh-water biflagellate that became one of the most widely studied photosynthetic unicellular organism thanks to its easily synchronization, rapid growth (doubling time ~ 8-12 hours), sequenced genome (Merchant et al., 2007) and the availability of numerous strains and mutants (http://www.chlamycollection.org/). *C. reinhardtii* possesses two equal apical flagella that allow it to swim and a cell wall composed by glycoproteins. A single chloroplast occupies a large volume of the cytoplasm (up to 50%, Figure 4.1). Unlike plants, the chloroplast of *C. reinhardtii* shows poorly stacked thylakoid membranes (Figure 4.1; see Engel et al., 2015 for a recent publication). The pyrenoid is also visible at the periphery of the chloroplast. Near the chloroplast, a primitive eye, the eyespot, recognizable as an orange spot (rich of carotenoids) mediates the perception of the light. This eye is essential for phototaxis (the ability to swim toward or away from a light source). *C. reinhardtii* is a widespread freshwater species, commonly found in temporary soil pools, eutrophic lakes, etc. In these habitats, the cells can experience drastic changes in light intensity (from total darkness to excessive photon flux intensities within few minutes). To cope with light fluctuations, *C. reinhardtii* has evolved a series of physiological photoacclimatative mechanisms to adjust its photosynthetic rate and to survive.

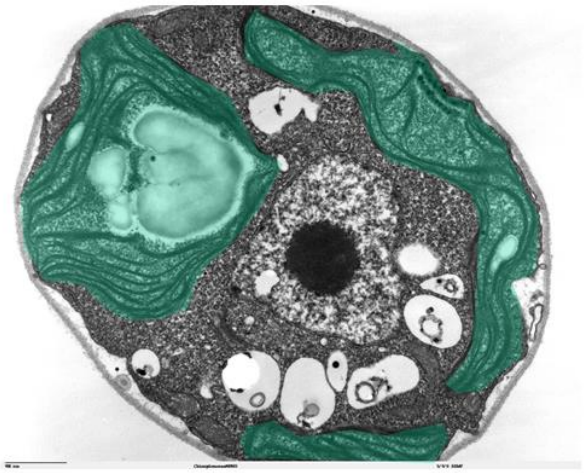

Figure 4.1 – **EM picture of *Chlamydomonas reinhardtii***. In green the chloroplast of *Chlamydomonas* is highlited (modified from http://remf.dartmouth.edu/imagesindex.html).

4.2.1 LHCSR

As mentioned earlier (section 1.6.1.1) the qE component of non-photochemical fluorescence quenching (NPQ) is the most efficient and rapid mechanism to regulate photosynthesis under excessive photon flux densities. In the green alga *Chlamydomonas reinhardtii* qE induction requires the nuclear-encoded chloroplast localized proteins LHCSRs (Ligh-Harvesting Complex Stress Related proteins, previously called Li818 Light Induced protein 818; Peers et al., 2009). Three genes encoding two LHCSRs isoforms are present in the genome of *C. reinhardtii* (Merchant et al., 2007). The *LHCSR3.1* (Cre08.g367500) and *LHCSR3.2* (Cre08.g367400) genes, which are 99% identical (775 out of the 780 base pairs) encode for the same 259 amino acid polypeptide LHCSR3, while the *LHCSR1* gene (Cre08.g365900) encodes for the LHCSR1 isoform. The proteins LHCSR1 and LHCSR3 have more than 80% identity (Bonente et al., 2011). In 2009, Peers and colleagues demonstrated that knock-out mutants of *LHCSR3.1* and *LHCSR3.2* have a largely reduced qE (Peers et al., 2009), concluding that LHCSR3 is the main qE effector protein in *C. reinhardtii*. In the double mutant of LHCSR3 and LHCSR1 no qE is detectable (Berteotti et al., 2016). LHCSR3 is a three helix protein located in the thylakoid membranes, which possess chlorophylls (Chl *a*/*b*) and carotenoids binding motifs (lutein, violaxanthin and zeaxanthin; Bonente et al., 2011). At variance with PSBS (the qE protein effector in higher plants; Li et al., 2000), which is contitutively accumulated in the thylakoids, LHCSR3 is induced by high light (Gagné & Guertin, 1992). However, LHCSR3 transcripts accumulate under environmental conditions inducing photo-oxidative stress, limitation of carbon dioxide (Miura et al., 2004), sulphur (Zhang et al., 2004) or iron (Naumann et al., 2007), as well as high light (Ledford et

al., 2004). Accumulation of LHCSR3 also requires active photosynthesis together with the Ca^{2+} binding protein CAS and Ca^{2+} signaling events (Petroutsos et al., 2011). This was later confirmed at the transcript level by Maruyama et al., 2014 who carefully studied the expression of *LHCSR1*, *LHCSR3.1* and *LHCSR3.2* at low and high light in the absence and presence of photosynthetic and Ca^{2+} signaling inhibitors. Yamano et al. (2008) showed that the transcription of LHCSR1 was repressed by low CO_2 while *LHCSR3.2* and *LHCSR3.1* were induced under low CO_2. *LHCSR1* transcriptional repression by low CO_2 was confirmed by Brueggemann et al., 2012 in a RNAseq study of cells shifted from high to low CO_2 conditions. Similarly, Fang et al., 2012 found that transcription of both *LHCSR3.1* and *LHCSR3.2* is upregulated in low CO_2 conditions and is under control of the CIA5 transcription factor that regulates transcription of genes for acclimation to low CO_2 such as inorganic carbon transporters and carbonic anhydrases.

LHCSRs proteins in *C. reinhardtii* possess a dual role acting as sensors of lumen acidification and as quenching site. Indeed LHCSR3 contains residues sensing luminal acidification (Ballottari et al., 2016), like PSBS. However, unlike PSBS, it also possess several pigment molecules (Bonente et al., 2011) and presumably act as a direct site of high light quenching (Tokutso & Minagawa, 2013; Ahn et al., 2008).

4.2.2 A facultative acetate flagellate

Chlamydomonas ability to survive in adverse conditions relies also to its metabolic flexibility and in particulal to its capacity to use organic carbon source via respiration in the dark (heterotrophy), to use inorganic carbon consuming CO_2 (photoautotrophy) or to combine the two carbon sources (mixotrophy). Depending on the prevailing mode of carbon assimilation, this versatile unicellular microalga is able to adjust its photosynthetic efficiency. It is well known, that the combination of both inorganic (CO_2) and an external organic carbon substrates leads to a synergetic effect of the two processes that enhances the productivity and growth of microalgae (Bhatnagar et al., 2010). For this reason, the central carbon metabolism play a crucial role balancing the production of energetic compounds (i.e carbohydrates and lipids) and photosynthetic efficiency.

The tricarboxylic acid cycle (TCA, also called Krebs cycle or citric acid cycle) is a key component of the central carbon metabolism, in which organic molecules are break down to produces reducing equivalents (NADH and $FADH_2$) to fuel the electron transport chain for cellular respiration.

The acetate metabolism in *C. reinhardtii* proceeds following its entry into the glyoxylate and the TCA cycle pathways. The conversion of fixed carbon into either carbohydrates or lipids involves different compartments of the cell: the chloroplast, the mitochondria and the cytosol. The TCA cycle takes place in mitochondria. Fuelled by ATP, the enzyme acetyl-CoA synthetase (ACS) converts acetate into acetyl-CoA a key metabolic compound involved in several physiological processes (i.e fatty acid and amino acid synthesis, the TCA and glyoxylate pathways, etc. Figure 4.2).

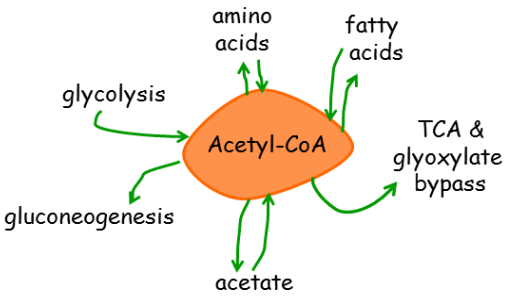

Figure 4.2 – **The central role of the Acetyl-CoA in central metabolism.** Representation of the physiological processes, which involves Acetyl-CoA (from Wolfe, 2015).

Acetate can also enter in the TCA cycle in a multiple-step reaction operated by two enzymes: the acetate kinase (ACK) and phosphate acetyltransferase (PAT; Wolfe, 2005; Ingram-Smith et al., 2006). This alga possess two parallel ACK-PAT pathways (ACK1-PAT2 localized in chloroplasts and ACK2-PAT1 localized in the mitochondria; Atteia et al., 2006, 2009; Terashima et al., 2010). Both ACKs and PATs are almost identical at amino acid sequences (similar for more than 70%; Yang et al., 2014). When one molecules of Acetyl CoA enters this cycle, it starts a series of oxidation-reduction reactions. The four-carbon molecule, oxaloacetate, is the first player of the cycle participating in the oxidation of the acetyl group (and also the last player because at the end of each cycle is regenerated). The overall pathway of the TCA cycle is represented in Figure 4.3 A. The enzymes involved in the cycle are: citrate synthase, aconitase, isocitrate dehydrogenase, α-ketoglutarate dehydrogenase, succinyl CoA synthetase, succinate dehydrogenase, fumarase and malate dehydrogenase. For every molecule of Acetyl-CoA that enter in the cycle 3 molecules of NADH, 1 molecule of $FADH_2$, 2 molecules of both ATP and CO_2 are produced (Johnson & Alric, 2013). The reduced compounds (NADH and $FADH_2$) are cosumed by the mitochondrial electron-transport chain generating a proton gradient across the membranes, which in turn fuels ATP synthesis. Alternatively, acetate can be metabolised via the glyoxylate cycle providing this microalga with

additional metabolic versatility. The glyoxylate cycle, is a five-steps reactions in which two enzymes (isocitrate lyase and malate synthase) bypass the two decarboxylation steps in the TCA cycle and permit the direct assimilation of carbon from Acetyl-CoA (Figure 4.3 B).

Starting from the initial observation that *C. reinhardtii* cells grown in presence of light and acetate (TAP medium) show no NPQ capacity (Finazzi et al., 2006), we have reinvestigated the link between acetate and photoprotection, as described in section 4.4

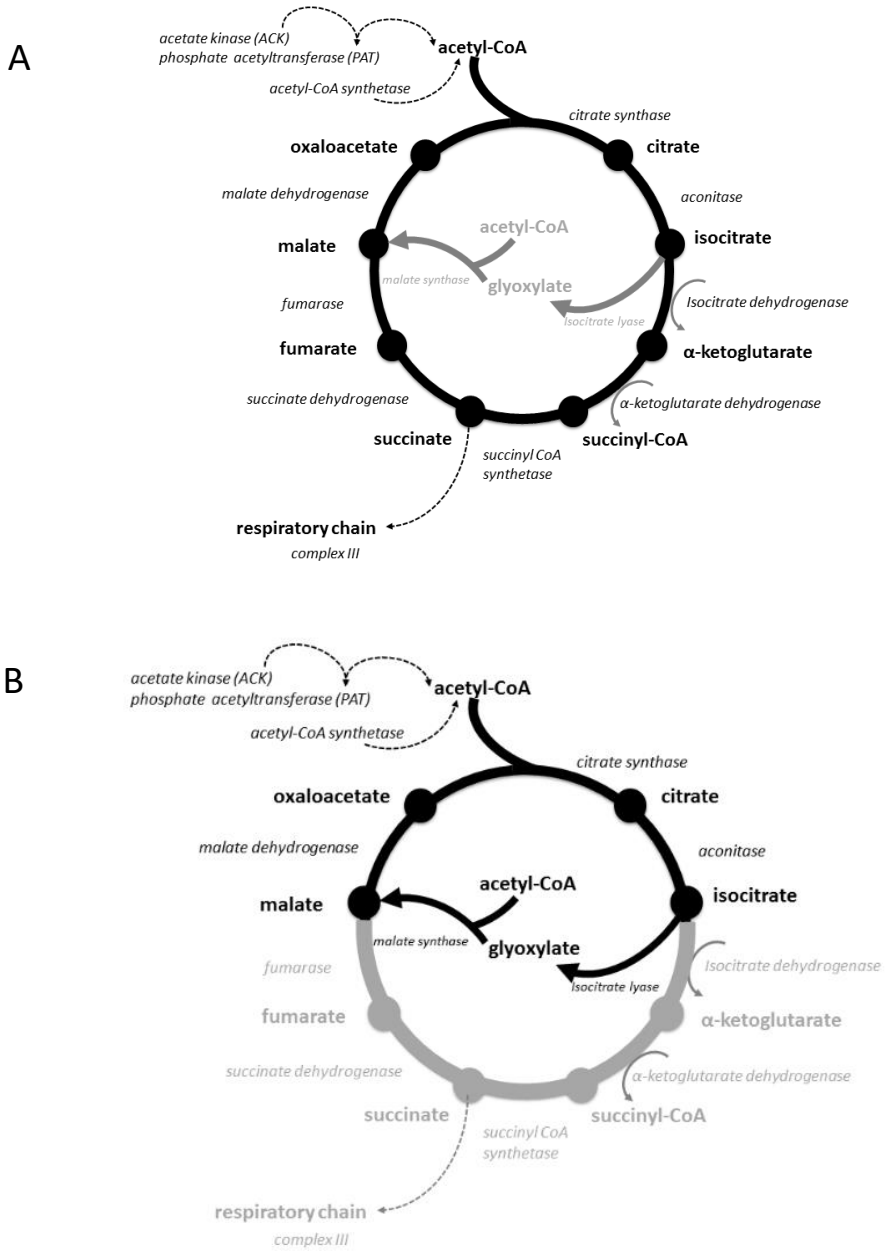

Figure 4.3 – **Schematic representation of acetate assimilation in *Chlamydomonas reinhardtii*.** (A) The tricarboxylic acid cycle. (B) the glyoxylate cycle.

4.2.3 Photoreceptors

Light is a crucial factor for photosynthetic organisms and its variability in time and space establishes their survival and performance in their natural environment. Its triple role can be briefly summarized as *i*. energy source for photosynthesis *ii.* environmental information converted by photoreceptor proteins into biological signals and *iii.* potential damage, when light absorbed overcomes the capacity for CO_2 fixation. Photosynthetic organisms evolved different strategies to cope with light fluctuating environments, which rely on sophisticated light-sensing system: the photoreceptors. A photoreceptor is a molecule that absorbs light and transduce its energy into a biological signal (Shropshire Jr. & Mohr, 1983). Typically, five types of photoreceptors (Figure 4.4) exist in plants: the UV Resistence locus 8 that absorb in the UV-B region at around 280-315 nm (Jenkins, 2014); the cryptochromes, that mediate the blue region (390-500 nm; Chaves et al.2011) as the phototropins (PHOT; Christie, 2007) and the members of the Zeitlupe protein family (Suetsugu & Wada, 2013); and finally the phytochromes, capable of absorbing the red (600–700 nm) and far-red regions (700–800 nm, Chen & Chory, 2011).

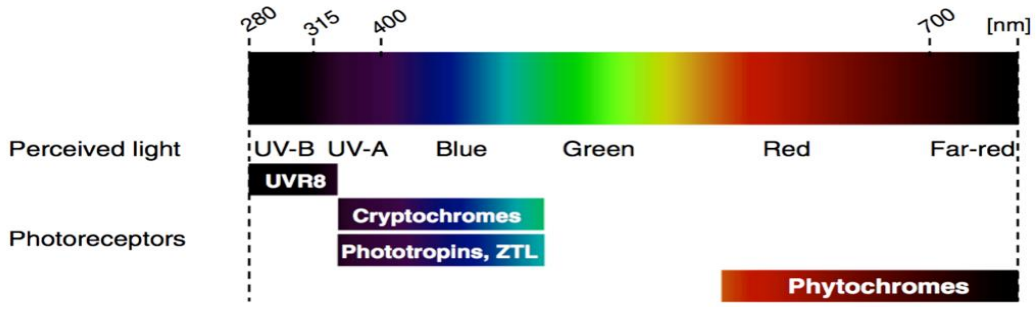

Figure 4.4 – **Photoreceptor proteins.** Scheme of the five types of photoreceptors found in plants (Heijde & Ulm, 2012)

4.2.3.1 Phototropin

In *C. reinhardtii*, phytochromes are missing (Figure 4.5) and the blue light responses are mediated by chryptochromes (Small et al., 1995) and phototropin (Huang et al., 2002). In this section, I will focus on the light-sensing perception operated by the blue-light photoreceptor phototropin in *C. reinhardtii* and on its link to photoprotection.

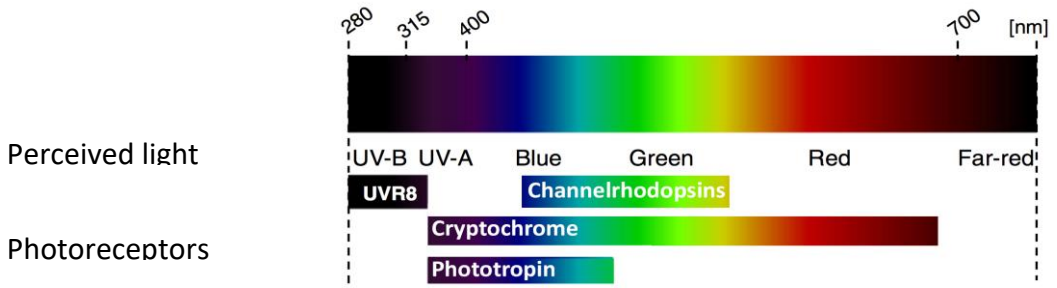

Figure 4.5 –**Photoreceptor proteins in *Chlamydomonas reinhardtii*.** Photoreceptors found in *Chlamydomonas reinhardtii* (Modified scheme from Heijde & Ulm, 2012).

In *C. reinhardtii,* phototropin is involved in the regulation of the cell cycle (Huang & Beck, 2003), in the eyespot development and phototactic behavior (Trippens et al., 2012) as well in the expression of light-regulated genes involved in chlorophyll and carotenoid biosynthesis (Im et al., 2006). Phototropins possess a serine-threonine kinase protein domain (PDK) at the C-terminus, and a photosensory region with two blue-light sensitive domains (called light oxygen and voltage domains, LOV1 and LOV2; Figure 4.6) at the N-terminus. The LOV domains are almost structurally identical and formed by a fold of ~110 amino acids tightly binding a flavin mononucleotide (FMN) cofactor, which acts as a chromophore (Tokutomi et al., 2008). While both LOV1 and LOV2 sense light, they probably do this in two different ways, as revealed by the findings that their quantum efficiency and photochemical reaction kinetics are different (Kasahara et al., 2002; Salomon et al., 2000). LOV1 is thought to be important for protein dimerization and acts as attenuator of phototropin activity (Matsuoka et al., 2007), whereas LOV2 has a central role in photoreceptor light activation and in the regulation of the kinase activity (Demarsy & Fankhauser, 2009). The PDK domain located at the C-terminus of the protein belongs to the AGC kinases family (cAMP-dependent protein kinase A, cGMP-dependent protein kinase G and phospholipid dependent protein C). This domain plays a crucial role in many biological processes, including cell growth, gene transcription and protein synthesis. The activation mechanism of phototropin by light involves *i.* blue-light sensing by the

LOV2 domain *ii.* conformational change and *iii.* autophosphorylation (Pfeifer et al., 2010) of several serine residues on the kinase domain (Christie, 2015). At variance with plants, where two PHOT exists, only a single phototropin has been identified in *C. reinhardtii* (Huang et al., 2002). The gene product is found in the plasma membrane of the cell body and in flagella (Huang et al., 2004). Proteomic studies also reveal its presence in the eyespot proteome (Schmidt et al., 2006).

Figure 4.6 – **Structure of the phototropin.** Schematic representation of the phototropin with at the N-terminal the two blue-light sensitive domains (LOV1 and LOV2) and at the C-terminal a serine-threonine kinase protein.

4.2.4 Okazaki large spectrograph

So far, no information was available on the possible link between light sensing and high light protection. In order to investigate this phenomenon, we employed the Okazaki Large Spectrograph (OLS, Ushio Inc., Tokyo, Japan) the largest spectrograph in the world used to measure the spectrum of NPQ *in vivo* (Figure 4.7 A). Equipped with light sources, a monochromator, and sample holders capable of exposing algae to a very monochromatic light (FWHM 1 nm) this instruments represented the state of the art choice for our purpose. So far, several photobiological experiments have been conducted on living organisms, biological molecules, and artificial organic molecules at the OLS (Watanabe et al., 1982; Otsuna et al., 2014). Using a 30 kW Xenon short arc lamp, the spectrograph projects (10 m in length) a spectrum of wavelengths ranging from 250 nm (ultraviolet) to 1000 nm (infrared, Figure 4.7 B) at light intensities up to 2000 µE m^{-2} s^{-1} with elevated specificity superior to regular spectrographs.

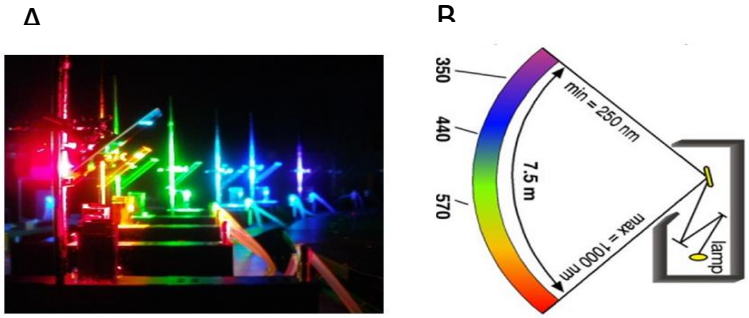

Figure 4.7 – **The largest spectrograph in the world**. (A) Picture of the Okazaki Large Spectrograph (OLS) http://www.nibb.ac.jp (B) Wavelength covered (modified from Otsuna et al., 2014).

4.3 Blue light perception by phototropin mediates regulation of photosynthetic light harvesting

4.3.1 Preface

The article presented in this chapter (Petroutsos et al., under revision in *Nature*) focuses on the model organism *C. reinhardtii*. In this section, we want to understand if besides light intensity, is there a role of the light quality in the induction of qE and LHCSR3?

This article clearly describe how the blue light perceived by the photoreceptor phototropin (PHOT) controls photoprotection by inducing the expression of the qE effector protein LHCSR3 in high light. More in detail, this control occurs via two steps: first, blue light is perceived by the photosensory regions (LOV domains) of this photoreceptor, probably activating PHOT via a conformational change. Then, a signal is transduced via the kinase domain of the activated PHOT. LHCSR3 induction by PHOT results in light dissipation in photosystem II, indicating that light sensing, utilization, and dissipation is a linked process in *C. reinhardtii*.

4.3.2 A blue light photoreceptor mediates the feedback regulation of photosynthesis

Dimitris Petroutsos[1], Ryutaro Tokutsu[2-4], Shinichiro Maruyama[5], Serena Flori[1], Andre Greiner[6], Leonardo Magneschi[1,7], Loic Cusant[1], Tilman Kottke[8], Maria Mittag[9], Peter Hegemann[6], Giovanni Finazzi[1], Jun Minagawa[2-4]

[1]Laboratoire de Physiologie Cellulaire et Végétale, UMR 5168, Centre National de la Recherche Scientifique (CNRS), Commissariat à l'Energie Atomique et aux Energies Alternatives (CEA), Université Grenoble Alpes, Institut National Recherche Agronomique (INRA), Institut de Biosciences et Biotechnologies de Grenoble, (BIG), CEA Grenoble, F-38054 Grenoble cedex 9, France

[2]Division of Environmental photobiology, National Institute for Basic Biology (NIBB), Nishigonaka 38, Myodaiji, Okazaki 444-8585, Japan

[3]Department of Basic Biology, School of Life Science, the Graduate University for Advanced Studies (SOKENDAI), Okazaki 444-8585, Japan

[4]Core Research for Evolutional Science and Technology (CREST), Japan Science and Technology Agency (JST), Saitama 332-0012, Japan

[5]Department of Environmental Life Sciences, Graduate School of Life Sciences, Tohoku University, Sendai 980-8578, Japan

[6]Humboldt University of Berlin, Institute of Biology, Experimental Biophysics. Invalidenstraße 42, D-10115, *Berlin, Germany*

[7]Institute of Plant Biology and Biotechnology, University of Münster, Münster 48143, Germany

[8]Physical and Biophysical Chemistry, Bielefeld University, 33615 Bielefeld, Germany

[9]Institute of General Botany and Plant Physiology, Friedrich Schiller University, 07743 Jena, Germany

Abstract

In plants and algae, light serves both as the energy source for photosynthesis and as a biological signal triggering cellular responses via specific sensory photoreceptors. Red light is perceived by bilin-containing phytochromes, blue light by the flavin-containing cryptochromes (CRYs) and/or phototropins (PHOTs; Jiao et al., 2007),the latter containing two photosensory LOV (light, oxygen, or voltage) domains (Christie, 2007). Photoperception spans several orders of light intensity (Briggs, 2014) ranging from far below the threshold for photosynthesis to values beyond the capacity of photosynthetic CO_2 assimilation. Excess light may cause oxidative damage and cell death unless it is prevented by enhanced thermal dissipation (energy quenching, qE), a key photoprotective response

(Li et al., 2009). Here, we show the existence of a molecular link between photoreception, photosynthesis, and photoprotection in the green alga *Chlamydomonas reinhardtii.* We show that PHOT controls qE by inducing the expression of the qE effector protein LHCSR3 (Light-Harvesting Complex Stress-Related Protein3) in high light. This control requires blue light perception by LOV domains, LHCSR3 induction through PHOT kinase, and light dissipation in photosystem II via LHCSR3. *phot* mutants display severely reduced fitness under excessive light conditions, indicating that light sensing, utilization, and dissipation is a concerted process playing a vital role in microalgal acclimation to environments of variable light intensities.

In oxygenic photosynthesis, light absorption by pigments (chlorophylls and carotenoids) embedded in the light harvesting complexes (LHCs) transfers energy to reaction centres, triggers electron flow from H_2O to NADPH, and generates a proton motive force across the chloroplast thylakoid membranes that is used for ATP synthesis. The generated ATP and NADPH molecules are consumed for CO_2 fixation in the Calvin-Benson cycle (Eberhard et al., 2008). Whenever light is absorbed beyond the CO_2 assimilation capacity, over-excitation of the photosystems leads to photodamage and possibly to cell death. Such negative consequences are prevented by non-photochemical quenching (NPQ), an intricate photoprotective process that dissipates excess absorbed energy. The major component of NPQ is high energy quenching (qE), which occurs at the LHCs of photosystem II (Horton et al., 1996). qE is driven by lumenal acidification under excess light, which modifies the LHCII pigment composition via the xanthophyll cycle and activates specific qE protein effectors (Niyogi & Truong, 2013). In the active state, these protein effectors (PSBS in plants and the light-harvesting complex stress-related (LHCSR) proteins in green algae; Peers et al., 2009; Tokutsu & Minagawa, 2013) increase the energy dissipation capacity of LHCII via a still unresolved mechanism (Ruban et al., 2007; Ahn et al., 2008). While plants constitutively express PSBS, the green alga *Chlamydomonas reinhardtii* only accumulates LHCSR3 (the major qE effector) following environmental stresses, including excess light and nutrient starvation (Finazzi & Minagawa, 2014). LHCSR3 induction requires Ca^{2+} signalling and active photosynthesis (Petroutsos et al., 2011; Maruyama et al., 2014) but the molecular mechanism behind this process is largely unknown.

4.3.2.1 Results and discussion

To gain insight into how LHCSR3 induction is regulated, we measured the light colour dependency (action spectrum) of qE induction in *C. reinhardtii.* Low light-acclimated cells were exposed for 4 hours to highly intense monochromatic light at different wavelengths between 400 and 720 nm, provided by the Okazaki Large Spectrograph (Watanabe et al., 1982), to induce LHCSR3. Then, kinetics of NPQ development were followed under saturating white light for 5 min (Figure 4.8 A). The extent of NPQ observed at the end of illumination was used to evaluate the action spectrum of qE (Figure 4.8 B) corresponding to the fraction of NPQ that is rapidly reversible in the dark. This spectrum was comparable to the spectrum of LHCSR3 accumulation (Figure 4.8 C), confirming the tight link between energy dissipation and LHCSR3 induction in this alga (Peers et al., 2009). We found that blue light was more effective than red light in inducing the qE response (Figure 4.8 A and B) and LHCSR3 accumulation (Figure 4.8 C), although the cells absorbed both almost equally (Figure 4.8 B, grey area). This finding suggests that a blue light-absorbing molecule (likely a blue light receptor) is involved in LHCSR3 accumulation in high light. To test this hypothesis, we compared NPQ kinetics (Figure 4.8 A), the action spectra of qE (Figure 4.8 B) and the induction of LHCSR3 (Figure 4.8 C) in wild-type (WT) and mutant *C. reinhardtii* cells lacking blue light receptors, either the animal-like cryptochrome (aCRY; Beel et al., 2012), or phototropin (PHOT; Zorin et al., 2009). *acry* cells (Supplementary Figure 4.12 A) showed WT levels of qE (Figure 4.8 B) and LHCSR3 accumulation (Figure 4.8 C) throughout the entire light spectrum, including red light, where aCRY acts (Beel et al., 2012) in the absence of phytochromes in *C. reinhardtii* (Merchant et al., 2007). Conversely, *phot* cells (Supplementary Figure 4.12 B) specifically lacked blue light induction of qE (Figure 4.8 B) and LHCSR3 accumulation (Figure 4.8 C), and therefore were more prone to photodamage (Figure 4.8 D). *phot* cells also showed a largely compromised induction of LHCSR3 and NPQ in high intensity white light at variance with WT and *acry* cells (Supplementary Figure 4.12 C, D and E). Their ability to accumulate photoprotective carotenoids via the xanthophyll cycle was, however, similar to that of WT and *acry* cells (Supplementary Figure 4.12 F and G). The phenotype of *phot* was similar to that of *npq4* (Figure 4.8 B and D), a deletion mutant of LHCSR3 (Peers et al., 2009) that we used as a qE lacking strain. PHOT-mediated blue light control of LHCSR3 accumulation was highly specific. Accumulation of representative subunits of the major photosynthetic complexes was comparable in all cell lines and wavelength-insensitive (Supplementary Figure 4.13). The photosynthetic electron transport rate (ETR) was somewhat reduced in *phot* cells, especially upon high light exposure (Supplementary Figure 4.12 H and I). Since photosynthesis is required for proper LHCSR3

accumulation (Petroutsos et al., 2011; Maruyama et al., 2014) the lower electron flow capacity of *phot* cells could diminish LHCSR3 induction. To evaluate this hypothesis, we titrated ETR in WT cells using variable concentrations of the herbicide 3-(3,4-dichlorophenyl)-1,1-dimethylurea (DCMU), which inhibits electron transfer in photosystem II. Addition of DCMU progressively reduced the ETR to a much lower extent in WT cells than in DCMU-free *phot* cells (Supplementary Figure 4.10 A). However, accumulation of LHCSR3 remained larger in DCMU-treated WT cells than in DCMU-untreated *phot* cells (Supplementary Figure 4.14 B). We therefore excluded the possibility that the diminished ETR observed in *phot* cells was the cause of the impaired LHCSR3 accumulation. We concluded instead that the impaired photoprotection in *phot* was the cause of the reduced ETR (Supplementary Figure 4.12 I) and enhanced photosensitivity (Fig 4.8 D), indicating that PHOT is a central actor of photoprotection in this alga.

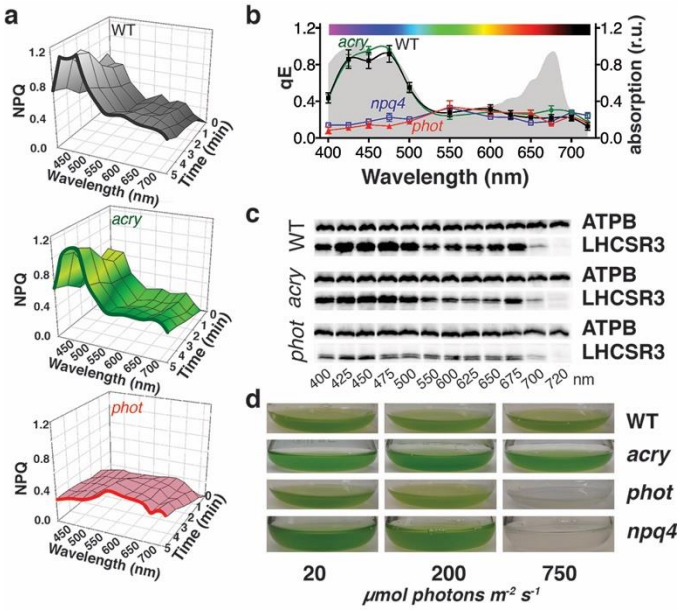

Figure 4.8 – **PHOT controls induction of LHCSR3 and qE and is crucial for survival in high light in *C. reinhardtii***. (A) Development of NPQ in WT (137c), *phot* and *acry* mutants during illumination with high intensity white light (750 µmol photons m^{-2} s^{-1}). Before the measurements, cells were exposed for 4 h to different wavelengths of actinic light (250 µmol photons m^{-2} s^{-1}) provided by the Okazaki Large Spectrograph (Watanabe et al., 1982) to induce LHCSR3, and dark acclimated for 30 min. (B) Action spectra of qE induction in WT (black), *acry* (green) *npq4* (blue) and *phot* (red) strains by 4h illumination with different wavelengths of actinic light (250 µmol photons m^{-2} s^{-1}). Grey area, absorption spectrum of WT cells. Data shown as mean ± SD (n = 3). (C) Immunoblot analysis of LHCSR3 accumulation. ATPB was used as loading control. (D) Erlenmeyer flasks containing WT, *acry*, *phot* and *npq4* after 16 h of light of 20, 200 and 750 µmol photons m^{-2} s^{-1}.

Phototropins are ubiquitous in plants and algae, and their function in light perception involves two structurally similar LOV domains (LOV1 and LOV2) at the N terminus and downstream signalling via a C-terminal Ser/Thr kinase domain (Christie, 2007). We dissected the role of the different PHOT domains in LHCSR3 induction using existing mutants (Trippens et al., 2012; Figure 4.9 A). Complementation of *phot* with the full-length cDNA of PHOT (strain PPHOT) restored PHOT protein (Supplementary Figure 4.15 A), *LHCSR3.1* and *LHCSR3.2* transcripts (both encoding for LHCSR3, Peers et al., 2009, Figure 4.9 B) and LHCSR3 protein (Figure 4.9 C) to a certain extent, which was nonetheless sufficient to largely rescue resistance to high light stress, (Figure 4.9 D and Supplementary Figure 4.15 B). Moreover, introduction of the *LHCSR3.1* gene into *phot* under the control of the strong, PHOT-independent *PsaD* promoter (strain PLHCSR3) also rescued qE and LHCSR3 levels (Supplementary Figure 4.16). Thereby, the univocal relationship between PHOT, LHCSR3 and photoprotection was confirmed. Conversely, complementation of *phot* with the truncated gene carrying only the photosensory domains LOV1 and LOV2 (strain PLOV) did not rescue either the protein or photosensitivity (Figure 4.9 C, D and Supplementary Figure 4.15 B). Finally, complementation with the kinase domain (strain PKIN) fully restored expression of LHCSR3 and photoprotection (Figure 4.9 C, D and Supplementary Figure 4.15 B).

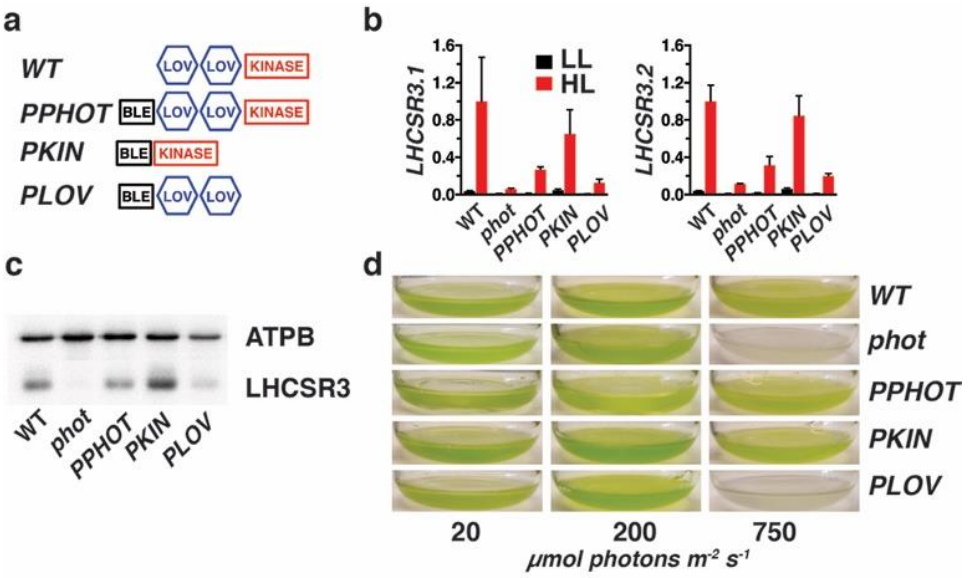

Figure 4.9 – **Role of the different PHOT domains in controlling LHCSR3**. (A) Schematic drawings of constructs used for the complementation of *phot* mutant. BLE, bleomycin resistance cassette; LOV, the light, oxygen, or voltage photosensory domain and KINASE, and the kinase domain of the *PHOT* gene**.** (B) *LHCSR3.1* and *LHCSR3.2* mRNA accumulation in WT (*cw15-302*), *phot*, and *phot* complemented with full-length PHOT (PPHOT), with the photosensory domains (PLOV) or with the kinase domain (PKIN) in low light (LL) or high light (HL). Mean values relative to an endogenous control gene encoding G protein subunit-like protein (GBLP) are calculated from three biological replicates and normalized to WT HL samples and shown as mean ± SD (n = 3). (C) Immunoblot analysis of LHCSR3 accumulation in the WT control and in the different *phot* mutants. ATPB was used as loading control. (D) Erlenmeyer flasks containing WT, *phot*, PPHOT, PLOV and PKIN after 20 h exposure to light of 20, 200 or 750 µmol photons m^{-2} s^{-1}.

In this line, however, LHCSR3 accumulation became light-color-independent (Figure 4.10 A and B), at variance with the WT (Figure 4.8 A, C) and the PPHOT strain (*phot* complemented with full-length PHOT; Figure 4.10 A and B). This indicates that removal of the LOV domains fully unleashed inhibition of the kinase activity as previously reported in plants (Kong et al., 2007). Deregulation of the PHOT kinase activity (PKIN) or removal of the kinase domain (*phot*, PLOV) did not alter LHCSR3 phosphorylation levels (Supplementary Figure 4.17), ruling out any link between PHOT and LHCSR3 phosphorylation. We also found that LHCSR3 accumulation remained light intensity-dependent in the PKIN strain (Figure 4.10 C, D), suggesting that in addition to PHOT, high light photosynthesis was required for accumulation of LHCSR3. In agreement with this interpretation, in another mutant generated by inserting an additional copy of the kinase domain into WT *C. reinhardtii* cells (WTKIN, Supplementary Figure 4.18) LHCSR3 accumulation also became largely wavelength-independent but was still light intensity-sensitive. Moreover, accumulation of LHCSR3 was fully blocked upon inhibition of photosynthesis by DCMU in the PKIN and WTKIN strains (Figure 4.10 C, D, Supplementary Figure 4.18 E). Additionally, LHCSR3 was not accumulated in the far-red part of the spectrum in all cell lines (720 nm; Figure 4.8 C, Figure 4.10 A, B, Supplementary Figure 4.18 C, D). This light is not absorbed by *C. reinhardtii* cells (Figure 4.8 B, grey area) and therefore does not activate photosynthesis.

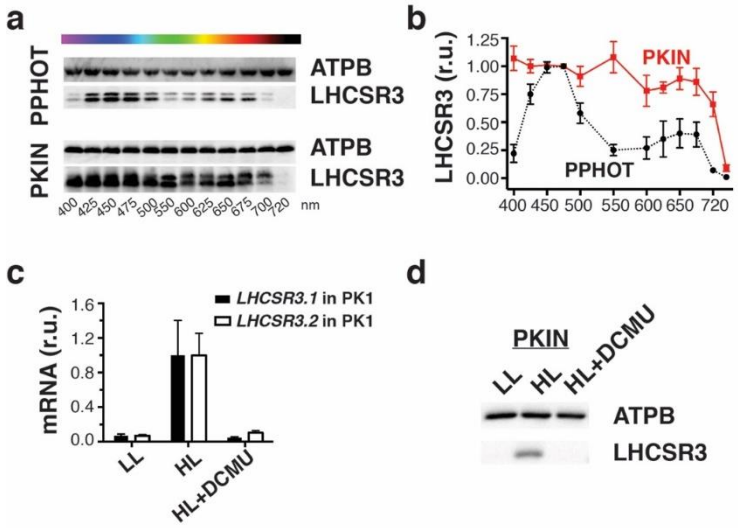

Figure 4.10 – **PHOT-dependent control of LHCSR3 expression requires blue light perception by LOV, signal transduction by the C-terminal kinase domain of PHOT and photosynthesis**. (A) Action spectrum of LHCSR3 accumulation in PPHOT (*phot* complemented by full-length PHOT) and PKIN (*phot* complemented by the kinase domain of PHOT). ATPB was used as loading control. (B) Densitometric quantification of LHCSR3 accumulation in PPHOT and PKIN (data normalized with ATPB) of Figure 4.10 A. Values are normalized to 475 nm and shown as mean ± SD (n = 3). (C) *LHCSR3.1* and *LHCSR3.2* mRNA accumulation in PKIN at LL and HL in the presence and absence of the PSII inhibitor DCMU. Values are normalized to HL and shown as mean ± SD (n = 3). (D) LHCSR3 protein accumulation in PK in LL and HL in the presence or absence of DCMU for 4h.

In *Arabidopsis,* PHOTs regulate the blue light-induced increase in cytosolic free Ca^{2+} (Harada et al., 2003; Babourina et al., 2002). Since PHOT controls LHCSR3 expression in *C. reinhardtii* (Figure 4.8) and Ca^{2+} is required for the accumulation of LHCSR3 (Petroutsos et al., 2011), a link between PHOT, Ca^{2+}, and LHCSR3 can be conceived. However, a ten-fold elevation of extracellular Ca^{2+} to 3.4 mM did not restore LHCSR3 accumulation in the *phot* mutant (Supplementary Figure 4.19 A). This finding led us to conclude that Ca^{2+} signalling is not modulating LHCSR3 in the absence of PHOT. We hypothesise that other second messengers (the cyclic nucleotides cAMP or cGMP) act as signalling molecules downstream of PHOT. We tested this hypothesis using a pharmacological approach and found that treatment of *phot* cells with 3-isobutyl-1-methylxanthine (IBMX), an inhibitor of cAMP/cGMP-phosphodiesterases, rescued LHCSR3 expression (Figure 4.11 A and Supplementary Figure 4.19 B). We confirmed this effect by incubating *phot* cells with dibutyrylated cGMP and cAMP (db-cGMP and db-cAMP; Figure 4.11 A), suggesting that in *C. reinhardtii*, cyclic nucleotides are not only critical in mating and phototaxis (Merchant et al., 2007) but are also involved in photoprotection through regulating LHCSR3 expression. On the other hand, induction of LHCSR3 in IBMX-treated WT or *phot* cells remained light intensity-dependent (Figure 4.11 A), implying that cAMP/cGMP require a high-light-photosynthesis-related signal to be effective on LHCSR3 accumulation.

While extensive research has focused on the nature and functions of the molecular actors involved in the sensing (photoreceptors) and utilization (photosynthetic complexes) of environmental light, the present work uncovers the molecular linkage between these two essential functions of photosynthetic organisms (Figure 4.11 B). Blue light perceived by phototropin controls photoprotection of the photosynthetic machinery (qE) in a green alga. The LOV domain of PHOT provides blue light sensitivity while its kinase domain performs signal transduction, possibly via a cyclic nucleotides monophosphate-signalling cascade. At some point downstream of PHOT, this signal integrates with another regulatory signal from the chloroplast that carries information about the amount of absorbed light that is not used by photosynthesis. This signal relies on photosynthetic electron transfer (Petroutsos et al., 2011; Maruyama et al., 2014) via an unknown mechanism. The integrated signal affects accumulation of *LHCSR3.1*/*LHCSR3.2* transcripts (Figure 4.9 B), mainly due to activation of transcription and partially due to stabilisation of the transcripts (Supplementary Figure 4.20). This contrasts with plant PHOTs that have been suggested to destabilize transcripts (Folta & Kaufman, 2003) while little evidence exists for their role in activation of transcription

(Christie, 2007). The LHCSR3 polypeptide is then imported into the chloroplast thylakoids, where it modulates qE (Figure 4.11 B).

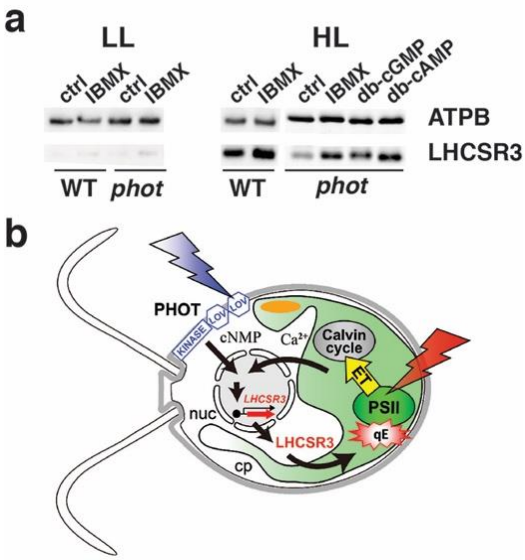

Figure 4.11 – **Possible signal transduction pathway for HL-induced expression of LHCSR3**. (A) Immunoblot analyses of LHCSR3 accumulation in WT (*cw15-302*) cells and in *phot* cells treated with the phosphodiesterase inhibitor IBMX, db-cAMP or db-cGMP after exposure to LL or HL for 20 h. (B) Schematic representation of the negative feedback regulation of photosynthesis (photoreception–photosynthesis–photoprotection link) in *C. reinhardtii*. cp, chloroplast; cNMP: cyclic nucleotides mono phosphate (cAMP or cGMP); ET, electron transport; nuc, nuclear; PSII, photosystem II.

4.3.2.2 Conclusions

Because LHCSR3 is “an ancient light harvesting protein” (Peers et al., 2009) found only in “lower plants” including green unicellular eukaryotic algae (chlorophytes), and mosses (Niyogi & Truong, 2013) as well as in Chromalveolata (algae derived by secondary endosymbiosis) we hypothesise that the molecular link for photoreception-photosynthesis-photoprotection discovered in this study has evolved in the environment in which photosynthesis started during evolution, namely the water columns, where blue light dominates the available spectrum. Consistent with this hypothesis, photoprotection in cyanobacteria, which are thought to share a common ancestry with chloroplasts, also relies on blue light. The cyanobacterial NPQ protein effector OCP (Orange Carotenoid Protein) binds a single blue light-absorbing carotenoid, and NPQ in cyanobacteria is also triggered by high intensity blue light (Kirilovsky & Kerfeld, 2013). Evidences also show a link between blue light and photoprotection in diatoms (Costa et al., 2013) via a still uncharacterised mechanism. On the other hand, the blue light-dependent control of photoprotection was apparently lost during colonisation of the land, where a new qE process evolved, which is based on a constitutively expressed protein (PSBS; Li et al., 2009). Land plants, however, seem to carry a remnant of ancestral qE control by blue light, called ‘qM’, because blue light still affects NPQ in these organisms, but only via the PHOT-triggered chloroplast movements that avoid high light (Cazzaniga et al., 2013).

The transition from water to the land was paralleled by the emergence of a second PHOT gene. Seed plants contain PHOT1, responding to low intensity blue light signals, and PHOT2, triggering high intensity blue light responses. Unicellular green algae, like *Chlorella variabilis*, *Ostreococcus tauri*, and *C. reinhardtii*, only contain one PHOT gene, which is the ortholog of PHOT2 (Galván-Ampudia & Offringa, 2007). However, in *C. reinhardtii* blue light triggers different biological responses depending on the photon fluence rate. Low intensity blue light (e.g. 1 µmol photons m^{-2} s^{-1}) triggers gametogenesis at low nitrogen abundance (Huang & Beck, 2003) and gene expression (Im et al., 2006) whereas blue light at higher intensities desensitizes the eyespot (Trippens et al., 2012) and induces LHCSR3 expression (e.g. 60 µmol photon m^{-2} s^{-1}, Supplementary Figure 4.21). Thus, we conclude that the same PHOT that ensures low light responses can trigger higher light signalling when acting in synergy with the photosynthetic signal. We propose that while the transition from the motile life form of algae to the sessile character of land plants led to an increased specialisation of the function of photoreceptors, this process occurred at the expense of some essential functions in water, likely the regulation of photoprotection reported here.

4.3.2.3 Materials and methods

Chemicals: Chemicals were purchased from Sigma (DCMU) and Enzo (3-isobutyl-1-methylxanthine (IBMX), dibutyryl cyclic AMP (db-cAMP), and dibutyryl cyclic GMP (db-cGMP)). Stock solutions of DCMU were prepared in ethanol (40 mM) or H_2O (40 µM); IBMX was dissolved in DMSO at 250 mM; db-CAMP and db-GMP were dissolved in H_2O.

Strains and conditions: *C. reinhardtii* strains were grown under 20 µmol photons m^{-2} s^{-1} in Tris-acetate-phosphate (TAP) media (Gorman & Levine, 1965) at 23 ^{o}C. In all experiments cells were transferred to Sueoka's high salt medium (Sueoka, 1960) at 2 million cells/mL and exposed to light intensities as described in the text and figure legends. Two *C. reinhardtii* WT strains, the *cw15-302* and 137c, were used as indicated in the Figure legends. The *phot* mutant was previously generated using a homologous recombination strategy (Zorin et al., 2009). For the different complemented lines of *phot*, *PsaD* promoter and terminator were used for the expression of full-length PHOT cDNA (strain PPHOT; clone PPHOT3 or PPHOT4), the LOV domains (strain PLOV; clone PLOV1) and the kinase domain (strain PKIN; clone PKIN1), N-terminally fused to the Zeocin resistance marker sh-*Ble,* (Trippens et al., 2012). Using the same strategy, overexpression of the PHOT kinase domain in the WT background resulted in the strain WTKIN (Trippens et al., 2012). For the PHOT-independent expression of LHCSR3, the *PsaD* promoter and terminator were fused to a full-length genomic *LHCSR3.1* gene. The generated construct with the *aphVII* marker gene was introduced into *phot* by electroporation with NEPA21 Super Electroporator (NEPAGENE, Japan). The transformants, PLHCSR3(B5) and PLHCSR3(G6), were screened for their resistance to 10 µg/mL hygromycin. The *acry* mutant, originally delivered in a SAG73.72 genetic background (Beel et al., 2012), was back-crossed three times to WT strain 137c. Unless otherwise stated, LL conditions corresponded to 20 µmol photons m^{-2} s^{-1} while HL conditions corresponded to 250 µmol photons m^{-2} s^{-1} of white light. All experiments were repeated three times to verify their reproducibility, unless otherwise stated.

Pigment and mRNA quantification: Extraction and quantification of chlorophyll and xanthophylls, calculation of the de-epoxidation state DES, and mRNA quantification by quantitative PCR were performed as described previously (Maruyama et al., 2014; Allorent et al., 2013). A gene encoding G protein subunit-like protein (GBLP; Schloss, 1990) was used as the endogenous control, and relative expression values relative to *GBLP* (Figure 2b and 3c) were calculated from three biological replicates, each of which contained three technical replicates. The primers used were *LHCSR3.1* (5'-

CACAACACCTTGATGCGAGATG-3' and 5'- CCGTGTCTTGTCAGTCCCTG-3'), *LHCSR3.2* (5'-TGTGAGGCACTCTGGTGAAG-3' and 5'-CGCCTGTTGTCACCATCTTA-3'), *GBLP* (5'-CAAGTACACCATTGGCGAGC-3' and 5'-CTTGCAGTTGGTCAGGTTCC-3'), and 18S rRNA (5'-AGCATGAGAGATGGCTACCACATC-3' and 5'-CATTCCAATTACCAGACGCGAAGC-3'). The mRNA stability experiments were performed in the presence of the transcription inhibitor actinomycin D (Wako, Japan) at 160 μg/mL (Gera & Baker, 1998). RT-PCR was performed using Light cycler 96 (Roche) with AptaTaqDNA GM with ROX (Roche).

Immunoblotting: Protein samples of whole cell extracts (0.5 μg chlorophyll, unless stated otherwise) were loaded on 7% or 13% SDS-PAGE gels and blotted onto nitrocellulose membranes. Antisera against D1, D2 and ATPB were from Agrisera (Vännäs, Sweden); previously described were antisera against *C. reinhardtii* aCRY (Beel et al., 2012), PHOT (LOV1 domain; Zorin et al., 2009), and all others (Takahashi et al., 2006; Iwai et al., 2010). ATPB was used as a loading control. An anti-rabbit horseradish peroxidase–conjugated antiserum was used for detection. The blots were developed with ECL detection reagent, and images of the blots were obtained using a CCD imager (ChemiDoc MP System, Bio-Rad). For the densitometric quantification of LHCSR3 data were normalized with ATPB. LHCSR3 appears as a double band in some of the western blots (i.e. Figure 4.10 and Supplementary Figures 4.13, 4.15, 4.17, 4.18, 4.19). The upper band represents the phosphorylated form of LHCSR3 (see Supplementary Figure 4.17). The extent of LHCSR3 phosphorylation was determined using a Phos-tag-based method as described (Longoni et al., 2015). For the de-phosphorylation of LHCSR3 whole cell extracts (1 μg total chlorophyll) were treated with either 20 U of calf intestine phosphatase (Promega) or 200 U of lambda protein phosphatase (New England Biolabs) in the presence of 0.05 (v/v) Triton X-100, at 30^{o}C for 1h.

Fluorescence-based measurements: Fluorescence-based photosynthetic parameters were measured with a fluorescence imaging setup previously described (Johnson et al., 2009). The photosynthetic electron transfer rate (ETR) was calculated as (Fm'-F)/Fm' * 0.84 * 0.5 * I (Petroutsos et al., 2009). qE was estimated as the fraction of NPQ that is rapidly inducible in the light and reversible in the dark, using the following equation: (Fm-Fm')/Fm'. F and Fm' are the fluorescence yields in steady state light and after a saturating pulse in the actinic light, respectively, Fm is the maximal fluorescence yield in dark-adapted cells, and I is the light irradiance in μmol photons m^{-2} s^{-1} (Petroutsos et al., 2009). Before NPQ measurements cells were exposed to high intensity light for

4 h unless otherwise mentioned to induce LHCSR3 and dark acclimated for 30 min. For NPQ measurements actinic light was set at 750 µmol photons m^{-2} s^{-1}. For action spectra measurements, 5 mL of concentrated cells (2 * 10^7 cells mL^{-1}) were placed in a petri dish and exposed to intense (250 µmol photons m^{-2} s^{-1}) monochromatic light (The spectral half width is 5.5 nm or less), provided by the Okazaki Large Spectrograph (Watanabe et al., 1982) for 4 h. Samples were then collected and subjected to immunoblotting (0.1 mL) as well as qE measurement (0.2 mL) with a fluorescence video-imaging system (Fluorocam, Photon System Instruments, Bruno, Czech Republic).

Contributions

D.P., R.T., J.M. and G.F. designed the study. D.P., R.T., S.M., S.F., L.M., L.C., J.M. and G.F. performed the experiments. D.P., R.T., S.M., A.G., L.M., T.K., M.M., P.H., J.M. and G.F. provided strains and analysed the data. D.P., R.T., J.M. and G.F. wrote the manuscript, and all authors revised and approved it.

Supplementary Figures

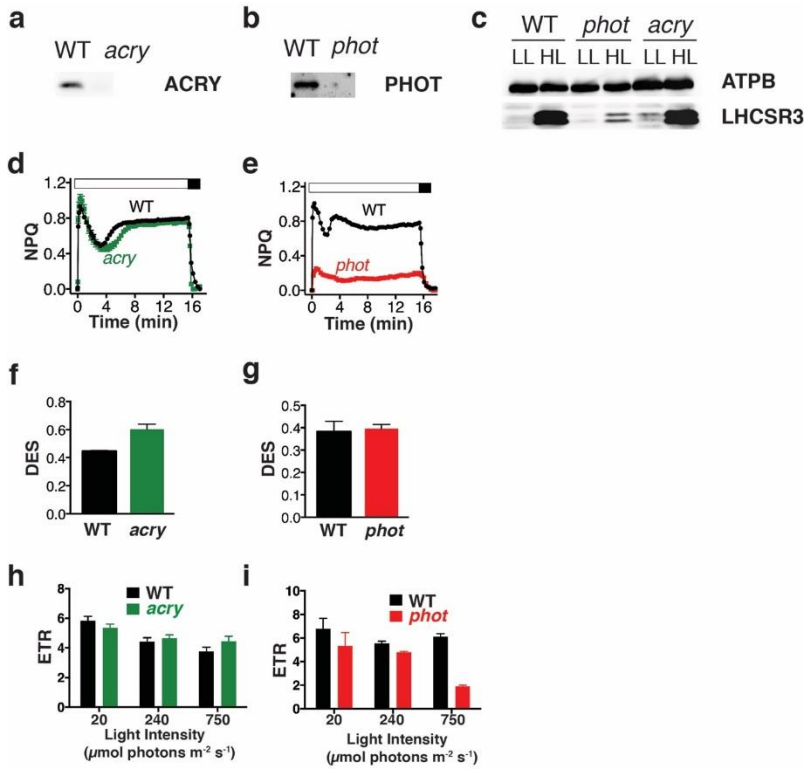

Supplementary Figure 4.12 – **Photosynthetic properties of *acry* and *phot* mutants**. (A) Immunoblot analysis of aCRY accumulation in WT (137c) and *acry* cells. The two strains were grown as described previously (Beel et al., 2012). Cells were harvested at the beginning of the light phase (LD2 phase; Beel et al., 2012). Whole cell samples with 2 µg of chlorophylls were loaded on each lane. (B) Immunoblotting analysis of PHOT in WT (*cw15-302*) and *phot* after 4 h exposure to high intensity white light. (C) Immunoblot analysis of LHCSR3, and ATPB in WT (137c), *phot* and *acry* in LL and after 4 h exposure to high intensity white light (HL). ATPB was used as loading control. (D) and (E), NPQ induction kinetics of WT (137c) and *acry* (D) and WT (*cw15-302*) and *phot* (E) after 4 h exposure to high intensity white light. qE was recorded for 16 min upon illumination with 440 µmol photons m^{-2} s^{-1} (*white bar*) followed by 2 min of darkness (*black bar*), to follow qE relaxation. f and g, Xanthophyll cycle de-epoxidation state (DES) indicating the ratio ([zeaxanthin] + 1/2 [antheraxanthin])/([zeaxanthin] + [antheraxanthin] + [violaxanthin]) in WT (137c) and *acry* (f) and WT and phot (g) cells after exposure HL for 4 h. (H) and (I), Electron transfer rate (ETR) of WT (137c) and *acry* (h) and WT (*cw15-302*) and phot (i) cells exposed at 20, 240 and 750 µmol photons m^{-2} s^{-1} for 10 h. ETR (µmol photons m^{-2} s^{-1}) was measured at actinic illumination of 41 µmol photons m^{-2} s^{-1}. Mean ± SD (n = 3).

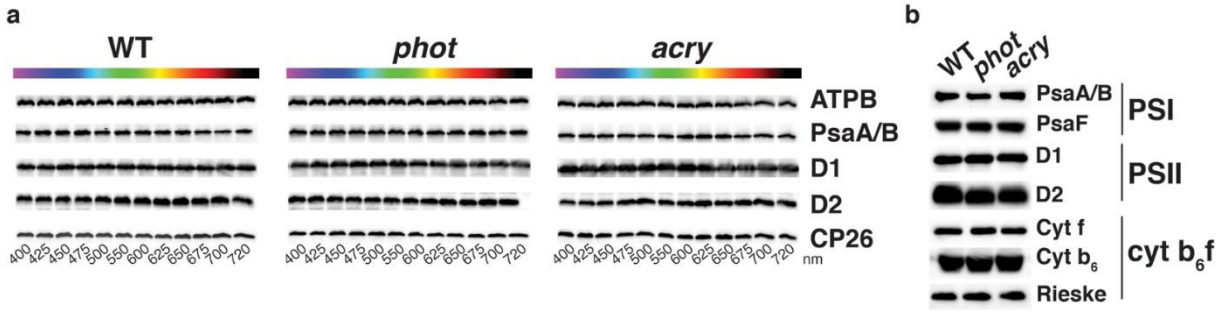

Supplementary Figure 4.13 –**Accumulation of major photosynthetic complexes is unaltered in the *phot* cells upon exposure to different wavelengths of visible light.** (A) Immunoblot analyses of ATPB, PsaA/B, D1, D2 and CP26 accumulation in WT (137c), *phot* and *acry* cells after 4 h exposure at 250 µmol photons m^{-2} s^{-1} of monochromatic light at the different wavelengths of the visible spectrum. (B) Immunoblot analyses of major photosynthetic complexes of PSII, Cyt $_{b6f}$ and PSII in WT, *phot* and *acry* after 4 h exposure at 250 µmol photons m^{-2} s^{-1} of white light.

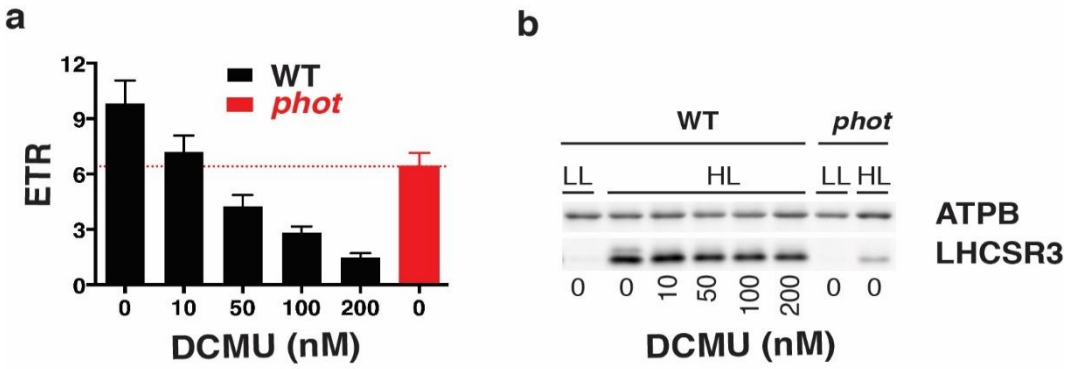

Supplementary Figure 4.14 – **Diminished LHCSR3 induction in *phot* is not caused by diminished photosynthesis**. (A) Comparison of ETR in DCMU-titrated WT cells and DCMU-untreated *phot* cells exposed to HL for 3 h. ETR (µmol photons m^{-2} s^{-1}) was measured upon exposure to light of 170 µmol photons m^{-2} s^{-1}. Mean ± SD (n = 3). (B) Immunoblotting analysis of LHCSR3 accumulations in the WT and *phot* samples described in Extended Data Figure 4a. ATPB was used as a loading control.

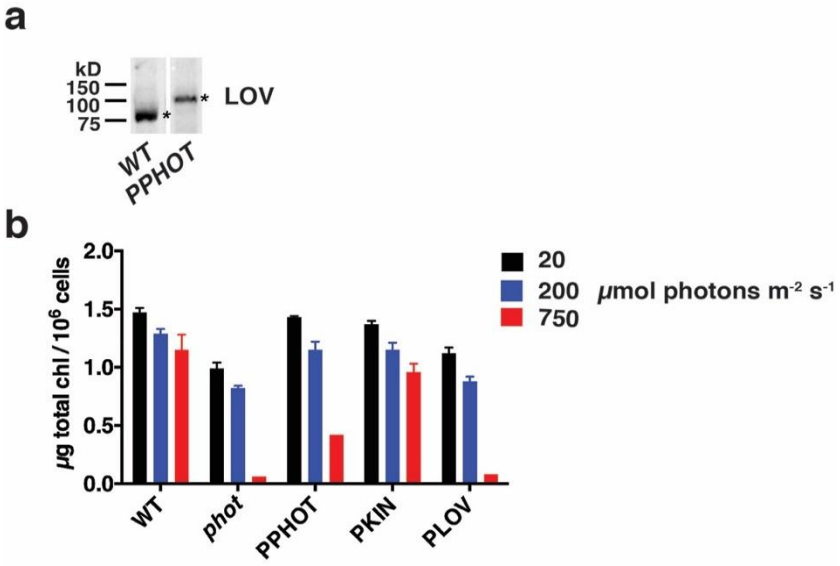

Supplementary Figure 4.15 – **PHOT protein levels pigment content in *phot* mutants**. (A) Immunoblotting analyses of PHOT accumulation in WT (*cw15-302*) and the PPHOT (*phot* complemented by a full-length PHOT). PPHOT expresses a fused PHOT-BLE protein, which has a higher molecular weight than the WT PHOT protein. (B) Total cellular chlorophyll (*a*+*b*) content in WT, *phot*, PPHOT, PLOV and PKIN cells exposed to light of 20, 200 or 750 µmol photons m^{-2} s^{-1} for 20 h as in Figure 4.9 D. Diminished chlorophyll content is a signature of pigment bleaching following photo-damage.

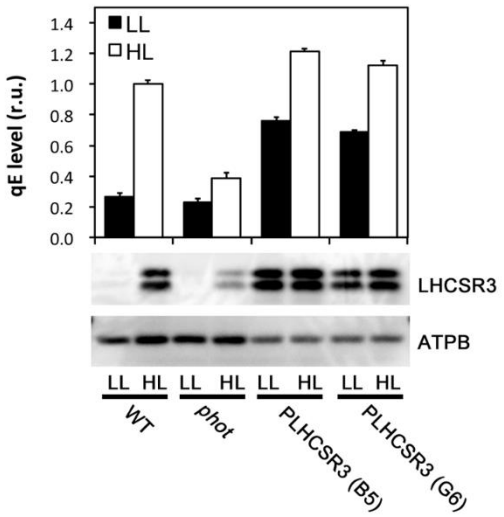

Supplementary Figure 4.16 – **PHOT-independent LHCSR3 expression restores photoprotection in the *phot* mutant.** Relative qE and LHCSR3 expression in WT (*cw15-302*), *phot*, and two *phot* transformant lines expressing the *LHCSR3.1* gene under the control of the *PsaD* promoter (PLHCSR3(B5) and PLHCSR3(G6)) in LL and HL conditions. ATPB was used as loading control. qE values were normalized to WT cells in HL conditions, and shown as mean ± SD (n = 3).

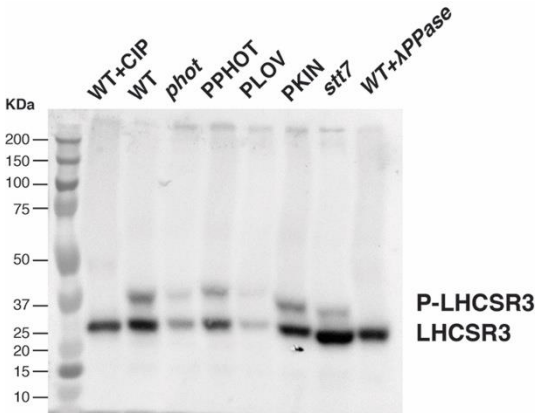

Supplementary Figure 4.17 – **Phosphorylation levels of LHCSR3 in *phot*, PPHOT, PLOV, PKIN, *stt7* and WT.** Assessment of the phosphorylation levels of LHCSR3 in WT (*cw15-302*), *phot* and in the different complemented lines (PPHOT, PLOV, PKIN) by a mobility shift detection of phosphorylated proteins (phos-tag). The upper and lower bands correspond to the phosphorylated and non-phosphorylated forms of LHCSR3 ("P-LHCSR3" and "LHCSR3"), respectively, which was confirmed by treatment of the samples with either calf intestinal phosphatase (CIP) or lambda protein phosphatase (λPP). The *stt7* mutant (Depège et al., 2003) was used to test the involvement of the chloroplastic serine/threonine kinase STT7 in the LHCSR3 phosphorylation. In this mutant LHCSR3 was mostly in the non-phosphorylated form while a STT7-independent phosphorylation was also evidenced in agreement with recent findings (Bergner et al., 2015).

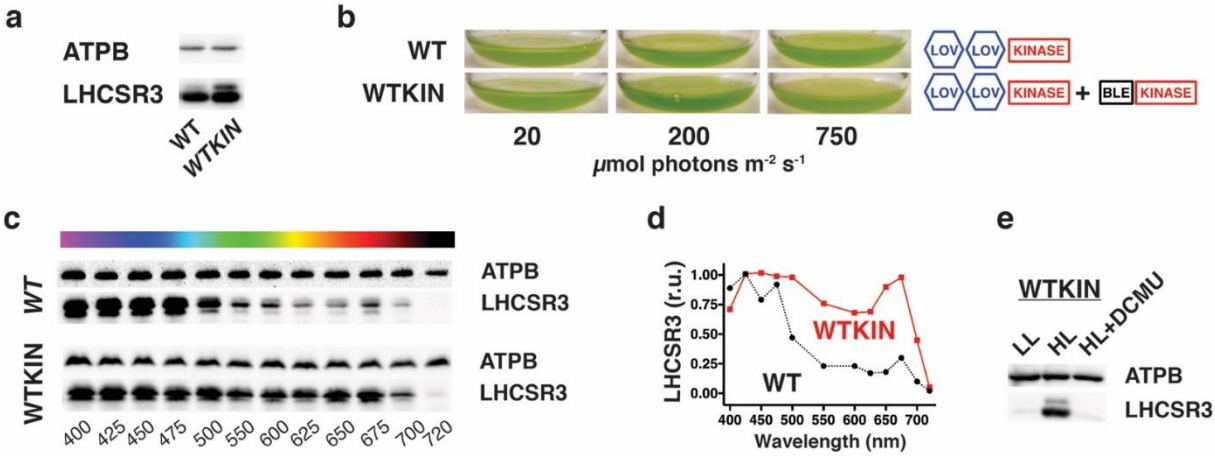

Supplementary Figure 4.18 – **Phenotypic traits of the WTKIN genotype.** (A) Immunoblot analyses of LHCSR3 accumulation after exposure to 240 µmol photons m^{-2} s^{-1} of white light for 20 h in WT (137c) and WTKIN cells and schematic drawings of the *PHOT* gene constructs in the two lines. ATPB was used as loading control. (B) Erlenmeyer flasks containing WT and WTKIN (expressing the kinase domain of PHOT in the WT background) after 20 h exposure to white light of 20, 200 and 750 µmol photons m^{-2} s^{-1}. (C) Action spectrum of LHCSR3 accumulation in WT and WTKIN. ATPB was used as a loading control. (D) Densitometric quantification of LHCSR3 accumulation in WT (137c) and WTKIN (data normalized to ATPB). (E) LHCSR3 protein accumulation in WTKIN at LL and HL in the absence and presence of the PSII inhibitor DCMU.

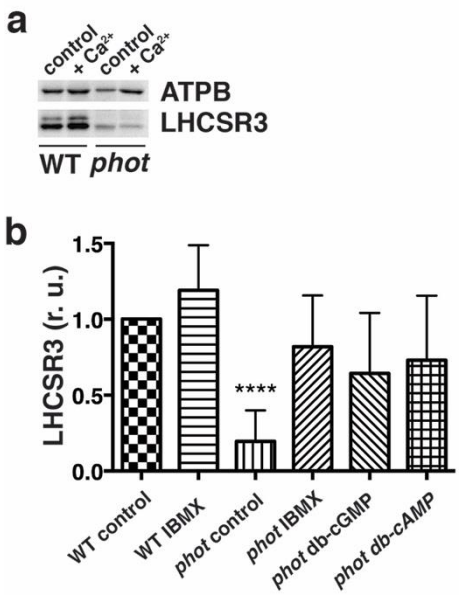

Supplementary Figure 4.19 – **Second messengers involved in the PHOT-dependent regulation of LHCSR3 expression.** (A) Immunoblotting analyses of LHCSR3 accumulation after exposure to high intensity of white light for 20 h in WT (*cw15-302*) and *phot* cells under control conditions (0.34 mM Ca^{2+}) or in the presence of increased Ca^{2+} concentration (3.4 mM Ca^{2+}). (B) Statistical analyses of LHCSR3 accumulation in high-light treated (HL) WT or *phot* cells in the absence (control) and presence of IBMX, db-cGMP and db-cAMP (see conditions as in Figure 4.11 A). Data are normalized to LHCSR3 levels of WT control cells). Mean ± SD (n = 3-6). Asterisks indicate statistical significant difference from WT control cells.

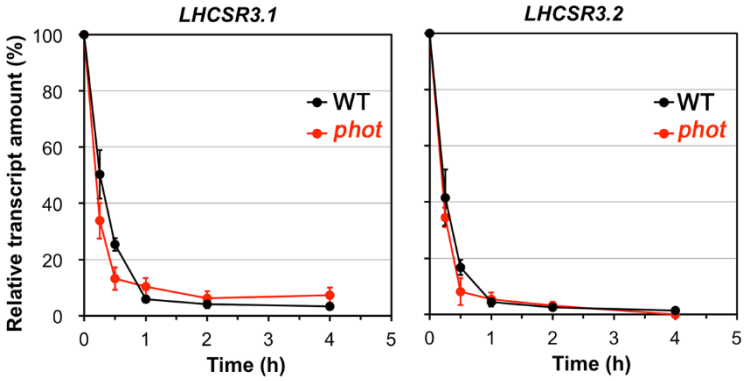

Supplementary Figure 4.20 – ***LHCSR3.1* and *LHCSR3.2* transcripts stability in WT and *phot* cells.**Relative amounts of *LHCSR3.1* and *LHCSR3.2* mRNA in WT (*cw15-302*; black) and in *phot* (red) were quantified by quantitative PCR. Cells exposed for 20 h to 470 nm LED light at 100 µmol photons m^{-2} s^{-1} were transfered to darkness at t=0 and treated with actinomycin D to stop further mRNA synthesis. mRNA samples were collected at 0, 0.25, 0.5, 1, 2, and 4 h after transition to darkness. *LHCSR3.1* and *LHCSR3.2* transcript amounts were normalised to the amounts of 18S rRNA as the endogenous control and their values were set at 100% at t=0 (n=3, mean ± s.d.).

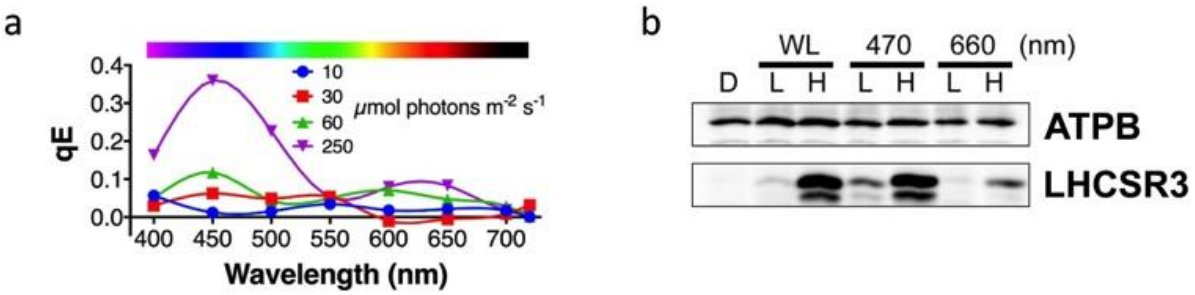

Supplementary Figure 4.21 – **qE and LHCSR3 induction requires high light in *C. reinhardtii*.** (A) Action spectrum of qE induction in WT cells as a function of the light intensity. (B) Immunoblot analysis of LHCSR3 accumulation in darkness (D) and under white (WL), blue (470 nm) and red (660 nm) light of low (LL; 20 µmol photons m^{-2} s^{-1}) and high intensity (HL; 250 µmol photons m^{-2} s^{-1}). ATPB was used as loading control.

4.3.3 Perspectives

Light is an essential factor for microalgae not only because it fuels carbon assimilation via the Calvin-Benson-Bassham cycle, but also because it acts as a signal in several processes related to growth and environmental responses. In this work, we have addressed the double role of light in regulating the photoprotective responses in *C. reinhardtii*. By using biochemical and spectroscopic approaches coupled with genetic analysis we have identified the molecular actors for this regulation revisiting the fundamental concepts of photoprotection in microalgae. Based on these promising results we hypothesized that other signals could exist which link light utilization for metabolism and light dissipation via NPQ. This was the starting point for the investigation presented in the following section.

4.4 Carbon metabolism controls photoprotection in *Chlamydomonas* via the light harvesting complex stress response protein LHCSR3

Flori et al., Manuscript in preparation.

4.4.1 Introduction

Photosynthesis is one of the most highly integrated and regulated process to efficient use of sunlight, while minimizing the damaging effects of excess light (Paul & Foyer, 2001). Among other photosynthetic organisms, *Chlamydomonas reinhardtii*, a member of the green algal lineage, has served as a model organism to study photosynthesis, mainly due to its ability, when grown heterotrophically in the dark, to maintain a normal green chloroplast that retains the capacity to perform oxygenic photosynthesis when illuminated. This has allowed the isolation of several photosynthetic mutants that would otherwise not be viable under phototrophic conditions (Grossman et al., 2007). Besides heterotrophic growth with acetate, *Chlamydomonas* may use carbon dioxide (CO_2) for photoautotrophy, and both carbon sources for mixotrophic growth (Harris, 1989). CO_2 is fixed via the Calvin-Benson-Bassham cycle in *Chlamydomonas* (Bassham et al., 1950). However like other aquatic phototrophs, this alga is often exposed to restricted CO_2 supplies because CO_2 diffusion is slower in water than in air. To overcome this problem *Chlamydomonas* possesses a CO_2-concentrating mechanism (CCM), that combines a series of carbonic anhydrases (CAs) to interconvert CO_2 and HCO_{3^-} with a complex series of ion pumps to actively transport HCO_{3^-} concentrating CO_2 at the site of fixation by RuBisCo within the pyrenoid (reviewed in Wang et al., 2015).

Acetate is incorporated into acetyl-CoA either as a one-step reaction, catalyzed by acetyl-CoA synthetase (ACS), or in two steps via acetate-phosphate, a reaction catalyzed by acetate kinase (ACK) and phosphate acetyltransferase (PAT; Wolfe, 2005). *Chlamydomonas* possess two parallel ACK-PAT pathways. Proteomic analyses have indicated that ACK1-PAT2 is localized in chloroplasts while ACK2-PAT1 is found in the mitochondria (Atteia et al., 2009; Terashima et al., 2010). Their localization was recently confirmed by their expression in *Chlamydomonas* as Venus fusion proteins (Yang et al., 2014). After binding to CoA, acetate reacts with oxaloacetate in the first step of the tricarboxylic acid (TCA) cycle and is then completely metabolized by this pathway, to generate 3 molecules of NADH, 1 molecule of FADH2, 2 molecules of both ATP and CO_2. The reduced compounds (NADH and FADH2) are consumed by the mitochondrial electron-transport chain

generating a proton gradient across the membranes, which produces additional ATP. Alternatively, acetate is metabolized by the glyoxylate cycle, as originally proposed by Kornberg and Krebs in 1957 to explain microbial growth on two-carbon compounds as the sole carbon source (Kornberg & Krebs, 1957). Three of the five enzymes that make up the pathway (citrate synthase, aconitate hydratase and malate dehydrogenase) are also found in the TCA cycle. The concerted action of the other two enzymes, isocitrate lyase and malate synthase, specific to the glyoxylate cycle, bypasses the two oxidative steps in which CO_2 is evolved, and explains formation of C4 acids from acetate. The C4 acids may then enter the gluconeogenesis cycle via phosphoenolpyruvate carboxykinase (Plancke et al., 2014). With the exception of the cytosolic isocitrate lyase all other enzymes of the glyoxylate cycle are localized in peroxisomal microbodies (Lauersen et al., 2016).

In *Chlamydomonas* both acetate assimilation and the induction of CCM triggered by inorganic carbon limitation are ATP-demanding processes. Therefore, alternative electron flow processes are switched on during phototrophic and mixotrophic growth conditions, to provide the extra ATP needed. This is typically the case of cyclic electron flow (CEF) around PSI, which is enhanced under low Ci, acetate assimilation (Lucker & Kramer, 2013). CEF starts from electrons accumulated at the acceptor side of PSI (reduced ferredoxin or NADPH), because of the ATP shortage. It recycles these electrons towards the intersystem electron transport chain, namely, the PQ pool or the cytochrome $_{b6/f}$ complex. By generating a thylakoid trans-membrane proton gradient, CEF produces the “extra” ATP for CO_2 assimilation (Allen, 2002) and is also involved in the establishment of nonphotochemical quenching (NPQ; Munekage et al., 2002).

NPQ is a photoprotective mechanism that dissipates absorbed light energy whenever absorbed beyond the CO_2 assimilation capacity (Li et al., 2009). The major component of NPQ is high energy quenching (qE), which mainly occurs at the light harvesting complexes of photosystem II (Horton et al., 1996). qE is driven by lumenal acidification under excess light, which modifies the LHCII pigment composition via the xanthophyll cycle and activates specific qE protein effectors (Niyogi & Truong, 2013). In vascular plants qE is modulated by the constitutively expressed protein PSBS (Li et al., 2000), while in *Chlamydomonas* qE requires the Light Harvesting Complex Stress-Response protein 3 (LHCSR3), a nucleus-encoded, chloroplast localized, inducible protein (Peers et al., 2009). LHCSR was originally identified as a light-induced transcript (called Li818; Gagné & Guertin, 1992). LHCSR3 transcripts accumulate under conditions known to induce photo-oxidative stress, including deprivation of carbon dioxide (Miura et al., 2004), sulphur (Zhang et al., 2004) or iron (Naumann et al., 2007), as well high light (Ledford et al., 2004). LHCSR3 induction requires Ca2+ signalling and

active photosynthesis (Petroutsos et al., 2011; Maruyama et al., 2014), but the molecular mechanism behind this process is largely unknown. As discussed above LHCSR3 transcription is under the control of the blue-light photoreceptor (see section 4.3).

Several biological processes have been described to be under nutritional control in *Chlamydomonas*, as exemplified by the control of sexuality by nitrogen (Sager & Granick, 1954), and the modulation of lipid biosynthesis by nitrogen, phosphorus or iron availability (Urzica et al., 2013). The metabolic status of the cells also defines different biological responses, as evidenced by the different strategies of acclimation of *Chlamydomonas* to Fe deficiency followed under phototrophic or mixotrophic conditions (Höhner et al., 2013). Because of its role in controlling the ATP cellular demand, acetate should deeply also affect photosynthetic responses (CO_2 assimilation, CEF and consequently NPQ) in *Chlamydomonas*. In this work we investigated the role of acetate and, more generally, of carbon metabolism in regulating photoprotection in this alga. We found that acetate is a potent inhibitor of NPQ, via a direct transcriptional control on the expression of the LHCSR3.

4.4.2 Results

LHCSR3 accumulation and NPQ capacity in Chlamydomonas are affected by acetate.

Previous results have indicated a very low NPQ capacity in *Chlamydomonas* cells grown in low light in the presence of acetate (Finazzi et al., 2006) at variance with the high NPQ observed in cells exposed to high light in minimal medium without acetate (Niyogi et al., 1997). Because the NPQ capacity relies on the slow (t1/2 of about two hours, Allorent et al., 2013) accumulation of LHCSR3 (the protein effector of the qE; Peers et al., 2009), we considered the possibility that acetate could exert a regulatory role on LHCSR3 itself. To test this possibility, we incubated *Chlamydomonas* cells overnight in HSM (in the absence and presence of acetate 20 mM) in LL (20 µmol photons m^{-2} s^{-1}) and shifted them to HL (250 µmol photons m^{-2} s^{-1}) for 4h. After 4 hours cells were collected and analyzed for their cellular LHCSR3 content and NPQ capacity.

We found that acetate largely repressed NPQ in HL-treated cells (Figure 4.22 A) and this correlated with a complete inhibition of LHCSR3 accumulation (Figure 4.22 B). Interestingly the presence of acetate abolished even the very low steady state NPQ observed in LL adapted cells (Figure 4.22 A). Since active photosynthetic electron flow is required for proper expression of LHCSR3 at the protein (Petroutsos et al., 2011) and transcript level (Maruyama et al., 2014) it was important to investigate if inhibition of LHCSR3 by acetate was due to a cease of photosynthesis in the presence of acetate or due to a more direct role of this metabolite on LHCSR3. We measure photosynthetic electron

transfer rate (ETR) in the presence and absence of acetate (Figure 4.22 C) and found that in LL conditions acetate had no impact on the photosynthetic performance of the cells whereas under HL conditions acetate grown cells had an ETR of ca. 35% lower compared to the phototrophic grown ones. This drop of photosynthetic activity in the presence of acetate is in agreement with previous findings (Fett & Coleman, 1994b) but cannot justify the complete abolishment of LHCSR3 expression since even a maintenance of 15% of ETR under high light is sufficient for proper accumulation of LHCSR3 (see section 4.3, Supplementary Figure 4.14 A).

In order to investigate if the inhibition of LHCSR3 by acetate occurs at the transcriptional level we used a strain that expresses the firefly luciferase under control of the LHCSR3.1 promoter in the WT background. This strain exhibits a WT-like NPQ induction (Figure 4.22 D) and LHCSR3 accumulation (Figure 4.22 E) after 4h exposure to HL in minimal medium. A LL to HL shift experiment revealed that luminescence (i.e. the accumulation of luciferase, which is in turn reflects LHCSR3 gene induction) was largely increased (here 46 fold induction) with fast kinetics, being complete after 1 hour of high light exposure. This time lenght is consistent with previous data obtained by measuring LHCSR3 mRNA accumulation in the WT (section 4.3). A comparison of luciferase activity levels in control (in minimal medium) and acetate-treated cells (Figure 4.22 G) indicates that acetate almost completely inhibits LHCSR3 expression similar to DCMU. Its effect was almost identical to that of DCMU, a photosynthesis inhibitor that was used as a positive control. Indeed this herbicide was previously shown to block LHCSR3 gene expression by qPCR (Maruyama et al., 2014).

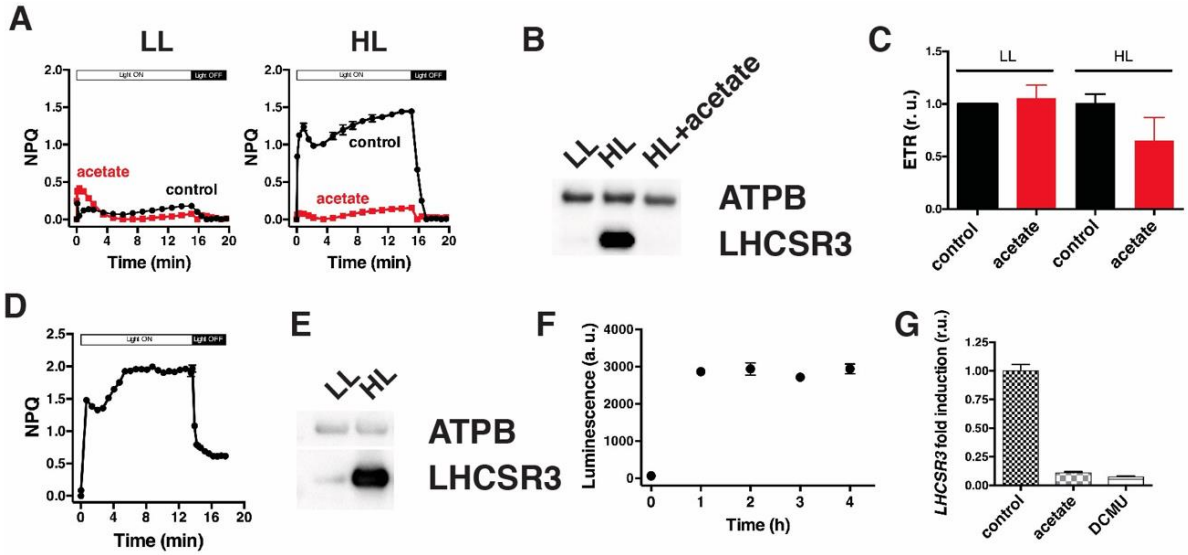

Figure 4.22 – **Acetate inhibits NPQ and LHCSR3 induction.** (A) NPQ induction kinetics of WT cells after overnight incubation in minimal medium at LL (20 µmol photons m^{-2} s^{-1}) or after 4 h exposure to HL (250 µmol photons m^{-2} s^{-1}) in the presence and absence of acetate. NPQ was recorded for 16 min upon illumination with 440 µmol photons m^{-2} s^{-1} (white bar) followed by 4 min of darkness (black bar), to follow NPQ relaxation. (B) Immunoblot analysis of LHCSR3, and ATPB of the samples described in (A). ATPB was used as loading control. (C) Electron transfer rate (ETR) of the samples described in (A). ETR (µmol photons m^{-2} s^{-1}) was measured at actinic illumination of 41 µmol photons m^{-2} s^{-1}. Mean ± SD (n = 3). (D) NPQ induction kinetics of *LHCSR3* Prom::Luc cells after 4h exposure to HL (250 µmol photons m^{-2} s^{-1}). (E) Immunoblot analysis of LHCSR3, and ATPB of *LHCSR3* Prom::Luc cells after 4h exposure to HL. ATPB was used as loading control. (F) Luminescence kinetics of *LHCSR3* Prom::Luc cells exposed to HL. (G) Fold induction of LHCSR3 based on luminescence measurements of *LHCSR3* Prom::Luc cells exposed to HL for two hours in minimal medium (control), acetate-containing medium or poisoned by DCMU. Data are normalized to the fold induction of control cells. Figure summarizes data of three to five experiments (average, SD).

In a different approach, we pre-incubated cells overnight in HL minimum medium to reach full accumulation of LHCSR3. We then added acetate and followed the kinetics of NPQ and LHCSR3 while keeping the cells in HL. Despite the exposure to HL, a condition that favors NPQ and LHCSR3 induction in control cells, acetate was still able to decrease NPQ (Figure 4.23 A) and photosynthetic activity measured as ETR (Figure 4.23 B). The decreased NPQ capacity was progressive and paralleled by a reduction of the cellular LHCSR3 content (Figure 4.23 C and D). The effect of acetate on LHCSR3 was specific as evidenced by the fact that another component of PSII, the D1 protein levels remain unaltered even 24 h after acetate was added, i.e. when most of the LHCSR3 had already disappeared.

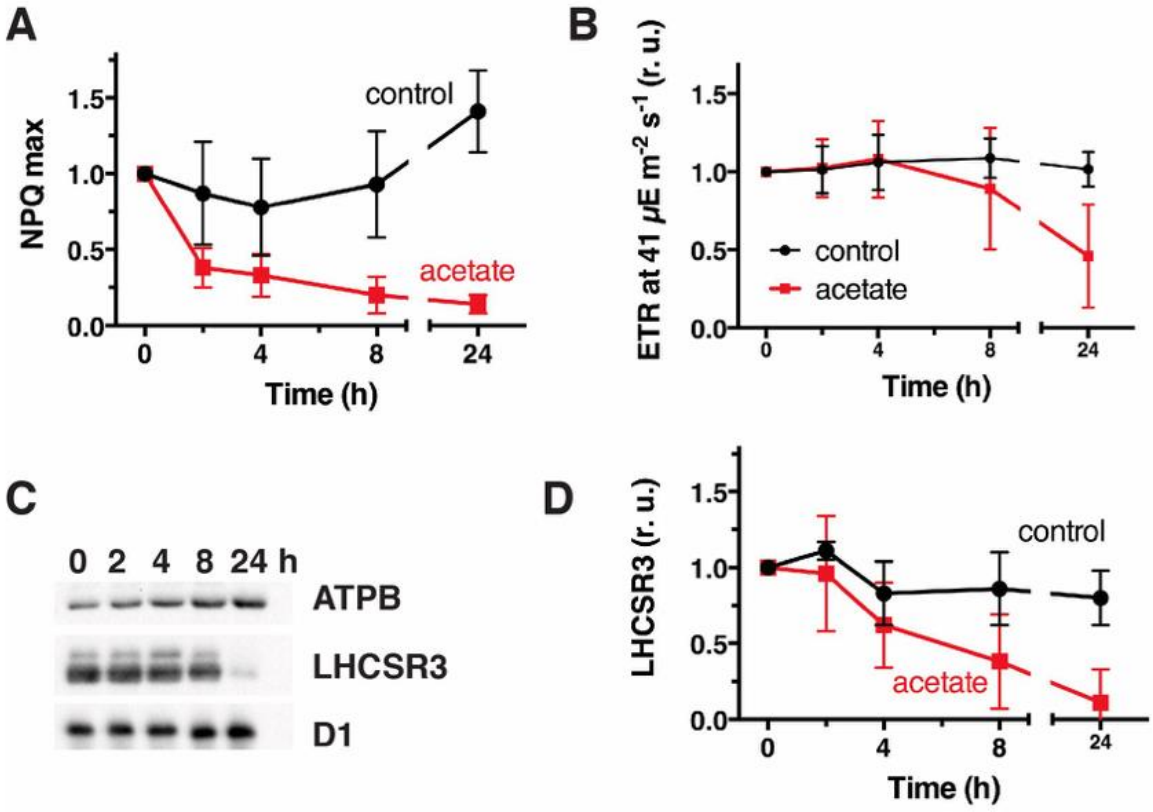

Figure 4.23 – **Acetate triggers LHCSR3 degradation in HL**. WT cells were incubated overnight in minimal (control) medium in HL (250 µmol photons m^{-2} s^{-1}) to reach the maximum accumulation of LHCSR3. Acetate was added (20 mM) and cells remained to HL for another 24h. (A) NPQ capacity (NPQ max) and (B) ETR kinetics in cells remaining in minimal (control) medium or having received 20 mM acetate. (C) Immunoblot analysis of LHCSR3, D1 and ATPB of cells described in (A). ATPB was used as loading control. (D) Densitometric analyses of LHCSR3 normalised to ATPB (1 = LHCSR3 in control conditions at t=0).

Previous data have shown that LHCSR3 gene expression stops abruptly after a HL to LL transition (t1/2 < 0.5 hour). Because LHCSR3 is absent in LL treated cells, we reasoned that the decline of NPQ and LHCSR3 during the HL to LL transition could offer an excellent opportunity to investigate LHCSR3 protein turnover. We started from cells that were we pre-loaded with LHCSR3 thanks to an overnight incubation in HL. After transferring them in LL conditions, samples were collected for 24 hours and LHCSR3 levels and NPQ capacity were measured (Figure 4.24 A and B). We found that LHCSR3 is a relatively stable protein that degrades slowly (t1/2 > 8h). Moreover, its degradation turned out to be independent in the presence of acetate. Interestingly even after 24 h after the shift to LL phototrophic cells (control) still retain a significant NPQ capacity (ca 50%) which is however abolished by acetate (Figure 4.24 C), despite the fact that this compound did not impact the photosynthetic performance of the cells (Figure 4.24 D).

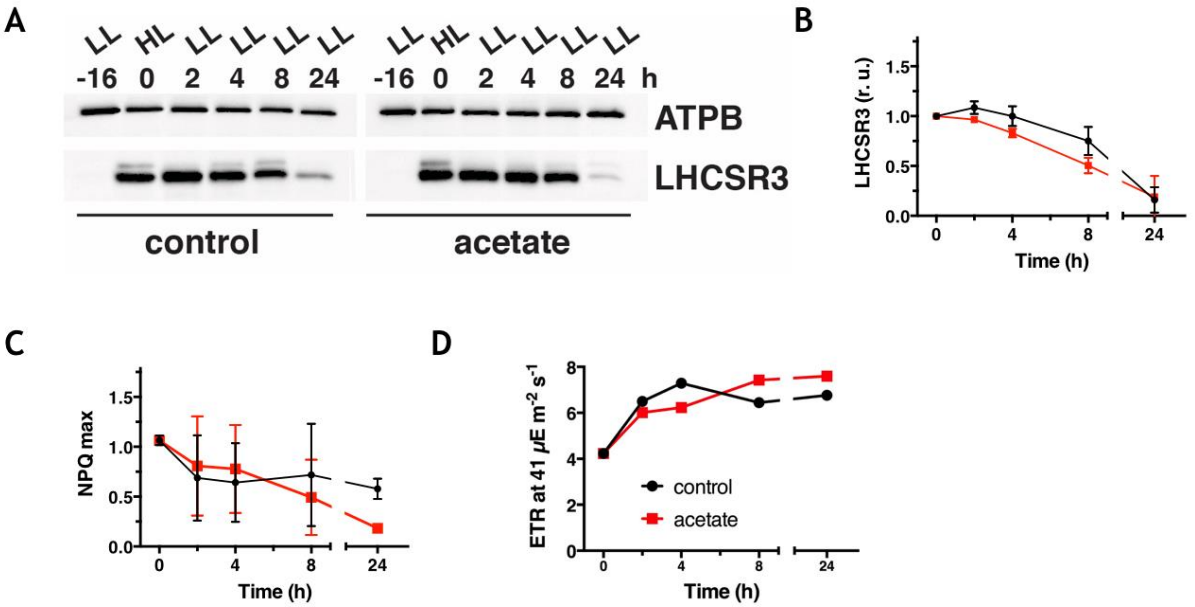

Figure 4.24 – **Acetate is not involved in LHCSR3 protein stability.** Cells acclimated to LL (20 µmol photons m^{-2} s^{-1}; t = -16h) were shifted to HL (250 µmol photons m^{-2} s^{-1}) overnight to reach the maximum accumulation of LHCSR3. Acetate was added (20 mM) and cells were transferred back to LL for another 24h. (A) Immunoblot analysis of LHCSR3, and ATPB of cells described in (B). ATPB was used as loading control. (B) Densitometric analyses of LHCSR3 normalised to ATPB (1 = LHCSR3 in control conditions at t=0). (C) NPQ capacity (NPQ max) and (D) ETR kinetics in cells remaining in minimal (control) medium or having received 20 mM acetate.

Acetate modulation of LHCSR3 reveals a metabolic control of NPQ in *Chlamydomonas*.

The data shown above indicate that acetate is a potent inhibitor of photoprotection in *Chlamydomonas*, because it reduces the expression of the LHCSR3 gene. This impacts LHCSR3 protein accumulation during LL to HL transitions (Figure 4.22) but also during HL conditions (Figure 4.23). Overall, these data show that LHCSR3 and NPQ are under control of acetate metabolism by the cell. To gain further insights into the link between acetate metabolism we tested the effect of this metabolite in the following mutants with altered acetate metabolisms: (i) *dum11*, defective in complex III (ubiquinol cytochrome c oxidoreductase) and thus unable to oxidize the reducing power produced by glycolysis, the pentose phosphate pathway and/ or TCA. This mutant can still produce some ATP via electron transport mediated through complex I (NADH dehydrogenase) and the alternative oxidase (AOX). The low ATP production in this mutant may be responsible for the absence of growth under heterotrophic conditions and the slower growth under mixotrophic conditions (Colin et al., 1995). (ii) *icl*, is a mutant lacking isocitrate lyase, a key enzyme of the glyoxylate cycle. This cycle plays an essential role in cell growth on acetate, and is important for gluconeogenesis as it bypasses the two oxidative steps of the tricarboxylic acid (TCA) cycle in which CO_2 is evolved. Although its respiratory complexes are unaltered, the *icl* mutant cannot grow on acetate in the dark while it shows reduced acetate assimilation and respiration in the light (Plancke et al., 2014). (iii) *ack1, ack2* and the double mutant *ack1ack2* lack either the chloroplastic (ACK1) or the mitochondrial (ACK2) or both the acetate kinases respectively. Acetate kinase catalyzes the phosphorylation of acetate to acetyl-P which is further converted to acetyl-CoA by phosphate acetyltransferase.

We found (Figure 4.25 A) that acetate was not able to inhibit LHCSR3 induction in the *dum11* and *icl* mutants in LL to HL shift experiments, indicating that impaired respiration of this compound was enough to make it ineffective. Moreover, no LHCSR3 degradation was observed when acetate was added in HL acclimated cells at variance with the WT (Figure 4.25 B). On the other hand, the three *ack* mutants tested showed a WT-like phenotype (Figure 4.25 A) suggesting that acetate entry via the acetyl CoA synthase was probably sufficient to promote its metabolism and therefore the control over LHCSR3 gene induction.

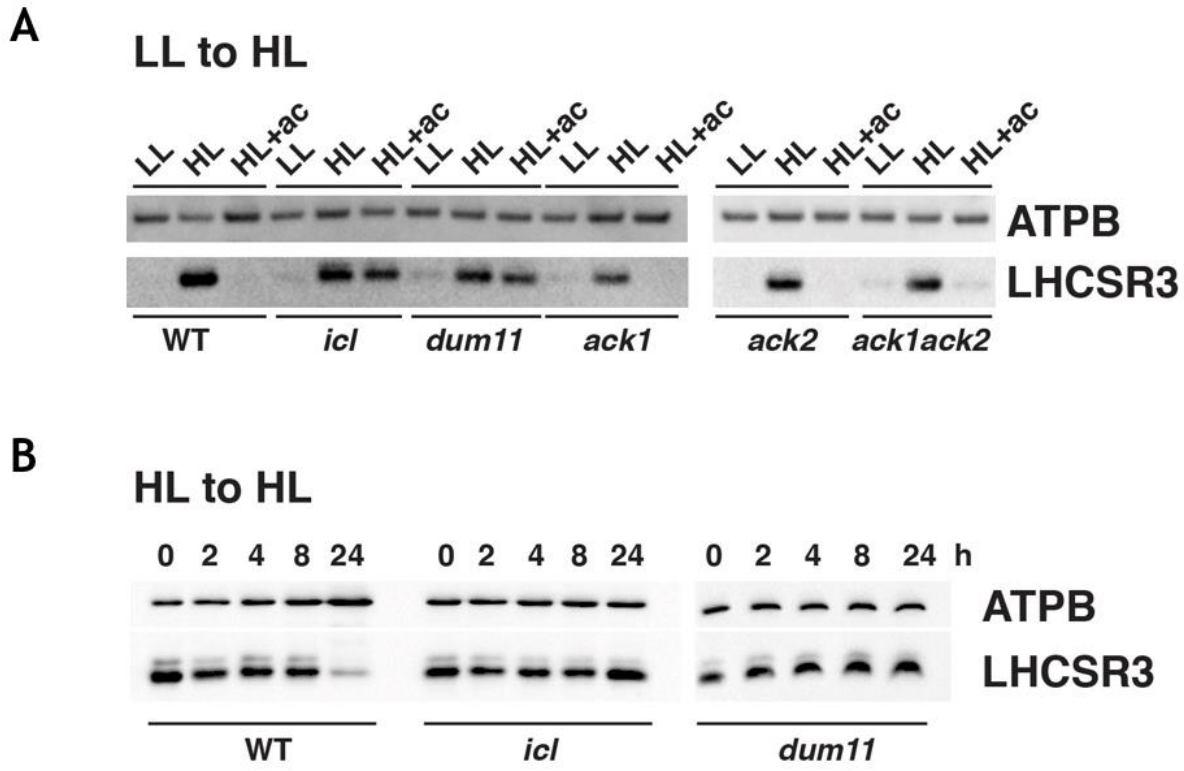

Figure 4.25 – **Differential response of LHCSR3 to acetate in selected metabolic mutants.** (A) WT and mutant cells acclimated to LL (20 µmol photons m^{-2} s^{-1}) were shifted to HL (250 µmol photons m^{-2} s^{-1}) for 4h in the presence and absence of acetate. Immunoblot analysis of LHCSR3, and ATPB. (B) WT and mutant cells were incubated overnight in minimal (control) medium in HL (250 µmol photons m^{-2} s^{-1}) to reach the maximum accumulation of LHCSR3. Acetate was added (20 mM) and cells remained to HL for another 24h. The figure shows the immunoblot analyses of LHCSR3 and ATPB at the indicated time points.

A key role of CO_2 and CCM in the regulation of the *LHCSR3* gene

Overall, the data of Figure 4.25 indicate that acetate controls LHCSR3 accumulation via a metabolic control, which involves respiration. Indeed, in both the *icl* and the *dum11* LHCSR3 accumulation in HL becomes acetate-insensitive. In these mutants respiration is compromised and therefore ATP levels are low, explaining their inability to grow heterotrophically on acetate. However they do grow on acetate mixotrophically, although their growth rates are compromised (Plancke et al., 2014; Colin et al., 1995). Therefore, acetate enters the cell in the mutants, suggesting that this metabolite per se is not the signaling molecule that triggers the inhibition of LHCSR3 transcription. Because acetate assimilation rate in *icl* and *dum11* mutants is slow, respiratory CO_2 released by these mutants should be lower in these mutants. The low CO_2 concentration could explain the differential response of LHCSR3 in WT and *icl* and *dum11* mutants. Indeed, the promoter region of LHCSR3.1 contains a conserved sequence motif termed EEC, an enhancer element for low CO_2 responses (Maruyama et al., 2014) also present in other low CO_2-inducible gene promoters in *C. reinhardtii* (Kucho et al., 2003; Yoshioka et al., 2004). In order to test this hypothesis, we performed LL to HL shift experiments in WT and the mutants *icl*, *dum11*, *ack1*, *ack2*, *ack1ack2* in control medium (minimal) and in medium supplemented with 2.5 mM bicarbonate. We found that $NaHCO_3$ suppressed LHCSR3 accumulation not only in WT and *ack* mutants but also in the acetate-insensitive in *icl* and *dum11* (Figure 4.26) pointing a control of CO_2 on LHCSR3 either direct or via CCM.

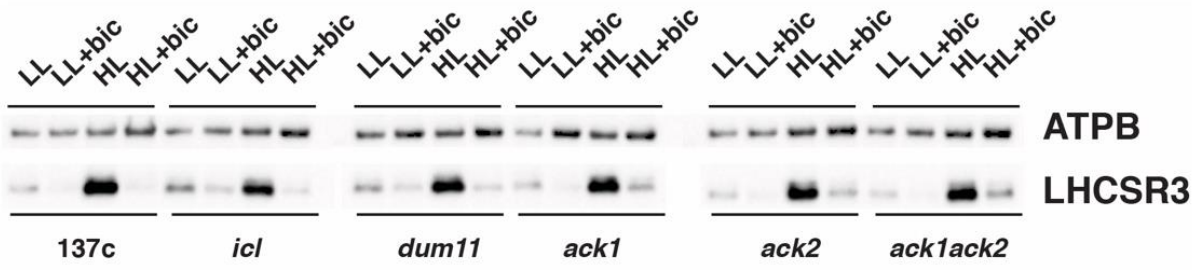

Figure 4.26 – **Bicarbonate inhibits LHCSR3 expression in WT and metabolic mutants.** WT and mutant cells acclimated to LL (20 µmol photons m^{-2} s^{-1}) were shifted to HL (250 µmol photons m^{-2} s^{-1}) for 4h in the presence and absence of 2.5 mM $NaHCO_3$. The figure shows the immunoblot analysis of LHCSR3, and ATPB.

We tested the effect of CO_2 on *LHCSR3* expression in the LHCSR3 Prom::Luc strain in LL to HL shift experiments for 2h where the culture medium was supplemented with saturating concentration of bicarbonate (2.5 mM $NaHCO_3$) and we saw that transcription of *LHCSR3* is inhibited by $NaHCO_3$ (Figure 4.27 A) to a similar extend of DCMU- or acetate-triggered inhibition (Figure 4.22 G). The shift from LL to HL induces the mitochondrial carbonic anhydrases CAH4/5 indicating an activation of CCM under HL conditions (Figure 4.27 B). Accumulation of protein levels of CAH4/5 perfectly follow the accumulation pattern of LHCSR3 protein, i.e. no expression in LL, high expression in HL, suppression in HL by acetate and bicarbonate (Figure 4.27 B). Moreover the mutant *cia5*, lacking a master regulator of CCM (Moroney et al., 1989; Fukuzawa et al., 2001) is unable to accumulate any detectable protein levels of either LHCSR3 or CAH4/5 (Figure 4.27 B). These data show a close interconnection of LHCSR3 and CCM which is further supported by earlier findings that CCM is inhibited by acetate (Fett & Coleman, 1994b; Moroney et al., 1987). Based on the above-mentioned reasoning we hypothesized that acetate-metabolism-derived intracellular CO_2 inactivates CCM and blocks LHCSR3 transcription.

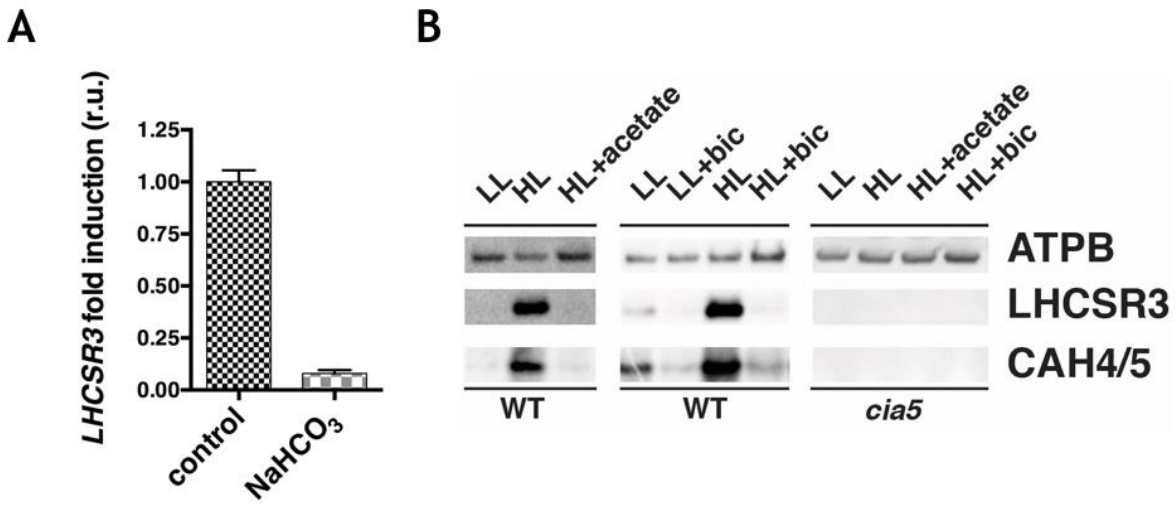

Figure 4.27 – **LHCSR3 is under control of CCM.** (A) Fold induction of *LHCSR3* based on luminescence measurements of *LHCSR3* Prom::Luc cells exposed to HL for two hours in minimal medium (control) and $NaHCO_3$-containing medium. Data are normalized to the fold induction of control cells. Figure summarizes data of three to five experiments (average, SD). (B) Immunoblot analyses of LHCSR3, CAH4/5 and ATPB in WT and *cia5* cells shifted from LL (20 µmol photons m^{-2} s^{-1}) to HL (250 µmol photons m^{-2} s^{-1}) in the absence (control) and presence of acetate (20 mM) or $NaHCO_3$ (2.5 mM).

4.4.3 Materials and methods

Chemicals: Stock solutions of DCMU were prepared in ethanol (40 mM). DCMU was used at a final concentration of 40 µM.

Strains and conditions: *C. reinhardtii* strains were grown under 20 µmol photons m^{-2} s^{-1} in Tris-acetate-phosphate (TAP) media (Gorman & Levine, 1965) at 23 ^{o}C containing 17.5 mM acetate. In all experiments cells were transferred to Sueoka's high salt medium (Sueoka, 1960) at 2 million cells/mL and exposed to light intensities as described in the text and figure legends. The strain 137c was used as wild type strain of *C. reinhardtii*. The mutants *icl*, *dum11*, *ack1*, *ack2* and *ack1ack2* are described in the text. We used a *pgrl1* strain backcrossed four times with the wild-type strain CC124 (Kukuczka et al., 2014). The 137c expressing the firefly luciferase under control of *LHCSR3.1* promoter (*LHCSR3* Prom::Luc) was kindly provided by the lab of Jun Minagawa (Okasaki, Japan). Unless otherwise stated, LL conditions corresponded to 20 µmol photons m^{-2} s^{-1} while HL conditions corresponded to 250 µmol photons m^{-2} s^{-1} of white light.

Immunoblotting: Protein samples of whole cell extracts (0.5 µg chlorophyll) were loaded on 4-20% SDS-PAGE gels and blotted onto nitrocellulose membranes. Antisera against D1, CAH4/5, ATPB were from Agrisera (Vännäs, Sweden). Anti-LHCSR3 was a kind gift from M. Hippler (University of Muenster). An anti-rabbit horseradish peroxidase–conjugated antiserum was used for detection. The blots were developed with ECL detection reagent, and images of the blots were obtained using a CCD imager (ChemiDoc MP System, Bio-Rad). LHCSR3 appears as a double band in some of the western blots. The upper band represents the phosphorylated form of LHCSR3.

Luminescence measurements: For the firefly luciferase activity measurements, 100 µL of cell suspension at 2 million cells/mL was mixed with 100 µL ONE-Glo™ Luciferase Assay mixture (Promega) containing luciferin, the substrate of firefly luciferase. Luminescence was recorded after 20 minutes of incubation with the Luciferase Assay mixture using a Spark® 10M luminescence microplate reader (Tecan).

Fluorescence-based measurements: Fluorescence-based photosynthetic parameters were measured with a fluorescence imaging setup previously described (Johnson et al., 2009). The photosynthetic electron transfer rate (ETR) was calculated as (Fm'-F)/Fm' * 0.84 * 0.5 * I (Petroutsos

et al., 2009). NPQ was calculated using the following equation: (Fm-Fm')/Fm'. F and Fm' are the fluorescence yields in steady state light and after a saturating pulse in the actinic light, respectively, Fm is the maximal fluorescence yield in dark-adapted cells, and I is the light irradiance in µmol photons m^{-2} s^{-1} (Genty et al., 1989).

4.4.4 Discussion

Photoprotection in *Chlamydomonas* largely relies on the expression of the qE effector protein LHCSR3. At variance with the situation in plants, where the qE effector protein PSBS is constitutively expressed, LHCSR3 is an inducible protein. Induction of LHCSR3 requires exposure to high light intensities (Peers et al., 2009), active photosynthetic electron flow and calcium signaling (Petroutsos et al., 2011; Maruyama et al., 2014). The data presented here unveils the existence of a metabolic regulation in the expression of LHCSR3, since acetate inhibits transcription of *LHCSR3* and NPQ capacity of *Chlamydomonas* (Figures 4.22).

LHCSR3 transcripts accumulate under environmental conditions known to induce photo-oxidative stress, including deprivation of sulphur (Zhang et al., 2004), of iron (Naumann et al., 2007) but also of carbon dioxide (Miura et al., 2004). Under low external inorganic carbon (C_i; CO_2 or HCO_{3-}) conditions *Chlamydomonas* cells activate the CO_2 concentrating mechanism (CCM), that enables survival and proliferation when the CO_2 concentration limits photosynthesis. These mechanisms mostly comprises C_i transporters and carbonic anhydrases (CAs), which catalyze interconversion of CO_2 and HCO_{3-} (Wang et al., 2015). Most of the C_i transporters and CAHs are under control of a zinc-finger type transcription regulator named CIA5 (or CCM1; Moroney et al., 1989; Fukuzawa et al., 2001), which is localized in the nucleus (Xiang & Weeks, 2001) and controls transcription of CO_2 responsive genes. Recently, a genome-wide transcriptomics study indicated that both LHCSR3.1 and LHCSR3.2 are under control of CIA5 (Fang et al., 2012), whereas the promoter region of LHCSR3.1 has been found to contain a conserved sequence motif termed EEC, an enhancer element for low CO_2 responses (Maruyama et al., 2014) also present in other low CO_2-inducible gene promoters in *C. reinhardtii* (Kucho et al., 2003; Yoshioka et al., 2004).

Exogenous addition of acetate boosts respiration (Matsuo & Obokata, 2006; Fett & Coleman, 1994a), induces expression of genes of the glyoxylate cycle incuding *ICL* (Hayashi et al., 2015) (Hayashi et al., 2015; Matsuo et al., 2011) and increases the number of peroxisomes (Hayashi et al., 2015) which has been identified as the site where the glyoxylate cycle takes place (Lauersen et al., 2016). This is why we selected metabolic/respiratory mutants to further pursue the study of acetate-

triggered inhibition of LHCSR3 (Figure 4.25). The acetate-insensitive phenotype of *icl* and *dum11* in terms of LHCSR3 induction allows excluding the possibility that acetate acts as a signal per se because both *icl* and *dum11* do assimilate acetate but at slow rates. The hypothesis that metabolic CO_2 produced by acetate assimilation inhibited LHCSR3 via intracellular gas exchanges sounded more plausible. A remote control of photosynthetic genes by the mitochondrial respiratory chain had been demonstrated in *Chlamydomonas* for the case of psaE mRNA (Matsuo & Obokata, 2006). Similarly, acetate repressed the expression of the genes encoding the small and large Rubisco subunits (Goldschmidt-Clermont, 1986). Acetate also inhibited CCM and carbonic anhydrases expression and it had been suggested that this could be due to respiratory CO_2 produced by acetate assimilation mimicking high CO_2 conditions in the cell (Eriksson et al., 1998; Fett & Coleman, 1994a). This could also explain the sensitivity of LHCSR3 to acetate. Indeed several lines of evidence already existed supporting a very tight interconnection of LHCSR3 and CCM: *i. LHCSR3* gene is induced under low CO_2 (Miura et al., 2004), *ii*. a genome-wide transcriptomics study identified both *LHCSR3.1* and *LHCSR3.2* as being under control of CIA5, the master regulator of CCM genes (Fang et al., 2012), *iii.* the promoter region of *LHCSR3.1* contains an enhancer element for low CO_2 responses (Maruyama et al., 2014) also present in other low CO_2-inducible gene promoters in C. *reinhardtii* (Kucho et al., 2003; Yoshioka et al., 2004). Our data confirmed this close interconnection of LHCSR3 and CCM because $NaHCO_3$ transcriptionally inhibits *LHCSR3* (Figure 4.26 A), the mitochondrial CAH4/5 perfectly co-expresses with LHCSR3 in LL to HL experiments in the presence and absence of acetate or bicarbonate and finally the mutant *cia5* does not expressed LHCSR3 (Figure 4.26 B). Addition of bicarbonate in the acetate-insensitive mutants *icl* and *dum11* rendered them WT-like because LHCSR3 was completely inhibited.

Contrary to plants that are ready to perform NPQ any time they experience excess light conditions thanks to constitutive expression of the qE effector protein PSBS (Li et al., 2000) and to marine diatoms that perform NPQ due to the constitutively expressed LHCX1 protein (Bailleul et al., 2010), *Chlamydomonas* relies to the relatively slowly induced protein LHCSR3. That leaves a time window of approximately two hours during which cells need to freshly synthesize LHCSR3 and therefore are not efficiently photoprotected by qE. It has been demonstrated that state transitions, another component of NPQ, cover this photoprotective gap in *Chlamydomonas* (Allorent et al., 2013). However, our data show that, once expressed, LHCSR3 is fairly stable and gets slowly degraded with a t1/2 that exceeds 8 h (Figure 4.24 A, B). This means that the cells will be ready to perform NPQ when brought back to high light. Indeed, after 8h in LL the cells retain 75% of their NPQ capacity

which remains at 50% after 24 h in LL.

When acetate is added to cells that have been acclimated to HL and cellular LHCSR3 levels are already at their maximum accumulation, the protein LHCSR3 starts getting degraded even though the cells still remain at HL conditions that would certainly benefit from efficient photoprotection (Figure 4.23). Nonetheless, no significant photoinhibition is detected, as evidenced by the finding that the D1 levels remained unaltered upon high light exposure in the presence of acetate (Figure 4.23 C). This apparent contradiction can be explained by the suggestion (Roach et al., 2013) that acetate changes the energetics of PSII and that mixotrophic cells are less susceptible to photoinhibition because they produce less $^1O_2$ compared to phototrophic cells. The drop in photosynthetic activity measured as ETR observed at the same conditions (Figure 4.22 B) could be an indication of enhancement of CEF in the presence of acetate, as has been suggested by others (Lucker & Kramer, 2013; Johnson & Alric, 2013). It seem therefore that acetate promotes a metabolic shift in *Chlamydomonas* (i.e. enhanced photoprotection capacity, modified redox potential of the PSI acceptor side, same as in Roach et al. 2013 and higher CEF) which reminds the situation described in photosynthetic anaerobic bacteria. In these organisms, the main purpose of photosynthesis is not to assimilate CO_2 but rather to generate ATP for housekeeping purposes (Finazzi, 2005). This is a condition that can also be expected in this alga when grown in the presence of an environment rich in organic carbon, were light penetration and oxygen concentration could be relative low.

Chapter 5

5.1 Concluding remarks

The chloroplast likely represents the most sophisticated light-harvesting and energy collector systems in nature. This flexible "molecular machine" can optimally perform under extremely variable environments (changes in nutrients, temperature, light quality or quantity). Within the chloroplast, three main sub-compartments can be easily identified *i*. the envelope, a membrane system that control exchanges of metabolites and proteins with the rest of the cell *ii.* the stroma the soluble space which hosts the enzymes required for carbon fixation and *iii.* the thylakoids, the internal membrane network. The presence of these chloroplast subcompartments reflects the necessity to confine different photosynthetic steps (i.e. light-harvesting, electron flow, carbon assimilation) in different compartments with different physio-chemical properties (light absorbing pigments must work in a nonpolar environment while CO_2 assimilation requires an aqueous space). A rapid and efficient interaction between these compartments is needed for optimum photosynthesis. My main contribution to the first part of this Ph.D project has been to investigate the physical strategies established by the diatom *P. tricornutum* to optimize the interaction between its different cells subcompartments.

At the cellular level, we observe contact points between the nucleus and the chloroplast (see Flori et al., in preparation, Chapter 2), which likely mediate a direct exchange of metabolites and "signals" as required for a proper dialog between the site where most of the photosynthetic genes are expressed (the nucleus) and the site where the gene products must operate (the chloroplast). Understanding the nature of these exchanges, as well as their possible involvement in retrograde signalling (i.e. signalling the redox state of the chloroplast to the nucleus to modify its gene expression profile) will constitute a major step in understanding cellular communication.

We also see contacts between the chloroplast and the mitochondria, which likely facilitate the exchange of reducing equivalents and ATP between the two organelles to optimise CO_2 assimilation in the light (Baileul et al., 2015). Investigating the nature of the protein exchangers present in these "junctions" by targeted proteomic analysis, will constitute a major achievement to elucidate the molecular mechanisms behind these energy exchanges. This is now possible thanks to the possibility to isolate intact chloroplast in *P. tricornutum,* which not only opens new stimulating opportunity of studying the different subcompartments of the chloroplast (envelope, thylakoids, etc.) still a mystery in diatoms, but also allow purifying patches of chloroplast envelope fused to mitochondrial memebranes.

At the subcellular level, we observe extensive contacts between the periplastidial membrane (PPM) and the inner nuclear envelope (iNE; Flori et al., 2016). A vesicular network (VN) fills the space between the PPM and the two innermost envelope membranes (oEM and iEM) and could be an important platform for the import of protein precursors to the chloroplast. The identification of the proteins generating the VN represents therefore an important challenge for future works. To achieve this goal a biochemical and structural approach should be applied through the correlative light electron microscopy technique (CLEM).

Finally, we see "linking membranes" connecting the different thylakoid layers, which optimize electron flow by facilitating the diffusion of the soluble electron carriers between the two photosystems. Thanks to this rapid connection, the two photosystems can be kept apart, to avoid useless energy spillover between them.

Overall, the major outcome of this part of my thesis was to reveal the sophisticated arrangement of the cellular compartment and to relate this structure to the global function and flexibility of a diatoms cell. A large spectrum of future investigations is possible. The new protocols I have developed during my Ph.D are now ready to be exploited to study cell grown in standard conditions and in conditions allowing rearrangements or modification of the cellular complexes (e.g. low light vs high light, nutrient starvation, etc.). In principle, it could be possible to use these findings to elucidate how microalgae interact with their environment and respond to stress conditions.

In the second part of this project, I have focused more on the "biological" mechanisms of the signalling between the different cell compartments focusing on the green alga *C. reinhardtii*. By integrating action spectra, genetic screening and spectroscopic analysis, we explored that different signals are involved in the regulation of photoprotection in this widespread model organism. In the first study, addressing the question if light colour is involved in the regulation of NPQ in *C. reinhardtii* we highlight the link between light sensing and dissipation via the photoreceptor phototropin.

We also reveal a feedback regulation between carbon assimilation for metabolism and photoprotection. In fact, depending on the prevailing mode of carbon assimilation (phototrophy vs mixotrophy, i.e. simultaneous utilisation of light and reduced carbon), this flexible microalga is able to adjust its photosynthetic machinery and to sustain growth under extreme and differentiated conditions. To obtain these results, I have established an innovative small-scale approach to investigate the regulation of photoprotective responses. Using the Biolog® microplates, I have been able to investigate the effect of 190 metabolites on growth, photosynthesis and photoprotection. This pioneering approach can open an interesting perspective for the future. In fact, the scale-up of

this metabolomic approach can confirm the experimental evidences obtained using the Biolog® technology. The selection, in liquid, of other central carbon metabolites involved in TCA and/or aminoacid metabolism was already tested, but due to the lack of time, the entire set of metabolites (190) was not verified entirely and this approach was not included in this manuscript of thesis. Furthermore, by combining these results with a data base reconstituting the metabolism in photosynthetic organisms (e.g. ChloroKB database) it will be possible to identify other key metabolic regulators of LHCSR3 and NPQ in *Chlamydomonas reinhardtii.*

5.2 List of acronyms

AA Antimycin A
ACS acetyl-CoA synthetase
ACK Acetate kinase
ADP Adenosine di-phosphate
AFM Atomic force microscopy
AIC Akaike information criterion
AOX Alternative oxidase
ATP Adenosine tri-phosphate
CAs Carbonic anhydrases
CBB Calvin-Benson-Bassham cycle
CBP Chlorophyll binding proteins
CCM CO_2-concentrating mechanism
CEF Cyclic electron flow
cERM Chloroplast endoplasmic reticulum
Chl Chlorophyll
Cyt Cytochrome
DCMU 3-(3,4-dichlorophenyl)-1,1-dimethylurea
Dd Diadinoxanthin
DDE Diadinoxanthin de-epoxidase
DGDG Digalactosyl-diacyl- glycerol
Dt Diatoxanthin
DTE Diatoxanthin epoxidase
ECS Electrochromic shift
EM Electron microscopy
ENV Envelope
ER Endoplasmic reticulum
ESAW Enriched Seawater medium
ETR Electron transport rate
$FADH_2$ Flavin adenine dinucleotide
FCCP (Trifluoromethoxy) phenylhydrazone
FCP Fucoxanthin chlorophyll-*a/c* binding proteins
Fd Ferredoxin
FIB-SEM Focus ion beam-scanning electron microscopy
FNR Fd-NADP+-oxidoreductase
Fm Maximal fluorescence after dark acclimation
Fm' Maximal fluorescence in the light acclimated state
Fv Variable Fluorescence after dark acclimation
GAP Glyceraldehyde 3-phosphate
HA Hydroxylamine
HL High light

HSM High salt medium (Sueoka's buffer)
IBMX 3-isobutyl-1-methylxanthine
IEM Inner envelope membrane
LEF Linear electron flow
LHCI Light harvesting complex I
LHCII Light harvesting complex II
LHCSRs Light harvesting complex stress related proteins
Li818 Light Induced protein 818
LL Low light
LOV Light oxygen and voltage domain
MGDG Monogalactosyl-diacyl- glycerol
NADH Nicotinamide adenine dinucleotide
NADPH Nicotinamide adenine dinucleotide phosphate
NPQ Non-photochemical quenching
OCP Orange carotenoid protein
OEM Outer envelope membrane
OLS Okazaki large spectrograph
PAM Pulse amplitude modulation
PAT Phosphate acetyltransferase
PBSs Phycobilisomes
PC Plastocyanin
PCA Principal components analysis
PDK Serine-threonine kinase protein domain
PG Phosphatidyldiacylgycerol
PHOT Phototropin
PMF Proton motive force
PPC Periplastidial compartment
PPM Periplastidial membrane
PQ Plastoquinone
PSI Photosystem I
PSII Photosystem II
PSBS PSII subunit S protein
PYR Pyrenoid
Q Quinone
qP Photochemical quenching
qE High-energy-state quenching
qI Photoinhibitory quenching
qT Quenching related to state transitions
ROS Reactive oxygen species
RuBisCo Ribulose-1,5-bisphosphate carboxylase/oxygenase
Ru5P Ribulose-5-phosphate
SDS-PAGE Sodium dodecyl sulphate - polyAcrylamide gel electrophoresis

SHAM Salicylhydroxamic acid
SQDG Sulfoquinovosyldiacylglycerol
TAP Tris-acetate phosphate buffer
TCA Tricarboxylic acid cycle
TEF Total electron flow
TEM transmission electron microscopy
VDE Violaxanthin de-epoxidase
VN Vesicular network
Vx Violaxanthin
WT Wild type
XC Xanthophyll cycle
ZEP Zeaxanthin epoxidase
Zx Zeaxanthin
ΔΨ Electric field
ΔpH Proton gradient

5.3 List of publications

This thesis is based on the following publications and manuscripts:

Chapter 2

Section 2.3.2 Benjamin Bailleul, Nicolas Berne, Omer Murik, Dimitris Petroutsos, Judit Prihoda, Atsuko Tanaka, Valeria Villanova, Richard Bligny, **Serena Flori**, Denis Falconet, Anja Krieger-Liszkay, Stefano Santabarbara, Fabrice Rappaport, Pierre Joliot, Leila Tirichine, Paul G. Falkowski, Pierre Cardol, Chris Bowler, Giovanni Finazzi 2015 “Energetic Coupling Between Plastids and Mitochondria Drives CO_2 Assimilation in Diatoms" *Nature*……37

Section 2.4.2 **Serena Flori**, Pierre-Henri Jouneau, Giovanni Finazzi, Eric Maréchal and Denis Falconet “Ultrastructure of the Periplastidial Compartment of *Phaeodactylum tricornutum” Protist…*……63

Section 2.5.2 **Serena Flori**, Pierre-Henri Jouneau, Benjamin Bailleul, Benoit Gallet, Leandro Estrozi, Christine Moriscot, Olivier Bastien, Simona Eicke, Alexander Schober, Carolina Rio Bartulos, Eric Maréchal, Peter G. Kroth, Dimitris Petroutsos, Samuel Zeeman, Cécile Breyton, Guy Schoehn, Denis Falconet, Giovanni Finazzi “Chloroplast thylakoid architecture optimizes photosynthesis in diatoms“ manuscript in preparation……84

Chapter 4

Section 4.3.2 Dimitris Petroutsos, Ryutaro Tokutsu, Shinichiro Maruyama*,* **Serena Flori**, Andre Greiner, Leonardo Magneschi, Loic Cusant, Tilman Kottke, Maria Mittag, Peter Hegemann, Jun Minagawa, Giovanni Finazzi “A Blue Light Photoreceptor Mediates the Feedback Regulation of Photosynthesis“ paper under revision to *Nature*……144

Section 4.4 **Serena Flori** and collaborators “Carbon metabolism controls photoprotection in *Chlamydomonas* via the light harvesting complex stress response protein LHCSR3” manuscript in preparation……165

5.4 List of figures

Chapter 1

Chapter 2

Figure 2.33 - **Structural arrangement of the photosynthetic membranes in *P. tricornutum.*** (A) Equilibrium plots for the components of the high potential chain. Redox signals of cyt c and P_{700} in the light were plotted against each other. The dotted lines represent simulations corresponding to different values of the equilibrium constant. The rate of electron flow is calculated from data in Supplementary Figure 2.40. (B) Cartoon representing a possible arrangement of the photosynthetic complexes in a likely 3 thylakoid layers arrangement of the photosynthetic membranes in *P. tricornutum*. The different PSI and PSII localization within the peripheral (green) and the core membranes (violet) is shown. PSI: photosystem 1; PSII: photosystem 2, FCP: fucoxanthin chlorophyll antenna protein, $Cytb_6f$: cytochrome b_6f complex……91

Supplementary Figure 2.34 - **PSI/cytochrome c stoichiometry and oxidation kinetics in *P. tricornutum*. Cyt c/PSI stoichiometry.** Cells were exposed to a saturating single turnover laser flash to generate 1 turnover per PSI and the amount of oxidized c-type cytochrome was calculated 300µs after the flash (i.e. when P700 is fully rereduced by the cytochromes) This amount was normalized to the total amount of cyt c oxidized in continuous light in the presence of DCMU (20µM). Because the flash oxidizes 33% of the cyt c type cytochromes, we conclude there are ~3 c-type cytochromes per PSI. (B) procedure employed to evaluate the rates of PSI oxidation in the light in the case of the total donors to PSI pool. Open bar: light on. Closed bar: light off. The slope measured after the light is switched off (S_D) allows calculating the dark rereduction rates of the PSI donor pool in the control (closed blue squares), DCMU treated samples (closed red circles) and DCMU + HA treated samples (closed green triangles). The sum of this rate plus the apparent oxidation rate in the light (S_L) .provides the real rate of oxidation of the total donors to PSI oxidation kinetics, (open symbols). See methods for further description……101

Supplementary Figure 2.35 **- Light energy spillover in *P. tricornutum* cells exposed to different light intensities.** (A) Fluorescence emission kinetics in the presence of DCMU 40 µM and HA 0.2 mM. Squares: control, triangles: DCMU; circles: DCMU and HA; open symbols 150 µm photons m^{-2} s^{-1}; closed symbols: 300 µm photons m^{-2} s^{-1}. (B) Fluorescence emission kinetics in the presence of DCMU 40 µM and HA 0.2 mM. Squares: control, triangles: DCMU; circles: DCMU and HA; open symbols: 590 µm photons m^{-2} s^{-1}; closed symbols: 1100 µm photons m^{-2} s^{-1} (C) Kinetics of oxidation of the entire pool of PSI electron donors at a light intensity of 150 µm photons m^{-2} s^{-1}. (D) Kinetics of oxidation of the entire pool of PSI electron donors at a light intensity of 300 µm photons m^{-2} s^{-1}in

Chapter 3

Chapter 4

5.5 Supplementary Materials

5.6 References

- Abida, H., Dolch, L.-J., Mei, C., Villanova, V., Conte, M., Block, M.A., Finazzi, G., Bastien, O., Tirichine, L., Bowler, C., et al. (2015). Membrane glycerolipid remodeling triggered by nitrogen and phosphorus starvation in *Phaeodactylum tricornutum*. Plant Physiology, 118.
- Ahn, T.K., Avenson, T.J., Ballottari, M., Cheng, Y.-C., Niyogi, K.K., Bassi, R., and Fleming, G.R. (2008). Architecture of a charge-transfer state regulating light harvesting in a plant antenna protein. Science *320*, 794-797.
- Akaike, H. (1974). A new look at the statistical model identification. IEEE transactions on automatic control *19*, 716-723.
- Akazaki, H., Kawai, F., Hosokawa, M., Hama, T., Chida, H., Hirano, T., Lim, B.-K., Sakurai, N., Hakamata, W., and Park, S.-Y. (2009). Crystallization and structural analysis of cytochrome c_6 from the diatom *Phaeodactylum tricornutum* at 1.5 Å resolution. Bioscience, biotechnology and Biochemistry *73*, 189-191.
- Albertsson, P.-Å.A. (2001). A quantitative model of the domain structure of the photosynthetic membrane. Trends in Plant Science, 349.
- Alboresi, A., Gerotto, C., Giacometti, G.M., Bassi, R., and Morosinotto, T. (2010). *Physcomitrella patens* mutants affected on heat dissipation clarify the evolution of photoprotection mechanisms upon land colonization. Proceedings of the National Academy of Sciences *107*, 11128-11133.
- Allen, J.F. (1975). Oxygen reduction and optimum production of ATP in photosynthesis. 599-600.
- Allen, J.F. (1992). Protein phosphorylation in regulation of photosynthesis. Biochimica et Biophysica Acta (BBA) - Bioenergetics *1098*, 275-335.
- Allen, J.F. (2002). Photosynthesis of ATP electrons, proton pumps, rotors, and poise. Cell *110*, 273-276.
- Allorent, G., Tokutsu, R., Roach, T., Peers, G., Cardol, P., Girard-Bascou, J., Seigneurin-Berny, D., Petroutsos, D., Kuntz, M., Breyton, C., et al. (2013). A dual strategy to cope with high light in *Chlamydomonas reinhardtii*. The Plant Cell *25*, 545-557.
- Amunts, A., Nelson, N., and Dumas, R. (2008). Functional organization of a plant photosystem I: Evolution of a highly efficient photochemical machine. Plant Physiology and Biochemistry *46*, 228-237.

- Anderson, J.M. (1986). Photoregulation of the composition, function, and structure of thylakoid membranes. Annual Review of Plant Biology *37*, 93.
- Anderson, J.M., Chow, W.S., and Park, Y.-I. (1995). The grand design of photosynthesis: acclimation of the photosynthetic apparatus to environmental cues. Photosynthesis Research *46*, 129-139.
- Anderson, J.M., Park, Y.-I., and Chow, W.S. (1998). Unifying model for the photoinactivation of photosystem II in vivo under steady-state photosynthesis. Photosynthesis Research *56*, 1-13.
- Anwaruzzaman, M., Chin, B.L., Li, X.-P., Lohr, M., Martinez, D.A., and Niyogi, K.K. (2004). Genomic analysis of mutants affecting xanthophyll biosynthesis and regulation of photosynthetic light harvesting in *Chlamydomonas reinhardtii*. Photosynthesis Research *82*, 265-276.
- Apt, K.E., Bhaya, D., and Grossman, A.R. (1994). Characterization of genes encoding the light-harvesting proteins in diatoms: biogenesis of the fucoxanthin chlorophylla/c protein complex. Journal of Applied Phycology *6*, 225-230.
- Apt, K.E., Korth-Pancic, P.G., and Grossman, A.R. (1996). Stable nuclear transformation of the diatom *Phaeodactylum tricornutum*. Molecular & general genetics *252,*5, 572-579.
- Aro, E.-M., Virgin, I., and Andersson, B. (1993). Photoinhibition of photosystem II. inactivation, protein damage and turnover. Biochimica et Biophysica Acta (BBA) - Bioenergetics *1143*, 113-134.
- Arvidsson, P.-O.A. and Sundby, C.A., (1999). A model for the topology of the chloroplast thylakoid membrane. Australian Journal of Plant Physiology, 687.
- Asada, K. (2000). The water–water cycle as alternative photon and electron sinks. Philosophical Transactions of the Royal Society of London B: Biological Sciences *355*, 1419-1431.
- Asada, K., Takahashi, M.-a., and Nagate, M. (1974). Assay and inhibitors of spinach superoxide dismutase. Agricultural and Biological Chemistry *38*, 471-473.
- Atteia, A., Adrait, A., Brugière, S., Tardif, M., van Lis, R., Deusch, O., Dagan, T., Kuhn, L., Gontero, B., Martin, W., et al. (2009). A proteomic survey of *Chlamydomonas reinhardtii* mitochondria sheds new light on the metabolic plasticity of the organelle and on the nature of the α-proteobacterial mitochondrial ancestor. Molecular Biology and Evolution *26*, 1533-1548.

- Atteia, A., van Lis, R., Gelius-Dietrich, G., Adrait, A., Garin, J., Joyard, J., Rolland, N., and Martin, W. (2006). Pyruvate formate-lyase and a novel route of eukaryotic ATP synthesis in *Chlamydomonas* mitochondria. The Journal of Biological Chemistry *281*, 9909-9918.
- Austin, J.R., II, and Staehelin, L.A. (2011). Three-dimensional architecture of grana and stroma thylakoids of higher plants as determined by electron tomography. Plant Physiology *155*, 1601-1611.
- Babourina, O., Newman, I., and Shabala, S. (2002). Blue light-induced kinetics of H+ and Ca2+ fluxes in etiolated wild-type and phototropin-mutant *Arabidopsis* seedlings. Proceedings of the National Academy of Sciences *99*, 2433-2438.
- Badger, M.R. (1985). Photosynthetic oxygen exchange. Annual Review of Plant Physiology *36*, 27-53.
- Bailleul, B., Rogato, A., de Martino, A., Coesel, S., Cardol, P., Bowler, C., Falciatore, A., and Finazzi, G. (2010). An atypical member of the light-harvesting complex stress-related protein family modulates diatom responses to light. In Proceedings of the National Academy of Sciences. *107* (42), 18214-18219.
- Bailleul, B., Berne, N., Murik, O., Petroutsos, D., Prihoda, J., Tanaka, A., Villanova, V., Bligny, R., Flori, S., Falconet, D., et al. (2015). Energetic coupling between plastids and mitochondria drives CO_2 assimilation in diatoms. Nature *524*, 366-369.
- Baker, N.R. (2008). Chlorophyll Fluorescence: A probe of photosynthesis in vivo. Annual review of Plant Biology *59*, 89-113.
- Ballottari, M., Dall'Osto, L., Morosinotto, T., and Bassi, R. (2007). Contrasting behavior of higher plant photosystem I and II antenna systems during acclimation. Journal of Biological Chemistry *282*(12), 8947-8958.
- Ballottari, M., Truong, T.B., De Re, E., Erickson, E., Stella, G.R., Fleming, G.R., Bassi, R., and Niyogi, K.K. (2016). Identification of pH-sensing sites in the light harvesting complex stress-related 3 protein essential for triggering Non-photochemical quenching in *Chlamydomonas reinhardtii*. Journal of Biological Chemistry *291*, 7334-7346.
- Barber, J. (1980). An explanation for the relationship between salt-induced thylakoid stacking and the chlorophyll fluorescence changes associated with changes in spillover of energy from photosystem II to photosystem I. FEBS Letters *118*, 1-10.
- Barber, J., and Andersson, B. (1992). Too much of a good thing: light can be bad for photosynthesis. Trends in Biochemical Sciences *17*, 61-66.

- Bassham, J.A., Benson, A.A., and Calvin, M. (1950). The Path of Carbon in Photosynthesis VIII. The Role of Malic Acid.
- Bassham, J.A. (2003). Mapping the carbon reduction cycle: a personal retrospective. Photosynthesis Research *76*, 35-52.
- Bedoshvili, Y., D., and Likhoshway, Y., V. (2012). The cell ultrastructure of diatoms - implications for phylogeny? INTECH Open Access Publisher.
- Bedoshvili, Y.D., Popkova, T.P., and Likhoshway, Y.V. (2009). Chloroplast structure of diatoms of different classes. Cell and Tissue Biology, 297.
- Beel, B., Prager, K., Spexard, M., Sasso, S., Weiss, D., Müller, N., Heinnickel, M., Dewez, D., Ikoma, D., Grossman, A.R., et al. (2012). A flavin binding cryptochrome photoreceptor responds to both blue and red light in *Chlamydomonas reinhardtii*. The Plant Cell *24*, 2992-3008.
- Beer, A., Gundermann, K., Beckmann, J., and Büchel, C. (2006). Subunit composition and pigmentation of fucoxanthin−chlorophyll proteins in diatoms: evidence for a subunit involved in diadinoxanthin and diatoxanthin binding. Biochemistry *45*, 13046-13053.
- Benson, A.A. (2002). Paving the path. Annual Review of Plant Biology *53*, 1.
- Benson, A. A., and Calvin, M. (1950). Carbon dioxide fixation by green plants. Annual Review of Plant Physiology *1*, 25-42.
- Berges, J.A., Franklin, D.J., and Harrison, P.J. (2001). Evolution of an artificial seawater medium: improvements in enriched seawater, artificial water over the last two decades. Journal of Phycology *37*, 1138-1145.
- Bergner, S.V., Scholz, M., Trompelt, K., Barth, J., Gäbelein, P., Steinbeck, J., Xue, H., Clowez, S., Fucile, G., and Goldschmidt-Clermont, M. (2015). State transitions7-dependent phosphorylation is modulated by changing environmental conditions, and its absence triggers remodeling of photosynthetic protein complexes. Plant Physiology *168*, 615-634.
- Berteotti, S., Ballottari, M., and Bassi, R. (2016). Increased biomass productivity in green algae by tuning non-photochemical quenching. Scientific reports *6*.
- Berthold, D.A., Babcock, G.T., and Yocum, C.F. (1981). A highly resolved, oxygen-evolving photosystem II preparation from spinach thylakoid membranes. FEBS Letters *134*, 231-234.
- Betterle, N., Ballottari, M., Zorzan, S., de Bianchi, S., Cazzaniga, S., Dall'Osto, L., Morosinotto, T., and Bassi, R. (2009). Light-induced dissociation of an antenna hetero-oligomer is needed

for non-photochemical quenching induction. Journal of Biological Chemistry *284*, 22, 15255-15266.

- Bhatnagar, A., Chinnasamy, S., and Das, K.C. (2010). Mixotrophic algae for the production of algae biofuel feedstock on wastewater. Patent number: WO2010123848A3.
- Bilger, W., and Björkman, O. (1990). Role of the xanthophyll cycle in photoprotection elucidated by measurements of light-induced absorbance changes, fluorescence and photosynthesis in leaves of *Hedera canariensis*. Photosynthesis Research *25*, 173-185.
- Bligny, R., and Douce, R. (2001). NMR and plant metabolism. Current Opinion in Plant Biology *4*, 191-196.
- Bohlin, K.H. (1897). Zur morphologie und biologie einzelliger algen.
- Bolte, K., Bullmann, L., Hempel, F., Bozarth, A., Zauner, S., and Maier, U.-G. (2009). Protein targeting into secondary plastids. Journal of Eukaryotic Microbiology *56*, 9-15.
- Bonente, G., Ballottari, M., Truong, T.B., Morosinotto, T., Ahn, T.K., Fleming, G.R., Niyogi, K.K., and Bassi, R. (2011). Analysis of LhcSR3, a protein essential for feedback de-excitation in the green alga *Chlamydomonas reinhardtii*. PLoS Biology *9*, 1-17.
- Bonente, G., Howes, B.D., Caffarri, S., Smulevich, G., and Bassi, R. (2008). Interactions between the photosystem II subunit PsbS and xanthophylls studied in vivo and in vitro. Journal of Biological Chemistry *283*,13, 8434-8445.
- Boonyareth, M., Saranak, J., Pinthong, D., Sanvarinda, Y., and Foster, K.W. (2009). Roles of cyclic AMP in regulation of phototaxis in *Chlamydomonas reinhardtii*. Biologia, 1058.
- Borkhsenious, O.N., Mason, C.B., and Moroney, J.V. (1998). The intracellular localization of ribulose-1,5-bisphosphate carboxylase/oxygenase in *Chlamydomonas reinhardtii*. Plant Physiology *116*, 1585-1591.
- Botté, C., Saïdani, N., Mondragon, R., Mondragón, M., Isaac, G., Mui, E., McLeod, R., Dubremetz, J.-F., Vial, H., Welti, R., et al. (2008). Subcellular localization and dynamics of a digalactolipid-like epitope in *Toxoplasma gondii*. Journal of Lipid Research *49*(4), 746-762.
- Botté, C.Y., Yamaryo-Botté, Y., Janouskovec, J., Rupasinghe, T., Keeling, P.J., Crellin, P., Coppel, R.L., Maréchal, E., McConville, M.J., and McFadden, G.I. (2011). Identification of plant-like galactolipids in *Chromera velia*, a photosynthetic relative of malaria parasites. The Journal of Biological Chemistry *286*, 29893-29903.
- Botté, C.Y., Yamaryo-Botté, Y., Rupasinghe, T.W.T., Mullin, K.A., MacRae, J.I., Spurck, T.P., Kalanon, M., Shears, M.J., Coppel, R.L., Crellin, P.K., et al. (2013). Atypical lipid composition

in the purified relict plastid (apicoplast) of malaria parasites. Proceedings of the National Academy of Sciences *110*, 7506-7511.

- Botté, C.Y., and Maréchal, E. (2014). Plastids with or without galactoglycerolipids. Trends in Plant Science *19*, 71-78.
- Bouck, G.B. (1969). Extracellular Microtubules. The origin, structure, and attachment of flagellar hairs in *Fucus* and *Ascophyllum antherozoids*. The Journal of Cell Biology, 446.
- Boudière, L., Michaud, M., Petroutsos, D., Rébeillé, F., Falconet, D., Bastien, O., Roy, S., Finazzi, G., Rolland, N., Jouhet, J., et al. (2014). Review: glycerolipids in photosynthesis: composition, synthesis and trafficking. Biochimica et Biophysica Acta (BBA) - Bioenergetics *1837*, 470-480.
- Bowler, C., Montagu, M.V., and Inze, D. (1992). Superoxide dismutase and stress tolerance. Annual Review of Plant Physiology and Plant Molecular Biology *43*, 83-116.
- Bowler, C., Allen, A.E., Badger, J.H., Grimwood, J., Jabbari, K., Kuo, A., Maheswari, U., Martens, C., Maumus, F., Otillar, R.P., et al. (2008). The *Phaeodactylum* genome reveals the evolutionary history of diatom genomes. Nature *456*, 239-244.
- Briggs, W.R. (2014). Phototropism: some history, some puzzles, and a look ahead. Plant Physiology 164, 13-23.
- Brueggeman, A.J., Gangadharaiah, D.S., Cserhati, M.F., Casero, D., Weeks, D.P., and Ladunga, I. (2012). Activation of the carbon concentrating mechanism by CO_2 deprivation coincides with massive transcriptional restructuring in *Chlamydomonas reinhardtii*. The Plant Cell *24*, 1860-1875.
- Büchel, C. (2015). Evolution and function of light harvesting proteins. Journal of Plant Physiology *172*, 62-75.
- Büchel, C., and Wilhelm, C. (1993). In vivo analysis of slow chlorophyll fluorescence induction kinetics in algae: progress, problems and perspectives. Photochemistry & Photobiology *58*, 137.
- Bullmann, L., Haarmann, R., Mirus, O., Bredemeier, R., Hempel, F., Maier, U.G., and Schleiff, E. (2010). Filling the gap, evolutionarily conserved Omp85 in plastids of *Chromalveolates*. Journal of Biological Chemistry *285*(9), 6848-6856.
- Cardol, P., Bailleul, B., Rappaport, F., Derelle, E., Béal, D., Breyton, C., Bailey, S., Wollman, F.A., Grossman, A., and Moreau, H. (2008). An original adaptation of photosynthesis in the

marine green alga *Ostreococcus*. Proceedings of the National Academy of Sciences *105*, 7881-7886.

- Cardol, P., Alric, J., Girard-Bascou, J., Franck, F., Wollman, F.-A., and Finazzi, G. (2009). Impaired respiration discloses the physiological significance of state transitions in *Chlamydomonas*. Proceedings of the National Academy of Sciences *106*, 15979-15984.
- Cavalier-Smith, T. (2003). Genomic reduction and evolution of novel genetic membranes and protein-targeting machinery in eukaryote-eukaryote chimaeras (meta-algae). Philosophical Transactions of the Royal Society: Biological Sciences *358*, 1429, 109-134.
- Cavalier-Smith, T. (2006). Cell evolution and Earth history: stasis and revolution. Philosophical Transactions of the Royal Society of London: Biological Sciences *361*, 1470, 969-1006.
- Cazzaniga, S., Dall' Osto, L., Kong, S.-G., Wada, M., and Bassi, R. (2013). Interaction between avoidance of photon absorption, excess energy dissipation and zeaxanthin synthesis against photooxidative stress in *Arabidopsis*. The Plant Journal: For Cell And Molecular Biology *76*, 568-579.
- Chaves, I., Pokorny, R., Byrdin, M., Hoang, N., Ritz, T., Brettel, K., Essen, L.-O., van der Horst, G.T., Batschauer, A., and Ahmad, M. (2011). The cryptochromes: blue light photoreceptors in plants and animals. Annual review of plant biology *62*, 335-364.
- Chen, M., and Chory, J. (2011). Phytochrome signaling mechanisms and the control of plant development. Trends in Cell Biology, 664.
- Cheniae, G. M., and Martin, I. F. (1971). Effects of Hydroxylamine on Photosystem II I. Factors Affecting the Decay of O2. Evolution in Plant Physiology *47*, 568-575.
- Christie, J.M. (2007). Phototropin blue-light receptors. Annual review of plant biology *58*, 21-45.
- Christie, J.M., Blackwood, L., Petersen, J., and Sullivan, S. (2015). Plant flavoprotein photoreceptors. Plant & Cell Physiology *56*, 401-413.
- Colin, M., Dorthu, M.P., Duby, F., Remacle, C., Dinant, M., Wolwertz, M.R., Duyckaerts, C., Sluse, F., and Matagne, R.F. (1995). Mutations affecting the mitochondrial genes encoding the cytochrome oxidase subunit I and apocytochrome b of *Chlamydomonas reinhardtii*. . Molecular and General Genetics MGG *249*: 179–184.

- Costa, B.S., Jungandreas, A., Jakob, T., Weisheit, W., Mittag, M., and Wilhelm, C. (2013). Blue light is essential for high light acclimation and photoprotection in the diatom *Phaeodactylum tricornutum*. Journal of experimental botany *64*, 483-493.
- Curtis, B.A.A., Tanifuji, G.A., Burki, F.A., Gruber, A.A., Irimia, M.A., Maruyama, S.A., Arias, M.C.A., Ball, S.G.A., Gile, G.H.A., Hirakawa, Y.A., et al. (2012). Algal genomes reveal evolutionary mosaicism and the fate of nucleomorphs. Nature, 59.
- Dalgaard, P. (2002). Introductory Statistics with R Springer–Verlag New York.
- Dall'Osto, L., Caffarri, S., and Bassi, R. (2005). A mechanism of nonphotochemical energy dissipation, independent from PsbS, revealed by a conformational change in the antenna protein CP26. The Plant Cell *17*, 1217-1232.
- Dang, K.-V., Plet, J., Tolleter, D., Jokel, M., Cuiné, S., Carrier, P., Auroy, P., Richaud, P., Johnson, X., and Alric, J. (2014). Combined increases in mitochondrial cooperation and oxygen photoreduction compensate for deficiency in cyclic electron flow in *Chlamydomonas reinhardtii*. The Plant Cell *26*, 3036-3050.
- Daum, B., Kuhlbrandt, W., and Gilliham, M. (2011). Electron tomography of plant thylakoid membranes. Journal of Experimental Botany *62*, 2393-2402.
- De Martino, A., Meichenin, A., Shi, J., Pan, K., and Bowler, C. (2007). Genetic and phenotypic characterization of *Phaeodactylum tricornutum* (Bacillariophyceae) accessions. Journal of Phycology, 992.
- De Riso, V., Raniello, R., Maumus, F., Rogato, A., Bowler, C., and Falciatore, A. (2009). Gene silencing in the marine diatom *Phaeodactylum tricornutum*. Nucleic acids research, *37*, 14, e96-e96.
- de Vargas, C., Audic, S., Henry, N., Decelle, J., Mahé, F., Logares, R., Lara, E., Berney, C., Le Bescot, N., Probert, I., et al. (2015). Ocean plankton. Eukaryotic plankton diversity in the sunlit ocean. Science *348*, 1261605-1261605.
- Dekker, J.P., and Boekema, E.J. (2005). Supramolecular organization of thylakoid membrane proteins in green plants. Biochimica et Biophysica Acta (BBA) - Bioenergetics *1706*, 12-39.
- Delosme, R., Olive, J., and Wollman, F.-A. (1996). Changes in light energy distribution upon state transitions: an in vivo photoacoustic study of the wild type and photosynthesis mutants from *Chlamydomonas reinhardtii*. Biochimica et Biophysica Acta (BBA) - Bioenergetics *1273*, 150-158.

- Demarsy, E., and Fankhauser, C. (2009). Higher plants use LOV to perceive blue light. Current Opinion in Plant Biology *12*, 69-74.
- Depège, N., Bellafiore, S., and Rochaix, J.-D. (2003). Role of chloroplast protein kinase Stt7 in LHCII phosphorylation and state transition in Chlamydomonas. Science *299*, 1572-1575.
- Dietz, K.-J., Turkan, I., and Krieger-Liszkay, A. (2016). Redox-and reactive oxygen species-dependent signalling in and from the photosynthesizing chloroplast. Plant physiology *171*, 1541-1550.
- Diner, B., and Joliot, P. (1976). Effect of the transmembrane electric field on the photochemical and quenching properties of photosystem II in vivo. Biochimica et Biophysica Acta (BBA) - Bioenergetics *423*, 479-498.
- Dittami, S.M., Michel, G., Collén, J., Boyen, C., and Tonon, T. (2010). Chlorophyll-binding proteins revisited - a multigenic family of light-harvesting and stress proteins from a brown algal perspective. BMC Evolutionary Biology *10*, 1-14.
- Dorrell, R.G., and Smith, A.G. (2011). Do red and green make brown? Perspectives on plastid acquisitions within chromalveolates. Eukaryotic cell *10*, 856-868.
- Eberhard, S., Finazzi, G., and Wollman, F.-A. (2008). The dynamics of photosynthesis. Annual Review of Genetics, 463.
- Engel, B.D., Schaffer, M., Kuhn Cuellar, L., Villa, E., Plitzko, J.M., and Baumeister, W. (2015). Native architecture of the *Chlamydomonas* chloroplast revealed by in situ cryo-electron tomography. Elife *4*.
- Eppard, M., and Rhiel, E. (1998). The genes encoding light-harvesting subunits of *Cyclotella cryptica* (Bacillariophyceae) constitute a complex and heterogeneous family. Molecular and General Genetics MGG *260*, 335-345.
- Eriksson, M., Villand, P., Gardeström, P., and Samuelsson, G. (1998). Induction and regulation of expression of a low-CO_2-induced mitochondrial carbonic anhydrase in *Chlamydomonas reinhardtii*. Plant Physiology *116*: 637–641.
- Falciatore, A., Casotti, R., Leblanc, C., Abrescia, C., and Bowler, C. (1999). Transformation of nonselectable reporter genes in marine diatoms. Marine Biotechnology *1*, 239-251.
- Falkowski, P.G., Katz, M.E., Knoll, A.H., Quigg, A., Raven, J.A., Schofield, O., and Taylor, F.J.R. (2004). The evolution of modern eukaryotic phytoplankton. Science *305*, 5682, 354.
- Falkowski, P.G., and LaRoche, J. (1991). Acclimation to spectral irradiance in algae. Journal of Phycology *27*, 8-14.

- Fang, W., Si, Y., Douglass, S., Casero, D., Merchant, S.S., Pellegrini, M., Ladunga, I., Liu, P., and Spalding, M.H. (2012). Transcriptome-wide changes in *Chlamydomonas reinhardtii* gene expression regulated by carbon dioxide and the CO_2-concentrating mechanism regulator CIA5/CCM1. The Plant Cell *24*, 1876-1893.
- Felsner, G., Sommer, M.S., Gruenheit, N., Hempel, F., Moog, D., Zauner, S., Martin, W., and Maier, U.G. (2011). ERAD components in organisms with complex red plastids suggest recruitment of a preexisting protein transport pathway for the periplastid membrane. Genome Biology and Evolution *3*, 140-150.
- Fett, J.P. and Coleman, J.R. (1994a). Regulation of periplasmic carbonic anhydrase expression in *Chlamydomonas reinhardtii* by acetate and pH. Plant Physiology *106*: 103–108.
- Fett, J.P. and Coleman, J.R. (1994b). Regulation of periplasmic carbonic anhydrase expression in *Chlamydomonas reinhardtii* by acetate and pH. Plant Physiology *106*: 103–108.
- Field, C.B., Behrenfeld, M.J., Randerson, J.T., and Falkowski, P. (1998). Primary production of the biosphere: integrating terrestrial and oceanic components. Science *281*, 237-240.
- Finazzi, G., and Rappaport, F. (1998). In vivo characterization of the electrochemical proton gradient generated in darkness in green algae and its kinetic effects on cytochrome b6f turnover. Biochemistry *37*, 9999-10005.
- Finazzi, G. (2005). The central role of the green alga *Chlamydomonas reinhardtii* in revealing the mechanism of state transitions. Journal of Experimental Botany *56*: 383–388.
- Finazzi, G., Johnson, G.N., Dall'Osto, L., Zito, F., Bonente, G., Bassi, R., and Wollman, F.-A. (2006). Nonphotochemical quenching of chlorophyll fluorescence in *Chlamydomonas reinhardtii*. Biochemistry *45*, 1490-1498.
- Finazzi, G., and Minagawa, J. (2014). High light acclimation in green microalgae in non-photochemical quenching and thermal energy dissipation in plants, algae and cyanobacteria. Advances in Photosynthesis and Respiration-Including Bioenergy and Related Processes, *40*, 24.
- Flori, S., Jouneau, P.-H., Finazzi, G., Maréchal, E., and Falconet, D. (2016). Ultrastructure of the periplastidial compartment of the diatom *Phaeodactylum tricornutum*. Protist *167*, 254-267.
- Folta, K.M., and Kaufman, L.S. (2003). Phototropin 1 is required for high-fluence blue-light-mediated mRNA destabilization. Plant molecular biology *51*, 609-618.

- Fristedt, R., Willig, A., Granath, P., Crèvecoeur, M., Rochaix, J.-D., and Vener, A.V. (2009). Phosphorylation of photosystem II controls functional macroscopic folding of photosynthetic membranes in *Arabidopsis*. The Plant Cell *21*, 3950-3964.
- Fukuzawa, H., Miura, K., Ishizaki, K., Kucho, K.-I., Saito, T., Kohinata, T., and Ohyama, K. (2001). Ccm1, a regulatory gene controlling the induction of a carbon-concentrating mechanism in *Chlamydomonas reinhardtii* by sensing CO_2 availability. Proceedings of the National Academy of Sciences *98*: 5347–5352.
- Gagné, G., and Guertin, M. (1992). The early genetic response to light in the green unicellular alga *Chlamydomonas eugametos* grown under light/dark cycles involves genes that represent direct responses to light and photosynthesis. Plant Molecular Biology *18*, 429-445.
- Galván-Ampudia, C.S., and Offringa, R. (2007). Plant evolution: AGC kinases tell the auxin tale. Trends in Plant Science *12*, 541-547.
- Genty, B., Briantais, J.-M., and Baker, N.R. (1989). The relationship between the quantum yield of photosynthetic electron transport and quenching of chlorophyll fluorescence. Biochimica et Biophysica Acta (BBA) *990*: 87–92.
- Gera, J.F., and Baker, E.J. (1998). Deadenylation-dependent and-independent decay pathways for α1-tubulin mRNA in *Chlamydomonas reinhardtii*. Molecular and cellular biology *18*, 1498-1505.
- Gibbs, S.P. (1962a). The ultrastructure of the chloroplasts of algae. Journal of Ultrastructure Research *7*, 418-435.
- Gibbs, S.P. (1962b). Nuclear envelope-chloroplast relationships in algae. The Journal of Cell Biology *14*, 433-444.
- Gibbs, S.P. (1962c). Chloroplast development in *Ochromonas danica*. The Journal of Cell Biology *15*, 343-361.
- Gibbs, S.P. (1979). The route of entry of cytoplasmically synthesized proteins into chloroplasts of algae possessing chloroplast ER. Journal of Cell Science *35*, 253-266.
- Gibbs, S.P. (1981). The chloroplast of some algal groups may have evolved from endosmbiotic eukaryotic algae. Annals of the New York Academy of Sciences *361*, 193.
- Goldschmidt-Clermont, M. (1986). The two genes for the small subunit of RuBP Carboxylase/oxygenase are closely linked in *Chlamydomonas reinhardtii*. Plant Molecular Biology *6*: 13–21.

- Goral, T.K., Johnson, M.P., Duffy, C.D.P., Brain, A.P.R., Ruban, A.V., and Mullineaux, C.W. (2012). Light-harvesting antenna composition controls the macrostructure and dynamics of thylakoid membranes in *Arabidopsis*. The Plant Journal *69*, 289-301.
- Gorman, D.S., and Levine, R. (1965). Cytochrome f and plastocyanin: their sequence in the photosynthetic electron transport chain of *Chlamydomonas reinhardii*. Proceedings of the National Academy of Sciences *54*, 1665-1669.
- Goss, R., Lepetit, B., and Wilhelm, C. (2006). Evidence for a rebinding of antheraxanthin to the light-harvesting complex during the epoxidation reaction of the violaxanthin cycle. Journal of Plant Physiology *163*, 585-590.
- Gould, S.B., Sommer, M.S., Kroth, P.G., Gile, G.H., Keeling, P.J., and Maier, U.-G. (2006). Nucleus-to-nucleus gene transfer and protein retargeting into a remnant cytoplasm of cryptophytes and diatoms. Molecular Biology and Evolution *23*, 2413-2422.
- Gould, S. B., Maier, U.-G., and Martin, William F. (2015). Protein import and the origin of red complex plastids. Current Biology *25*, R515-R521.
- Green, B.R., and Durnford, D.G. (1996). The chlorophyll-carotenoid proteins of oxygenic photosynthesis. Annual Review of Plant Physiology and Plant Molecular Biology *47*, 685-714.
- Grosche, C., Hempel, F., Bolte, K., Zauner, S., and Maier, U.G. (2014). The periplastidal compartment: a naturally minimized eukaryotic cytoplasm. Current Opinion in Microbiology *22*, 88-93.
- Grossman, A.R., Croft, M., Gladyshev, V.N., Merchant, S.S., Posewitz, M.C., Prochnik, S., and Spalding, M.H. (2007). Novel metabolism in *Chlamydomonas* through the lens of genomics. Current Opinion in Plant Biology *10*: 190–198.
- Grouneva, I., Rokka, A., and Aro, E.-M. (2011). The thylakoid membrane proteome of two marine diatoms outlines both diatom-specific and species-specific features of the photosynthetic machinery. Journal of Proteome Research *10*, 5338-5353.
- Gruber, A., Vugrinec, S., Hempel, F., Gould, S.B., Maier, U.-G., and Kroth, P.G. (2007). Protein targeting into complex diatom plastids: functional characterisation of a specific targeting motif. Plant Molecular Biology *64*(5), 519-530.
- Guillard, R.R. (1975). Culture of phytoplankton for feeding marine invertebrates. In Culture of marine invertebrate animals. (Springer, 29-60).
- Hager, A. (1967). Studies on the backward-reactions in the xanthophyll-cycle of *Chlorella*, *Spinacia* and *Taxus*. Planta *76*, 138-148.

- Hansma, P.K., Cleveland, J.P., Radmacher, M., Walters, D.A., Hillner, P.E., Bezanilla, M., Fritz, M., Vie, D., Hansma, H.G., Prater, C.B., et al. (1994). Tapping mode atomic force microscopy in liquids. Applied Physics Letters *64*, 1738-1740.
- Harada, A., Sakai, T., and Okada, K. (2003). Phot1 and phot2 mediate blue light-induced transient increases in cytosolic Ca2+ differently in Arabidopsis leaves. Proceedings of the National Academy of Sciences *100*, 8583-8588.
- Harris, E.H. (1989). An overview of the genus *Chlamydomonas*. In the *Chlamydomonas* sourcebook (Elsevier), 1–24.
- Hayashi, Y., Sato, N., Shinozaki, A., and Watanabe, M. (2015). Increase in peroxisome number and the gene expression of putative glyoxysomal enzymes in *Chlamydomonas* cells supplemented with acetate. Journal of Plant Research *128*: 177–185.
- Hasegawa, E., Hayashi, H., Asakura, S., and Kamiya, R. (1987). Stimulation of in vitro motility of *Chlamydomonas* axonemes by inhibition of cAMP-dependent phosphorylation. Cell Motility & the Cytoskeleton *8*, 302.
- Heijde, M., and Ulm, R. (2012). UV-B photoreceptor-mediated signalling in plants. Trends in Plant Science *17*, 230-237.
- Heiny, S.R., Pautz, S., Recker, M., and Przyborski, J.M. (2014). Protein Traffic to the Plasmodium falciparum apicoplast: evidence for a sorting branch point at the golgi. Traffic *15*, 1290-1304.
- Heinz, E., and Lithgow, T. (2014). A comprehensive analysis of the Omp85/TpsB protein superfamily structural diversity, taxonomic occurrence, and evolution. Frontiers in Microbiology *5*, 1-13.
- Hempel, F., Bozarth, A., Sommer, M.S., Zauner, S., Przyborski, J.M., and Maier, U.-G. (2007). Transport of nuclear-encoded proteins into secondarily evolved plastids. Biological Chemistry *388*, 899-906.
- Hempel, F., Bullmann, L., Lau, J., Zauner, S., and Maier, U.G. (2009). ERAD-derived preprotein transport across the second outermost plastid membrane of diatoms. Molecular Biology and Evolution *26*, 1781-1790.
- Herbstova, M., Tietz, S., Kinzel, C., Turkina, M.V., and Kirchhoff, H. (2012). Architectural switch in plant photosynthetic membranes induced by light stress. Proceedings of the National Academy of Sciences *109*, 20130-20135.

- Hill, R., and Bendall, F.A.Y. (1960). Function of the Two Cytochrome Components in Chloroplasts: A Working Hypothesis. Nature *186*, 136.
- Hiller, R.G., Wrench, P.M., Gooley, A.P., Shoebridge, G., and Breton, J. (1993). The major intrinsic light-harvesting protein of *Amphidinium*: characterization and relation to other light-harvesting proteins. Photochemistry and Photobiology *57*(1), 125-131.
- Holdsworth, R.H. (1971). The isolation and partial characterization of the pyrenoid protein of *Eremosphaera viridis*. The Journal of Cell Biology *51*, 499-513.
- Horton, P., Ruban, A.V., and Walters, R.G. (1996). Regulation of light harvesting in green plants. Annual Review of Plant and Plant Molecular Biology, *47*: 655–684.
- Hosmer, J.D.W., Lemeshow, S., and Sturdivant, R.X. (2013). Applied Logistic Regression. John Wiley & Sons.
- Höhner, R., Barth, J., Magneschi, L., Jaeger, D., Niehues, A., Bald, T., Grossman, A., Fufezan, C., and Hippler, M. (2013). The metabolic status drives acclimation of iron deficiency responses in *Chlamydomonas reinhardtii* as revealed by proteomics based hierarchical clustering and reverse genetics. Molecular Cell Proteomics *12*: 2774–2790.
- Howe, C.J., Schlarb-Ridley, B.G., Wastl, J., Purton, S., and Bendall, D.S. (2006). The novel cytochrome c6 of chloroplasts: a case of evolutionary bricolage? Journal of Experimental Botany *57*, 13-22.
- Huang, K., Merkle, T., and Beck, C.F. (2002). Isolation and characterization of a *Chlamydomonas* gene that encodes a putative blue-light photoreceptor of the phototropin family. Physiologia Plantarum *115*, 613-622.
- Huang, K., and Beck, C.F. (2003). Phototropin is the blue-light receptor that controls multiple steps in the sexual life cycle of the green alga *Chlamydomonas reinhardtii*. Proceedings of the National Academy of Sciences *100*, 6269-6274.
- Huang, K., Kunkel, T., and Beck, C.F. (2004). Localization of the blue-light receptor phototropin to the flagella of the green alga *Chlamydomonas reinhardtii*. Molecular Biology of The Cell *15*, 3605-3614.
- Im, C.-S., Eberhard, S., Kaiyao, H., Beck, C.F., and Grossman, A.R. (2006). Phototropin involvement in the expression of genes encoding chlorophyll and carotenoid biosynthesis enzymes and LHC apoproteins in *Chlamydomonas reinhardtii*. Plant Journal *48*, 1-16.
- Inda, L.A., Erdner, D.L., Peleato, M.L., and Anderson, D.M. (1999). Cytochrome c6 isolated from the marine diatom *Thalassiosira weissflogii*. Phytochemistry *51*, 1-4.

- Ingram-Smith, C., Martin, S.R., and Smith, K.S. (2006). Acetate kinase: not just a bacterial enzyme. Trends in Microbiology *14*, 249-253.
- Iwai, M., Yokono, M., Inada, N., and Minagawa, J. (2010). Live-cell imaging of photosystem II antenna dissociation during state transitions. Proceedings of the National Academy of Sciences *107*, 2337-2342.
- Jansson, S. (1999). A guide to the Lhc genes and their relatives in *Arabidopsis*. Trends in Plant Science *4*, 236-240.
- Jarvis, P., and Soll, J. (2001). Review: Toc, Tic, and chloroplast protein import. Biochimica et Biophysica Acta (BBA) - Molecular Cell Research *1541*, 64-79.
- Jenkins, G.I. (2014). The UV-B photoreceptor UVR8: from structure to physiology. The Plant Cell, 21.
- Jiao, Y., Lau, O.S., and Deng, X.W. (2007). Light-regulated transcriptional networks in higher plants. Nature Reviews Genetics *8*, 217-230.
- Joët, T., Cournac, L., Horvath, E.M., Medgyesy, P., and Peltier, G. (2001). Increased sensitivity of photosynthesis to antimycin A induced by inactivation of the chloroplast ndhB gene. Evidence for a participation of the NADH-dehydrogenase complex to cyclic electron flow around photosystem I. Plant Physiology *125*, 1919-1929.
- Johnson, X., and Alric, J. (2013). Central carbon metabolism and electron transport in *Chlamydomonas reinhardtii*: metabolic constraints for carbon partitioning between oil and starch. Eukaryotic Cell *12*, 776-793.
- Johnson, X., Vandystadt, G., Bujaldon, S., Wollman, F.-A., Dubois, R., Roussel, P., Alric, J., and Béal, D. (2009). A new setup for in vivo fluorescence imaging of photosynthetic activity. Photosynthesis Research *102*, 85-93.
- Joliot, P., and Delosme, R. (1974). Flash-induced 519 nm absorption change in green algae. Biochimica et Biophysica Acta (BBA)-Bioenergetics *357*, 267-284.
- Joliot, P., and Joliot, A. (1989). Characterization of linear and quadratic electrochromic probes in *Chlorella sorokiniana* and *Chlamydomonas reinhardtii*. Biochimica et Biophysica Acta (BBA)-Bioenergetics *975*, 355-360.
- Joliot, P.A., and Finazzi, G. (2010). Proton equilibration in the chloroplast modulates multiphasic kinetics of non-photochemical quenching of fluorescence in plants. Proceedings of the National Academy of Sciences *107*, 12728-12733.

- Junge, W., Sielaff, H., and Engelbrecht, S. (2009). Torque generation and elastic power transmission in the rotary FOF1-ATPase. Nature *459*, 364-370.
- Kana, T.M., Darkangelo, C., Hunt, M.D., Oldham, J.B., Bennett, G.E., and Cornwell, J.C. (1994). Membrane inlet mass spectrometer for rapid high-precision determination of N2, O2, and Ar in environmental water samples. Analytical Chemistry *66*, 4166-4170.
- Kasahara, M., Swartz, T.E., Olney, M.A., Onodera, A., Mochizuki, N., Fukuzawa, H., Asamizu, E., Tabata, S., Kanegae, H., Takano, M., et al. (2002). Photochemical Properties of the Flavin Mononucleotide-Binding Domains of the Phototropins from *Arabidopsis*, *Rice*, and *Chlamydomonas reinhardtii*. Plant Physiology *129*, 762-773.
- Keeling, P.J. (2004). Diversity and evolutionary history of plastids and their hosts. American Journal of Botany *91*, 1481-1493.
- Khatoon, M., Inagawa, K., Pospíšil, P., Yamashita, A., Yoshioka, M., Lundin, B., Horie, J., Morita, N., Jajoo, A., Yamamoto, Y., et al. (2009). Quality control of photosystem II: Thylakoid unstacking is necessary to avoid further damage to the D1 protein and to facilitate D1 degradation under light stress in spinach thylakoids. Journal of Biological Chemistry *284*, 25343-25352.
- Kilian, O., and Kroth, P.G. (2005). Identification and characterization of a new conserved motif within the presequence of proteins targeted into complex diatom plastids. Plant Journal *41*, 175-183.
- Kinoshita, H., Nagasaki, J., Yoshikawa, N., Yamamoto, A., Takito, S., Kawasaki, M., Sugiyama, T., Miyake, H., Weber, A.P., and Taniguchi, M. (2011). The chloroplastic 2-oxoglutarate/malate transporter has dual function as the malate valve and in carbon/nitrogen metabolism. The Plant Journal *65*, 15-26.
- Kirchhoff, H., Mukherjee, U., and Galla, H.J. (2002). Molecular architecture of the thylakoid membrane: lipid diffusion space for plastoquinone. Biochemistry, 4872.
- Kirchhoff, H., Schöttler, M.A., Maurer, J., and Weis, E. (2004). Plastocyanin redox kinetics in spinach chloroplasts: evidence for disequilibrium in the high potential chain. Biochimica et Biophysica Acta (BBA) - Bioenergetics *1659*, 63-72.
- Kirchhoff, H., Hall, C., Wood, M., Herbstova, M., Tsabari, O., Nevo, R., Charuvi, D., Shimoni, E., and Reich, Z. (2011). Dynamic control of protein diffusion within the granal thylakoid lumen. Proceedings of the National Academy of Sciences *108*, 20248-20253.

- Kirchhoff, H. (2013). Architectural switches in plant thylakoid membranes. Photosynthesis research *116*, 2-3, 481-487.
- Kirilovsky, D., and Kerfeld, C.A. (2012). The orange carotenoid protein in photoprotection of photosystem II in cyanobacteria. Biochimica et Biophysica Acta (BBA) - Bioenergetics *1817*, 158-166.
- Kirilovsky, D., and Kerfeld, C.A. (2013). The orange carotenoid protein: a blue-green light photoactive protein. Photochemical & Photobiological Sciences *12*, 1135-1143.
- Kolber, Z.S., Van Dover, C.L., Niederman, R.A., and Falkowski, P.G. (2000). Bacterial photosynthesis in surface waters of the open ocean. Nature *407*, 177-179.
- Kong, S.-G., Kinoshita, T., Shimazaki, K.-i., Mochizuki, N., Suzuki, T., and Nagatani, A. (2007). C-terminal kinase fragment of *Arabidopsis* phototropin 2 triggers constitutive phototropin responses. The Plant Journal *51*(5), 862-873.
- Kornberg, H.L. and Krebs, H.A. (1957). Synthesis of cell constituents from C2-units by a modified tricarboxylic acid cycle. Nature.
- Kucho, K.-I., Yoshioka, S., Taniguchi, F., Ohyama, K., and Fukuzawa, H. (2003). Cis-acting elements and DNA-binding proteins involved in CO_2-responsive transcriptional activation of Cah1 encoding a periplasmic carbonic anhydrase in *Chlamydomonas reinhardtii*. Plant Physiology *133*: 783–793.
- Kouřil, R., Dekker, J.P., and Boekema, E.J. (2012). Supramolecular organization of photosystem II in green plants. Biochimica et Biophysica Acta (BBA) -Bioenergetics *1817,* 1, 2-12.
- Kowalczyk, N., Rappaport, F., Boyen, C., Wollman, F.-A., Collén, J., and Joliot, P. (2013). Photosynthesis in *Chondrus crispus*: The contribution of energy spill-over in the regulation of excitonic flux. Biochimica et Biophysica Acta (BBA) - Bioenergetics *1827*, 834-842.
- Krause, G.H. (1988). Photoinhibition of photosynthesis. An evaluation of damaging and protective mechanisms. Physiologia Plantarum *74*, 566-574.
- Krieger-Liszkay, A., Fufezan, C., and Trebst, A. (2008). Singlet oxygen production in photosystem II and related protection mechanism. Photosynthesis Research *98*, 551-564.
- Kroth, P.G., Chiovitti, A., Gruber, A., Martin-Jezequel, V., Mock, T., Parker, M.S., Stanley, M.S., Kaplan, A., Caron, L., Weber, T., et al. (2008). A Model for carbohydrate metabolism in the diatom *Phaeodactylum tricornutum* deduced from comparative whole genome analysis. PLoS ONE *3*, 1-14.

- Kukuczka, B., Magneschi, L., Petroutsos, D., Steinbeck, J., Bald, T., Powikrowska, M., Fufezan, C., Finazzi, G., and Hippler, M. (2014). Proton gradient regulation5-like1-mediated cyclic electron flow is crucial for acclimation to anoxia and complementary to nonphotochemical quenching in stress adaptation. Plant Physiology *165*: 1604–1617.
- Külheim, C., Ågren, J., and Jansson, S. (2002). Rapid regulation of light harvesting and plant fitness in the field. Science *297*, 5578, 91.
- Lacoste-Royal, G., and Gibbs, S.P. (1987). Immunocytochemical localization of ribulose-1,5-bisphosphate carboxylase in the pyrenoid and thylakoid region of the chloroplast of *Chlamydomonas reinhardtii*. Plant Physiology *83*, 602-606.
- Lau, J.B., Stork, S., Moog, D., Sommer, M.S., and Maier, U.G. (2015). N-terminal lysines are essential for protein translocation via a modified ERAD system in complex plastids. Molecular Microbiology, 609.
- Lauersen, K.J., Willamme, R., Coosemans, N., Joris, M., Kruse, O., and Remacle, C. (2016). Peroxisomal microbodies are at the crossroads of acetate assimilation in the green microalga *Chlamydomonas reinhardtii*. Algal Research *16*: 266–274.
- Lavaud, J., Rousseau, B., van Gorkom, H.J., and Etienne, A.-L. (2002). Influence of the diadinoxanthin pool size on photoprotection in the marine planktonic diatom *Phaeodactylum tricornutum*. Plant Physiology *129* (3), 1398-1406.
- Lavaud, J., and Lepetit, B. (2013). An explanation for the inter-species variability of the photoprotective non-photochemical chlorophyll fluorescence quenching in diatoms. BBA - Bioenergetics *1827*, 294-302.
- Lavaud, J., Six, C., and Campbell, D.A. (2016). Photosystem II repair in marine diatoms with contrasting photophysiologies. Photosynthesis Research, 189.
- Ledford, H., Baroli, I., Shin, J., Fischer, B., Eggen, R., and Niyogi, K. (2004). Comparative profiling of lipid-soluble antioxidants and transcripts reveals two phases of photo-oxidative stress in a xanthophyll-deficient mutant of *Chlamydomonas reinhardtii*. Molecular Genetics and Genomics *272*, 470-479.
- Lebart, L., Piron, A., Lebart, M., Morineau, A., and Piron, M. (2000). Statistique exploratoire multidimensionnelle; Dunod, Paris, 3e édition.
- Lemaire, C., Wollman, F.-A., and Bennoun, P. (1988). Restoration of phototrophic growth in a mutant of *Chlamydomonas reinhardtii* in which the chloroplast atpB gene of the ATP

synthase has a deletion: an example of mitochondria-dependent photosynthesis. Proceedings of the National Academy of Sciences *85*, 1344-1348.

- Lepetit, B., Goss, R., Jakob, T., and Wilhelm, C. (2012). Molecular dynamics of the diatom thylakoid membrane under different light conditions. Photosynthesis research *111*(1-2), 245-257.
- Lepetit, B., Sturm, S., Rogato, A., Gruber, A., Sachse, M., Falciatore, A., Kroth, P.G., and Lavaud, J. (2013). High light acclimation in the secondary plastids containing diatom *Phaeodactylum tricornutum* is triggered by the redox state of the plastoquinone pool. Plant Physiology *161*, 853-865.
- Levitan, O., Dinamarca, J., Hochman, G., and Falkowski, P.G. (2014). Diatoms: a fossil fuel of the future. Trends in Biotechnology, 117.
- Ley, A.C., and Butler, W.L. (1977). Energy transfer from photosystem II to photosystem I in *Porphyridium cruentum*. Biochimica et Biophysica Acta (BBA) *462*, 290-294.
- Li, X.-P., Bjorkman, O., Shih, C., Grossman, A.R., Rosenquist, M., Jansson, S., and Niyogi, K.K. (2000). A pigment-binding protein essential for regulation of photosynthetic light harvesting. Nature *403*, 391-395.
- Li, X.-P., Phippard, A., Pasari, J., and Niyogi, K.K. (2002). Structure–function analysis of photosystem II subunit S (PsbS) in vivo. Functional Plant Biology *29*, 1131-1139.
- Li, Z., Wakao, S., Fischer, B.B., and Niyogi, K.K. (2009). Sensing and responding to excess light. Annual Review of Plant Biology *60*, 239-260.
- Liu, L.-N., and Scheuring, S. (2013). Investigation of photosynthetic membrane structure using atomic force microscopy. Trends in Plant Science *18*(5), 277-286.
- Lohr, M. (2011). Carotenoid metabolism in phytoplankton. Phytoplankton Pigments: Characterization, Chemotaxonomy and Applications in Oceanography, 113-161.
- Longoni, P., Douchi, D., Cariti, F., Fucile, G., and Goldschmidt-Clermont, M. (2015). Phosphorylation of the light-harvesting complex II isoform Lhcb2 is central to state transitions. Plant Physiology *169*, 2874-2883.
- Lucker, B., and Kramer, D.M. (2013). Regulation of cyclic electron flow in *Chlamydomonas reinhardtii* under fluctuating carbon availability. Photosynthesis Research *117*, 449-459.
- Maréchal, E., and Cesbron-Delauw, M.F. (2001). The apicoplast: a new member of the plastid family. Trends in Plant Science *6*, 200-205.

- Martinson, T.A., Ikeuchi, M., and Plumley, F.G. (1998). Oxygen-evolving diatom thylakoid membranes. Biochimica et Biophysica Acta (BBA) - Bioenergetics *1409*(2), 72-86.
- Maruyama, S., Tokutsu, R., and Minagawa, J. (2014). Transcriptional regulation of the stress-responsive light harvesting complex genes in *Chlamydomonas reinhardtii*. Plant & Cell Physiology *55*, 1304-1310.
- Massana, R., Gobet, A., Audic, S., Bass, D., Bittner, L., Boutte, C., Chambouvet, A., Christen, R., Claverie, J.-M., Decelle, J., et al. (2015). Marine protist diversity in European coastal waters and sediments as revealed by high-throughput sequencing. Environmental Microbiology, 4035.
- Matsuo, M. and Obokata, J. (2006). Remote control of photosynthetic genes by the mitochondrial respiratory chain. The Plant Joural *47*: 873–882.
- Matsuo, M., Hachisu, R., Tabata, S., Fukuzawa, H., and Obokata, J. (2011). Transcriptome analysis of respiration-responsive genes in *Chlamydomonas reinhardtii*: mitochondrial retrograde signaling coordinates the genes for cell proliferation with energy-producing metabolism. Plant and Cell Physiology *52*: 333–343.
- Matsuoka, D., Iwata, T., Zikihara, K., Kandori, H., and Tokutomi, S. (2007). Primary processes during the light-signal transduction of phototropin. Photochemistry & Photobiology *83*, 122-130.
- McFadden, G.I. (2014). Origin and evolution of plastids and photosynthesis in eukaryotes. Cold Spring Harbor perspectives in biology *6*, 4, a016105.
- McFadden, G.I., and van Dooren, G.G. (2004). Evolution: red algal genome affirms a common origin of all plastids. Current Biology *14*, R514-R516.
- Melis, A. (1982). Kinetic analysis of P-700 photoconversion: effect of secondary electron donation and plastocyanin inhibition. Archives of Biochemistry and Biophysics *217*, 536-545.
- Melis, A. (1991). Dynamics of photosynthetic membrane composition and function. Biochimica et Biophysica Acta (BBA) - Bioenergetics *1058*, 87-106.
- Menke, W. (1962). Structure and Chemistry of Plastids. Annual Review of Plant Physiology *13*, 27.
- Merchant, S.S., Prochnik, S.E., Vallon, O., Harris, E.H., Karpowicz, S.J., Witman, G.B., Terry, A., Salamov, A., Fritz-Laylin, L.K., Marechal-Drouard, L., et al. (2007). The *Chlamydomonas* genome reveals the evolution of key animal and plant functions. Science *318*, 245-251.

- Miura, K., Yamano, T., Yoshioka, S., Kohinata, T., Inoue, Y., Taniguchi, F., Asamizu, E., Nakamura, Y., Tabata, S., and Yamato, K.T. (2004). Expression profiling-based identification of CO_2-responsive genes regulated by CCM1 controlling a carbon-concentrating mechanism in *Chlamydomonas reinhardtii*. Plant Physiology *135*, 1595-1607.
- Moog, D., Stork, S., Zauner, S., and Maier, U.-G. (2011). In silico and in vivo investigations of proteins of a minimized eukaryotic cytoplasm. Genome Biology and Evolution *3*, 375-382.
- Moroney, J.V., Kitayama, M., Togasaki, R.K., and Tolbert, N.E. (1987). Evidence for inorganic carbon transport by intact chloroplasts of *Chlamydomonas reinhardtii*. Plant Physiology *83*: 460–463.
- Moroney, J.V., Husic, H.D., Tolbert, N.E., Kitayama, M., Manuel, L.J., and Togasaki, R.K. (1989). Isolation and characterization of a mutant of *Chlamydomonas reinhardtii* deficient in the CO_2 concentrating mechanism. Plant Physiology *89*: 897–903.
- Müller, P., Li, X.-P., and Niyogi, K.K. (2001). Non-photochemical quenching. A response to excess light energy. Plant Physiology *125*, 1558-1566.
- Munekage, Y., Hojo, M., Meurer, J., Endo, T., Tasaka, M., and Shikanai, T. (2002). PGR5 is involved in cyclic electron flow around photosystem I and is essential for photoprotection in *Arabidopsis*. Cell *110*: 361–371.
- Murata, N., Takahashi, S., Nishiyama, Y., and Allakhverdiev, S.I. (2007). Photoinhibition of photosystem II under environmental stress. Biochimica et Biophysica Acta (BBA) - Bioenergetics *1767*, 414-421.
- Mustardy, L., Buttle, K., Steinbach, G., and Garab, G. (2008). Three-dimensional architecture of the granum-stroma thylakoid membrane system revealed by electron tomography. Photosynthesis. Energy from the Sun. Springer Netherlands, 767-770.
- Mustardy, L., and Garab, G. (2003). Granum revisited. A three-dimensional model - where things fall into place. Trends in Plant Science *8*, 117-122.
- Nagy, G., Ünnep, R., Zsiros, O., Tokutsu, R., Takizawa, K., Porcar, L., Moyet, L., Petroutsos, D., Garab, G., Finazzi, G., et al. (2014). Chloroplast remodeling during state transitions in *Chlamydomonas reinhardtii* as revealed by noninvasive techniques in vivo. Proceedings of the National Academy of Sciences *111*, 5042-5047.
- Nakamura, A., Suzawa, T., Kato, Y., and Watanabe, T. (2005). Significant species-dependence of P700 redox potential as verified by spectroelectrochemistry: Comparison of spinach and Theromosynechococcus elongatus. FEBS letters *579*, 2273-2276.

- Nakano, Y., and Asada, K. (1987). Purification of ascorbate peroxidase in spinach chloroplasts; its inactivation in ascorbate-depleted medium and reactivation by monodehydroascorbate radical. Plant and cell physiology *28*, 131-140.
- Nath, K., Jajoo, A., Poudyal, R.S., Timilsina, R., Park, Y.S., Aro, E.-M., Nam, H.G., and Lee, C.H. (2013). Towards a critical understanding of the photosystem II repair mechanism and its regulation during stress conditions. FEBS Letters, 3372.
- Naumann, B., Busch, A., Allmer, J., Ostendorf, E., Zeller, M., Kirchhoff, H., and Hippler, M. (2007). Comparative quantitative proteomics to investigate the remodeling of bioenergetic pathways under iron deficiency in *Chlamydomonas reinhardtii*. Proteomics *7*, 3964-3979.
- Nawrocki, W.J., Santabarbara, S., Mosebach, L., Wollman, F.-A., and Rappaport, F. (2016). State transitions redistribute rather than dissipate energy between the two photosystems in *Chlamydomonas*. Nature Plants *2*, 16031.
- Neidhardt, J., Benemann, J.R., Zhang, L., and Melis, A. (1998). Photosystem-II repair and chloroplast recovery from irradiance stress: relationship between chronic photoinhibition, light-harvesting chlorophyll antenna size and photosynthetic productivity in *Dunaliella salina* (green algae). Photosynthesis Research *56*, 175-184.
- Nelson, N., and Ben-Shem, A. (2005). The structure of photosystem I and evolution of photosynthesis. BioEssays *27*, 914-922.
- Nelson, N., and Yocum, C.F. (2006). Structure and function of photosystems I and II. Annual Review of Plant Biology *57*, 521-565.
- Nisbet, R.E.R., Kilian, O., and McFadden, G.I. (2004). Diatom genomics: genetic acquisitions and mergers. Current Biology *14*, R1048-R1050.
- Niyogi, K.K. (1999). Photoprotection revisited: genetic and molecular approaches. Annual Review of Plant Physiology and Plant Molecular Biology *50*, 333-359.
- Niyogi, K.K., Bjorkman, O., and Grossman, A.R. (1997). *Chlamydomonas* xanthophyll cycle mutants identified by video imaging of chlorophyll fluorescence quenching. The Plant Cell *9*: 1369–1380.
- Niyogi, K.K., and Truong, T.B. (2013). Evolution of flexible non-photochemical quenching mechanisms that regulate light harvesting in oxygenic photosynthesis. Current Opinion in Plant Biology *16*, 307-314.
- Nymark, M., Valle, K.C., Hancke, K., Winge, P., Andresen, K., Johnsen, G., Bones, A.M., and Brembu, T. (2013). Molecular and photosynthetic responses to prolonged darkness and

subsequent acclimation to re-illumination in the diatom *Phaeodactylum tricornutum*. PLoS ONE *8*, 1-19.

- Ort, D.R., and Baker, N.R. (2002). A photoprotective role for O2 as an alternative electron sink in photosynthesis? Current Opinion in Plant Biology *5*, 193-198.
- Osmond, B., Badger, M., Maxwell, K., Björkman, O., and Leegood, R. (1997). Too many photons: photorespiration, photoinhibition and photooxidation. Trends in Plant Science *2*, 119-121.
- Otsuna, H., Shinomiya, K., and Ito, K. (2014). Parallel neural pathways in higher visual centers of the *Drosophila* brain that mediate wavelength-specific behavior. Frontiers In Neural Circuits *8*, 8-8.
- Oudot-Le Secq, M.-P., Grimwood, J., Shapiro, H., Armbrust, E.V., Bowler, C., and Green, B.R. (2007). Chloroplast genomes of the diatoms *Phaeodactylum tricornutum* and *Thalassiosira pseudonana*: comparison with other plastid genomes of the red lineage. Molecular Genetics and Genomics *277*(4), 427-439.
- Owens, T.G. (1986). Light-Harvesting Function in the Diatom *Phaeodactylum tricornutum*: II. Distribution of excitation energy between the photosystems. Plant Physiology *80*, 739-746.
- Paolillo, D.J., Falk, R.H., and Reighard, J.A. (1967). The effect of chemical fixation on the fretwork of chloroplasts. Transactions of the American Microscopical Society 225.
- Paolillo, D.J., Jr. (1970). The three-dimensional arrangement of intergranal lamellae in chloroplasts. Journal of Cell Science *6*, 243-255.
- Paul, M.J. and Foyer, C.H. (2001). Sink regulation of photosynthesis. Journal of Experimental Botany *52*: 1383.
- Peers, G., Truong, T.B., Ostendorf, E., Busch, A., Elrad, D., Grossman, A.R., Hippler, M., and Niyogi, K.K. (2009). An ancient light-harvesting protein is critical for the regulation of algal photosynthesis. Nature *462*, 518-521.
- Peltier, G., and Thibault, P. (1985). Uptake in the light in *Chlamydomonas*: evidence for persistent mitochondrial respiration. Plant Physiology *79*, 225-230.
- Peschke, M., Moog, D., Klingl, A., Maier, U.G., and Hempel, F. (2013). Evidence for glycoprotein transport into complex plastids. Proceedings of the National Academy of Sciences *110*, 10860-10865.

- Petersen, J., Förster, K., Turina, P., and Gräber, P. (2012). Comparison of the H+/ATP ratios of the H+-ATP synthases from yeast and from chloroplast. Proceedings of the National Academy of Sciences *109*, 11150-11155.
- Petroutsos, D., Terauchi, A.M., Busch, A., Hirschmann, I., Merchant, S.S., Finazzi, G., and Hippler, M. (2009). PGRL1 participates in iron-induced remodeling of the photosynthetic apparatus and in energy metabolism in *Chlamydomonas reinhardtii*. The Journal of Biological Chemistry *284*, 32770-32781.
- Petroutsos, D., Busch, A., Jan, xdf, en, I., Trompelt, K., Bergner, S.V., Weinl, S., Holtkamp, M., Karst, U., et al. (2011). The chloroplast calcium sensor CAS is required for photoacclimation in *Chlamydomonas reinhardtii*. The Plant Cell *23*, 2950-2963.
- Petroutsos, D., Amiar, S., Abida, H., Dolch, L.-J., Bastien, O., Rébeillé, F., Jouhet, J., Falconet, D., Block, M.A., McFadden, G.I., et al. (2014). Review: Evolution of galactoglycerolipid biosynthetic pathways – From cyanobacteria to primary plastids and from primary to secondary plastids. Progress in Lipid Research *54*, 68-85.
- Pfeifer, A., Mathes, T., Lu, Y., Hegemann, P., and Kottke, T. (2010). Blue light induces global and localized conformational changes in the kinase domain of full-length phototropin. Biochemistry *49*, 1024-1032.
- Plancke, C. et al. (2014). Lack of isocitrate lyase in *Chlamydomonas* leads to changes in carbon metabolism and in the response to oxidative stress under mixotrophic growth. The Plant Journal *77*: 404–417.
- Prihoda, J., Tanaka, A., De Paula, W.B.M., Allen, J.F., Tirichine, L., Bowler, C., and Teige, M. (2012). Chloroplast-mitochondria cross-talk in diatoms. Journal of Experimental Botany *63*, 1543-1557.
- Radmer, R.J., and Kok, B. (1976). Photoreduction of O_2 primes and replaces CO_2 assimilation. Plant Physiology *58*, 336-340.
- Raven, J.A., and Geider, R.J. (2003). Adaptation, acclimation and regulation in algal photosynthesis. Photosynthesis in Algae (Springer, 385-412).
- Rivasseau, C., Seemann, M., Boisson, A., Streb, P., Gout, E., Douce, R., Rohmer, M., and Bligny, R. (2009). Accumulation of 2-C-methyl-D-erythritol 2, 4-cyclodiphosphate in illuminated plant leaves at supraoptimal temperatures reveals a bottleneck of the prokaryotic methylerythritol 4-phosphate pathway of isoprenoid biosynthesis. Plant, Cell & Environment *32*, 82-92.

- Roach, T., Sedoud, A., and Krieger-Liszkay, A. (2013). Acetate in mixotrophic growth medium affects photosystem II in *Chlamydomonas reinhardtii* and protects against photoinhibition. Biochimica et Biophysica Acta (BBA) *1827*: 1183–1190.
- Round, F.E. (1990). The diatoms: biology & morphology of the genera / F. E. Round, R. M. Crawford, D. G. Mann. Cambridge University Press.
- Ruban, A.V., Berera, R., Ilioaia, C., Stokkum, I.H.M.v., Kennis, J.T.M., Pascal, A.A., Amerongen, H.v., Robert, B., Horton, P., and Grondelle, R.v. (2007). Identification of a mechanism of photoprotective energy dissipation in higher plants. Nature *450,* 7169, 575-578.
- Ruban, A.V., and Johnson, M.P. (2015). Visualizing the dynamic structure of the plant photosynthetic membrane. Nature Plants *1*, 15161.
- Sager, R. and Granick, S. (1954). Nutritional control of sexuality in *Chlamydomonas reinhardi*. The Journal of General Physiology *37*: 729–742.
- Salomon, M., Christie, J.M., Knieb, E., Lempert, U., and Briggs, W.R. (2000). Photochemical and mutational analysis of hte FMN-binding domains of the plant blue light receptor, phototropin. Biochemistry, 9401.
- Salvi, D., Rolland, N., Joyard, J., and Ferro, M. (2008). Purification and proteomic analysis of chloroplasts and their sub-organellar compartments. Methods in Molecular Biology *432*, 19-36.
- Santabarbara, S., Redding, K.E., and Rappaport, F. (2009). Temperature dependence of the reduction of P700+ by tightly bound plastocyanin in vivo. Biochemistry *48*, 10457-10466.
- Scheuring, S., and Sturgis, J.N. (2009). Atomic force microscopy of the bacterial photosynthetic apparatus: plain pictures of an elaborate machinery. Photosynthesis Research *102*, 2-3, 197-211.
- Schindelin, J., Arganda-Carreras, I., Frise, E., Kaynig, V., Longair, M., Pietzsch, T., Preibisch, S., Rueden, C., Saalfeld, S., Schmid, B., et al. (2012). Fiji: an open-source platform for biological-image analysis. Nature Methods *9*, 676-682.
- Schleiff, E., and Becker, T. (2011). Common ground for protein translocation: access control for mitochondria and chloroplasts. Nature Reviews Molecular Cell Biology *12*, 48-59.
- Schleiff, E., Maier, U.G., and Becker, T. (2011). Omp85 in eukaryotic systems: one protein family with distinct functions. Biological Chemistry *392*, 21-27.
- Schloss, J.A. (1990). A *Chlamydomonas* gene encodes a G protein β subunit-like polypeptide. Molecular and General Genetics *221*, 443-452.

- Schmidt, M., Gessner, G., Luff, M., Heiland, I., Wagner, V., Kaminski, M., Geimer, S., Eitzinger, N., Reissenweber, T., Voytsekh, O., et al. (2006). Proteomic analysis of the eyespot of *Chlamydomonas reinhardtii* provides novel insights into its components and tactic movements. The Plant Cell, 1908.
- Shikanai, T. (2007). Cyclic electron transport around photosystem I: genetic approaches. Annual Review of Plant Biology *58*, 199-217.
- Shimoni, E., Rav-Hon, O., Ohad, I., Brumfeld, V., and Reich, Z. (2005). Three-dimensional organization of higher-plant chloroplast thylakoid membranes revealed by electron tomography. The Plant Cell, 2580.
- Shropshire, W., Jr., and Mohr, H. (1983). Photomorphogenesis. Encyclopedia of Plant Physiology. New Series.
- Siaut, M., Heijde, M., Mangogna, M., Montsant, A., Coesel, S., Allen, A., Manfredonia, A., Falciatore, A., and Bowler, C. (2007). Molecular toolbox for studying diatom biology in *Phaeodactylum tricornutum*. Gene *406*, 23-35.
- Small, G.D., Min, B., and Lefebvre, P.A. (1995). Characterization of a *Chlamydomonas reinhardtii* gene encoding a protein of the DNA photolyase/blue light photoreceptor family. Plant Molecular Biology *28*, 443-454.
- Smith, B.M., Morrissey, P.J., Guenther, J.E., Nemson, J.A., Harrison, M.A., Allen, J.F., and Melis, A. (1990). Response of the photosynthetic apparatus in *Dunaliella salina* (Green Algae) to irradiance stress. Plant Physiology *93*, 1433-1440.
- Sommer, M.S., Daum, B., Gross, L.E., Weis, B.L.M., Mirus, O., Abram, L., Maier, U.-G., Kühlbrandt, W., and Schleiff, E. (2011). Chloroplast Omp85 proteins change orientation during evolution. Proceedings of the National Academy of Sciences *108*, 13841-13846.
- Sommer, M.S., Gould, S.B., Lehmann, P., Gruber, A., Przyborski, J.M., and Maier, U.-G. (2007). Der1-mediated preprotein import into the periplastid compartment of chromalveolates? Molecular Biology and Evolution *24*, 918-928.
- Spetea, C., Pfeil, B.E., Schoefs, B. (2012). Phylogenetic analysis of the thylakoid ATP/ADP carrier reveals new insights into its function restricted to green plants. Frontiers in Plant Science 9, 2-110.
- Staehelin, L.A. (2003). Chloroplast structure: from chlorophyll granules to supra-molecular architecture of thylakoid membranes. Photosynthesis Research *76*, 185-196.

- Stork, S., Moog, D., Przyborski, J.M., Wilhelmi, I., Zauner, S., and Maier, U.G. (2012). Distribution of the SELMA translocon in secondary plastids of red algal origin and predicted uncoupling of ubiquitin-dependent translocation from degradation. Eukaryotic Cell *11*, 1472-1481.
- Stork, S., Lau, J., Moog, D., and Maier, U.-G. (2013). Three old and one new: protein import into red algal-derived plastids surrounded by four membranes. Protoplasma, 1013.
- Sueoka, N. (1960). Mitotic replication of deoxyribonucleic acid in *Chlamydomonas reinhardi*. Proceedings of the National Academy of Sciences *46*, 83-91.
- Suetsugu, N., and Wada, M. (2013). Evolution of three LOV blue light receptor families in green plants and photosynthetic stramenopiles: phototropin, ZTL/FKF1/LKP2 and aureochrome. Plant & Cell Physiology *54*, 8-23.
- Sukenik, A., Bennett, J., and Falkowski, P. (1987). Light-saturated photosynthesis — Limitation by electron transport or carbon fixation? Biochimica et Biophysica Acta (BBA) - Bioenergetics *891*, 205-215.
- Sundby, C., McCaffery, S., and Anderson, J.M. (1993). Turnover of the photosystem II D1 protein in higher plants under photoinhibitory and nonphotoinhibitory irradiance. The Journal of Biological Chemistry 268, 25476-25482.
- Tabachnick, B.G., and Fidell, L.S., (2012). Using multivariate statistics (Pearson, London, ed. 6).
- Taddei, L. et al. (2016). Multisignal control of expression of the LHCX protein family in the marine diatom *Phaeodactylum tricornutum*. Journal of Experimental Botany.
- Takahashi, H., Iwai, M., Takahashi, Y., and Minagawa, J. (2006). Identification of the mobile light-harvesting complex II polypeptides for state transitions in *Chlamydomonas reinhardtii*. Proceedings of the National Academy of Sciences *103*, 477-482.
- Takeuchi, F., Futamura, Y., Yoshikura, H., and Yamamoto, K. (2003). Statistics of trinucleotides in coding sequences and evolution. Journal of Theoretical Biology *222*, 139-149.
- Tamayo, J., and Garcia, R. (1996). Deformation, contact time, and phase contrast in tapping mode scanning force microscopy. Langmuir *12*, 4430-4435.
- Tanaka, A., De Martino, A., Amato, A., Montsant, A., Mathieu, B., Rostaing, P., Tirichine, L., and Bowler, C. (2015). Ultrastructure and membrane traffic during cell division in the marine pennate diatom *Phaeodactylum tricornutum*. Protist *166*, 506.

- R Development Core Team. R (2008). A language and environment for statistical computing. (R Foundation for Statistical Computing, Vienna) ISBN 3-900051-07-0), http://www.R-project.org.
- Terashima, M., Specht, M., Naumann, B., and Hippler, M. (2010). Characterizing the anaerobic response of *Chlamydomonas reinhardtii* by quantitative proteomics. Molecular and Cellular Proteomics *9*: 1514–1532.
- Ting, C.S., and Owens, T.G. (1993). Photochemical and nonphotochemical fluorescence quenching processes in the diatom *Phaeodactylum tricornutum*. Plant Physiology *101*, 1323-1330.
- Tokutomi, S., Matsuoka, D., and Zikihara, K. (2008). Review: Molecular structure and regulation of phototropin kinase by blue light. Biochimica et Biophysica Acta (BBA) - Proteins and Proteomics *1784*, 133-142.
- Tokutsu, R., and Minagawa, J. (2013). Energy-dissipative supercomplex of photosystem II associated with LHCSR3 in *Chlamydomonas reinhardtii*. Proceedings of the National Academy of Sciences *110*, 10016-10021.
- Tokuyasu, K.T. (1973). A technique for ultramicrotomy of cell suspensions and tissues. The Journal of Cell Biology *57*, 551-565.
- Trippens, J., Greiner, A., Schellwat, J., Neukam, M., Rottmann, T., Lu, Y., Kateriya, S., Hegemann, P., and Kreimer, G. (2012). Phototropin influence on eyespot development and regulation of phototactic behavior in *Chlamydomonas reinhardtii*. The Plant Cell *24*, 4687-4702.
- Ünlü, C., Drop, B., Croce, R., and van Amerongen, H. (2014). State transitions in *Chlamydomonas reinhardtii* strongly modulate the functional size of photosystem II but not of photosystem I. Proceedings of the National Academy of Sciences *111*, 3460-3465.
- Urzica, E.I., Vieler, A., Hong-Hermesdorf, A., Page, M.D., Casero, D., Gallaher, S.D., Kropat, J., Pellegrini, M., Benning, C., and Merchant, S.S. (2013). Remodeling of membrane lipids in iron-starved *Chlamydomonas*. Journal of Biological Chemistry *288*: 30246–30258.
- Van de Meene, A.M., and Pickett-Heaps, J.D. (2004). Valve morphogenesis in the centric diatom *Rhizosolenia setigera* (Bacillariophyceae, Centrales) and its taxonomic implications. European Journal of Phycology *39*, 93-104.

- van Dooren, G.G., Schwartzbach, S.D., Osafune, T., and McFadden, G.I. (2001). Translocation of proteins across the multiple membranes of complex plastids. Biochimica et Biophysica Acta (BBA) *1541*, 34-53.
- Van Dooren, G.G., Waller, R.F., Joiner, K.A., Roos, D.S., and McFadden, G.I. (2000). Traffic jams: protein transport in *Plasmodium falciparum*. Parasitology Today *16*, 421-427.
- Vardi, A., Bidle, K.D., Kwityn, C., Hirsh, D.J., Thompson, S.M., Callow, J.A., Falkowski, P., and Bowler, C. (2008). A diatom gene regulating nitric-oxide signaling and susceptibility to diatom-derived aldehydes. Current Biology: CB *18*, 895-899.
- Vartanian, M., Desclés, J., Quinet, M., Douady, S., and Lopez, P.J. (2009). Plasticity and robustness of pattern formation in the model diatom *Phaeodactylum tricornutum*. New Phytologist *182*, 429-442.
- Veith, T., Brauns, J., Weisheit, W., Mittag, M., and Büchel, C. (2009). Identification of a specific fucoxanthin-chlorophyll protein in the light harvesting complex of photosystem I in the diatom *Cyclotella meneghiniana*. Biochimica et Biophysica Acta (BBA) - Bioenergetics *1787*, 905-912.
- Wang, Y., Stessman, D.J., and Spalding, M.H. (2015). The CO2 concentrating mechanism and photosynthetic carbon assimilation in limiting CO_2: how *Chlamydomonas* works against the gradient. The Plant Journal *82*: 429–448
- Waring, J., Klenell, M., Bechtold, U., Underwood, G.J.C., and Baker, N.R. (2010). Light-induced responses of oxygen photoreduction, reactive oxygen species production and scavenging in two diatom species. Journal of Phycology *46*, 1206-1217.
- Watanabe, M., Furuya, M., Miyoshi, Y., Inoue, Y., Iwahashi, I., and Matsumoto, K. (1982). Design and performance of the Okazaki large spectrograph for photobiological research. Photochemistry & Photobiology *36*, 491.
- Weigel, M., Pesaresi, P., and Leister, D. (2003). Tracking the function of the cytochrome c6-like protein in higher plants. Trends in Plant Science *8*, 513-517.
- Whitmarsh, J. Govindjee (1999) The photosynthetic process. Singhal GS, Renger G, Sopory SK, Irrgang KD and Govindjee, Concepts in Photobiology. Photosynthesis and Photomorphogenesis, 11-51.
- Wishnick, M., and Lane, M.D. (1969). Inhibition of Ribulose Diphosphate Carboxylase by cyanide inactive ternary complex of enzyme, ribulose diphosphate, and cyanide. Journal of Biological Chemistry *244*, 55-59.

- Witt, H. (1979). Energy conversion in the functional membrane of photosynthesis. Analysis by light pulse and electric pulse methods: The central role of the electric field. Biochimica et Biophysica Acta (BBA) - Reviews on Bioenergetics *505*, 355-427.
- Witt, H., Bordignon, E., Carbonera, D., Dekker, J.P., Karapetyan, N., Teutloff, C., Webber, A., Lubitz, W., and Schlodder, E. (2003). Species-specific differences of the spectroscopic properties of P700: analysis of the influence of non-conserved amino acid residues by site-directed mutagenesis of photosystem I from *Chlamydomonas reinhardtii*. Journal of Biological Chemistry *278*, 46760-46771.
- Wittpoth, C., Kroth, P.G., Weyrauch, K., Kowallik, K.V., and Strotmann, H. (1998). Functional characterization of isolated plastids from two marine diatoms. Planta *206* (1), 79-85.
- Wolfe, A.J. (2005). The acetate switch. Microbiology and molecular biology reviews *69,* 12-50.
- Wunder, T., Martin, R., Löffelhardt, W., Schleiff, E., and Steiner, J.M. (2007). The invariant phenylalanine of precursor proteins discloses the importance of Omp85 for protein translocation into cyanelles. BMC Evolutionary Biology *7*, 236-236.
- Xiang, Y. and Weeks, D.P. (2001). The Cia5 gene controls formation of the carbon concentrating mechanism in *Chlamydomonas reinhardtii*. Proceedings of the National Academy of Sciences *98*: 5341–5346.
- Yamano, T., Miura, K., and Fukuzawa, H. (2008). Expression analysis of genes associated with the induction of the carbon-concentrating mechanism in *Chlamydomonas reinhardtii*. Plant Physiology *147*, 340-354.
- Yang, W., Catalanotti, C., D'Adamo, S., Wittkopp, T.M., Ingram-Smith, C.J., Mackinder, L., Miller, T.E., Heuberger, A.L., Peers, G., Smith, K.S., et al. (2014). Alternative acetate production pathways in *Chlamydomonas reinhardtii* during dark anoxia and the dominant role of chloroplasts in fermentative acetate production. The Plant Cell, 4499–4518.
- Yokono, M., Nagao, R., Tomo, T., and Akimoto, S. (2015). Regulation of excitation energy transfer in diatom PSII dimer: How does it change the destination of excitation energy? Biochimica et Biophysica Acta (BBA)-Bioenergetics *1847*, 1274-1282.
- Yoon, H.S., Hackett, J.D., Ciniglia, C., Pinto, G., and Bhattacharya, D. (2004). A molecular timeline for the origin of photosynthetic eukaryotes. Molecular Biology and Evolution *21*, 809-818.

- Yoshioka, S., Taniguchi, F., Miura, K., Inoue, T., Yamano, T., and Fukuzawa, H. (2004). The novel Myb transcription factor LCR1 regulates the CO_2-responsive gene Cah1, encoding a periplasmic carbonic anhydrase in *Chlamydomonas reinhardtii*. The Plant Cell *16*: 1466–1477.
- Zhang, Z., Shrager, J., Jain, M., Chang, C.-W., Vallon, O., and Grossman, A.R. (2004). Insights into the survival of *Chlamydomonas reinhardtii* during sulfur starvation based on microarray analysis of gene expression. Eukaryotic Cell *3*, 1331-1348.
- Zorin, B., Lu, Y., Sizova, I., and Hegemann, P. (2009). Nuclear gene targeting in *Chlamydomonas* as exemplified by disruption of the PHOT gene. Gene *432*, 91-96.
- Zhu, S.-H., and Green, B.R. (2010). Photoprotection in the diatom *Thalassiosira pseudonana*: Role of LI818-like proteins in response to high light stress. Biochimica et Biophysica Acta (BBA) - Bioenergetics *1797*, 1449-1457

5.7 Acknowledgements

This Ph.D project has brought me around the world! It is difficult to describe how this experience deeply changed my person. I had the chance to visit incredible places and discover different cultures. This journey led me also to connect with incredible people who has inspired me and helped me during these 3 years.

All my gratitude goes to these people.

First of all, I would like to thank Dr. Christelle Breton, Prof. Claire Remacle, Dr. Xenie Johnson, Dr. Maurizio Ribera D'Alcalà and Prof. Jun Minagawa for accepting to valuate my work of thesis.

I would like to deeply thank my Ph.D supervisor Dr. Giovanni Finazzi who gave me the opportunity to join the AccliPhot consortium. During this period, thanks to his supervision he taught me how to become an independent scientist. I will always be grateful to him for this choice.

To Dr. Dimitris Petroutsos, for the constant support and help during these years.

Many thanks also to Dr. Denis Falconet for the everyday kindness and for refreshing my passion for science.

I would like to take the opportunity also to thank the director of the Cell and Plant Physiology Laboratory Dr. Norbert Rolland who accepted me in the Lab.

To all the colleagues at the PCV Lab and CEA. My gratitudes goes especially to: Cecile Giustini, Gilles Curien, Marcel Kuntz, Leonardo Magneschi, Michel Matringe, Lucas Moyet, Daniel Salvi, Fabrizio Iacono and Eric Marechal. A "super merci" also goes to Sophie, Danielle and Nassima always there for any questions.

A special thank goes to Martino, Valeria and Matteo my buddies in this busy journey called Ph.D! It was AWESOME to find you here. Thanks for every minute spent together!!

To my "French" family: Xenia, Raquel, Lucilla, Valeria B. and the group of Españoles + Italianos 2.0.

To the AccliPhot team that turns every meeting in a funny adventure!

Finally, to "the pillars of my heart" my family for the continuous support over the years.

Now is the moment to find new adventures and discover new seas!